

Vanessa Isabel da Silva Mendes

Preparation and Pre-clinical Evaluation of New Pentacyclic Triterpenoids

Doctoral Thesis in Pharmaceutical Sciences in the specialty of Pharmaceutical Chemistry supervised by Professor Jorge António Ribeiro Salvador and presented to the Faculty of Pharmacy of the University of Coimbra

August/2016



UNIVERSIDADE DE COIMBRA



***Preparation and Pre-clinical Evaluation of New
Pentacyclic Triterpenoids***

Thesis

submitted to the

Faculty of Pharmacy,

University of Coimbra

in Partial Fulfillment

of the Requirements

for the Degree of

Doctor of Philosophy in Pharmaceutical Sciences

in the specialty of

Pharmaceutical Chemistry

By

Vanessa Isabel da Silva Mendes

Coimbra, 2016



***Preparation and Pre-clinical Evaluation of New
Pentacyclic Triterpenoids***

Work developed under the scientific supervision of:

Professor Jorge António Ribeiro Salvador, PhD

Laboratory of Pharmaceutical Chemistry, Faculty of Pharmacy, University of
Coimbra

With the collaboration of:

Professor Varsha Gandhi, PhD

Department of Experimental Therapeutics, Division of Cancer Medicine,
The University of Texas MD Anderson Cancer Center, Houston, TX, USA

This thesis was developed in the Laboratory of Pharmaceutical Chemistry of the Faculty of Pharmacy of the University of Coimbra, in the Center for Neuroscience and Cell Biology (CNC), University of Coimbra, and in The University of Texas MD Anderson Cancer Center.

This work was financially supported by Fundação para a Ciência e a Tecnologia under the Programa Operacional Potencial Humano (POPH) of Quadro de Referência Estratégica Nacional (QREN) Portugal 2007-2013:

SFRH/BD/77419/2011



Front cover

The chemical structures of ursolic acid (UA, 1), derivative 3.2, and of the best derivatives of each experimental chapter (3.17, 4.2 and 5.12) are shown. Representative images of effect of two concentrations of compounds 3.17 and 4.2 on the spheroid culture model of the H460 cell line are shown.

According to the current legislation, any copying, publication, or use of this thesis or parts thereof shall not be allowed without written permission.

Aos meus pais,
ao meu irmão,
ao meu sobrinho,
à minha família
e aos meus amigos,

obrigada pelo vosso incentivo, carinho e apoio que me guiaram nesta
jornada.

*Sometimes our light goes out but is blown into flame by another human
being. Each of us owes deepest thanks to those who have rekindled this
light.*

Albert Schweitzer

Agradecimentos | Acknowledgements

Para caminhar o longo percurso até esta tese de doutoramento, houve contributos de natureza diversa que não devem deixar de ser realçados. Por essa razão, desejo expressar os meus sinceros agradecimentos:

Ao Professor Jorge António Ribeiro Salvador, gostaria de agradecer a oportunidade e a confiança que sempre teve em mim, a constante disponibilidade, o apoio, a orientação e a competência científica, bem como o espírito inovador e positivo. Agradeço ainda as sugestões e a revisão científica do presente texto. Foi um privilégio poder trabalhar e aprender com o professor ao longo destes anos.

I would like to thank Professor Varsha Gandhi for welcoming me in her lab, for your constant support, mentorship, and enthusiasm with this work. It was honor to work under your supervision and be able to appreciate your incessant dedication to science and education.

I would like to thank Doctor Geoffrey A. Bartholomeusz for the opportunity to work in his laboratory and providing all the conditions that I needed to perform the first biological assays presented in this thesis. It was an honor to be a part of the easy, constant, and wonderful collaborations between all the MDACC laboratories.

A todos os docentes e funcionários do Laboratório de Química Farmacêutica da Faculdade de Farmácia da Universidade de Coimbra, gostaria de agradecer a simpatia, a convivência, todo o apoio prestado, e os ensinamentos científicos e de vida.

Aos funcionários da biblioteca do Pólo das Ciências da Saúde e do Departamento de Química da Universidade de Coimbra, agradeço todo o apoio e disponibilidade.

Aos Professores José António Paixão e Maria Teresa Duarte, agradeço a disponibilidade e o apoio prestados no trabalho de difração de raios-X deste projeto.

Ao Pedro Cruz, à Fátima Nunes, e à Sílvia Gramacho, gostaria de agradecer o paciente trabalho técnico desenvolvido de elucidação estrutural das inúmeras amostras.

À Fundação para a Ciência e a Tecnologia, agradeço o apoio financeiro sob a forma de uma bolsa de doutoramento (SFRH/BD/77419/2011).

Aos meus colegas do Laboratório de Química Farmacêutica, com quem trabalhei ao longo deste anos, gostaria de agradecer o companheirismo, a disponibilidade e o apoio. Agradeço também a amizade, o interesse, a troca de ideias, e todos os momentos agradáveis e divertidos que partilhamos.

I would like to thank all my colleagues in Doctor Varsha Gandhi's lab for welcoming me into the laboratory, their assistance and friendship. It was a pleasure to have known and worked with you.

Aos meus pais e ao meu irmão, gostaria de agradecer o apoio incondicional, a paciência infinita, o incentivo que sempre me deram, o carinho e a compreensão. Sem vós, sem os vossos conselhos, exemplos de trabalho, dedicação e humanidade, não teria chegado a bom porto.

À minha avó e a toda a minha família, agradeço o apoio incondicional, as palavras de apoio, e o interesse que sempre demonstraram pelo meu trabalho.

Aos meus amigos, perto ou longe, a família que escolhemos, gostaria de agradecer os momentos de convívio, o apoio, e a compreensão pelas incontáveis ausências.

I would like to thank all my friends from Houston for their friendship, happy moments and support. You made Houston feel like home to me.

A todos os que, direta ou indiretamente, estiveram comigo:

Muito Obrigada!

Thank you!

Table of Contents

ABSTRACT	I
RESUMO	III
LIST OF ABBREVIATIONS	VII
LIST OF FIGURES	XIII
LIST OF TABLES	XVII
LIST OF SCHEMES	XIX
THESIS ORGANIZATION	XXI
CHAPTER 1	1
1. INTRODUCTION	2
1.1. CANCER.....	2
1.1.1. <i>Biology of cancer</i>	3
1.1.1.1. <i>Targeting apoptosis in cancer therapy</i>	4
1.1.1.2. <i>Targeting autophagy in cancer therapy</i>	8
1.1.2. <i>Lung cancer</i>	10
1.2. NATURAL PRODUCTS IN CANCER.....	13
1.3. TERPENES: GENERAL CONSIDERATIONS.....	18
1.3.1. <i>Triterpenes: pentacyclic triterpenoids</i>	19
1.3.2. <i>Ursolic acid</i>	21
1.3.2.1. <i>General activities of ursolic acid</i>	22
1.3.2.2. <i>Anticancer activity of ursolic acid</i>	22
1.3.2.3. <i>Semisynthetic derivatives with anticancer activity</i>	26
CHAPTER 2	41
GENERAL OBJECTIVES	41
CHAPTER 3	45
SYNTHESIS AND CYTOTOXIC ACTIVITY OF NOVEL A-RING MODIFIED URSOLIC ACID DERIVATIVES IN NSCLC	45
3.1. INTRODUCTION	46
3.2. RESULTS AND DISCUSSION	50
3.2.1. <i>Chemistry</i>	50
3.2.2. <i>Biological studies</i>	61
3.2.2.1. <i>Evaluation of in vitro anticancer activity</i>	61
3.2.2.2. <i>Effect of compound 3.17 on cellular DNA, RNA, and protein synthesis</i>	67
3.2.2.3. <i>Effect of compound 3.17 on the cell cycle distribution</i>	68
3.2.2.4. <i>Effect of compound 3.17 on gene expression profile</i>	69
3.2.2.5. <i>Apoptosis-inducing effect of compound 3.17 evaluated by annexin V-Cy5/PI assay</i>	70
3.2.2.6. <i>Effect of compound 3.17 on the levels of apoptosis-related proteins</i>	72
3.2.2.7. <i>Effect of compound 3.17 treatment on autophagy</i>	73
3.2.2.8. <i>Effect of compound 3.17 on the levels of autophagy-related proteins</i>	76
3.2.2.9. <i>Proposed mechanism of action</i>	78

3.3. CONCLUSION	80
3.4. EXPERIMENTAL SECTION	81
3.4.1. Chemistry.....	81
3.4.1.1. General.....	81
3.4.1.2. Synthetic procedures.....	83
3.4.2. Biology.....	98
3.4.2.1. Cell lines and culture	98
3.4.2.2. Materials.....	98
3.4.2.3. Viability assay.....	99
3.4.2.4. Macromolecule synthesis assay.....	100
3.4.2.5. Cell cycle assay.....	100
3.4.2.6. RNA isolation and array hybridization	101
3.4.2.7. Annexin V-Cy5/PI flow cytometric assay.....	102
3.4.2.8. Acridine orange staining.....	102
3.4.2.9. Protein extraction and immunoblot assay.....	103
3.4.2.10. Reverse Phase-Protein Array (RPPA)	104
3.4.2.11. Data and statistical analysis.....	105
CHAPTER 4	107
SYNTHESIS AND CYTOTOXIC ACTIVITY OF NEW OXIME AND NITRILE URSOLIC ACID DERIVATIVES IN NSCLC.....	107
4.1. INTRODUCTION	108
4.2. RESULTS AND DISCUSSION	109
4.2.1. Chemistry.....	109
4.2.2. Biological studies	131
4.2.2.1. Evaluation of <i>in vitro</i> anticancer activity.....	131
4.2.2.2. Effect of compound 4.2 on cellular DNA, RNA, and protein synthesis.....	135
4.2.2.3. Effect of compound 4.2 on the cell cycle distribution.....	136
4.2.2.4. Effect of compound 4.2 on gene expression profile	137
4.2.2.5. Apoptosis-inducing effect of compound 4.2 evaluated by annexin V-Cy5/PI assay	137
4.2.2.6. Effect of compound 4.2 on the levels of apoptosis-related proteins.....	139
4.2.2.7. Effect of compound 4.2 treatment on autophagy.....	140
4.2.2.8. Effect of compound 4.2 on the levels of autophagy-related proteins	143
4.3. CONCLUSION	144
4.4 EXPERIMENTAL SECTION	145
4.4.1. Chemistry.....	145
4.4.1.1. General.....	145
4.4.1.2. Synthetic procedures.....	147
4.4.2. Biology.....	167
4.4.2.1. Cell lines and culture, materials and assays	167
CHAPTER 5	169
SYNTHESIS AND CYTOTOXIC ACTIVITY OF NEW ESTERS AND ALPHA,BETA-UNSATURATED CARBONYL DERIVATIVES OF URSOLIC ACID IN NSCLC	169
5.1. INTRODUCTION	170

5.2. RESULTS AND DISCUSSION	172
5.2.1. Chemistry.....	172
5.2.2. Biological studies.....	187
5.2.2.1. Evaluation of <i>in vitro</i> anticancer activity.....	187
5.2.2.2. Effect of compound 5.12 on cellular DNA, RNA, and protein synthesis.....	191
5.2.2.3. Effect of compound 5.12 on the cell cycle distribution.....	192
5.2.2.4. Apoptosis-inducing effect of compound 5.12 evaluated by annexin V-Cy5/PI assay	194
5.2.2.5. Effect of compound 5.12 treatment on autophagy.....	195
5.2.2.6. Effect of compound 5.12 on protein expression profile	197
5.3. CONCLUSION.....	202
5.4 EXPERIMENTAL SECTION.....	203
5.4.1. Chemistry.....	203
5.4.1.1. General.....	203
5.4.1.2. Synthetic procedures.....	204
5.4.2. Biology.....	218
5.4.2.1. Cell lines and culture, materials and assays.....	218
CHAPTER 6	219
CONCLUDING REMARKS.....	219
CHAPTER 7	223
REFERENCES	223

Abstract

Lung cancer is the most commonly diagnosed cancer and a leading cause of cancer-related deaths worldwide. Lung cancer can be classified as non-small cell lung cancer (NSCLC) or small-cell lung cancer (SCLC), with NSCLC being the most common type (85%). The high mortality rate for patients with lung cancer has been attributed to the difficulty in obtaining an early diagnosis, a high potential for metastasis, and relative insensitivity to chemotherapy. Despite novel therapeutic strategies, the overall 5-year survival rate in many countries remains less than 15%. These statistics highlight the need for the development of new clinical agents.

Pentacyclic triterpenoids (PTs) are a large and structurally diverse group of natural products, widely present in several medicinal plants, fruits and vegetables. Medicinal plants containing PTs have been used for centuries in traditional medicine for the treatment of several diseases. Moreover, natural PTs have been extensively reported to possess a wide range of biological activities, including anticancer activity. From a biological point of view, some of the most important and active PTs include betulinic, oleanolic, glycyrrhetic and ursolic (UA) acids. UA has interesting biological properties that could be explored for the design and synthesis of more effective anticancer derivatives. Additionally, UA can be considered as a potential lead, due to its promising multitarget anticancer activity, low toxicity and commercial availability.

The main goal of this PhD thesis was to design, synthesize and evaluate new ursane derivatives as potential anti-NSCLC agents. This work followed three main semisynthetic strategies to modify the ursane scaffold. The first one involved expansion and cleavage of the A-ring, as well as introduction of N-containing groups. The second one aimed at the introduction of oximes and nitrile groups at A-ring. Finally, the third semisynthetic strategy was based on the introduction of esters (saturated or unsaturated), and of an α,β -unsaturated carbonyl system (with an endo- or exocyclic double bond) at A-ring.

The novel ursane derivatives synthesized were fully characterized using IR, MS and NMR techniques, and their anticancer activity was evaluated against NSCLC cell lines.

Based on the anticancer results obtained, the structure-activity relationships demonstrated that the most active compounds displayed a cleaved A-ring coupled with a secondary amide bearing a small alkyl side chain (**3.17**), an oxime group conjugated with a carbonyl function at A-ring (**4.2**), a cleaved A-ring bearing nitrile and imidazole groups (**4.16**), and an α,β -unsaturated ketone system with an exocyclic double bond conjugated with a heteroaromatic ring at A-ring (**5.12**).

The most active compounds were further tested in a 3D culture model, specifically a multicellular spheroid, which is able to mimic more closely the *in vivo* tumor microenvironment. Importantly, even in a 3D model, compounds **3.17** and **4.2** were active albeit a slight increase in the IC₅₀ value.

The preliminary studies on the anticancer mechanism demonstrated that the newly synthesized derivatives are able to induce cell death via apoptosis, through activation of the extrinsic pathway, and to induce autophagy. Furthermore, these compounds appear to inherit the multitarget potential of UA, by affecting the levels of different proteins involved in the process of cell death.

Overall, this work contributed with three new panels of novel ursolic acid derivatives with *in vitro* anticancer activity in 2D and 3D culture models. These derivatives can be promising candidates for the development of new anti-NSCLC agents.

Keywords:

Pentacyclic triterpenoids, Ursolic acid, Semisynthetic derivatives, Lung cancer, Monolayer culture model, Spheroid culture model, Apoptosis, Autophagy.

Resumo

O cancro do pulmão é dos tipos de cancro mais frequentemente diagnosticados e a principal causa de morte por cancro no mundo. O cancro do pulmão pode ser classificado como carcinoma pulmonar não de pequenas células (CPNPC) ou como carcinoma pulmonar de pequenas células (CPPC), sendo o CPNPC o tipo mais comum (85%). A elevada taxa de mortalidade em doentes com cancro do pulmão tem sido atribuída à dificuldade em obter um diagnóstico precoce, ao elevado potencial de formação de metástases, e à relativa insensibilidade à quimioterapia. Apesar das novas estratégias terapêuticas, a taxa de sobrevivência global aos 5 anos, em muito países, continua a ser inferior a 15%. Estas estatísticas destacam a necessidade para o desenvolvimento de novos agentes clínicos.

Os triterpenóides pentacíclicos (TPs) representam um grupo de produtos naturais abundante e estruturalmente diverso, que estão presentes em várias plantas medicinais, frutas e vegetais. As plantas medicinais contendo TPs têm constituído ao longo dos séculos uma base para a medicina tradicional no tratamento de várias doenças. Os TPs naturais têm sido extensivamente estudados pela vasta gama de atividades biológicas, incluindo a atividade anticancerígena. Do ponto de vista biológico, alguns dos TPs mais importantes e ativos incluem os ácidos betulínico, oleanólico, glicirretínico e ursólico (AU). O AU tem propriedades biológicas interessantes que poderão ser exploradas para o *design* e síntese de novos derivados anticancerígenos mais eficazes. Além disso, o AU pode ser considerado como um potencial *lead* devido à sua promissora atividade anticancerígena multifuncional, à sua baixa toxicidade e à sua disponibilidade comercial.

O principal objetivo desta tese de doutoramento foi o *design*, a síntese e a avaliação de novos derivados do tipo ursano como potenciais agentes contra o CPNPC. Este trabalho seguiu principalmente três estratégias de semissíntese para modificar a estrutura do ácido

ursólico: 1) expansão e clivagem do anel A, assim como, introdução de grupos contendo o elemento azoto; 2) introdução de grupos oxima e nitrilo no anel A; 3) e introdução de ésteres (saturados ou não saturados) e de um sistema carbonilo α,β -insaturado (com dupla ligação endocíclica ou exocíclica) no anel A.

Os novos derivados do tipo ursano sintetizados foram totalmente caracterizados através de técnicas de espectroscopia de infravermelho, ressonância magnética nuclear e espectrometria de massa, e a sua atividade anticancerígena foi avaliada em linhas celulares de CPNPC.

Com base nos resultados da atividade anticancerígena, as relações estrutura-atividade obtidas permitiram demonstrar que os compostos mais ativos exibem um anel A clivado e acoplado com uma amida secundária com uma pequena cadeia lateral alquílica (**3.17**), um anel A contendo um grupo oxima acoplado a um grupo carbonilo (**4.2**), um anel A clivado contendo um grupo nitrilo e um grupo imidazole (**4.16**), e um anel A com um sistema carbonilo α,β -insaturado, com dupla ligação exocíclica, conjugado com um anel heteroaromático (**5.12**).

Os compostos mais ativos foram testados num modelo de cultura 3D (esferóide multicelular), o qual mimetiza de forma mais próxima o microambiente tumoral *in vivo*. De facto, mesmo num modelo 3D, os compostos **3.17** e **4.2** foram ativos, apenas com um ligeiro aumento do valor de IC_{50} .

Os estudos preliminares sobre o mecanismo de ação anticancerígena demonstraram que os novos derivados do AU induzem morte celular por apoptose, através da ativação da via extrínseca, assim como autofagia. Além disso, estes compostos parecem herdar o potencial multifuncional do AU, afectando os níveis de diferentes proteínas envolvidas nos mecanismos de morte celular.

Em suma, este trabalho contribuiu com três novos grupos de derivados do ácido ursólico com atividade anticancerígena *in vitro*, em modelos de cultura 2D e 3D. Estes novos

derivados podem ser considerados como candidatos promissores para o desenvolvimento de novos agentes anti-CPNPC.

Palavras-chave:

Triterpenóides pentacíclicos, Ácido ursólico, Derivados semissintéticos, Cancro do pulmão, Modelo de cultura em monocamada, Modelo cultura esferóide, Apoptose, Autofagia.

List of abbreviations

2D	Two-dimensional
3D	Three-dimensional
4E-BP	Eukaryotic translation initiation factor 4E-binding protein
5-FU	5-fluorouracil
ABCG2	ATP-binding cassette sub-family G member 2
ADP	Adenosine diphosphate
 AEG	Astrocyte elevated gene
Akt	Protein kinase B
ALK	Anaplastic lymphoma kinase
AMP	Adenosine monophosphate
AMPK	AMP-activated protein kinase
Apaf-1	Apoptotic protease-activating factor 1
Atg	Autophagy-related protein
ATP	Adenosine triphosphate
AVO	Acidic vascular organelle
AXL	Tyrosine-protein kinase receptor UFO
Bcl-2	B-cell lymphoma 2
BH	Bcl-2 homology domain
br	broad signal (NMR)
BRAF	Serine/threonine kinase B-Raf
CaMKK	Calcium/calmodulin-dependent kinase kinase
CBMI	1,1'-carbonylbis(2-methylimidazole)
CDI	1,1'-carbonyldiimidazole
CDK	Cyclin-dependent kinase
CDT	1,1'-carbonyl-di-(1,2,4-triazole)
Chl	Chloroquine
CHOP	C/EBP homologous protein
c-Kit	KIT proto-oncogene receptor tyrosine kinase
COSY	Homonuclear correlation spectroscopy (NMR)
COX	Cyclooxygenase

CXCL12	C-X-C motif chemokine 12
CXCR4	C-X-C chemokine receptor type 4
d	Doublet (NMR)
DAST	(Dimethylamino)sulfur trifluoride
DCC	N,N'-dicyclohexylcarbodiimide
Dd	Doublet of doublets (NMR)
DED	Death effector domain
DISC	Death-inducing signaling complex
DMAP	4-(dimethylamino)pyridine
DMAPP	Dimethylallyl diphosphate
DMSO	Dimethyl sulfoxide
DNA	Deoxyribonucleic acid
dq	Doublet of quartets (NMR)
DR	Death receptor
dt	Doublet of triplets (NMR)
EGFR	Epidermal growth factor receptor
eIF2α	Eukaryotic translation initiation factor 2 α
eIF4e	Eukaryotic translation initiation factor 4E
EML4	Echinoderm microtubule-associated protein-like 4
ER	Endoplasmic reticulum
ERK	Extracellular signal-regulated kinase
EZH2	Enhancer of zeste homolog 2
FACS	Fluorescence-activated cell sorting
FADD	Fas-associated death domain
FBS	Fetal bovine serum
FLIP	FLICE-inhibitory protein
FOXM1	Forkhead box M1
FPP	Farnesyl diphosphate
GAPDH	Glyceraldehyde 3-phosphate dehydrogenase
GGPP	Geranylgeranyl diphosphate
GPP	Geranyl diphosphate
GSK3β	Glycogen synthase kinase 3 β
HER3	Human epidermal growth factor receptor 3
HIF-1α	Hypoxia-inducible factor-1 α

HMBC	Heteronuclear multiple bond coherence (NMR)
HMQC	Heteronuclear multiple quantum coherence (NMR)
HTA 2.0	Human Transcriptome Array 2.0
IAP	Inhibitor of apoptosis protein
IC₅₀	Half-maximal inhibitory concentration
ICAM	Intercellular adhesion molecule
IGFR	Insulin-like growth factor
IL	Interleukin
IPP	Isopentenyl diphosphate
IR	Infrared
<i>J</i>	Coupling constant (NMR)
JNK	c-Jun N-terminal Kinase
KRAS	V-Ki-ras2 Kirsten rat sarcoma viral oncogene homolog
LC3	Microtubule-associated proteins 1A/1B-light chain 3
LKB1	Liver kinase B1
<i>m</i>	Multiplet (NMR)
<i>M</i>⁺	Molecular ion (MS)
MAPK	Mitogen-activated protein kinase
Mcl-1	Induced myeloid leukemia cell differentiation protein
<i>m</i>-CPBA	<i>meta</i> -chloroperbenzoic acid
MET	Proto-oncogene receptor tyrosine kinase MET
miR	MicroRNA
MMP	Matrix metalloproteinase
Mp	Melting point
MS	Mass spectrometry
mTOR	Mammalian target of rapamycin
MYT1	Myelin transcription factor 1
<i>m/z</i>	Ion mass/charge ratio (MS)
ND	Not determined
NF-κB	Nuclear factor kappa-light-chain-enhancer of activated B cells
NMR	Nuclear magnetic resonance
NO	Nitric oxide
NOESY	Nuclear overhauser effect spectroscopy (NMR)
NSCLC	Non-small cell lung cancer

P	Phosphate
p70S6K	Ribosomal protein S6 kinase beta-1
PAI-1	Plasminogen activator inhibitor-1
PARP	Poly (ADP-ribose) polymerase
PERK	Protein kinase RNA-like endoplasmic reticulum kinase
PI	Propidium iodide
PI3K	Phosphoinositide 3-kinase
PIK3CA	phosphatidylinositol-4,5-bisphosphate 3-kinase catalytic subunit alpha
PIK3-p110	PI3K catalytic subunit p110
PKC	Protein kinase C
PKL1	Polo-like kinase 1
PS	Phosphatidylserine
PT	Pentacyclic triterpenoid
<i>p</i>-TsCl	<i>para</i> -toluenesulfonyl chloride
PVDF	Polyvinylidene difluoride
QIT-MS	Quadrupole/Ion Trap Mass Spectrometer
Rb	Retinoblastoma protein
Rictor	Rapamycin-insensitive companion of mammalian target of rapamycin
RNA	Ribonucleic acid
ROS	Reactive oxygen species
ROS1	Proto-oncogene tyrosine-protein kinase ROS
RPMI	Roswell Park Memorial Institute medium
RPPA	Reverse-phase protein array
r.t.	Room temperature
RTK	Receptor tyrosine kinase
S	Serine
s	Singlet (NMR)
S6	Ribosomal protein S6
S6K	S6 kinase
SAPK	Stress-activated protein kinase
SAR	Structure-activity relationship
SCLC	Small-cell lung cancer
SD	Standard deviation

SDS	Sodium dodecyl sulfate
SHP-1	Src homology region 2 domain-containing phosphatase-1
Smac	Second mitochondria-derived activator of caspase
SP1	Transcription factor Sp1 (specificity protein 1)
STAT3	Signal transducer and activator of transcription 3
T	Threonine
t	Triplet (NMR)
T3P	<i>n</i> -Propylphosphonic anhydride
tBid	Truncated Bid
THF	Tetrahydrofuran
TIMP-2	Tissue inhibitor of metalloproteinase-2
TLC	Thin-layer chromatography
TNFR	Tumor necrosis factor receptor
UA	Ursolic acid
u-PA	Urokinase-type plasminogen activator
VEGF	Vascular endothelial growth factor
VEGFR	Vascular endothelial growth factor receptor
VPS34/PI3K	Phosphoinositide 3-kinase Class III
XIAP	X-linked inhibitor of apoptosis protein
ZIP	Zeta-interacting protein
δ	Chemical shift (NMR)

List of figures

Figure I. Chemical structure of ursolic acid (UA).	XXII
Figure 1.1. Estimated percentage of new cancer cases (incidence) and death (mortality) for men and woman, in 2012, according to GLOBOCAN 2012 data.	2
Figure 1.2. Acquired capabilities, enabling characteristics, and emerging hallmarks of cancer... 4	
Figure 1.3. Simplified scheme of the extrinsic and intrinsic apoptosis pathways, as well as mechanisms contributing to apoptosis evasion.	5
Figure 1.4. Simplified scheme of the macroautophagy pathway.	9
Figure 1.5. Schematic algorithm for first-, second-, and third-line therapy in advanced non-small cell lung cancer (NSCLC).	12
Figure 1.6. Total new approved agents between 1981 and 2014.....	14
Figure 1.7. Total new approved anticancer agents between 1981 and 2014.	15
Figure 1.8. Schematic scheme showing monofunctional (left) versus multifunctional (right) drugs.....	18
Figure 1.9. Simplified scheme of the isoprenoid biosynthetic pathway.	19
Figure 1.10. Simplified scheme of the biosynthesis of some triterpenoids.	20
Figure 1.11. Chemical structure of ursolic acid (UA).	21
Figure 1.12. Main positions of the chemical modifications performed on the UA scaffold.....	26
Figure 1.13. Schematic representation of UA ester derivatives (1.30–1.47).	31
Figure 1.14. Schematic representation of C28 amide derivatives of UA (1.48–1.68).	33
Figure 1.15. Schematic representation of C28 amide derivatives of UA (1.69–1.76).	34
Figure 1.16. Schematic representation of C28 derivatives of UA (1.77–1.83).	36
Figure 3.1. Chemical structure of <i>n</i> -propylphosphonic anhydride (T3P).	47
Figure 3.2. Chemical structures of DAST and Selectfluor fluorinating reagents.....	49
Figure 3.3. ¹ H NMR spectrum of compound 3.6 recorded in CDCl ₃	52

Figure 3.4. ^{13}C NMR spectrum of compound 3.6 recorded in CDCl_3 .	53
Figure 3.5. ^1H NMR spectrum of compound 3.7 recorded in CDCl_3 .	54
Figure 3.6. ^{13}C NMR spectrum of compound 3.7 recorded in CDCl_3 .	55
Figure 3.7. ^1H NMR spectrum of compound 3.8 recorded in CDCl_3 .	57
Figure 3.8. ^{13}C NMR spectrum of compound 3.8 recorded in CDCl_3 .	57
Figure 3.9. IR spectrum of compound 3.8.	58
Figure 3.10. ^1H NMR spectrum of compound 3.17 recorded in CDCl_3 .	60
Figure 3.11. ^{13}C NMR spectrum of compound 3.17 recorded in CDCl_3 .	60
Figure 3.12. Schematic representation of the multicellular spheroid culture model.	64
Figure 3.13. Phenotypic changes in the H460 spheroid model treated with UA (top panel) and 3.17 (bottom panel) for 96h.	67
Figure 3.14. Effect of compound 3.17 treatment on the global DNA, RNA, and protein synthesis in the H460 cell line.	68
Figure 3.15. Effect of compound 3.17 on the cell cycle distribution.	69
Figure 3.16. Induction of H460 cell death by compound 3.17.	71
Figure 3.17. Effect of compound 3.17 on the levels of apoptosis-related proteins.	73
Figure 3.18. Effect of compound 3.17 treatment on induction of autophagy in the H460 cell line.	74
Figure 3.19. Effect of autophagy inhibition on 3.17-induced cell death.	76
Figure 3.20. Effect of compound 3.17 on the levels of autophagy-related proteins.	78
Figure 3.21. Possible anticancer mechanism of compound 3.17.	80
Figure 4.1. ^1H NMR spectrum of compound 4.2 recorded in CDCl_3 .	111
Figure 4.2. ^{13}C NMR spectrum of compound 4.2 recorded in CDCl_3 .	112
Figure 4.3. IR spectrum of compound 4.2.	113
Figure 4.4. ORTEP diagram of compound 4.3 crystallized from methanol.	113
Figure 4.5. ^1H NMR spectrum of compound 4.4 recorded in CDCl_3 .	114
Figure 4.6. ^{13}C NMR spectrum of compound 4.4 recorded in CDCl_3 .	115
Figure 4.7. NOESY NMR spectrum of compound 4.4 recorded in CDCl_3 .	116

Figure 4.8. NOESY correlation for compound 4.4	116
Figure 4.9. Proposed reaction mechanism of the “abnormal” Beckmann rearrangement for the formation of compound 4.15.....	119
Figure 4.10. ¹ H NMR spectrum of compound 4.5 recorded in CDCl ₃	120
Figure 4.11. ¹³ C NMR spectrum of compound 4.5 recorded in CDCl ₃	121
Figure 4.12. ¹ H NMR spectrum of compound 4.15 recorded in CDCl ₃	122
Figure 4.13. ¹³ C NMR spectrum of compound 4.15 recorded in CDCl ₃	122
Figure 4.14. IR spectrum of compound 4.5.	123
Figure 4.15. ¹ H NMR spectrum of compound 4.16 recorded in CDCl ₃	125
Figure 4.16. ¹³ C NMR spectrum of compound 4.16 recorded in CDCl ₃	126
Figure 4.17. ORTEP diagram of compound 4.16 crystallized from acetonitrile.....	126
Figure 4.18. ¹ H NMR spectrum of compound 4.19 recorded in CDCl ₃	128
Figure 4.19. ¹³ C NMR spectrum of compound 4.19 recorded in CDCl ₃	128
Figure 4.20. IR spectrum of compound 4.19.	129
Figure 4.21. ¹ H NMR spectrum of compound 4.20 recorded in CDCl ₃	130
Figure 4.22. ¹³ C NMR spectrum of compound 4.20 recorded in CDCl ₃	130
Figure 4.23. Phenotypic changes in the H460 spheroid model treated with UA (top panel), compound 4.2 (middle panel), and compound 4.16 (bottom panel) for 96 h.....	134
Figure 4.24. The effect of treatment with compound 4.2 on the global DNA (A), RNA (B), and protein (C) synthesis in the H460 cell line.	135
Figure 4.25. Effect of compound 4.2 on the cell cycle distribution.....	136
Figure 4.26. Induction of H460 cell death by compound 4.2.	138
Figure 4.27. Effect of compound 4.2 on the levels of apoptosis-related proteins.	140
Figure 4.28. Effect of compound 4.2 treatment on induction of autophagy in the H460 cell. ...	141
Figure 4.29. Effect of autophagy inhibition on 4.2-induced cell death.	142
Figure 4.30. Effect of compound 4.2 on the levels of autophagy-related proteins.....	144
Figure 5.1. Mechanism of the base-catalyzed aldol condensation reaction.	171
Figure 5.2. ¹ H NMR spectrum of compound 5.1 recorded in CDCl ₃	174

Figure 5.3. ^1H NMR spectrum of compound 5.2 recorded in CDCl_3 .	175
Figure 5.4. ^1H NMR spectrum of compound 5.4 recorded in CDCl_3 .	176
Figure 5.5. ^1H NMR spectrum of compound 5.5 recorded in CDCl_3 .	177
Figure 5.6. ^{13}C NMR spectrum of compound 5.1 recorded in CDCl_3 .	178
Figure 5.7. ^{13}C NMR spectrum of compound 5.4 recorded in CDCl_3 .	178
Figure 5.8. DEPT-135 NMR spectrum of compound 5.4 recorded in CDCl_3 .	179
Figure 5.9. ^1H NMR spectrum of compound 5.6 recorded in CDCl_3 .	181
Figure 5.10. ^{13}C NMR spectrum of compound 5.6 recorded in CDCl_3 .	181
Figure 5.11. ^1H NMR spectrum of compound 5.7 recorded in CDCl_3 .	182
Figure 5.12. ^{13}C NMR spectrum of compound 5.7 recorded in CDCl_3 .	183
Figure 5.13. ^1H NMR spectrum of compound 5.12 recorded in CDCl_3 .	185
Figure 5.14. ^{13}C NMR spectrum of compound 5.12 recorded in CDCl_3 .	185
Figure 5.15. NOESY NMR spectrum of compound 5.12 recorded in CDCl_3 .	186
Figure 5.16. Detailed NOESY NMR spectrum of compound 5.12.	187
Figure 5.17. Phenotypic changes in the H460 spheroid model treated with UA (top panel), and compound 5.12 (bottom panel) for 96 h.	190
Figure 5.18. The effect of treatment with compound 5.12 on the global DNA, RNA, and protein synthesis in the H460 cell line.	191
Figure 5.19. Effect of compound 5.12 on the cell cycle distribution.	193
Figure 5.20. Induction of H460 cell death by compound 5.12.	195
Figure 5.21. Effect of compound 5.12 treatment on induction of autophagy in the H460 cell line.	196
Figure 5.22. Effect of compound 5.12 on the RTKs and PI3K/Akt/mTOR pathway.	198
Figure 5.23. Simplified scheme of the cell cycle, its regulation, and the effect of compound 5.12 on the cell cycle.	201

List of tables

Table 1.1. Example of natural products and their derivatives, with anticancer activity used in clinical practice	16
Table 1.2. Examples of sources of ursolic acid in nature.....	21
Table 1.3. Examples of the anticancer activity, and mechanism of action/targets of UA in different cancer cell lines.....	23
Table 1.4. The inhibitory activities (IC ₅₀) of UA and derivatives (1.1–1.7) for the inhibition of the production of NO in mouse macrophages.....	27
Table 1.5. Inhibition of the proliferation of cancer cell lines by the UA derivatives 1.8–1.11. ¹³⁷ ..	28
Table 1.6. Inhibition of the proliferation of cancer cell lines by UA and derivatives 1.12–1.22. ^{138,139}	29
Table 1.7. Inhibition of the proliferation of cancer cell lines by UA and derivatives 1.23–1.29. ¹⁴⁰	30
Table 1.8. Inhibition of the proliferation of cancer and non-tumor (HELFL) cell lines by UA derivatives 1.30–1.47. ¹⁴¹⁻¹⁴³	32
Table 1.9. Inhibition of the proliferation of cancer and non-tumor (HELFL) cell lines by the UA derivatives 1.48–1.76. ¹⁴³⁻¹⁴⁶	35
Table 1.10. Inhibition of the proliferation of cancer and non-tumor (FR-2) cell lines by the UA derivatives 1.77–1.83. ¹⁴⁸⁻¹⁵⁰	37
Table 1.11. Inhibition of the proliferation of cancer cell lines by UA, 5-FU and derivatives 1.84–1.87. ¹⁵¹	37
Table 1.12. Inhibition of the proliferation of cancer and non-tumor (FR-2) cell lines by UA, 5-FU, and derivatives 1.88–1.98. ^{152,153}	38
Table 1.13. Inhibition of the proliferation of cancer cell lines by UA and derivatives 1.99–1.104. ^{141,154}	40
Table 3.1. The inhibitory activities (IC ₅₀) of UA (3.1) and derivatives 3.2–3.17 in the NSCLC cell lines.....	62

Table 3.2. The inhibitory activities (IC_{50}) of UA, derivative 3.2, and the most potent derivatives (3.15–3.17) in spheroid model of the H460 and H322 NSCLC cell lines.....	66
Table 4.1. The inhibitory activities (IC_{50}) of UA and derivatives 4.1–4.20 in the NSCLC cell lines.	131
Table 4.2. The inhibitory activities (IC_{50}) of UA, and the most potent derivatives (4.2 and 4.16) in the spheroid model of the NSCLC cell lines H460 and H322.	133
Table 5.1. The inhibitory activities (IC_{50}) of UA and derivatives 5.1–5.14 in the NSCLC cell lines.	188
Table 5.2. The inhibitory activities (IC_{50}) of UA, and the most potent derivative 5.12 in the spheroid model of the NSCLC cell line H460.	189

List of schemes

Scheme 3.1. Mechanism of action of T3P for the amide-bond formation.	48
Scheme 3.2. Synthesis of the fluorolactone derivative 3.2.	50
Scheme 3.3. Synthesis of derivatives 3.3–3.5.	51
Scheme 3.4. Synthesis of the derivative 3.6.	52
Scheme 3.5. Synthesis of the amide derivative 3.7.	54
Scheme 3.6. Synthesis of the nitrile derivative 3.8.	56
Scheme 3.7. Synthesis of the amide derivatives 3.9–3.17.	59
Scheme 4.1. Synthesis of derivatives 4.1 and 4.2.	109
Scheme 4.2. Synthesis of derivatives 4.3 and 4.4.	110
Scheme 4.3. Synthesis of derivatives 4.5–4.15.	118
Scheme 4.4. Synthesis of derivatives 4.16–4.18.	124
Scheme 4.5. Synthesis of derivatives 4.19 and 4.20.	127
Scheme 5.1. Synthesis of derivatives 5.1–5.5.	173
Scheme 5.2. Synthesis of derivatives 5.6–5.9.	180
Scheme 5.3. Synthesis of derivatives 5.10–5.14.	184

Thesis organization

This thesis is divided in seven chapters:

The first chapter focuses on the theoretical background, which supports the work developed, being sub-divided into the different areas that comprise this thesis. The first section includes introductory remarks about cancer and lung cancer. The second section is related to the importance of natural products in medicinal chemistry. The last subsection focuses on the therapeutic potential of the pentacyclic triterpenoids (PTs), and reviews the antitumor properties of ursolic acid (a PTs) and its main reported derivatives.

The second chapter describes the scope and the aims of this thesis.

The following chapters up until the fifth are dedicated to the synthesis and biological evaluation of the new ursolic acid derivatives, which include the experimental procedures used in their synthesis, the structural elucidation, and the biological studies.

Chapter six states the major findings and the concluding remarks of this work.

The last chapter provides the supporting references cited throughout this thesis.

In chapters one, and three to five, the ursane-type derivatives were numbered sequentially, with the first number identifying the chapter where they were mentioned for the first time.

The chemical structures of the newly synthesized compounds were numbered based on the ursolic acid scaffold.

The reader is advised to consider the following representation of the chemical structure of ursolic acid (Fig. 1), with the carbons numbered, for better understanding of the structural elucidation discussed in chapters three to five:

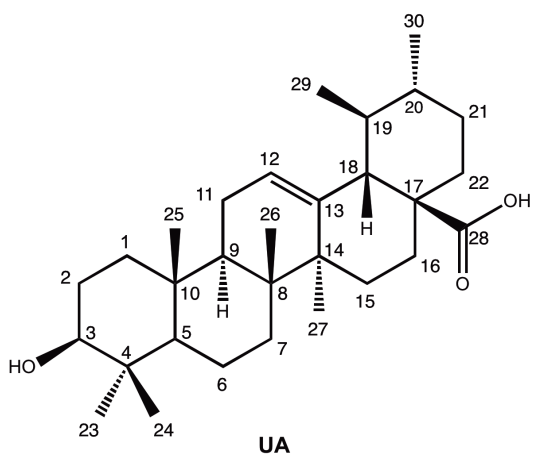
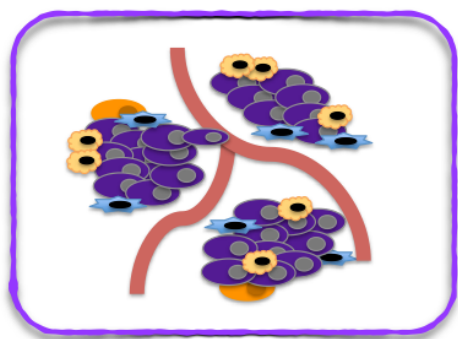


Figure I. Chemical structure of ursolic acid (**UA**).

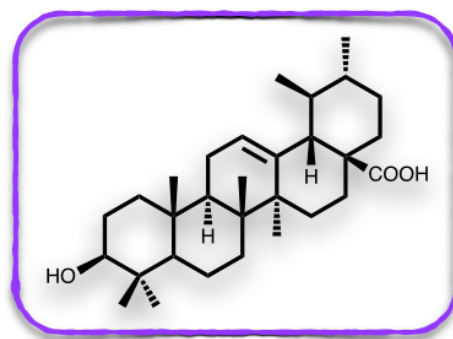
The nomenclature of the new derivatives followed the guidelines established by the IUPAC Commission on the nomenclature of organic chemistry. Moreover, some compounds mentioned during this work have been designated using their trivial name.

Chapter 1

Introduction



Cancer



Pentacyclic triterpenoids

Jorge A. R. Salvador; Ana S. Leal; Daniela P. S. Alho; Bruno M. F. Gonçalves; Ana S. Valdeira; **Vanessa I. S. Mendes**, and Youngkui Jing, *Highlights of pentacyclic triterpenoids in the cancer settings*, in *Studies in Natural Products Chemistry*, In: Atta-ur-Rahman Editor, Elsevier 41, 33–73 (2014).

1. Introduction

1.1. Cancer

Cancer is a term used to describe a complex group of diseases, characterized by deregulated growth and spread of abnormal cells, that potentially can invade and/or spread to other tissues and form new colonies, called metastases. The abnormal cells result from a series of missteps in the genome that lead to anomalies in the control of cell proliferation.^{1,2} According to GLOBOCAN 2012 (excluding non-melanoma skin cancer), an estimate of 14.1 million new cancer cases and 8.2 million cancer-related deaths occurred worldwide in 2012. The most commonly diagnosed cancers worldwide were lung, breast and colorectal cancers; and the most common causes of death by cancer were lung, liver and stomach cancers (Fig. 1.1). The incidence of cancer in women and men vary according to the type of cancer. Breast and prostate cancers have a pronounced incidence in female and male genders, respectively (Fig. 1.1).^{3,4}

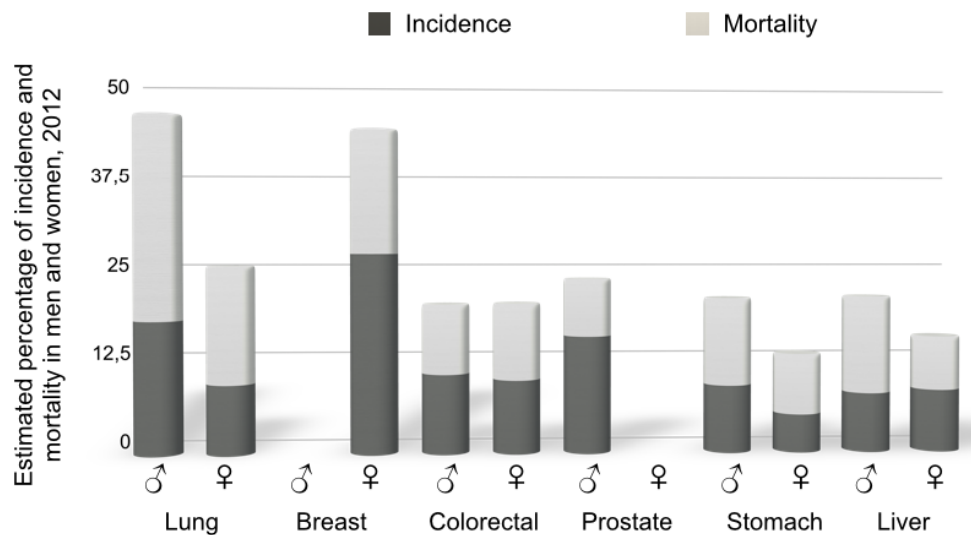


Figure 1.1. Estimated percentage of new cancer cases (incidence) and death (mortality) for men and women, in 2012, according to GLOBOCAN 2012 data.

1.1.1. Biology of cancer

Tumors are complex tissues composed of several distinct cell types, tumorigenic and non-tumorigenic, with a distinctive microenvironment, where they participate in heterotypic interactions with one another.⁵⁻⁷ Normal cells evolve to the neoplastic state progressively, in a multistep process, acquiring particular hallmark capabilities, that enable them to become tumorigenic and, finally, malignant (Fig. 1.2).^{5,6} Cancer cells acquire the ability to auto-sustain proliferation for an undetermined period of time, in the absence of an exogenous growth stimulus, and by evading growth suppressors. In order to reach the replicative immortality, cancer cells display deregulated signaling pathways that allow them to resist the cell death programs, namely apoptosis, autophagy and necrosis. In addition, cancer cells have also been shown to evade destruction by the immune system. Moreover, during tumor development, cancer cells are able to induce and sustain angiogenesis to form a neovasculature; this provides additional nutrients and oxygen, as well as a system to evacuate the metabolic waste, allowing them to compensate the inefficient supply from the normal vascularization. Furthermore, cancer cells also show reprogramming of the energy metabolism to fuel the cell growth, division and proliferation. One of the last stages in the tumor progression is the invasion of the surrounding tissues and metastasizing to new locations, in order to form new colonies.^{5,6}

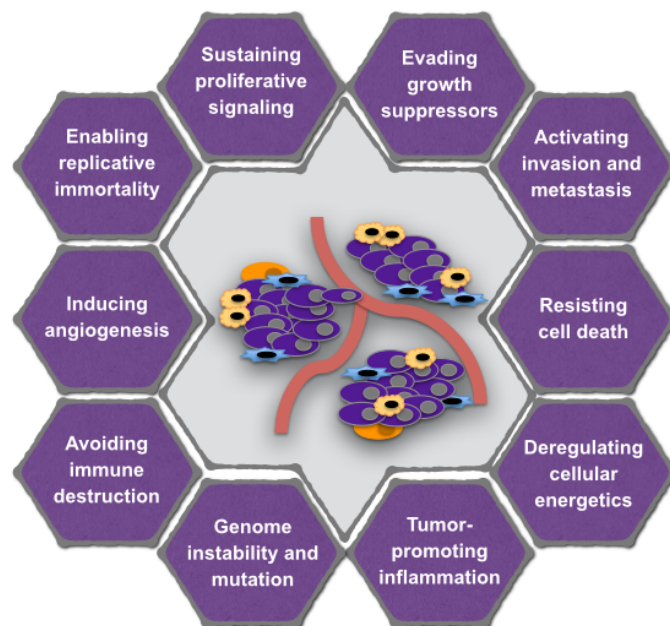


Figure 1.2. Acquired capabilities, enabling characteristics, and emerging hallmarks of cancer. Adapted from literature^{5,6}.

1.1.1.1. Targeting apoptosis in cancer therapy

The programmed cell death is a fundamental cellular response that plays a crucial role in the development and homeostasis in normal tissues by eliminating unnecessary and unwanted cells.⁸ Three main forms of programmed cell death have been described: apoptosis (type I), autophagy (type II) and necrosis (type III), which are characterized by specific morphological features.⁹

Apoptosis (“self-killing”) is characterized by specific morphological and biochemical changes of the dying cell, including cell shrinkage, chromatin condensation and nuclear fragmentation, cytoplasmic membrane blebbing, and formation of apoptotic bodies. During apoptosis, essentially no inflammatory reaction is induced, because there is no release of the cellular constituents into the surrounding interstitial tissue, and the apoptotic bodies are cleared by phagocytosis, avoiding damage to the neighboring cells.⁹⁻¹⁵

Chapter 1 | Introduction

Apoptosis can be initiated by two main pathways: the extrinsic pathway or death receptor pathway, which culminates in the activation of caspase-8; and the intrinsic pathway or mitochondrial pathway, which leads to caspase-9 activation (Fig. 1.3). These two pathways are connected, and the molecules in one pathway can influence the other. There is an additional pathway that is associated to the T-cell mediated cytotoxicity involving perforin-granzyme-mediated cell death. All three pathways converge in the execution phase, which is initiated by the cleavage and activation of the executioner caspases (caspase-3, -6 and -7).^{8,10,11,13,15-18}

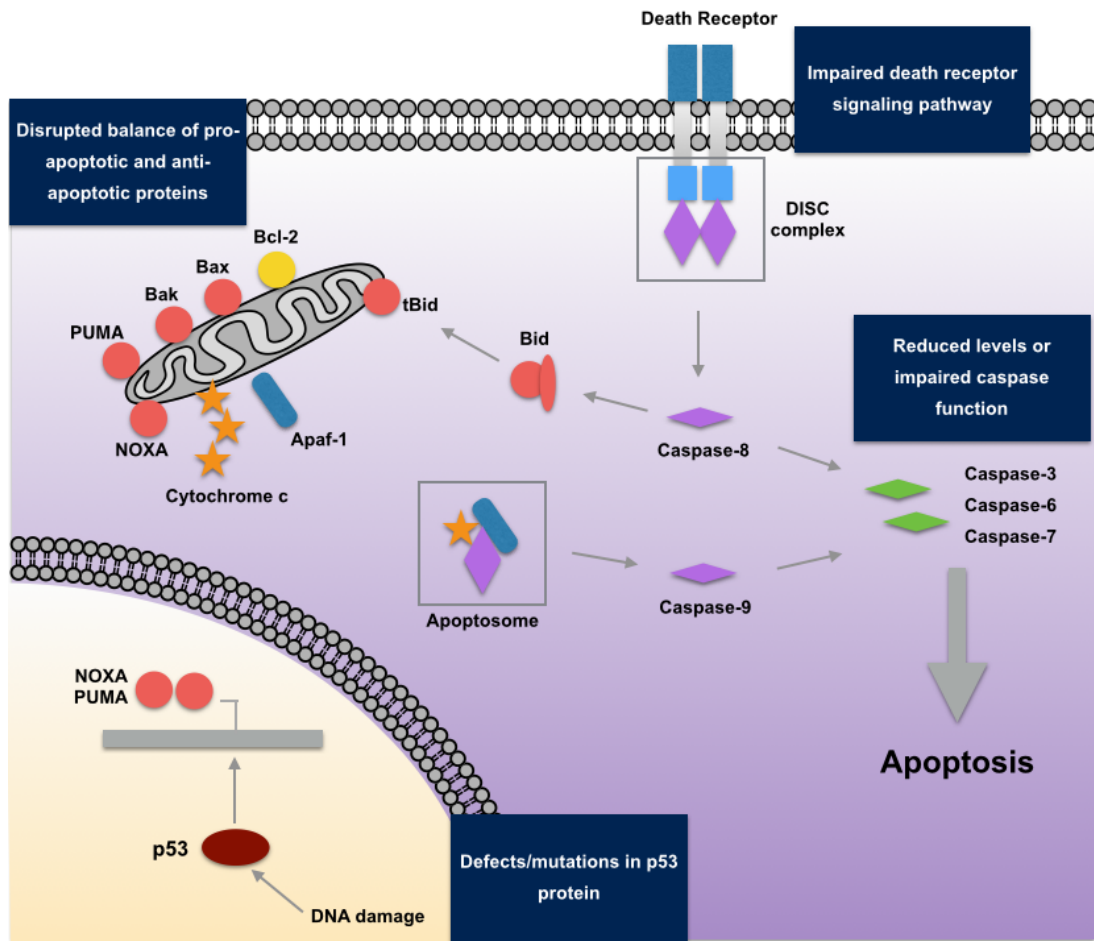


Figure 1.3. Simplified scheme of the extrinsic and intrinsic apoptosis pathways, as well as mechanisms contributing to apoptosis evasion (highlight by the dark blue box).

Chapter 1 | Introduction

The extrinsic pathway is activated following the binding of specific ligands to their cognate cell-surface death receptor (DR). Upon binding, the receptors oligomerize and recruit adapter proteins, such as Fas-associated death domain (FADD) and tumor necrosis factor receptor (TNFR)-associated death domain proteins. The adapter proteins recruit and aggregate several molecules of procaspase-8 via the death effector domains (DEDs), forming the death-inducing signaling complex (DISC), which in turn promotes the autoprocessing and activation of caspase-8. The active caspase-8 then proteolytically cleaves and activates the executioner caspases (Fig. 1.3).^{10,11,13,15,17-19}

The intrinsic pathway is mediated by the mitochondria. In response to apoptotic stimuli, pro-apoptotic members of Bcl-2 family alter the permeability of mitochondrial membrane, resulting in opening of the mitochondrial permeability transition pore, loss of the mitochondrial transmembrane potential, and release of pro-apoptotic molecules, such as cytochrome c and Smac/DIABLO. Once released into the cytosol, cytochrome c binds to the apoptotic protease-activating factor 1 (Apaf-1) in an ATP-dependent manner, to form a complex that recruits procaspase-9. This complex, known as apoptosome, then promotes the activation of caspase-9, which in turn activates the downstream executioner caspases (Fig. 1.3).^{10,11,13,15,17-19}

The Bcl-2 family is comprised of pro-apoptotic (e.g., Bax, Bak and Bad) and anti-apoptotic proteins (e.g., Bcl-2, Bcl-xL and Bcl-w). These proteins bind to each other, forming a complex network of homo- and heterodimers. The relative ratios of anti- and pro-apoptotic Bcl-2 family members dictate the ultimate sensitivity or resistance of cells to the apoptotic stimulus. All BH3-only molecules (e.g., PUMA, NOXA and Bim) require multi-domain BH3 proteins (Bax and Bak) to apply their intrinsic pro-apoptotic activities.^{10-12,17,18}

The extrinsic and intrinsic pathways can crosstalk through caspase-8-mediated proteolysis of Bid, a Bcl-2 family protein with BH3-only domain. Once activated, the resulting truncated Bid (tBid) is translocated to the mitochondria to induce the release of cytochrome c, thus activating the intrinsic pathway.^{10,11,17,19} The extrinsic and intrinsic pathways converge in the

Chapter 1 | Introduction

execution phase, leading to the activation of the effector caspases (-3, -6 and -7), which are responsible for the cleavage of several substrates, including poly (ADP-ribose) polymerase (PARP), DNA, proteins and enzymes, eventually causing the morphological and biochemical changes observed in the apoptotic cells.^{10,11,17,18}

As mentioned previously, evasion of cell death is one of the essential hallmarks in the malignant transformation of a cell, as it confers enhanced survival ability to the neoplastic cells, allowing their characteristic uncontrolled proliferation.^{5,6} Furthermore, deregulation of apoptosis has been implicated in drug resistance. There are several mechanisms by which evasion of apoptosis may occur (Fig. 1.3), namely disruption of the balance of pro- and anti-apoptotic proteins, such as a deregulated ratio of the Bcl-2 family members. This can be due to an overexpression of the anti-apoptotic members, underexpression of the pro-apoptotic members, or a combination of both.^{6,14-16,20,21} Defects in the tumor suppressor protein p53 have been linked to more than 50% of human cancers. This protein, known as “guardian of the genome”, is a regulator of the gene transcription, controlling genes that are important for cell cycle, DNA repair, and apoptosis. It has been demonstrated that cancer cells harboring a mutated p53 protein have decreased apoptosis, contributing to their proliferation.^{14-16,21,22} A deregulated expression of the family of inhibitor of apoptosis proteins (IAPs), which are endogenous inhibitors of caspases, has also been reported in many cancers. For example, survivin has been found overexpressed in several cancers, such as NSCLC. Another mechanism of evasion of apoptosis involves reduced levels or impaired caspase function, as well as impaired death receptor signaling.^{15,16,20}

As evasion of apoptosis is one of the prominent hallmarks of cancer, there is a therapeutic interest in developing drugs that promote cell death, in order to tip the balance of the cellular fate of cancer cells toward apoptosis. In fact, in clinical practice there are several cancer therapeutic drugs that promote cancer cell apoptosis.^{15-17,20,21,23,24}

1.1.1.2. Targeting autophagy in cancer therapy

Macroautophagy (hereafter referred as autophagy) is a catabolic process involved in the degradation of the cellular organelles and proteins through the lysosomal machinery. The morphological characteristics of autophagy include vacuolization, degradation of cytoplasmic contents, and slight chromatin condensation. Briefly, the autophagy pathway begins with the sequestration of the cytoplasmic constituents into double-membrane vesicles, known as autophagosomes. Then they are fused with lysosomes to form autolysosomes, where the sequestered contents are degraded and recycled (Fig. 1.4).²⁵⁻²⁷ This highly evolutionarily conserved multistep process is executed and regulated by a large group of distinct autophagy-related proteins (Atg) that direct the encapsulation of the cytoplasmic cargo inside of the autophagosome. The Atg proteins can be divided into four groups based on their functional properties: the Atg1/Unc-51-like kinase complex, involved in the autophagy induction; the Atg8/LC3 and Atg12 conjugation systems, involved in the expansion of the autophagosome; the class III phosphatidylinositol 3-kinase complex, which includes Beclin-1/Atg6; and the transmembrane protein Atg9 and its associated proteins, involved in the recycling of lipids and proteins.²⁵⁻²⁸ The mammalian target of rapamycin (mTOR), a conserved serine/threonine kinase, is a known regulator of autophagy that acts as a sensor of the metabolic state of a cell, and as a regulator of the bioenergetic pathways, and cell growth. In the presence of nutrients, autophagy is maintained at basal levels through mTOR-mediated phosphorylation and inhibition of the Atg1 initiation complex. However, under starvation conditions, mTOR is inactivated leading to Atg1 activation and autophagy induction.²⁵⁻²⁷

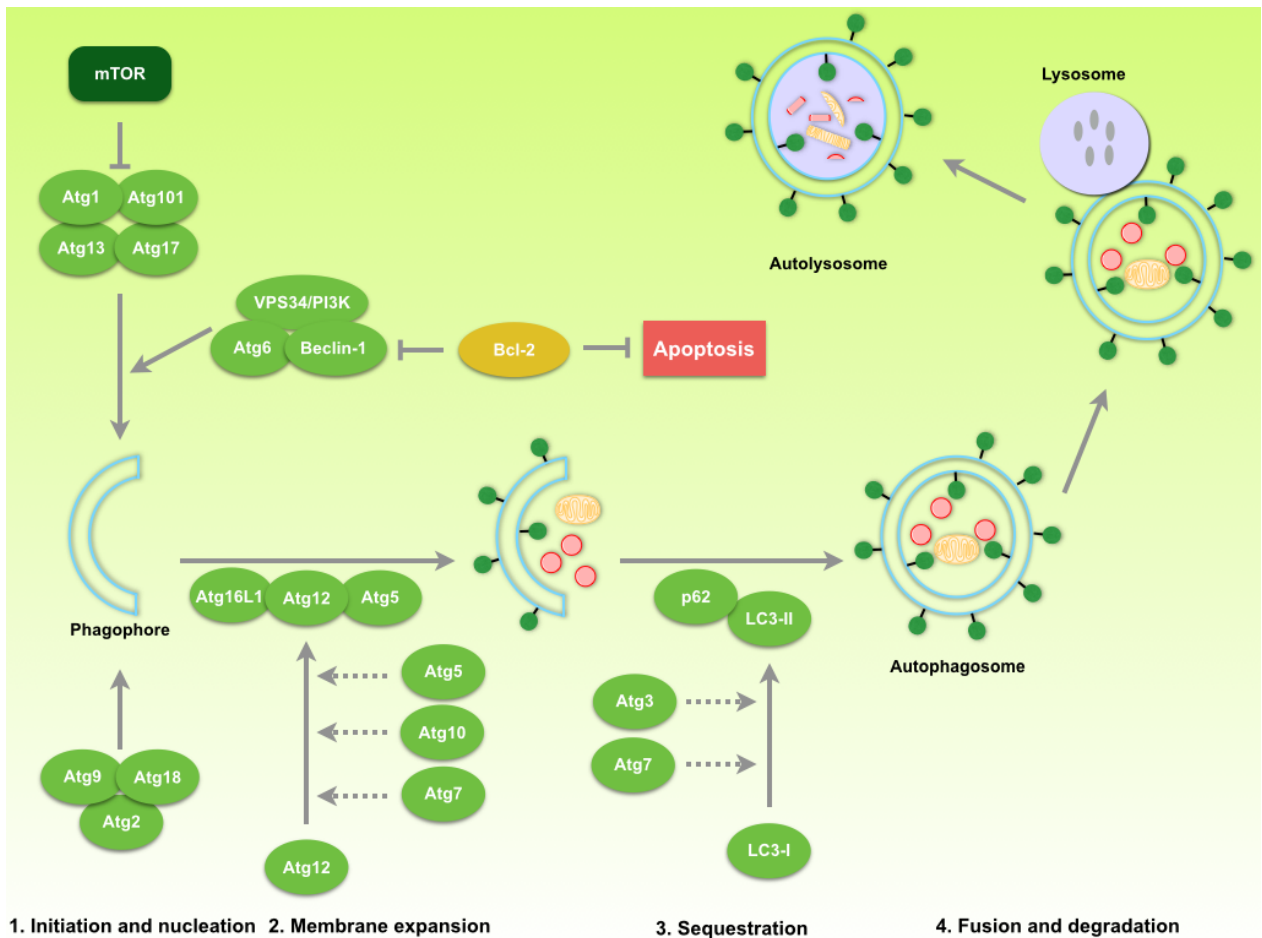


Figure 1.4. Simplified scheme of the macroautophagy pathway.

Under specific conditions, such as starvation and hypoxia, autophagy can be strongly induced to act as a pro-survival mechanism, as it enables the cell to break down cellular organelles, allowing the resulting catabolites to be recycled and used for biosynthesis and energy metabolism. However, under other conditions, activated autophagy can also act as an executioner of cell death, known as autophagic cell death, or type II programmed cell death. While the mechanism of autophagic cell death is still unclear, there is evidence that autophagy may promote cell death by the selective degradation of a survival protein, or that maintaining high levels of autophagy results in the demise of the cell due to energy limitations.^{28,29}

A crosstalk between autophagy and other cell death pathways has been described. The interplay between autophagy and apoptosis can be identified from the extensive molecular

Chapter 1 | Introduction

crosstalk between autophagy and apoptosis-related proteins. One of such interactions occurs within the Beclin-1/Bcl-2 complex (Fig. 1.4). Beclin-1, that has a critical role in the autophagosome formation, is inhibited by Bcl-2, which is an anti-apoptotic member of the Bcl-2 family.^{25,30,31}

Autophagy can act as a “double-edge sword” in cancer treatment. While autophagy can be induced in cancer cells as an adaptation mechanism leading to resistance to chemo- and radiotherapies, other cancer cells displayed reduced autophagic capacity when compared to normal cells. For example, mono-allelic deletion of Beclin-1 gene has been found in 50 and 75% of sporadic human breast and ovarian cancers, respectively, and Beclin-1 transfection was able to induce autophagy and inhibit tumor growth.³¹

Taking into account this dichotomy in the autophagy, the design of cancer treatments that modulate autophagy becomes quite complex. However, recent data suggest that therapeutic interventions enhancing or decreasing autophagy, depending on the context, can be beneficial for the cancer treatment.^{26,28,30}

1.1.2. Lung cancer

Lung cancer is a heterogeneous disease that has historically been divided into two main types, non-small cell lung cancer (NSCLC) and small-cell lung cancer (SCLC), with different disease patterns and treatment strategies for each type. The most common type is NSCLC (85%), which includes such subclasses as adenocarcinoma, squamous cell carcinoma, and large cell carcinoma.³² Despite advances in diagnostics and therapeutics, the outcome for patients with lung cancer remains poor. A substantial proportion of patients with lung cancer show tumor spread at the time of diagnosis, and 40% of patients with NSCLC have distant metastases.^{33,34} The high mortality rate for patients with lung cancer has been attributed to the

Chapter 1 | Introduction

difficulty in obtaining an early diagnosis, a high potential for metastasis, the heterogeneous histology and biology, and the relative insensitivity to chemotherapy.^{33,35}

Lung cancer is one of the most heavily mutated and genomically altered cancers.³⁶ The most widely recognized genomic alterations include epidermal growth factor receptor (*EGFR*) mutations, and echinoderm microtubule-associated protein-like 4-anaplastic lymphoma kinase (*EML4-ALK*) rearrangements.^{33,37} Other genetic mutations found in the NSCLC include alterations in V-Ki-ras2 Kirsten rat sarcoma viral oncogene homolog (*KRAS*), phosphatidylinositol-4,5-bisphosphate 3-kinase catalytic subunit alpha (*PIK3CA*), proto-oncogene B-Raf (*BRAF*), proto-oncogene receptor tyrosine kinase MET (*MET*), liver kinase B1 (*LKB1*), and proto-oncogene tyrosine-protein kinase ROS (*ROS1*) genes.^{33,38,39} *LKB1* (also known as serine/threonine kinase 11) is the second most commonly mutated tumor suppressor in sporadic lung cancer, after *TP53*.⁴⁰ *LKB1* is mutated in at least 15–30% of NSCLCs, although the frequency may be higher due to the difficulty in detecting inactivating lesions.^{41,42} Interestingly, roughly half of the NSCLCs with *LKB1* mutations also bear activating *KRAS* mutations, and current estimates suggest that 7–10% of all NSCLCs are commutated for *KRAS* and *LKB1*.⁴¹ NSCLC patients harboring *LKB1/KRAS* mutations tend to have a poorer prognosis compared to patients with *KRAS*-mutated NSCLC without concomitant *LKB1* mutation, suggestion that loss of *LKB1* induces a more aggressive cancer phenotype.^{43,44}

Surgery is the standard treatment for early stage lung cancer, in medically operable patients, and chemo- and radiotherapy are the prevailing treatment for patients with advanced NSCLC.³³ Platinum-based chemotherapy remains the standard systemic therapy for the majority of patients with advanced NSCLC (Fig. 1.5), which is based on the combination of a platinum drug (carboplatin or cisplatin) and a third-generation cytotoxic agent, such as gemcitabine, paclitaxel or vinorelbine.^{33,37,45,46} Nowadays, chemotherapy can be tailored based on the histopathology of the primary tumor, and on the response to induction chemotherapy. There are evidence-based data showing that patients with non-squamous NSCLC benefit from

Chapter 1 | Introduction

pemetrexed-containing regimens, due to the high content of thymidylate synthase in the primary tumor. Data from several clinical trials have shown that patients with tumors harboring activating mutations of *EGFR* and *ALK* rearrangements benefit from treatment with EGFR and ALK tyrosine kinase inhibitors, such as gefitinib and crizotinib, respectively (Fig. 1.5).^{33,37}

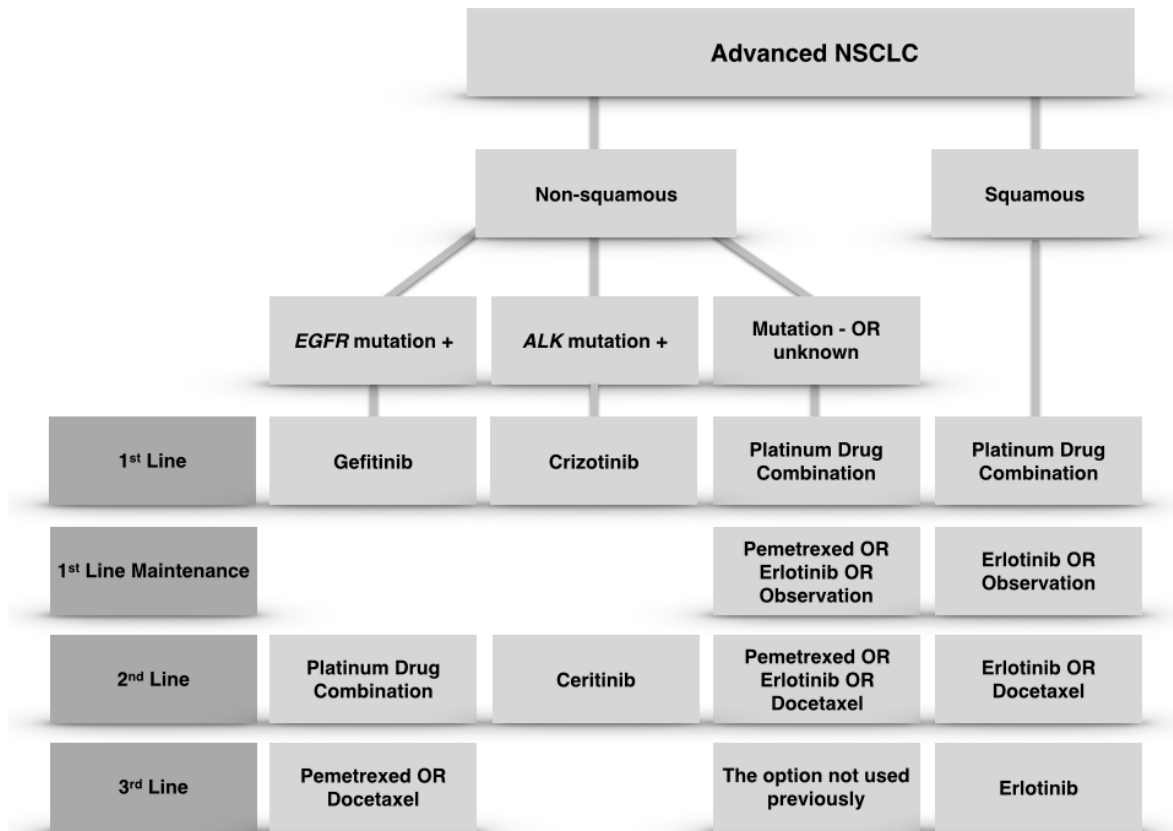


Figure 1.5. Schematic algorithm for first-, second-, and third-line therapy in advanced non-small cell lung cancer (NSCLC). Adapted from literature.^{47,48}

Despite the high response and progression-free survival rates to EGFR and ALK tyrosine kinase inhibitors, the majority of patients develop resistance within approximately 1 year.³⁷ There are two main mechanisms for acquired resistance to tyrosine kinase inhibitors: the target gene undergoes a second mutation or amplification, resulting in inefficient binding of the target; and the activation of a parallel signaling pathway, as seen in *MET* amplification as a secondary event

in *EGFR*-mutated cancers.³³ Moreover, several escape mechanisms have been reported for the lung cancer cells to counteract the current therapeutic interventions, such mechanism include enhanced antiapoptotic gene expression (Bcl-2, survivin), loss of the apoptosis effector molecules (caspases), enhanced expression of multidrug resistance proteins, and enhanced expression of immuneresistance genes.⁴⁹

Despite the novel therapeutic strategies, the overall 5-year survival rate in many countries remains less than 15%.³² These statistics highlight the need for the development of new clinical agents for the treatment of lung cancer.

1.2. Natural products in cancer

The role of natural products as a source of medicines has been recognized since ancient times.⁵⁰ Despite major scientific and technological progress in combinatorial chemistry, drugs derived from natural products still continue to play an important role in the development of the current therapeutic armamentarium. Considering all approved drugs worldwide, between 1981 and 2014, 50% were natural products, based or inspired thereon (Fig. 1.6). In the area of cancer, between 1981 and 2014, 78% were small molecules. If the higher molecular weight materials are removed (biological and vaccines), reducing the overall number to 136 (100%), 83% were either natural products per se or based thereon, or mimicked the natural products in one form or another (Fig. 1.7).⁵¹

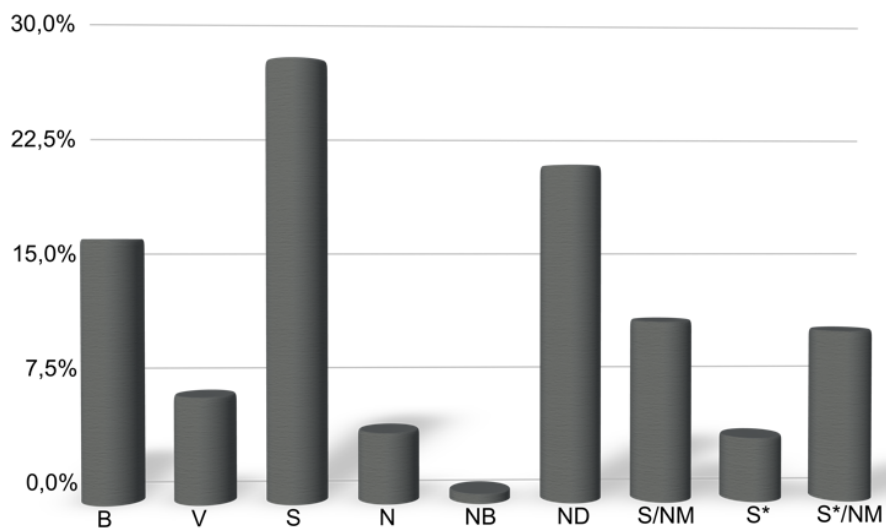


Figure 1.6. Total new approved agents between 1981 and 2014. B, biological; V, vaccine; S, totally synthetic drug, with no natural product conception; N, unmodified natural product; NB, natural product “botanical”; ND, modified natural product, usually a semisynthetic modification; S/NM, synthetic compound showing natural product mimicking properties; S*, synthetic compound with a natural product pharmacophore; S*/NM, total synthesis with a natural product pharmacophore, showing natural product mimicking properties. Adapted from literature.⁵¹

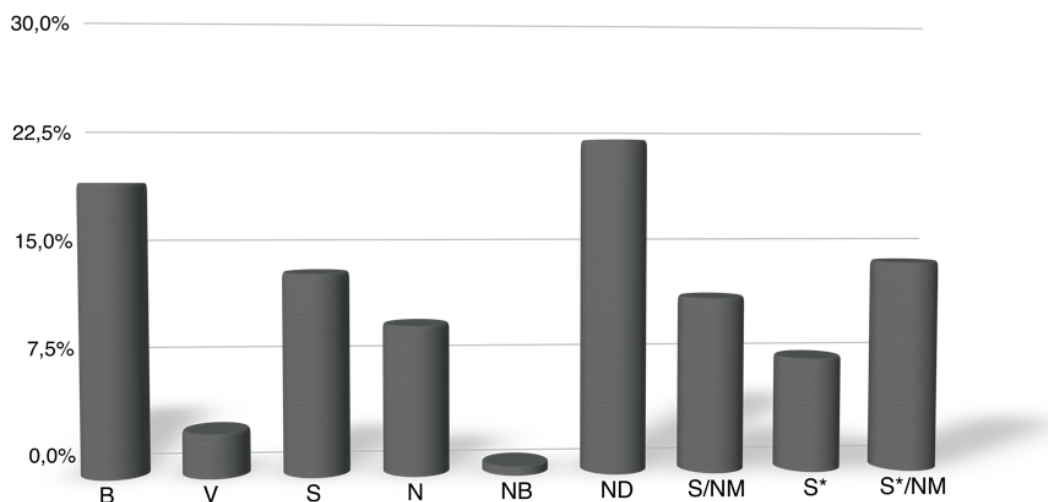


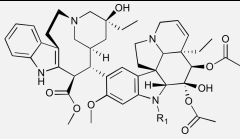
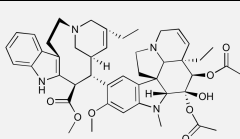
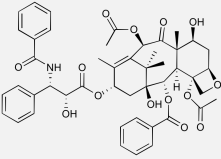
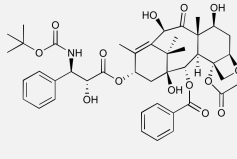
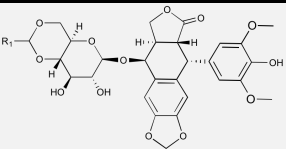
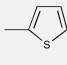
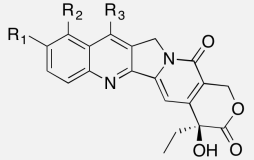
Figure 1.7. Total new approved anticancer agents between 1981 and 2014. B, biological; V, vaccine; S, totally synthetic drug, with no natural product conception; N, unmodified natural product; NB, natural product “botanical”; ND, modified natural product, usually a semisynthetic modification; S/NM, synthetic compound showing natural product mimicking properties; S*, synthetic compound with a natural product pharmacophore; S*/NM, total synthesis with a natural product pharmacophore, showing natural product mimicking properties. Adapted from literature.⁵¹

Recently, there has been a renewed interest in “rediscovering natural products”. In 2003, this was emphasized by Berkowitz commenting on natural products, “We would not have the top-selling drug class today, the statins; the whole field of angiotensin antagonists and angiotensin-converting-enzyme inhibitors; the whole area of immunosuppressives, nor most of the anticancer and antibacterial drugs. Imagine all of these drugs not being available to physicians or patients today”.^{52,53} It is evident that nature has played and will continue to play, a vital role in the drug discovery process.

Several natural products and derivatives are still used in cancer treatment. Importantly, all of these natural products have led to significant biological discoveries related to their unique and novel mechanism of action (Table 1.1).⁵⁴⁻⁵⁶

Chapter 1 | Introduction

Table 1.1. Example of natural products and their derivatives, with anticancer activity used in clinical practice. Data from literature.^{50,54,55,57}

Anticancer agents	Chemical Structure	Mechanism of Action	Source
Vinca alkaloids Vinblastine Vincristine Vinorelbine	  Vinblastine: R ₁ =CH ₃ Vinorelbine Vincristine: R ₁ =CHO	Tubulin-interactive agent	<i>Catharanthus roseus</i>
Taxanes Paclitaxel Docetaxel	  Paclitaxel Docetaxel	Tubulin-interactive agent	<i>Taxus brevifolia</i>
Podophyllotoxin derivatives Etoposide Teniposide	 Etoposide: R ₁ =CH ₃ Teniposide: R ₁ = 	Topoisomerase II inhibitor	<i>Podophyllum peltatum</i>
Camptothecin derivatives Topotecan Irinotecan	 Topotecan: R ₁ =OH, R ₂ =CH ₂ N(CH ₃) ₂ , R ₃ =H Irinotecan: R ₁ =OCOPiperidinePiperidine, R ₂ =H, R ₃ =CH ₂ CH ₃	Topoisomerase I inhibitor	<i>Camptotheca acuminata</i>

Natural products have been evolutionarily selected to bind to biological macromolecules, a property that led to the recognition of the natural product scaffold as a “privileged structure”, representing an excellent template for the development of novel biologically active compounds. This natural product-like scaffold has the necessary compromise of flexibility and rigidity to present the functional groups in a favorable spatial arrangement to biomolecular targets. However, natural products did not undergo evolutionary selection to serve as human

Chapter 1 | Introduction

therapeutics, and hence need to be optimized to have the desired potency, selectivity, and pharmacokinetic properties of a clinically useful drug.⁵⁵ Optimization of the basic scaffold to improve these properties can be accomplished by a semisynthetic approach.

As discussed previously, cancer is a complex disease with multiple altered pathways, and thus the inhibition of single targets may not be sufficient to cure this disease. The clinical development of resistance towards specific small molecule inhibitors, such as erlotinib, supports this point of view. The complexity underlying cancer highlights the need for the development of strategies that would target the intricate cancer network, in order to modulate the different hallmarks of cancer, and hence treat cancer as a complex disease. Contrarily to the conventional approach of developing monofunctional targeted drugs, which affect specifically one target, it has been proposed that multifunctional drugs be developed that would target the activity of different regulatory pathways, affecting as much hallmarks of cancer as possible (Fig. 1.8). This approach seems to represent a more realistic strategy to treat cancer as a complex disease. The “promiscuous” character of natural products, previously associated with dirty drugs, has recently attracted interest as templates for the development of such multifunctional anticancer drugs. It seems that during evolution, plants have overcome the resistance of pathogenic microorganisms towards phytochemicals by the development of multitarget compounds. This evolutionary approach of using “promiscuous” compounds as a defense mechanism may also support the development of natural products for cancer treatment.^{58,59}

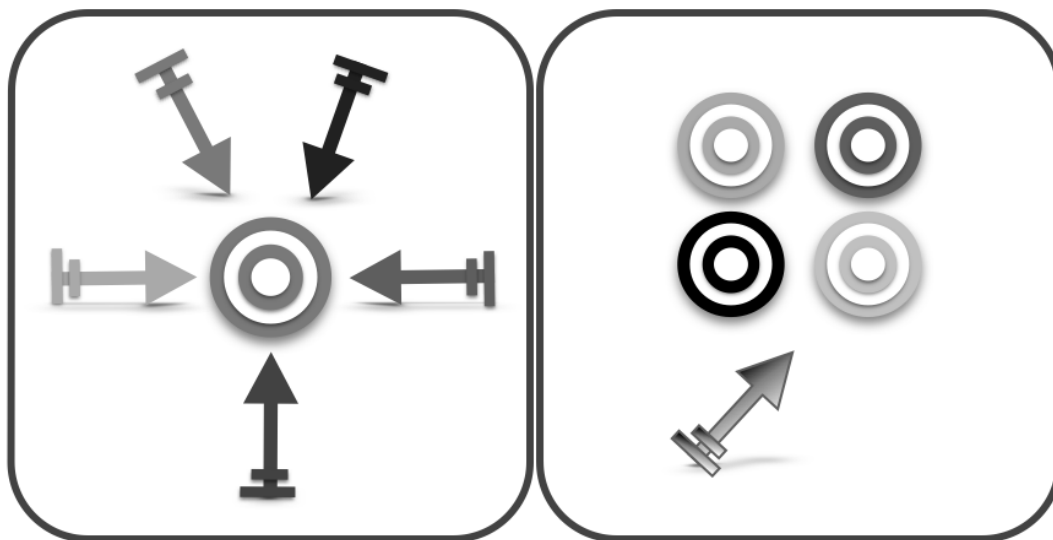


Figure 1.8. Schematic scheme showing monofunctional (left) versus multifunctional (right) drugs.

1.3. Terpenes: general considerations

Terpenes or isoprenoids are the largest and most structurally diverse class of natural products. These compounds are ubiquitous components of our diet, and are considered relatively nontoxic to humans. Terpenes display a wide range of biological activities, and have been used for centuries in the traditional medicine for the treatment of human diseases.⁶⁰⁻⁶³

Terpenes are essentially synthesized by the initial condensation of the C_5 substrates, isopentenyl diphosphate (IPP) and dimethylallyl diphosphate (DMAPP), to form geranyl diphosphate (GPP, C_{10}), farnesyl diphosphate (FPP, C_{15}), or geranylgeranyl diphosphate (GGPP, C_{20}) (Fig. 1.9). They can further undergo condensation, cyclization, and post-transnational modifications. Overall, these compounds are traditionally known as derivatives of the isoprene, a five-carbon acyclic chain (C_5H_8). Based on the number of building blocks, terpenes are commonly classified as monoterpenes (C_{10}), sesquiterpenes (C_{15}), diterpenes (C_{20}), triterpenes (C_{30}), and tetraterpenes (C_{40}) (Fig. 1.9).⁶⁰⁻⁶²

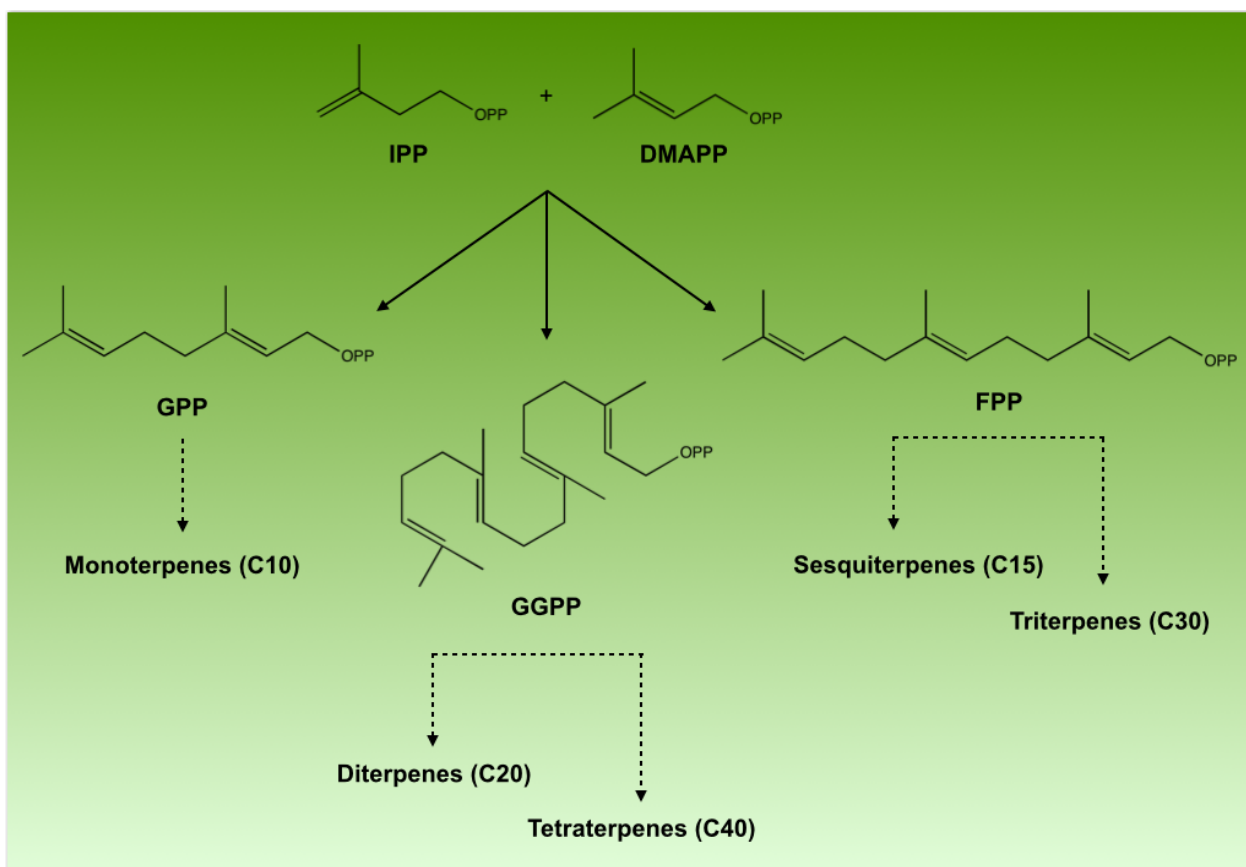


Figure 1.9. Simplified scheme of the isoprenoid biosynthetic pathway. IPP, isopentenyl diphosphate; DMAPP, dimethylallyl diphosphate; GPP, geranyl diphosphate; FPP, farnesyl diphosphate; GGPP, geranylgeranyl diphosphate.

1.3.1. Triterpenes: pentacyclic triterpenoids

Triterpenes are a large and structurally diverse group of terpenes, widely present in several medicinal plants.^{58,64,65} Triterpenes, containing six isoprene units with the basic molecular formula $C_{30}H_{48}$, are derived from squalene or related acyclic 30-carbon precursors.^{64,66} Triterpenoids are oxo-functionalized triterpenes derived from the intramolecular condensation of the 2,3-oxidosqualene to give different classes of triterpenoids, which are subsequently converted into a vast array of triterpenoid ring scaffolds (Fig. 1.10).^{64,67,68} According to the diverse features of their skeletons, triterpenoids can be divided into acyclic, mono-, bi-, tri-, tetra- and pentacyclic triterpenoids.^{66,69} Natural pentacyclic triterpenoids (PTs) have been extensively

Chapter 1 | Introduction

reported to possess a wide range of biological activities, such as antitumor, anti-inflammatory, antiviral, antidiabetic, antibacterial, antiparasitic, analgesic, and cardio-, hepato- and gastro-protective, among others activities.⁶⁹ From a biological point of view, some of the most important and active PTs include betulinic, oleanolic, glycyrrhetic and ursolic (UA) acids.^{67,70,71}

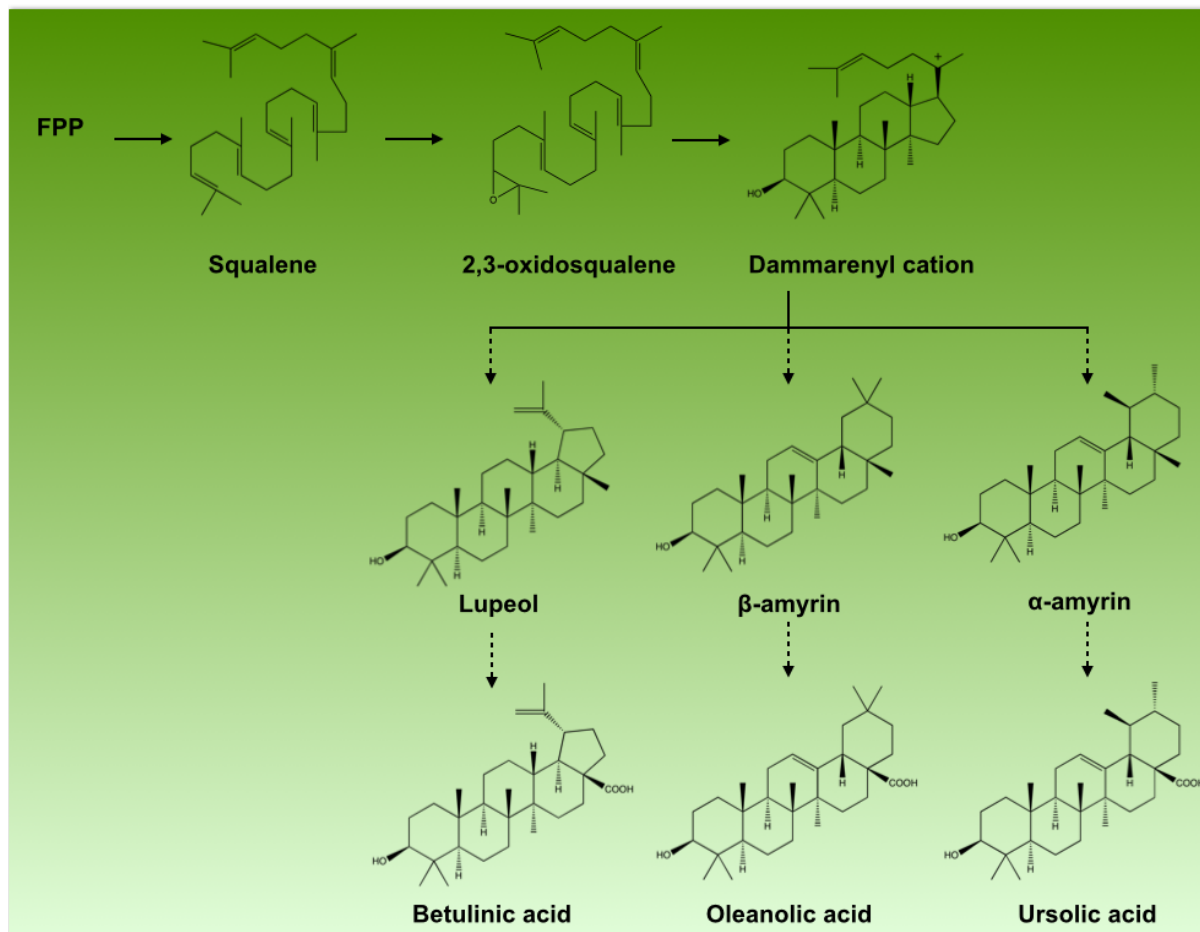


Figure 1.10. Simplified scheme of the biosynthesis of some triterpenoids. FPP, farnesyl diphosphate.

1.3.2. Ursolic acid

Ursolic acid (3 β -hydroxy-urs-12-en-28-oic acid) (**UA**) (Fig. 1.11) is a pentacyclic triterpenoid present in a wide variety of plants (Table 1.2), and an integral part of the human diet. This compound can be found in the form of a free acid, or as an aglycone of triterpenoid saponins.

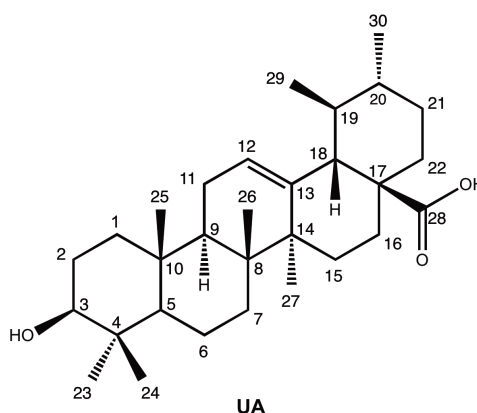


Figure 1.11. Chemical structure of ursolic acid (**UA**).

Table 1.2. Examples of sources of ursolic acid in nature.

Entry	Source	Common name	Ref.
1	<i>Actinidia arguta</i>	Hardy kiwi	72
2	<i>Arctostaphylos uva-ursi</i>	Bearberry	73
3	<i>Calluna vulgaris</i>	Common Heather	74
4	<i>Crataegus pinnatifida</i>	Chinese hawthorn	75
5	<i>Eucalyptus camaldulensis</i>	River red gum	76
6	<i>Lavandula angustifolia</i>	Lavender	77
7	<i>Malus domestica</i>	Golden-red apple	78
8	<i>Melissa officinalis</i>	Lemon balm	79
9	<i>Perilla frutescens</i>	Perilla	80
10	<i>Plantago major</i>	Broadleaf plantain	81
11	<i>Prunus mume</i>	Japanese apricot	82
12	<i>Rosmarinus officinalis</i>	Rosemary	83
13	<i>Salvia officinalis</i>	Common sage	84
14	<i>Sambucus ebulus</i>	Dwarf elder	85
15	<i>Vaccinium macrocarpon</i>	Large cranberry	86

1.3.2.1. General activities of ursolic acid

Medicinal plants containing **UA** have been used in folk medicine long before it was known which its constituents were responsible for their therapeutic effectiveness. The isolation and identification of **UA** revealed a wide range of biological activities, including antitumor, anti-inflammatory, immunomodulatory, antioxidant, antidiabetic, antibacterial, antiviral, antiulcer, hepatoprotective, analgesic, diuretic and anti-atherosclerotic.^{67,70,87-89} The anticancer effects of **UA** will be discussed below, in brief.

1.3.2.2. Anticancer activity of ursolic acid

UA has been implicated in the prevention and protection against tumors. The anticancer activity of **UA** has been reported in a wide variety of cancer cell lines (Table 1.3), as well as *in vivo*.^{67,70,87,89,90} Its antitumor activity has been attributed to its ability to prevent tumorigenesis⁹¹, to inhibit cancer cell proliferation^{92,93}, progression⁹⁴, invasion⁹⁵, and angiogenesis^{96,97}, to induce apoptosis⁹⁸⁻¹⁰⁰ and differentiation^{101,102}, to promote chemosensitization¹⁰³, and to induce cell cycle arrest^{104,105} (Table 1.3). The signaling pathways involved in the **UA** activity may vary in different cancer cells lines, and different signaling pathways may be regulated successively or simultaneously, and synergized to contribute to the **UA** overall anticancer effect.¹⁰⁶

Table 1.3. Examples of the anticancer activity, and mechanism of action/targets of **UA** in different cancer cell lines.

Entry	Cancer type	Cell line	Mechanism of action/targets ^a
1	Brain	U87 Rat C6 glioma	Inhibition of proliferation ^{107,108} ; G1-phase arrest (↓cyclin-E, -D1,-D3 and CDK4; ↑p21 ^{Waf1} , p27 ^{Kip1}); induction of autophagy via ROS-dependent ER stress (↑ROS production; ↑intracellular calcium concentration; ER stress-mediated PERK/eIF2a/CHOP pathway involvement; CaMKK-AMPK-mTOR signaling cascade; ↑Beclin-1; LC3-II). ¹⁰⁷ Inhibition of proliferation; inhibition of invasion through suppression of the association ZIP/p62 with PKC-ξ, and downregulation of MMP-9 expression. ⁹⁵
2	Bladder	T24	Inhibition of proliferation; ER stress-induced apoptosis. ¹⁰⁹
3	Breast	MCF-7 MDA-MB- 231	Inhibition of proliferation; induction of apoptosis by suppression of FOXM1 protein expression. ¹¹⁰ Inhibition of proliferation; inhibition of migration and invasion through inhibition of the JNK, Akt and mTOR pathway, and NF-κB expression, with downregulation of MMP-2 and u-PA expression, and upregulation of TIMP-2 and PAI-1. ¹¹¹
4	Cervix uteri	HeLa SNG-II HEC108	Inhibition of proliferation; induction of apoptosis through the intrinsic pathway (↑cytochrome c, caspase-9 and -3) with modulation of the members of Bcl-2 family (↓Bcl-2 and Bcl-xL; ↑Bax and Bak); downregulation of the phosphorylation of ERK1/2 and p38 proteins. ¹¹² Induction of apoptosis with inhibition of PI3K/Akt and MAPK pathways. ¹¹³
5	Colorectal	HCT116 HT29 Caco-2	Inhibition of proliferation; inhibition of c-FLIP, Bcl-2, survivin, Bcl-xL, cyclin D1, MMP-9, VEGF, and ICAM-1; inhibition of NF-κB activation; inhibition of metastasis; induction of apoptosis and chemosensitization. ¹¹⁴
6	Fibrosarcoma	HT1080	Inhibition of invasion by downregulation of MMP-9. ¹¹⁵
7	Gastric	BGC-823 NUGC-3	Inhibition of proliferation; G1-phase arrest; induction of apoptosis (↑caspase-3 and Bax); inhibition of invasion; upregulation of miR-133a. ⁹³ Inhibition of proliferation; inhibition of DNA polymerase, and DNA topoisomerases I and II. ¹¹⁶
8	Hepatic	HepG2 Hep3B Huh-7 HA22T	Inhibition of proliferation; G1-phase arrest; induction of apoptosis (↑caspase-3, ↓survivin and AEG-1) via AMPK activation and GSK3β phosphorylation. ¹¹⁷ Antiangiogenic properties; downregulation of HIF-1α, VEGF, IL-8, and u-PA; decreased invasion and migration. ¹¹⁸

Chapter 1 | Introduction

Entry	Cancer type	Cell line	Mechanism of action/targets ^a
Table 1.3. continued			
9	Leukemia	U937 Jurkat HL-60	Induction of differentiation by activation of the PI3K/Akt signaling pathway. ¹⁰² Induction of apoptosis via inactivation of Akt, activation of JNK, and downregulation of Mcl-1. ⁹⁸
10	Lymphoma	Daudi	Inhibition of viability; induction of calcium-dependent apoptosis. ¹¹⁹
11	Lung	H1299 H1650 H1975 PC9 A549	Inhibition of proliferation; induction of apoptosis; SAPK/JNK-mediated inhibition of SP1 with inhibition of EZH2 and DNA methyltransferase 1. ¹²⁰ Inhibition of proliferation and metastasis; inhibition of epithelial-mesenchymal transition by suppressing AEG-1 via repression of the NF- κ B signaling pathway. ¹²¹
12	Multiple myeloma	U266	Inhibition of proliferation; chemosensitization; G1-phase arrest; induction of apoptosis; inhibition of STAT3 activation by expression of the tyrosine phosphatase SHP-1. ¹⁰³
13	Ovarian	SKOV3 A2780 HEY	Inhibition of proliferation; chemosensitization; downregulation of HIF-1 α and ABCG2 levels. ¹²² Inhibition of proliferation; induction of apoptosis (\uparrow caspase-9 and -3, \downarrow c-Myc, Bcl-xL and AEG-1) by GSK3 β phosphorylation and β -catenin degradation. ¹²³
14	Pancreatic	AsPC-1 MIA PaCa-2 Panc-28 PANC-1 Capan-1	Inhibition of proliferation; induction of apoptosis; suppression of NF- κ B activation and regulated proteins; chemosensitization. ¹²⁴ Inhibition of proliferation; induction of apoptosis by induction of JNK pathway, and suppression of PI3K/Akt/NF- κ B signaling pathway. ¹²⁵
15	Prostate	LNCaP PC-3 DU145	Inhibition of proliferation; induction of apoptosis (\uparrow caspase-3, \downarrow Bcl-2, Bcl-xL and survivin) by modulation of PI3K/Akt/mTOR pathway. ¹²⁶ Inhibition of CXCR4/CXCL12 signaling axis, by downregulation of mRNA expression, inhibition of NF- κ B activation and modulation of chromatin immunoprecipitation activity; inhibition of CXCL12-induced migration and invasion. ¹²⁷
16	Thyroid	MTC-SK ARO	Inhibition of proliferation; induction of apoptosis. ¹²⁸ Inhibition of proliferation; induction of differentiation; inhibition of the endogenous reverse transcriptase. ¹⁰⁸
17	Skin	A375 B16F-10	Inhibition of proliferation; induction of differentiation; inhibition of the endogenous reverse transcriptase. ¹⁰⁸ Inhibition of proliferation; induction of apoptosis. ¹²⁹

^aABCG2: ATP-binding cassette sub-family G member 2; AEG: astrocyte elevated gene; Akt: protein kinase B; AMPK: adenosine monophosphate (AMP)-activated protein kinase; Bcl-2: B-cell lymphoma gene-2; CaMKK: Calcium/calmodulin-dependent kinase kinase; CDK: cyclin-dependent kinase; CHOP: C/EBP homologous protein; CXCL12: C-X-C motif chemokine 12; CXCR4: C-X-C chemokine receptor type 4; DNA: deoxyribonucleic acid; eIF2 α : eukaryotic translation initiation

Chapter 1 | Introduction

factor 2 α ; ERK: Ras/Raf extracellular signal-regulated kinase; ER: endoplasmic reticulum; EZH2: zeste 2 polycomb repressive complex 2 subunit; FLIP: FLICE-inhibitory protein; FOXM1: forkhead box M1; GSK3 β : glycogen synthase kinase 3 β ; HIF-1 α : hypoxia-inducible factor-1 α ; ICAM: intercellular adhesion molecule; IL: interleukin; JNK: c-Jun N-terminal kinase; LC3: microtubule-associated protein 1A/1B-light chain 3; MAPK: mitogen-activated protein kinase; miR: microRNA; MMP: matrix metalloproteinase; mTOR: mammalian target of rapamycin; NF- κ B: nuclear factor kappa-light-chain-enhancer of activated B cells; PAI-1: plasminogen activator inhibitor-1; PERK: protein kinase RNA-like endoplasmic reticulum kinase; PI3K: phosphoinositide 3-kinase; PKC: protein kinase C; ROS: reactive oxygen species; SAPK: stress-activated protein kinase; SHP-1: src homology region 2 domain-containing phosphatase-1; SP1: transcription factor Sp1 (specificity protein 1); STAT3: signal transducer and activator of transcription 3; TIMP-2: tissue inhibitor of metalloproteinase-2; u-PA: urokinase-type plasminogen activator; VEGF: vascular endothelial growth factor; ZIP: zeta-interacting protein.

UA is able to affect different pathways that are found deregulated in cancer, such as the MAPK/ERK and PI3K/Akt/mTOR signaling cascades that play critical roles in the development of resistance to apoptosis and drugs in cancer cells (Table 1.3).^{112,113,125,126} **UA** has also been shown to modulate the NF- κ B activity, which has been demonstrated to be abnormally expressed in different cancer cells, and to be correlated with uncontrolled proliferation (Table 1.3, entries 3, 5, 11, 14 and 15).^{125,129} Furthermore, inhibition of the FOXM1 expression by **UA** has been reported on the MCF-7 cells (Table 1.3, entry 3).¹¹⁰ FOXM1 has been recognized as an important target, as its upregulation may contribute to genomic instability and malignant transformation.^{87,110} Programmed cell death, namely apoptosis and autophagy, has also shown to be induced upon treatment with **UA** in several cancer cells lines (Table 1.3).^{67,89,107,130} Additionally, the effect of **UA** in the endogenous reverse transcriptase has been implicated in its ability to suppress growth and induce differentiation in cancer cells (Table 1.3, entries 16 and 17).¹⁰⁸ Other effects of **UA** that contribute to its anticancer activity include its antimetastatic, anti-angiogenic, and anti-inflammatory properties, and its ability to promote chemosensitization to other anticancer agents (Table 1.3).^{67,89}

Taking into account the different anticancer effects of **UA**, this compound can be considered as a multifunctional drug that is able to modulate the intricate cancer network,

highlighting the importance of acting on cancer as a complex disease. Therefore, **UA** can be considered as a potential lead for the development of new anticancer drugs, due to its promising multitarget anticancer activity, low toxicity and commercial availability.^{67,89,131}

1.3.2.3. Semisynthetic derivatives with anticancer activity

The **UA** scaffold has been modified in order to improve its anticancer activity. The main chemical modifications performed so far have focused mostly at the C2 position on A-ring, on the alcohol group at C3, at C11 and C12 positions on C-ring, and on the carboxylic acid at position C28 (Fig. 1.12). Some of the semisynthetic derivatives obtained have displayed improved anticancer activity in several cancer cell lines compared with **UA**.^{67,131} Some of the main derivatives prepared will be discussed hereinafter.

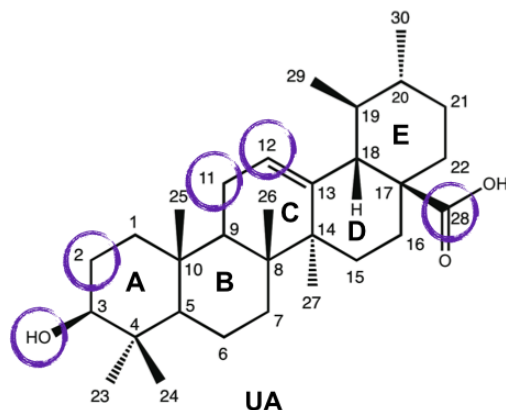


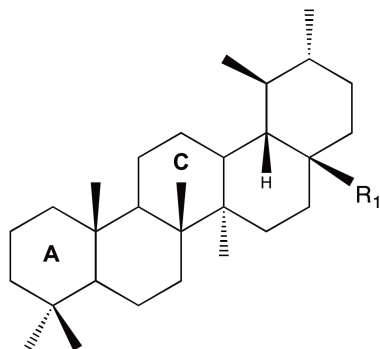
Figure 1.12. Main positions of the chemical modifications performed on the **UA** scaffold.

UA was first investigated for its anti-inflammatory properties which were associated to its ability to inhibit nitric oxide (NO) production and cyclooxygenase (COX) activation.^{132,133} Honda *et al* synthesized a series of new **UA** derivatives that significantly inhibited the production of NO

Chapter 1 | Introduction

in mouse macrophages. Most of the semisynthetic derivatives showed better activity compared with **UA** (Table 1.4).¹³⁴⁻¹³⁶

Table 1.4. The inhibitory activities (IC_{50}) of **UA** and derivatives (**1.1–1.7**) for the inhibition of the production of NO in mouse macrophages.



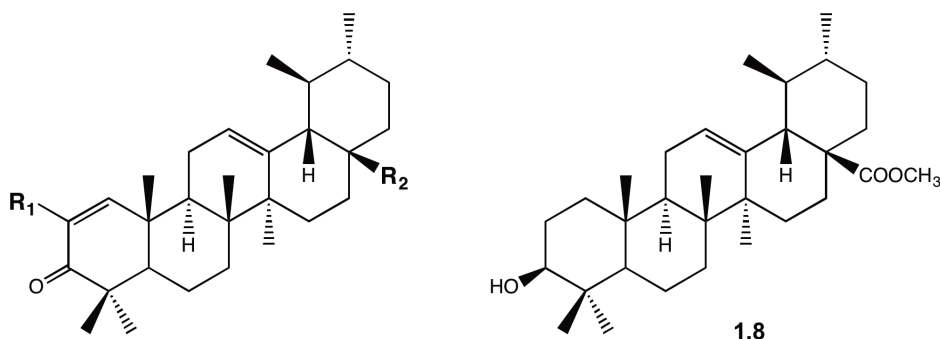
Entry	Comp.	A-ring	C-ring	R ₁	IC ₅₀ (μM)	Ref.
1	UA	-	-	-	Toxic ^a	134-136
2	1.1			CO ₂ H	17.6	134
3	1.2			CO ₂ H	5.1	134
4	1.3			CO ₂ CH ₃	8.9	135
5	1.4			CO ₂ H	6.2	135,136
6	1.5			CO ₂ CH ₃	5.1	135,136
7	1.6			CO ₂ H	0.8	135
8	1.7			CO ₂ CH ₃	0.1	135

^aUA was toxic to cells above 10 μM and was not active below 10 μM.

Chapter 1 | Introduction

Compared with the methyl ursolate **1.8**, the derivatives of **UA** with a cyano (**1.9**) and trifluoromethyl (**1.10**) groups at position C2 in the A-ring, coupled with an 1-en-3-one moiety, showed an enhanced growth inhibition in the 253JB-V, KU7, PANC-1 and Panc-28 cancer cell lines (Table 1.5).¹³⁷

Table 1.5. Inhibition of the proliferation of cancer cell lines by the **UA** derivatives **1.8–1.11**.¹³⁷



Entry	Comp.	R ₁	R ₂	Cell line/IC ₅₀ (μM)			
				253JB-V	KU7	PANC-1	Panc-28
1	1.8	-	-	6.1	9.0	11.8	10.6
2	1.9	CN	COOCH ₃	0.2	0.3	0.5	1.0
3	1.10	CF ₃	COOCH ₃	0.2	0.5	0.7	1.1
4	1.11	I	COOCH ₃	4.9	6.0	6.9	13.5

Salvador *et al* prepared a series of derivatives containing an α,β -unsaturated ketone moiety at A-ring (Table 1.6), and found that most of these derivatives exhibited significantly enhanced anticancer activity.^{138,139} The introduction of a Michael acceptor, such as 2-cyano group, coupled with an 1-en-3-one moiety in the A-ring, combined with a fluorolactone moiety (**1.21** and **1.22**), improved the cytotoxic activity against several cancer cell lines. Compound **1.22** induced cell cycle arrest at the G1 phase with upregulation of p21^{waf1}, and apoptosis with upregulation of NOXA and downregulation of c-FLIP in the AsPC-1 cell line.¹³⁹

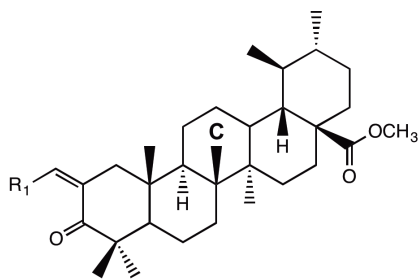
Table 1.6. Inhibition of the proliferation of cancer cell lines by **UA** and derivatives **1.12–1.22**.^{138,139}


Fig. 1.6.1

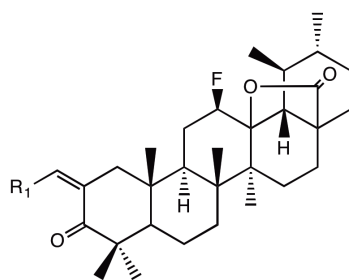


Fig. 1.6.2

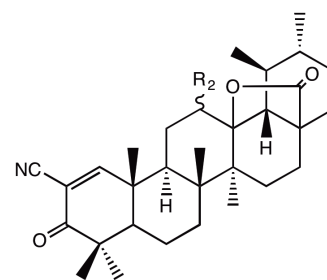


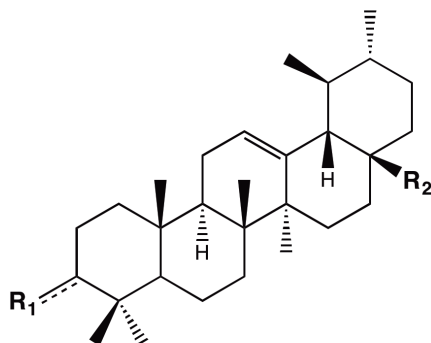
Fig. 1.6.3

Entry	Comp.	R ₁	C-ring	R ₂	Cell line/IC ₅₀ (μM)						
					AsPC-1	Panc-1	MIA PaCa-2	HepG-2	MCF7	A549	PC-3
1	UA	-	-	-	12.6	14.9	10.4	15.0	12.3	11.4	20.8
Figure 1.6.1											
2	1.12			-	2.3	18.2	24.3	27.6	9.4	12.2	12.9
3	1.13			-	2.1	14.4	8.3	8.5	3.5	18.7	5.7
4	1.14			-	8.1	12.1	7.8	7.9	12.5	12.9	9.5
5	1.15			-	5.8	5.1	7.3	2.0	5.3	5.6	6.8
6	1.16			-	2.1	5.6	5.6	4.0	2.2	5.3	3.5
7	1.17			-	1.9	3.5	4.0	3.2	2.3	4.9	3.0
Figure 1.6.2											
8	1.18		-	-	1.1	4.6	6.0	6.8	2.8	9.5	4.0
9	1.19		-	-	1.0	21.4	28.1	-	-	-	-
10	1.20		-	-	7.5	10.1	10.2	10.6	7.0	16.2	5.6
Figure 1.6.3											
11	1.21	-	-		0.5	14.3	2.1	3.0	2.2	10.0	2.0
12	1.22	-	-		0.7	1.8	0.9	0.5	0.7	0.9	0.9

Chapter 1 | Introduction

Structural modifications at positions C3 and C28 of the **UA** scaffold are by far the most commonly reported in the literature. Improvement of the cytotoxic activity was observed with the acetylursolic **1.23**, 3-oxo **1.24**, and hydroxyimino **1.25** derivatives, when compared with **UA** against the leukemia cell line HL-60 (Table 1.7, entries 2–4).¹⁴⁰ Furthermore, the introduction of a 3 β -amino group afforded a derivative (**1.26**) that was 30-fold more potent than **UA** and its α -counterpart (**1.27**) against HL-60 cells (Table 1.7, entries 5 and 6).¹⁴⁰ This result suggests that the configuration at C3 is critical for the cytotoxic activity. The introduction of aminoalkyl groups at position C28 (derivatives **1.28** and **1.29**) resulted in a significant improvement of the cytotoxicity compared with the parent compound (Table 1.7, entries 7 and 8).¹⁴⁰

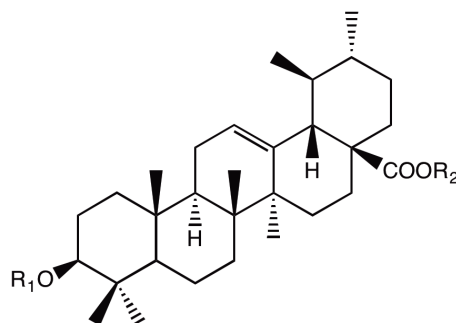
Table 1.7. Inhibition of the proliferation of cancer cell lines by **UA** and derivatives **1.23–1.29**.¹⁴⁰



Entry	Comp.	R ₁	R ₂	Cell line/ED ₅₀ (μg/ml)			
				HL-60	BGC	Bel-7402	HeLa
1	UA	▶OH	COOH	72.0	53.7	45.0	49.4
2	1.23	▶OAc	COOH	55.9	100.0	58.4	50.0
3	1.24	≡O	COOH	19.5	60.0	58.5	76.5
4	1.25	≡NOH	COOH	53.3	53.3	38.1	50.1
5	1.26	▶NH ₂	COOCH ₃	2.0	2.5	1.7	2.4
6	1.27	⋯NH ₂	COOCH ₃	79.5	>100.0	39.6	55.2
7	1.28	▶OH	CONH(CH ₂) ₉ NH ₂	5.0	30.0	8.0	-
8	1.29	▶OAc	CONH(CH ₂) ₉ NH ₂	5.0	35.0	95.0	-

Chapter 1 | Introduction

Several ester derivatives of ursolic acid (**1.30–1.47**) (Fig. 1.13) were synthesized and evaluated for their cytotoxic activity in several cell lines (Table 1.8).¹⁴¹⁻¹⁴³



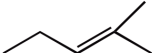
- | | |
|--|---|
| 1.30 $R_1=H$; $R_2=CH_2CH_3$ | 1.39 $R_1=H$; $R_2=(CH_2)_2ONO_2$ |
| 1.31 $R_1=H$; $R_2=CH_2CH_2CH_3$ | 1.40 $R_1=H$; $R_2=(CH_2)_3ONO_2$ |
| 1.32 $R_1=H$; $R_2=CH(CH_3)_2$ | 1.41 $R_1=H$; $R_2=(CH_2)_4ONO_2$ |
| 1.33 $R_1=H$; $R_2=CH_2CH_2CH_2CH_3$ | 1.42 $R_1=COCHCHCH_3$; $R_2=H$ |
| 1.34 $R_1=H$; $R_2=CH_2CH_2CH_2CH_2CH_3$ | 1.43 $R_1=COCH_2CH_2COOH$; $R_2=H$ |
| 1.35 $R_1=H$; $R_2=CH_2CH_2CH_2CH_2CH_2CH_3$ | 1.44 $R_1=COCH_2CH_3$; $R_2=H$ |
| 1.36 $R_1=H$; $R_2=$  | 1.45 $R_1=COCH_2CH_2CH_3$; $R_2=H$ |
| 1.37 $R_1=H$; $R_2=CH_2CH_2OH$ | 1.46 $R_1=COCH_3$; $R_2=CH_2CH(OH)CH_2OH$ |
| 1.38 $R_1=H$; $R_2=CH_2CH(OH)CH_2OH$ | 1.47 $R_1=COCH_3$; $R_2=CH_2CH_2OH$ |

Figure 1.13. Schematic representation of **UA** ester derivatives (**1.30–1.47**).

Chapter 1 | Introduction

Table 1.8. Inhibition of the proliferation of cancer and non-tumor (HELFL) cell lines by **UA** derivatives **1.30–1.47**.¹⁴¹⁻¹⁴³

Entry	Comp.	Cell line/IC ₅₀ (μM)							
		NTUB1	HT-29	HepG2	BCG-823	GES-1	SH-SY5Y	HeLa	HELFL
1	1.30	13.5	-	70.8	69.3	-	66.3	29.2	81.9
2	1.31	18.3	-	89.1	79.7	-	92.5	48.0	>100
3	1.32	8.0	-	-	-	-	-	-	-
4	1.33	15.6	-	>100	>100	-	>100	63.2	>100
5	1.34	27.8	-	-	-	-	-	-	-
6	1.35	26.2	-	-	-	-	-	-	-
7	1.36	10.9	-	-	-	-	-	-	-
8	1.37	19.5	-	-	-	-	-	-	-
9	1.38	-	-	44.2	20.5	154.3	-	-	-
10	1.39	-	-	79.6	84.2	-	71.1	36.2	68.1
11	1.40	-	-	87.4	98.3	-	89.6	69.4	82.6
12	1.41	-	-	>100	>100	-	>100	>100	>100
13	1.23	14.3	24.0	37.7	19.4	92.9	-	-	-
14	1.42	11.9	-	-	-	-	-	-	-
15	1.43	8.7	-	-	-	-	-	-	-
16	1.44	>30	-	-	-	-	-	-	-
17	1.45	>30	-	-	-	-	-	-	-
18	1.46	-	18.4	27.5	15.7	155.4	-	-	-
19	1.47	-	23.6	29.8	17.2	137.2	-	-	-

Treatment of the bladder cancer cell line NTUB1 with 40 μM of compound **1.32** increased the production of ROS, inhibited tubulin polymerization, induced cell cycle arrest, and ultimately apoptosis.¹⁴¹ BCG-823 stomach cancer cells treated with compound **1.46** showed an accumulation of cells in the sub-G1 phase, and induction of apoptosis, with upregulation of caspase-3, and downregulation of Bcl-2 and survivin. Moreover, compound **1.46** promoted tumor growth reduction in a mouse model, with low toxicity to the host.¹⁴²

In addition to **1.28** and **1.29**, a series of C28 amide derivatives of **UA** (**1.48–1.76**) (Fig. 1.14 and 1.15) were synthesized and tested against several cancer cell lines (Table 1.9).¹⁴³⁻¹⁴⁷

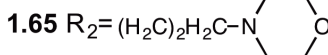
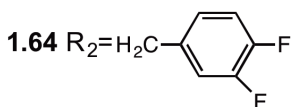
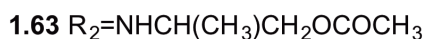
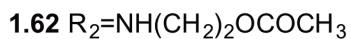
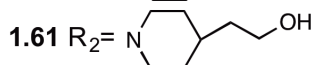
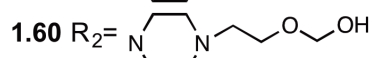
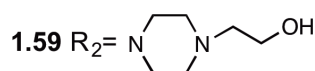
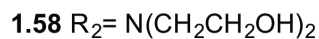
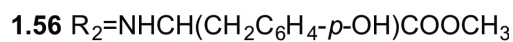
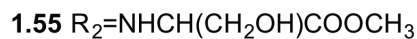
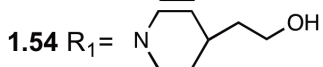
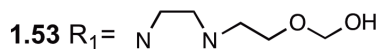
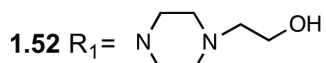
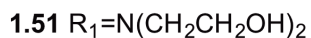
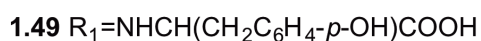
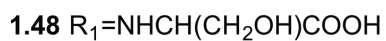
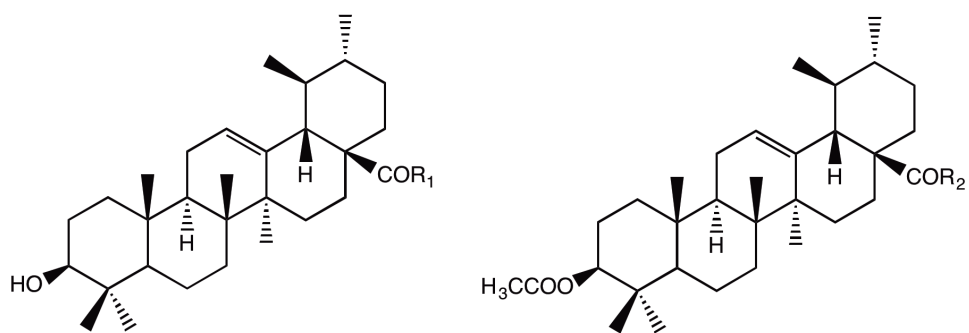
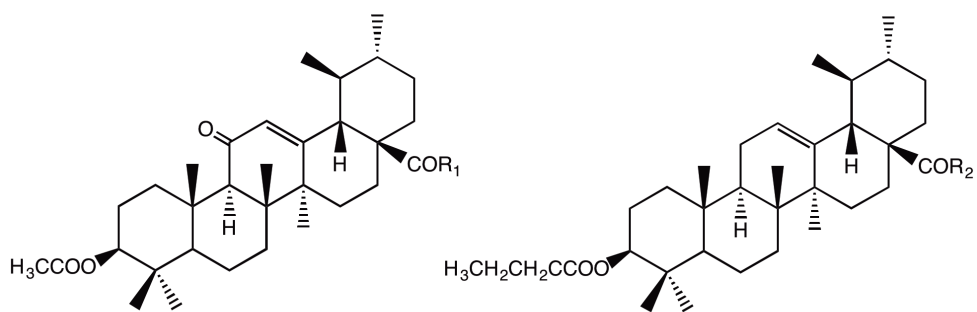


Figure 1.14. Schematic representation of C28 amide derivatives of UA (1.48–1.68).

Chapter 1 | Introduction

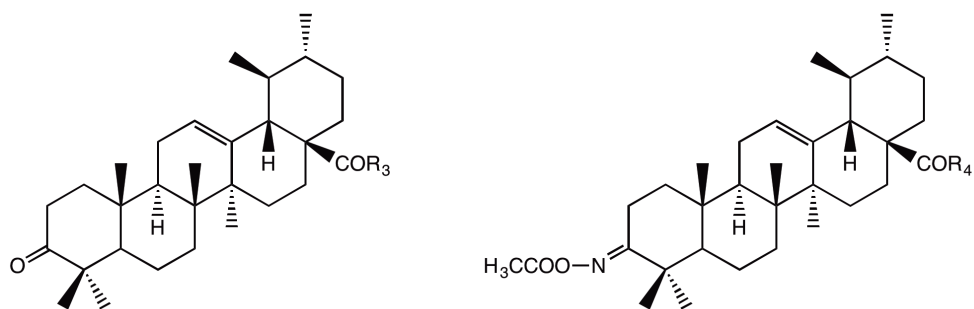


1.69 $R_1 = \text{NHC}_6\text{H}_5$

1.71 $R_2 = \text{NHCH}_2\text{COOCH}_3$

1.70 $R_1 = \text{NHCH}(\text{CH}_3)\text{CH}_2\text{OH}$

1.72 $R_2 = \text{NHCH}_2\text{C}_6\text{H}_5$



1.73 $R_3 = \text{NHCH}_2\text{CH}_2\text{CH}_2\text{OH}$

1.75 $R_4 = \text{NHC}_6\text{H}_5$

1.74 $R_3 = \text{HN}-\text{C}_6\text{H}_4-\text{OCH}_3$

1.76 $R_4 = \text{HN}-\text{C}_6\text{H}_4-\text{HOH}_2\text{C}$

Figure 1.15. Schematic representation of C28 amide derivatives of **UA** (**1.69–1.76**).

Chapter 1 | Introduction

Table 1.9. Inhibition of the proliferation of cancer and non-tumor (HELf) cell lines by the **UA** derivatives **1.48–1.76**.¹⁴³⁻¹⁴⁶

Entry	Comp.	Cell line/IC ₅₀ (μM)					
		HepG2	BCG-823	SH-SY5Y	HeLa	HELf	SKOV3
1	1.48	83.0	79.3	72.2	41.7	60.3	-
2	1.49	>100	>100	>100	>100	>100	-
3	1.50	82.4	78.3	65.0	32.3	52.8	-
4	1.51	35.7	39.3	21.4	14.4	36.9	-
5	1.52	>100	98.3	>100	52.3	32.8	-
6	1.53	36.7	35.0	30.3	23.8	28.7	-
7	1.54	>100	>100	>100	67.3	>100	-
8	1.55	35.3	29.0	37.2	20.6	22.3	-
9	1.56	>100	83.0	>100	67.0	35.8	-
10	1.57	46.6	48.5	49.4	16.3	27.8	-
11	1.58	20.3	15.5	13.2	10.9	38.1	-
12	1.59	20.5	13.9	11.7	7.2	31.0	-
13	1.60	15.3	12.8	9.5	6.3	38.9	-
14	1.61	59.4	51.3	40.1	12.4	30.0	-
15	1.62	-	>10	-	-	-	6.1
16	1.63	-	8.3	-	-	-	2.2
17	1.64	-	>10	-	>10	-	>10
18	1.65	-	4.5	-	2.7	-	7.4
19	1.66	-	-	-	-	-	-
20	1.67	-	-	-	-	-	-
21	1.68	-	-	-	5.44	-	-
22	1.69	-	>10	-	>10	-	>10
23	1.70	-	>10	-	>10	-	>10
24	1.71	-	5.6	-	>10	-	-
25	1.72	-	>10	-	>10	-	>10
26	1.73	-	>10	-	-	-	>10
27	1.74	-	>10	-	-	-	>10
28	1.75	21.2	8.1	-	9.3	-	-
29	1.76	23.7	9.2	-	13.8	-	-

Compound **1.58** induced apoptosis and cell cycle arrest at the S phase in the HepG2 cancer cell line in a time- and dose-dependent manner, with upregulation of caspase-3. *In vivo* studies using H22 xenografts in Kumming mice revealed an anticancer effect of compound **1.58** when compared to the control group.¹⁴³ Compounds **1.62** and **1.63** were also able to induce apoptosis and cell cycle arrest at the S phase in HeLa cells.¹⁴⁴

Chapter 1 | Introduction

Wang *et al* prepared a series of C28 piperazine-thiourea derivatives, and their anticancer activities were evaluated against five cancer cell lines (MGC-803, HCT 116, T24, HepG2 and A549), and a non-tumor cell line (HL-7702). The most active derivative **1.77** (Fig. 1.16, Table 1.10, entry 1) induced apoptosis, with upregulation of caspase-8, -9 and -3, and G1-phase arrest in the HepG2 cell line.¹⁴⁸ Furthermore, Yang and co-workers prepared a series of derivatives containing an acyl piperazine moiety at C28 (Fig. 1.16). Compounds **1.78** and **1.79** (Fig. 1.16, Table 1.10, entries 2–3) were the most active ones, and the preliminary mechanism of action showed that derivative **1.78** was able to induce apoptosis in the MGC-803 cell line.¹⁴⁹ In addition, a series of **UA**-triazolyl derivatives were prepared by Bhat *et al*, with compounds **1.80–1.83** being the most active derivatives (Fig. 1.16, Table 1.10, entries 4–7).¹⁵⁰

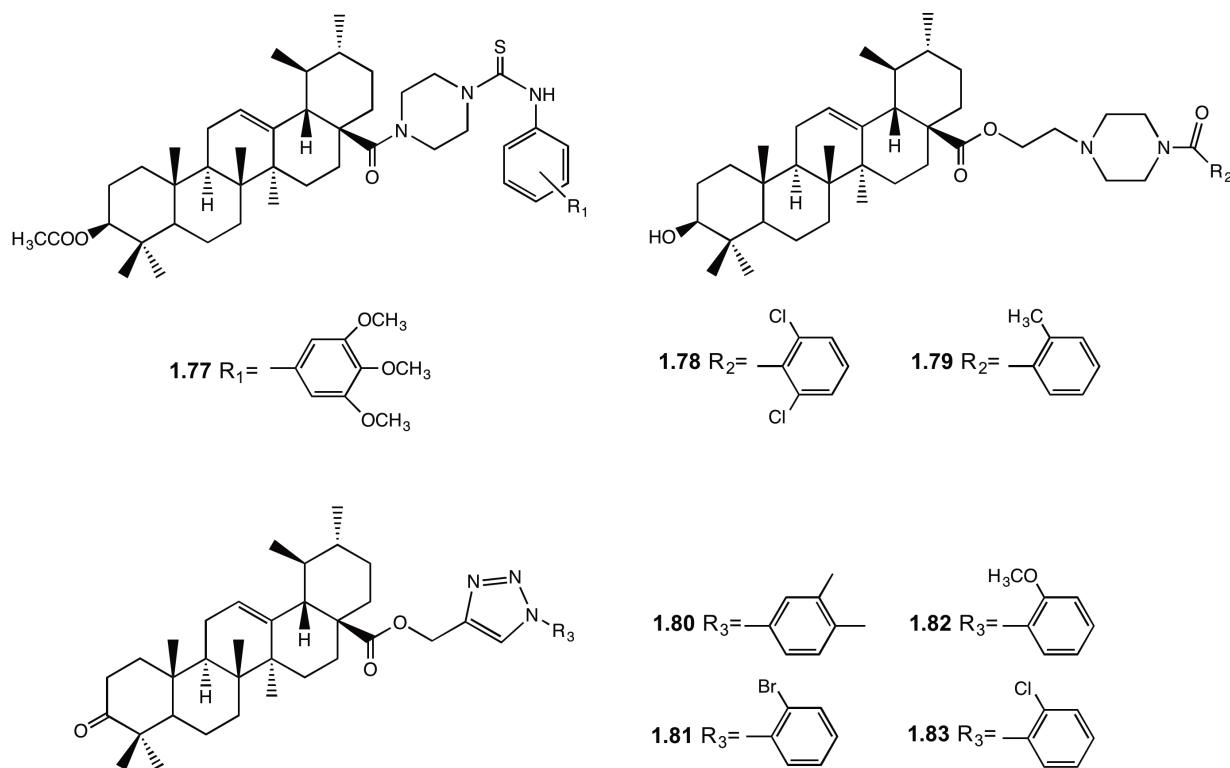


Figure 1.16. Schematic representation of C28 derivatives of **UA** (**1.77–1.83**).

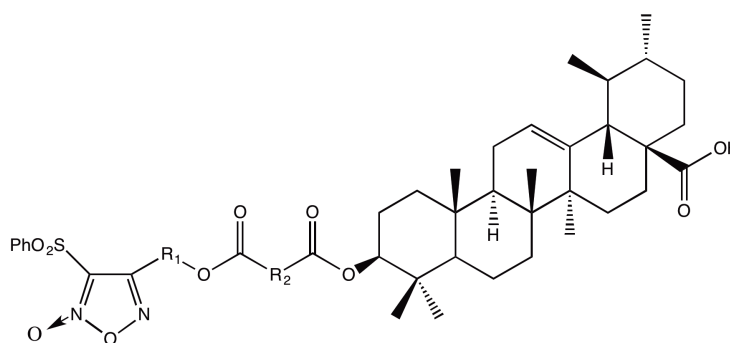
Chapter 1 | Introduction

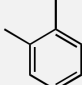
Table 1.10. Inhibition of the proliferation of cancer and non-tumor (FR-2) cell lines by the **UA** derivatives **1.77–1.83**.¹⁴⁸⁻¹⁵⁰

Entry	Comp.	Cell line/IC ₅₀ (μM)								
		MGC-803	HCT 116	T24	HepG2	A549	MCF-7	THP-1	HL-7702	FR-2
1	1.77	9.8	19.0	13.6	5.4	11.1	-	-	>100	-
2	1.78	2.5	-	-	-	-	-	-	-	-
3	1.79	3.6	-	-	-	-	-	-	-	-
4	1.80	-	<0.1	-	-	0.5	5.5	0.9	-	10
5	1.81	-	15	-	-	2.9	<0.1	<0.1	-	69
6	1.82	-	0.3	-	-	<0.1	<0.1	<0.1	-	>50
7	1.83	-	9.1	-	-	0.2	<0.1	<0.1	-	>50

A series of furoxan-based NO-donating **UA** derivatives were synthesized, and their cytotoxic activities were evaluated against HepG2 cancer cells (Table 1.11). Derivatives **1.84–1.87** (Table 1.11, entries 3–6) were more active than **UA** (Table 1.11, entry 1) and 5-fluorouracil (**5-FU**) (Table 1.11, entry 2) in the inhibition of HepG2 cell growth.¹⁵¹

Table 1.11. Inhibition of the proliferation of cancer cell lines by **UA**, **5-FU** and derivatives **1.84–1.87**.¹⁵¹

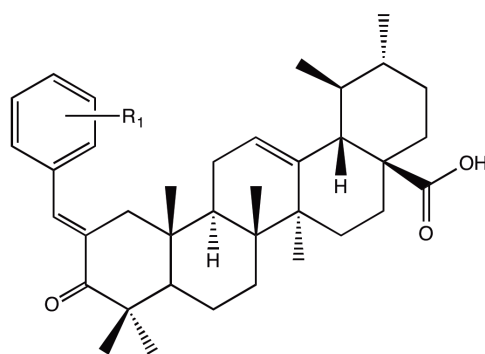


Entry	Comp.	R ₁	R ₂	Cell line/ IC ₅₀ (μM)
				HepG2
1	UA	-	-	21.1
2	5-FU	-	-	16.0
3	1.84	O(CH ₂) ₂	(CH ₂) ₂	3.2
4	1.85	O(CH ₂) ₂ (CH ₃)CH	(CH ₂) ₂	5.4
5	1.86	O(CH ₂) ₄	(CH ₂) ₂	4.9
6	1.87	O(CH ₂) ₂ (CH ₃)CH		9.8

Chapter 1 | Introduction

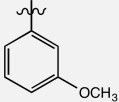
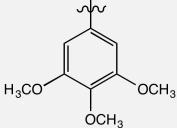
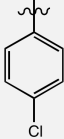
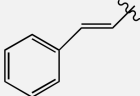
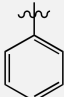
A library of ursolic acid-benzylidene derivatives was designed, synthesized, and evaluated against a panel of four cancer cell lines, and a non-tumor cell line (FR-2) (Table 1.12). The most active derivative **1.92** induced apoptosis, cell cycle arrest at the G1 phase, accumulation of cytochrome c in the cytosol, and increased expression of caspase-9 and -3, in the HCT-116 cell line.¹⁵²

Table 1.12. Inhibition of the proliferation of cancer and non-tumor (FR-2) cell lines by **UA**, **5-FU**, and derivatives **1.88–1.98**.^{152,153}



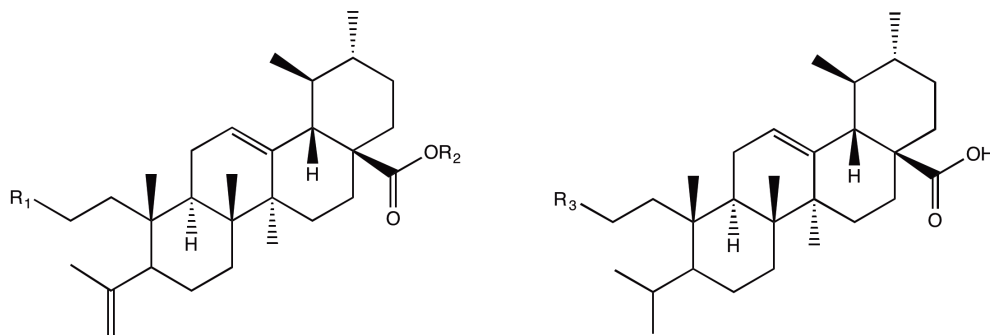
Entry	Comp.	R ₁	Cell line/IC ₅₀ (μM)				
			A549	HCT-116	MCF-7	THP1	FR-2
1	UA	-	33	42	37	9.1	31
2	5-FU	-	1.4	2.3	2.0	1.7	-
3	1.88		6.4	5.0	30	1.1	44
4	1.89		2.0	12	5.0	14	69
5	1.90		2.0	5.0	4.1	4.1	70
6	1.91		2.1	15	5.0	4.1	70
7	1.92		0.6	≤0.1	5.5	0.9	0.8
8	1.93		0.5	2.1	5.0	0.9	8.6

Chapter 1 | Introduction

Entry	Comp.	R ₁	Cell line/IC ₅₀ (μM)				
			A549	HCT-116	MCF-7	THP1	FR-2
Table 1.12 continued							
9	1.94		0.7	23	4.2	12	40
10	1.95		<0.9	<0.9	4.0	9.1	35
11	1.96		2.9	15	4.1	12	69
12	1.97		0.7	2.1	12	16	38
13	1.98		18	14	23	16	70

Compound **1.98** was able to inhibit the expression of CD133⁺, a marker for the isolation and identification of cancer stem cells, in a dose- and time-dependent manner in PLC/PRF/5 and Huh7 HCC cells. Treatment with compound **1.98** increased the CD133⁺ HCC cancer stem cells differentiation, decreased their self-renewal and tumorigenic capacity, and increased their sensitivity to the chemotherapeutic drugs doxorubicin and vincristine.¹⁵³

The cleavage of the A-ring of the ursane scaffold has also been explored (Table 1.13).^{141,154} The preliminary data suggests that compound **1.100** induces G2/M-phase arrest, and apoptosis in the NUTB1 cell line, through increased production of ROS.¹⁴¹

Table 1.13. Inhibition of the proliferation of cancer cell lines by **UA** and derivatives **1.99–1.104**.^{141,154}

Entry	Comp.	R ₁	R ₂	R ₃	Cell line/IC ₅₀ (μM)	
					NRP.152	NTUB1
1	UA	-	-	-	>5.0	-
3	1.99	CN	H	-	>5.0	-
4	1.100	COOH	H	-	>5.0	25.5
5	1.101	CHO	H	-	2.4	-
6	1.102	-	-	CH ₂ NH ₂	0.3	-
7	1.103	COOCH ₃	H	-	-	>30
8	1.104	COOCH ₃	CH ₃	-	-	15.6

As discussed in this subsection, the anticancer activity of **UA** can be improved by specific structural modifications of its basic scaffold. Moreover, the semisynthetic derivatives appear to preserve the multitarget anticancer activity of the parent compound. However, further research is needed to explore additional structural modifications of the **UA** scaffold to develop novel and more active **UA** derivatives with enhanced druggability. Therefore, there is an interest in the design and synthesis of new **UA** derivatives that could act as novel anticancer agents, particularly with anti-lung cancer activity.

Chapter 2

General objectives



Chapter 2 | General objectives

Non-small cell lung cancer (NSCLC) is a leading cause of cancer-related deaths worldwide. Despite novel therapeutic strategies, the overall 5-year survival rate in many countries remains less than 15%. The layer of complexity in cancer biology and the drug resistance often found, highlight the need for the development of new anticancer agents with novel mechanisms of action.

Natural triterpenoids, in particular ursane-type pentacyclic triterpenoids, have interesting biological properties that could be explored for the design and synthesis of more effective anticancer derivatives. Ursolic acid (**UA**) can be considered a potential lead, due to its promising multitarget anticancer activity, low toxicity and commercial availability.

Given these considerations, the aim of this thesis is to develop new **UA** derivatives, and evaluate their anticancer activity against at least one lung cancer cell line.

The synthesis of the novel **UA** derivatives was design based on three main semisynthetic strategies:

- i) Expansion and cleavage of the A-ring, as well as introduction of nitrogen-containing groups (chapter 3);
- ii) Introduction of oxime and nitrile groups at A-ring (chapter 4);
- iii) Introduction of esters (saturated or unsaturated), and of an α,β -unsaturated carbonyl system (with an endo- or exocyclic double bond) at A-ring (chapter 5).

The structural elucidation of the new synthesized compounds should be achieved through different techniques, such as infrared (IR) spectroscopy, mass spectrometry (MS), and nuclear magnetic resonance (NMR).

The anticancer activity of the newly semisynthetic derivatives should be tested against at least one lung cancer cell line, in a two-dimensional (2D) and three-dimensional (3D) culture models, in order to establish an IC_{50} .

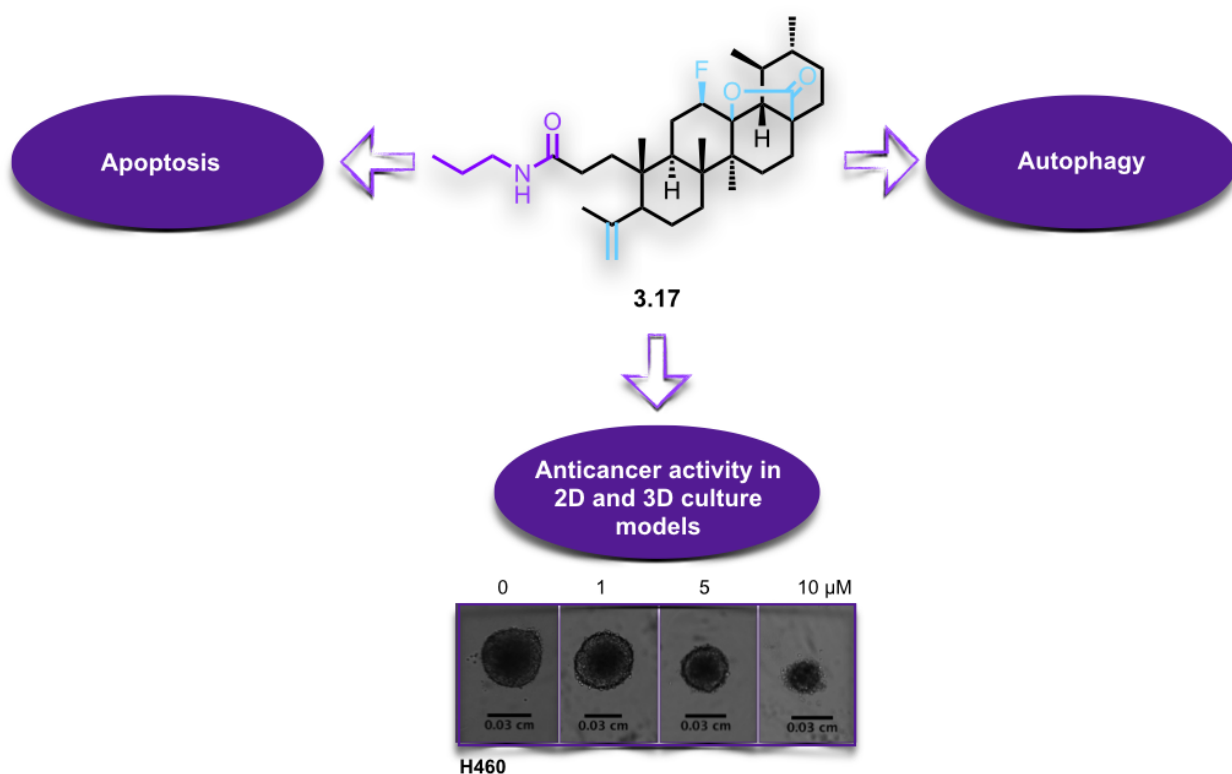
Chapter 2 | General objectives

The preliminary mechanism of action of the most active compound of each panel should be explored through the use of several techniques, such as liquid scintillation counting, FACS and immunoblot techniques, in order to explore the effect of the compounds on the DNA, RNA and protein synthesis rates, on the cell cycle distribution, on the induction of apoptosis and autophagy, as well as on expression levels of specific proteins. These studies should shed some light on the possible anticancer mechanism of the most active compounds found for each panel of **UA** derivatives.

The final objective of this research work is to select the best compounds for *in vivo* evaluation of their anticancer activity.

Chapter 3

Synthesis and cytotoxic activity of novel A-ring modified ursolic acid derivatives in NSCLC



Vanessa I. S. Mendes, Geoffrey A. Bartholomeusz, Mary Ayres, Varsha Gandhi, and Jorge A. R. Salvador, *Synthesis and cytotoxic activity of novel A-ring cleaved ursolic acid derivatives in human non-small cell lung cancer cells*, *European Journal of Medicinal Chemistry* 123, 317–331 (2016).

3.1. Introduction

The cleavage of the A-ring of **UA** has been a relatively less explored strategy to obtain new and more potent derivatives, which encouraged us to develop and synthesize a series of new **UA** derivatives with a cleaved A-ring coupled with additional modifications at C3.

The introduction of nitrogen-containing groups was explored, namely the formation of a lactam, several amides, and a nitrile group. Nitrogen-containing groups offer versatile properties that could improve the biological and pharmacokinetic profile of compounds. The amide function, for example, is one of the most fundamental chemical building blocks found in nature. It represents the main chemical bonds that link amino acid building blocks together to form proteins, and it is present in a vast number of synthetic structures.¹⁵⁵⁻¹⁵⁷ For example, the amide bond is found in 25% of known pharmaceuticals on the market,¹⁵⁸ and it was present in 2/3 of drug candidates which were surveyed by three leading pharmaceutical companies in 2006.¹⁵⁹

Typically, the amide bond is formed through the condensation of a carboxylic acid and an amine with release of one equivalent of water. The amide bond is usually formed via an activated carboxylic acid, which usually takes place by converting the –OH of the acid into a good leaving group prior to treatment with the amine. The activation of the carboxylic acid can be accomplished using coupling reagents, such as acid chlorides, among others.^{157,160}

n-Propylphosphonic anhydride, more commonly referred as T3P (or PPA) (Fig. 3.1) is an efficient coupling reagent that has been employed for the conversion of carboxylic acids to aldehydes and amides, amides to nitriles, and formamides to isonitriles, as well as for the synthesis of heterocycles, Weinreb amides, β -lactams, hydroxamic acids, acyl azides, esters, imidazopyridines, and dihydropyrimidinones.¹⁶¹⁻¹⁶³ This reagent has low toxicity, long shelf life stability, easy handling (commercially available as a 50% solution in different organic solvents,

Chapter 3 | Synthesis and cytotoxic activity of novel UA derivatives

such as ethyl acetate (EtOAc) and tetrahydrofuran (THF)), and its water-soluble by-products are extracted easily into the aqueous solution.¹⁶⁰

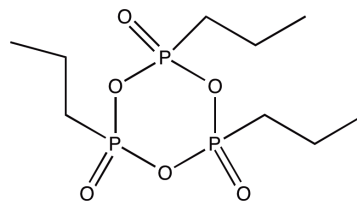
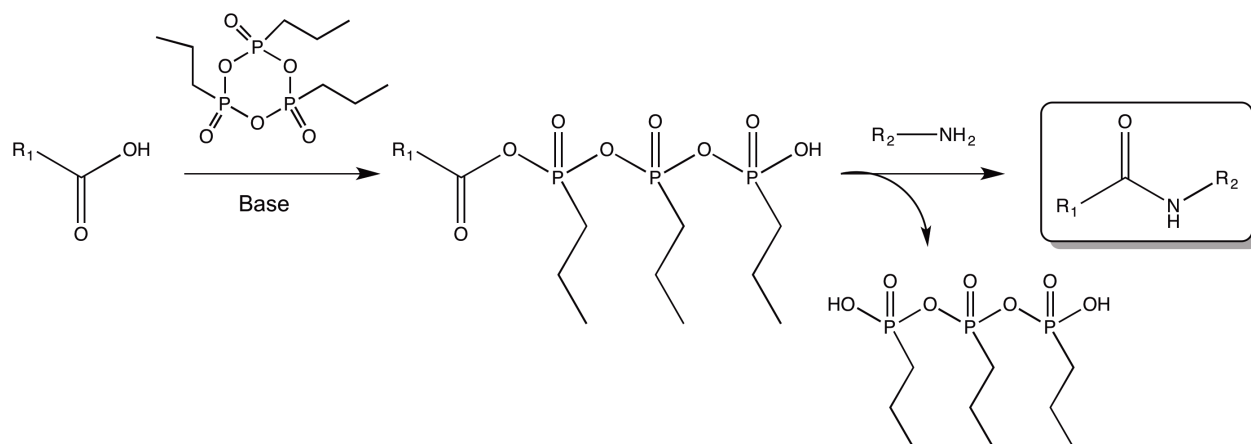


Figure 3.1. Chemical structure of *n*-propylphosphonic anhydride (T3P).

Wissmann and Kleiner first introduced T3P in 1980, as a novel coupling reagent to prepare several peptide derivatives, that displayed a better performance than other phosphorous analogues and *N,N'*-dicyclohexylcarbodiimide (DCC), due to its good solubility, long shelf life, and low susceptibility towards racemization.¹⁶⁴ To form an amide bond, T3P first converts the hydroxyl of the carboxylic acid into a leaving group, by forming an anhydride, and then reacts with the amine derivative to yield the corresponding amide. The resulting by-product is miscible with water and easily removed during the workup (Scheme 3.1).¹⁶⁵ Meudt and co-workers have patented a novel process for the preparation of nitriles using T3P with elimination of water. Hence, nitriles could be obtained by reacting T3P with carboxamides or ammonium salts of carboxylic acids, or carboxylic acids in the presence of ammonia or ammonium salts.^{166,167}

Chapter 3 | Synthesis and cytotoxic activity of novel UA derivatives



Scheme 3.1. Mechanism of action of T3P for the amide-bond formation.

The introduction of fluorine, a small and highly electronegative atom, in key positions of a biologically active molecule can result in a profound pharmacological effect. Hence, the presence of a fluorine atom has been shown to improve the metabolic and chemical stability, membrane permeability, and binding affinity of different molecules.¹⁶⁸⁻¹⁷⁰ Furthermore, strategies using the fluorine atom are already widely used and established by medicinal chemists in drug discovery. In fact, the fluorine atom is a prominent element in marketed drugs and development candidates. While in 1970 there were only about 2% of fluorine-containing drugs on the market, the current number has grown to about 25%.¹⁷¹⁻¹⁷³ Anticancer fluorinated compounds are commonly used in clinical practice, and some examples are the antimetabolite drugs 5-fluorouracil and gemcitabine, the anti-estrogenic drug fulvestrant, and the protein kinase inhibitors gefitinib and sorafenib.^{173,174}

Fluorinated organic compounds can be obtained from nucleophilic, electrophilic and radical forms of fluorinating reagents. Nucleophilic reagents, such as (dimethylamino)sulfur trifluoride (DAST) (Fig. 3.2), use a fluoride anion as the reaction active specie. On the other hand, electrophilic reagents use an fluoronium cation “F⁺” as the source of active species, usually in a N-F type-reagent, such as 1-chloromethyl-4-fluoro-1,4-diazoniabicyclo[2.2.2]octane bis(tetrafluoroborate) (Selectfluor[®]) (Fig. 3.2). In addition, a fluorinated building block can also be

Chapter 3 | Synthesis and cytotoxic activity of novel UA derivatives

used as a fluorine source, which has both a fluorine atom and a leaving group in the molecule.¹⁷⁵⁻¹⁷⁷

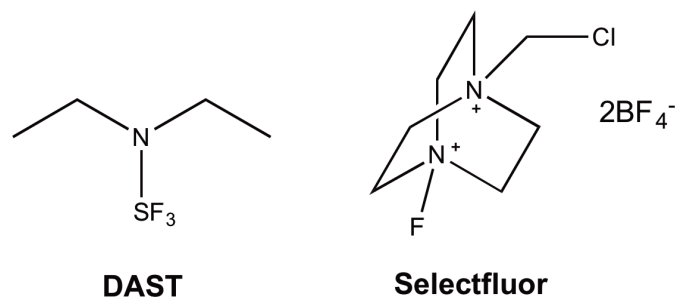


Figure 3.2. Chemical structures of DAST and Selectfluor fluorinating reagents.

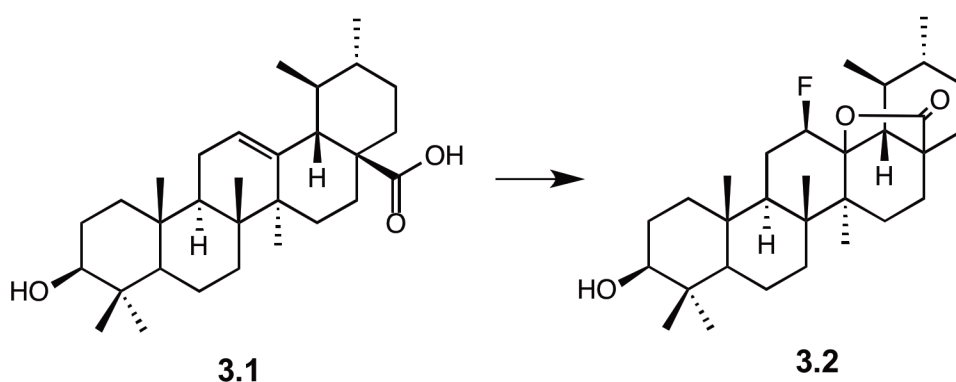
Our research group previously developed a 12 β -fluoro-13,28 β -lactone **UA** scaffold (**3.2**), using Selectfluor[®] as the electrophilic fluorinating reagent to introduce a fluorine atom into the C12 position, through reaction with the double bond. Selectfluor is a crystalline white solid reagent, stable at high temperatures, easy to work, and the resulting by-products are usually easy to removed by an aqueous workup.¹⁷⁸ In a medium without a nucleophilic donor, with solvents and temperature conditions optimized, the free carboxylic acid at the position C28 of **UA** behaves as a nucleophilic donor, leading to loss of the proton and cyclization at C13, with formation of a lactone group.¹³⁹ Taking into account the interesting results obtained with the fluorolactone ursane scaffold, and the interesting properties of the fluorine atom, this strategy was further explored in order to develop novel **UA** derivatives.

This chapter describes the synthesis of new fluorolactone ursolic acid derivatives with a modified A-ring. Ring expansion and cleavage was explored, as well as introduction of nitrogen-containing groups. The structures of the newly synthesized compounds were fully elucidated by IR, MS and NMR techniques. The *in vitro* anticancer activity was tested against NSCLC cell lines, in monolayer and spheroid cultures models, and the most active compound was selected for preliminary studies on its mechanism of action.

3.2. Results and discussion

3.2.1. Chemistry

The synthetic route began with the formation of 12 β -fluoro-13,28 β -lactone (**3.2**) via reaction of **UA** (**3.1**) with Selectfluor fluorinating reagent in a mixture of nitromethane and dioxane (3:2) at 80 °C, with yields above 60% (Scheme 3.2).¹³⁹ The fluorination reaction was selected as the first step of the synthetic scheme, prior to Jones oxidation (**3.3**), because some functional groups synthesized can also be fluorinated, resulting in a mixture of fluorinated compounds. The fluorolactone moiety is chemically stable, and allows several post-fluorination modifications using controlled acidic and basic conditions.



Scheme 3.2. Synthesis of the fluorolactone derivative **3.2**.

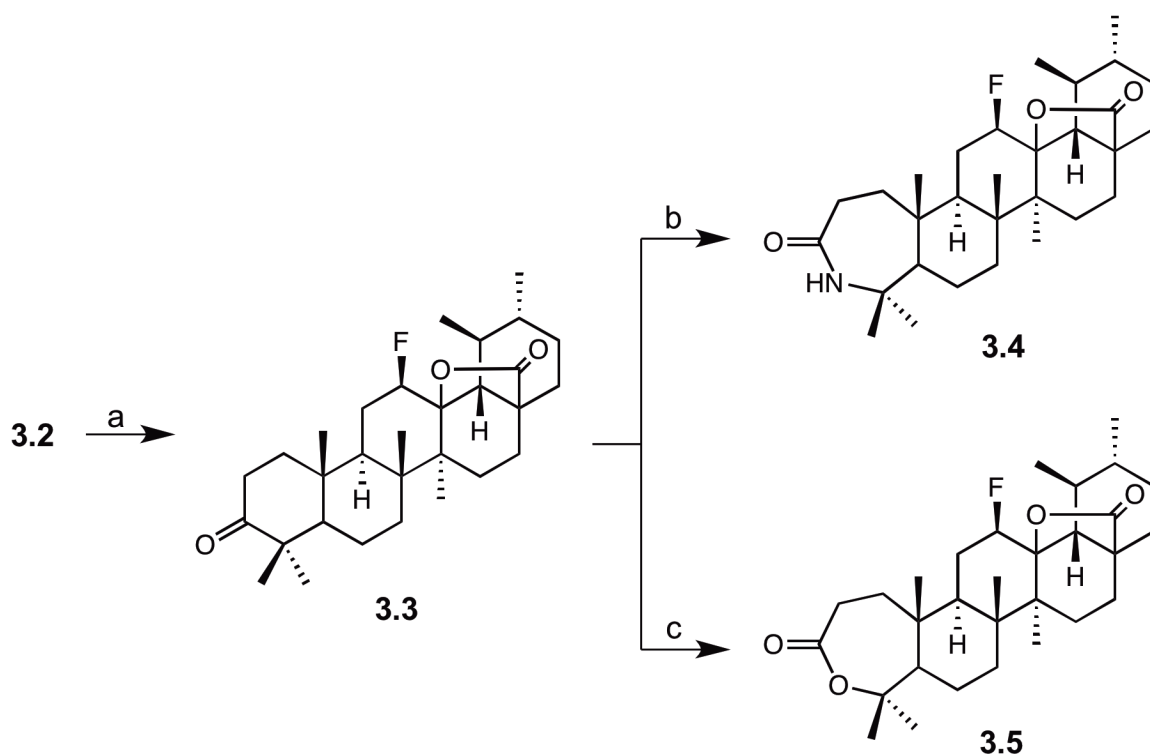
Reagents and conditions: Selectfluor, nitromethane, dioxane, 80 °C, 24 h.

The introduction of the 12 β -fluorolactone moiety was confirmed by the presence in the ¹H NMR spectra of a double triplet or double quartet at 4.55 – 5.00 ppm, with a coupling constant of around 45 Hz, characteristic of the geminal proton for the β -fluorine. In the ¹³C NMR spectra, it was possible to observe a doublet for the signal of C12 (88.50 – 89.50 ppm) and of C13 (91.50 –

Chapter 3 | Synthesis and cytotoxic activity of novel UA derivatives

92.00 ppm), with coupling constants of 186 and 14 Hz, respectively. This profile of ^1H and ^{13}C NMR spectra is characteristic of the β -isomer.¹³⁹

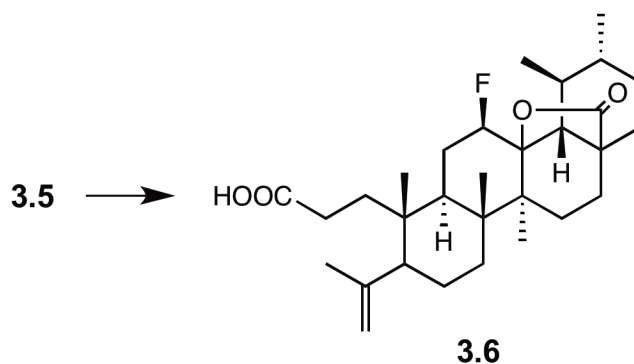
The oxidation of the 3β -hydroxyl group of **3.2** to obtain derivative **3.3** was achieved via Jones oxidation (Scheme 3.3). The treatment of 3-oxo-derivative **3.3** with NaN_3 in glacial acetic acid and sulfuric acid afforded lactam **3.4**, while the treatment of compound **3.3** with *m*-chloroperbenzoic acid (*m*-CPBA) in CHCl_3 afforded lactone **3.5**, with yields around 60% (Scheme 3.3).



Scheme 3.3. Synthesis of derivatives **3.3–3.5**.

Reagents and conditions: a) Jones reagent, acetone, ice; b) i - glacial acetic acid, sulfuric acid, NaN_3 , 65 °C; ii - 30 °C, 5 h; c) *m*-CPBA 77%, CHCl_3 , r.t., 120 h.

For the formation of amide derivatives, lactone **3.5** was cleaved using *p*-toluenesulfonic acid monohydrate in CH_2Cl_2 to give **3.6** (Scheme 3.4).



Scheme 3.4. Synthesis of the derivative **3.6**.

Reagents and conditions: *p*-toluenesulfonic acid monohydrate, CH₂Cl₂, r.t., 24 h.

The cleavage of A-ring with formation of a carboxylic acid and unsaturation at C4(23) position (**3.6**) was confirmed by the presence in the ¹H NMR spectrum of two singlets for the protons of the double bond of carbon 23 at 4.88 and 4.67 ppm (Fig. 3.3).

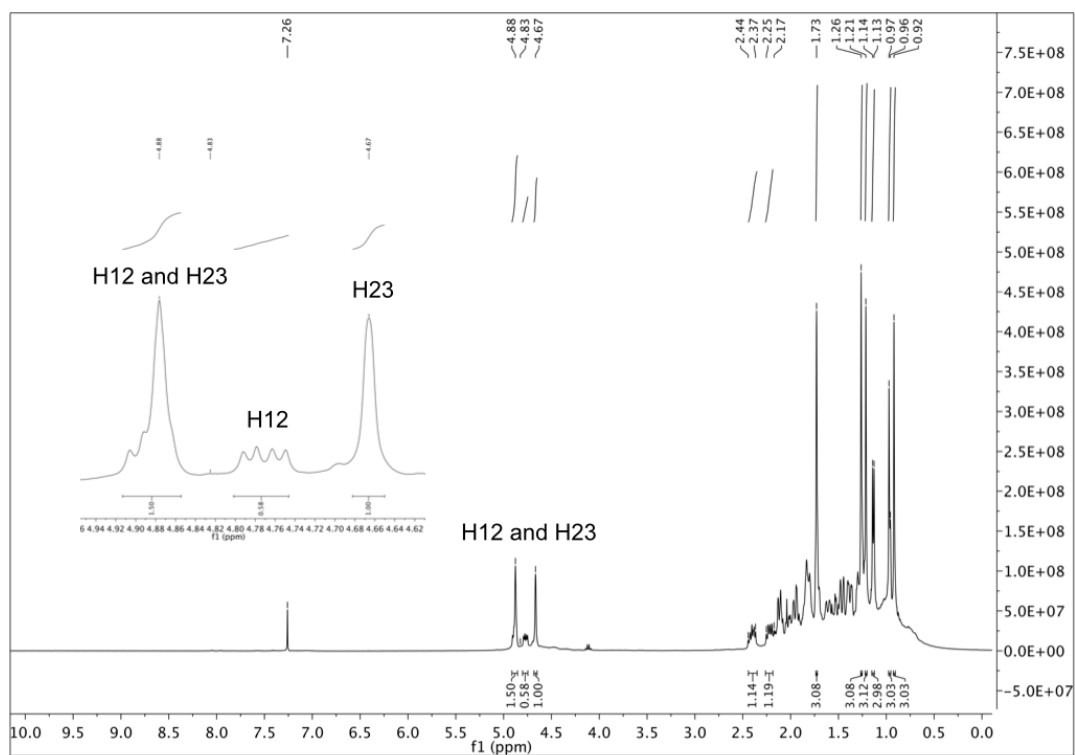


Figure 3.3. ¹H NMR spectrum of compound **3.6** recorded in CDCl₃.

Chapter 3 | Synthesis and cytotoxic activity of novel UA derivatives

In the ^{13}C NMR spectrum, the carbon of the carboxylic acid of compound **3.6** was observed at 179.71 ppm, close to the carbonyl carbon signal of the fluorolactone (179.02 ppm). Unsaturation at C4(23) was observed at 146.85 and 114.26 ppm, which was determined as a quaternary carbon (C4) and as a secondary carbon (C23), respectively, by ^{13}C (Fig. 3.4) and DEPT-135 NMR spectra.

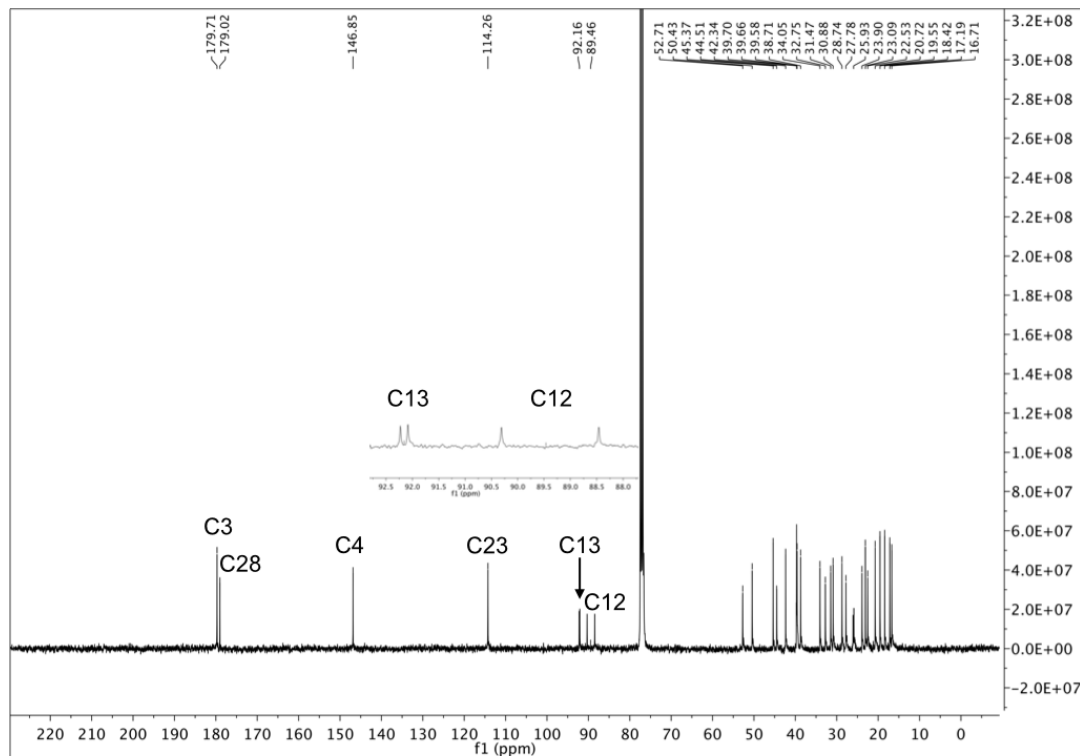
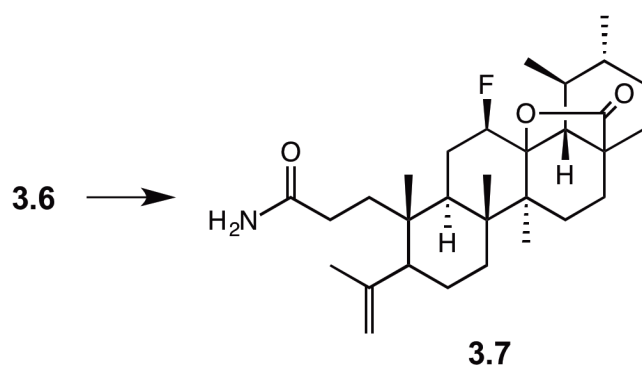


Figure 3.4. ^{13}C NMR spectrum of compound **3.6** recorded in CDCl_3 .

Compound **3.6** was first treated with oxalyl chloride and then reacted with cold 25% ammonium aqueous solution to generate the primary amide **3.7** (Scheme 3.5). T3P was not used in the formation of this amide because the amine available was in an aqueous solution, and the presence of water would quench the reagent, resulting in lower yields.



Scheme 3.5. Synthesis of the amide derivative **3.7**.

Reagents and conditions: i - oxalyl chloride, dry CH_2Cl_2 , r.t., 15h; ii - cold 25% ammonium aq. solution, dry THF, 2 h.

The introduction of the amide function in compound **3.7** was confirmed in the ^1H NMR spectrum by a broad singlet at 5.79 ppm for the protons of the amide function (Fig. 3.5). The carbonyl carbon of the amide group was observed in the ^{13}C NMR spectrum at 176.14 ppm (Fig. 3.6).

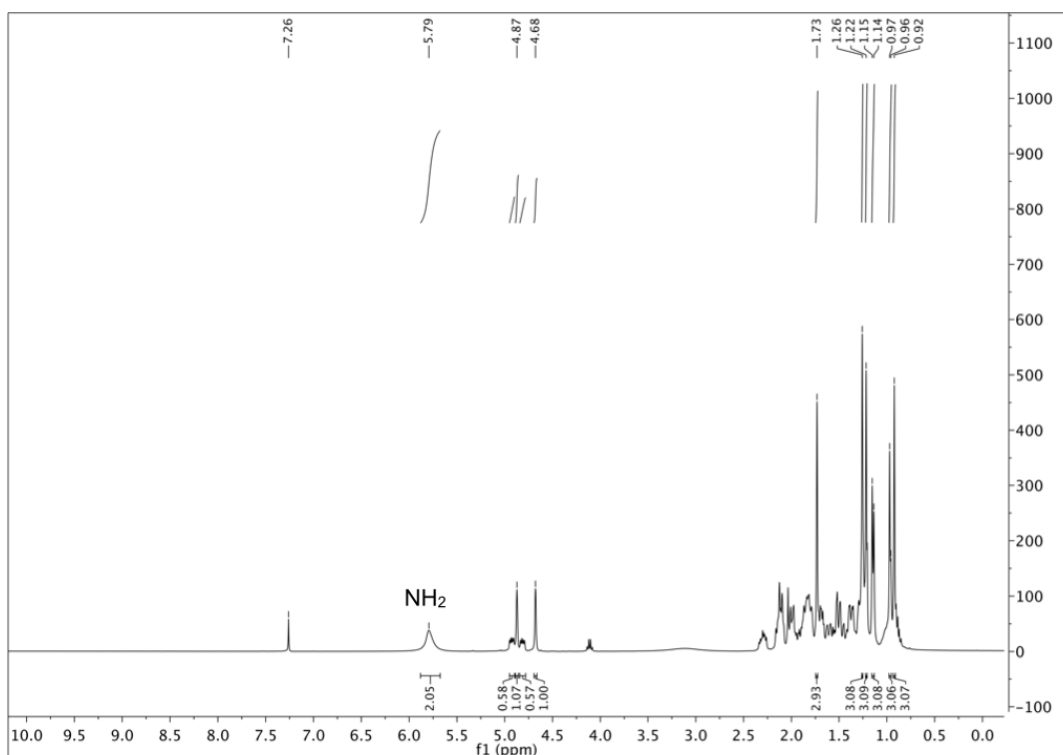


Figure 3.5. ^1H NMR spectrum of compound **3.7** recorded in CDCl_3 .

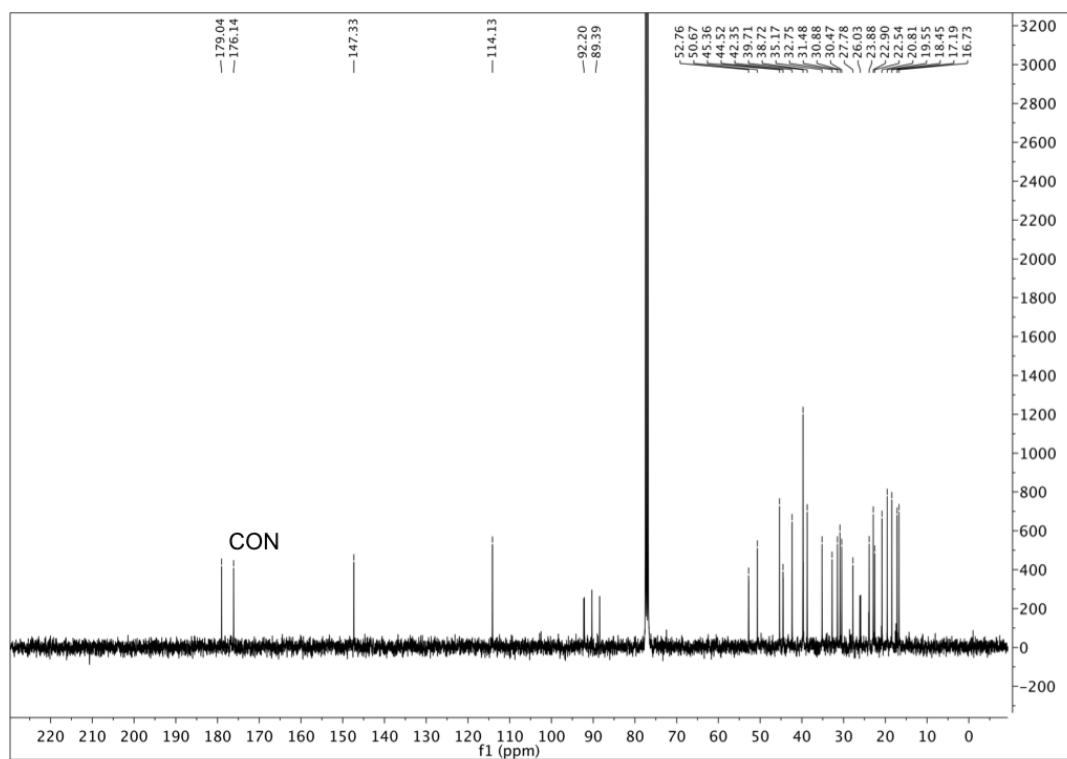
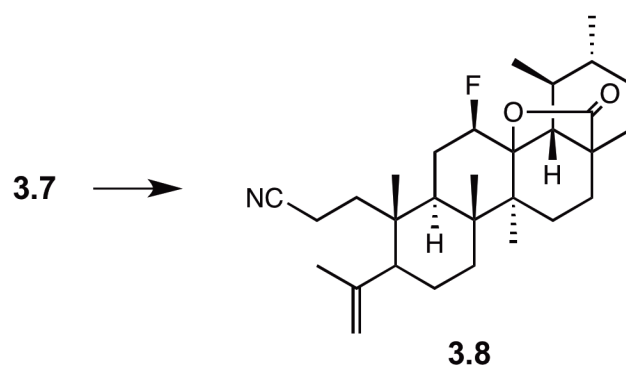


Figure 3.6. ^{13}C NMR spectrum of compound **3.7** recorded in CDCl_3 .

The reagent T3P[®] (*n*-propylphosphonic anhydride solution, 50 wt. % in THF) was used to prepare a nitrile derivative (**3.8**) and several amide derivatives (**3.9–3.17**) (Schemes 3.6 and 3.7).

Compound **3.8** was obtained by dehydration of the amide **3.7** with T3P (50 wt. % in THF) in a mixture of THF/EtOAc and triethylamine (Et_3N) at 77 °C for 5h (Scheme 3.6).



Scheme 3.6. Synthesis of the nitrile derivative **3.8**.

Reagents and conditions: T3P (50 wt. % in THF), THF/EtOAc, Et₃N, 77 °C, 5 h.

The nitrile derivative **3.8** was confirmed in the ¹H NMR spectrum by the disappearance of the proton signal of the NH group (Fig. 3.7), and in the ¹³C NMR spectrum by the disappearance of the carbonyl carbon signal at 173 ppm and appearance of the carbon signal of the nitrile group at 120.39 ppm (Fig. 3.8). In the IR spectrum, the band for CN stretching vibration was observed at 2237 cm⁻¹ (Fig. 3.9).

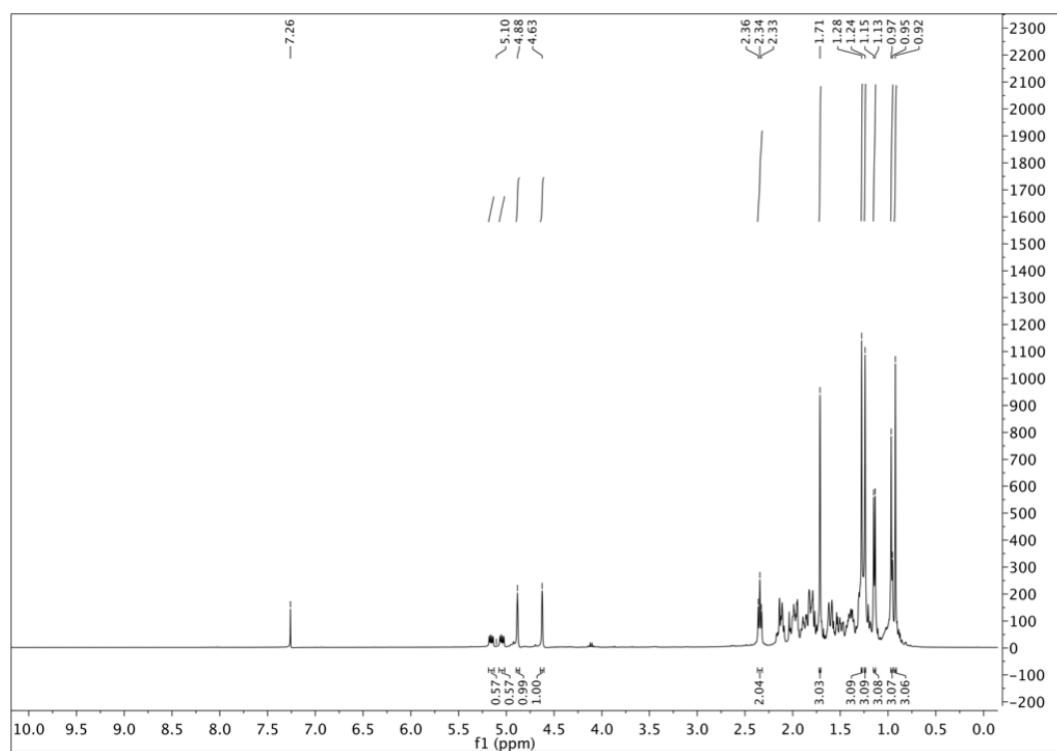


Figure 3.7. ^1H NMR spectrum of compound 3.8 recorded in CDCl_3 .

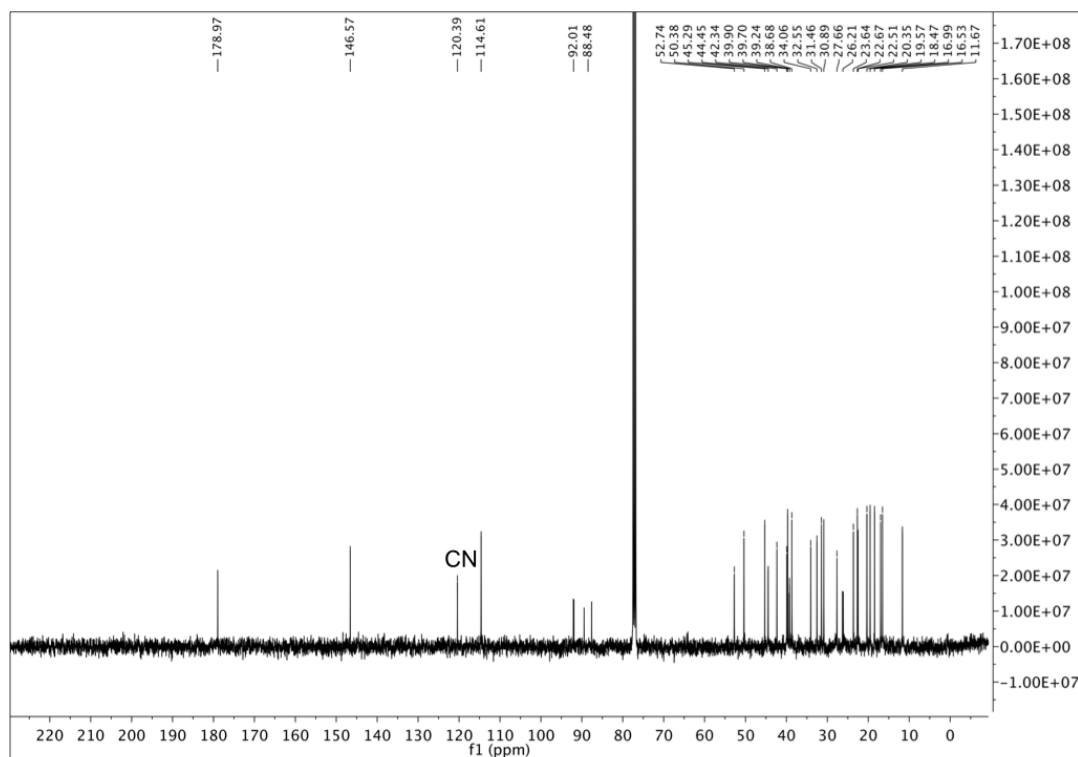


Figure 3.8. ^{13}C NMR spectrum of compound 3.8 recorded in CDCl_3 .

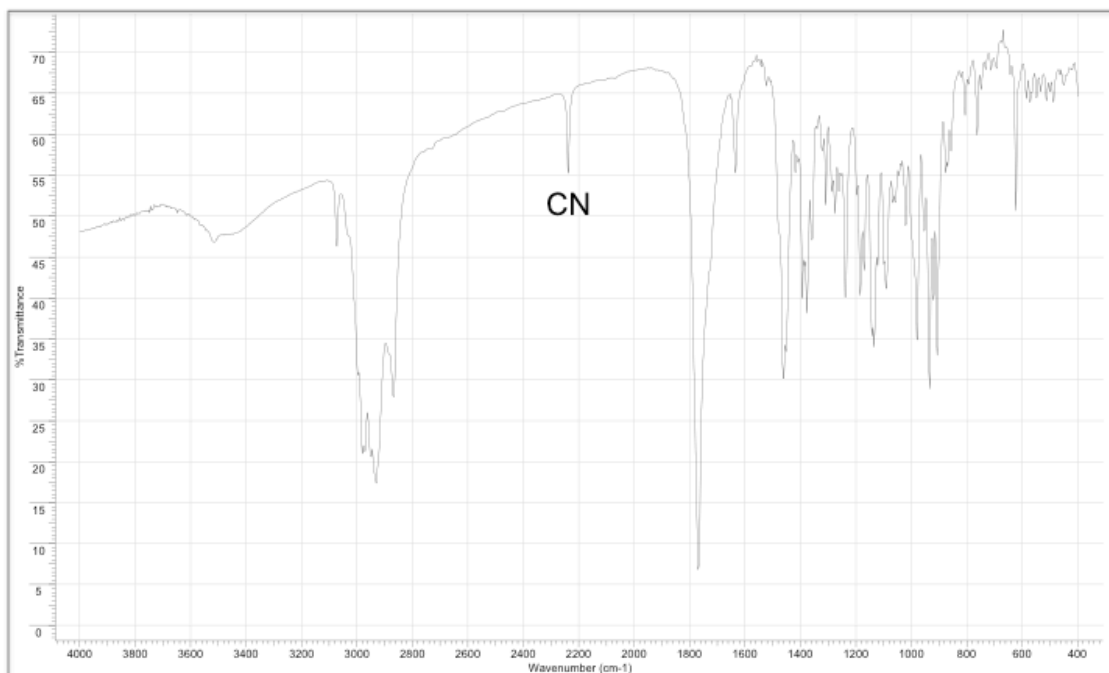
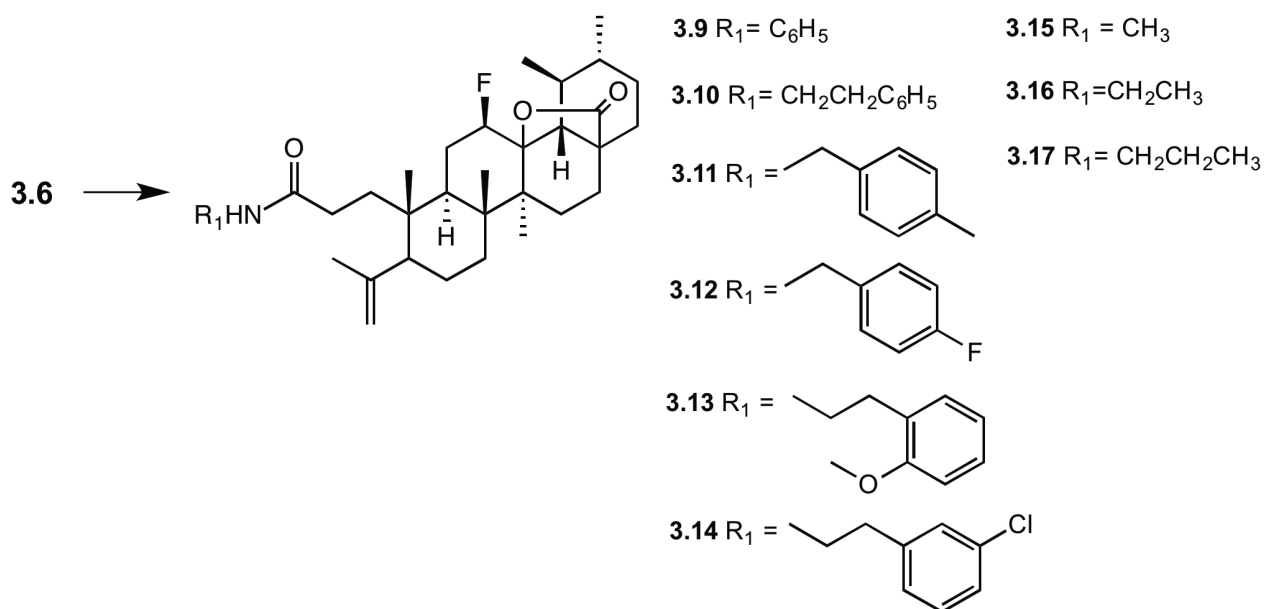


Figure 3.9. IR spectrum of compound 3.8.

The free carboxylic acid group of compound **3.6**, in the presence of T3P (50 wt. % in THF) and Et₃N in THF in an ice bath, reacted with several amines to yield the respective amide derivatives (**3.9–3.17**) (Scheme 3.7). The selected amines have an aromatic side chain (**3.9–3.14**), or a small aliphatic side chain (**3.15–3.17**), in order to evaluate the influence of different substituents on the anticancer activity.

Chapter 3 | Synthesis and cytotoxic activity of novel UA derivatives



Scheme 3.7. Synthesis of the amide derivatives **3.9–3.17**.

Reagents and conditions: T3P (50 wt. % in THF), dry THF, Et_3N , R_1NH_2 , ice bath; **3.9**: 7.3 h; **3.10**: 2.75 h; **3.11**, **3.13–3.15**, and **3.17**: 5 h; **3.12**: 4 h; **3.16**: 3 h.

In the 1H NMR spectra, it was possible to observe a broad singlet or triplet for the proton of the several amides around the chemical shifts of 5.3 and 5.7 ppm. The carbonyl carbon of the amide was observed in the region of 173 ppm in the ^{13}C NMR spectra. Figures 3.10 and 3.11 represent the 1H and ^{13}C NMR spectra of the amide derivative **3.17**.

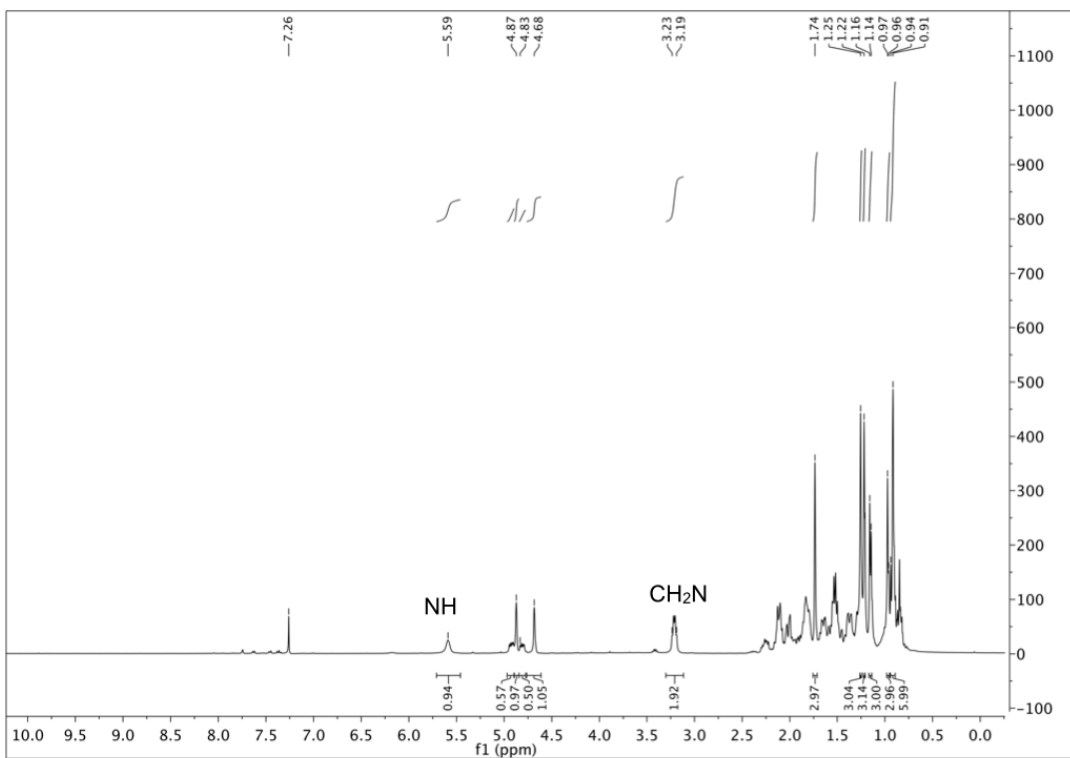


Figure 3.10. ^1H NMR spectrum of compound **3.17** recorded in CDCl_3 .

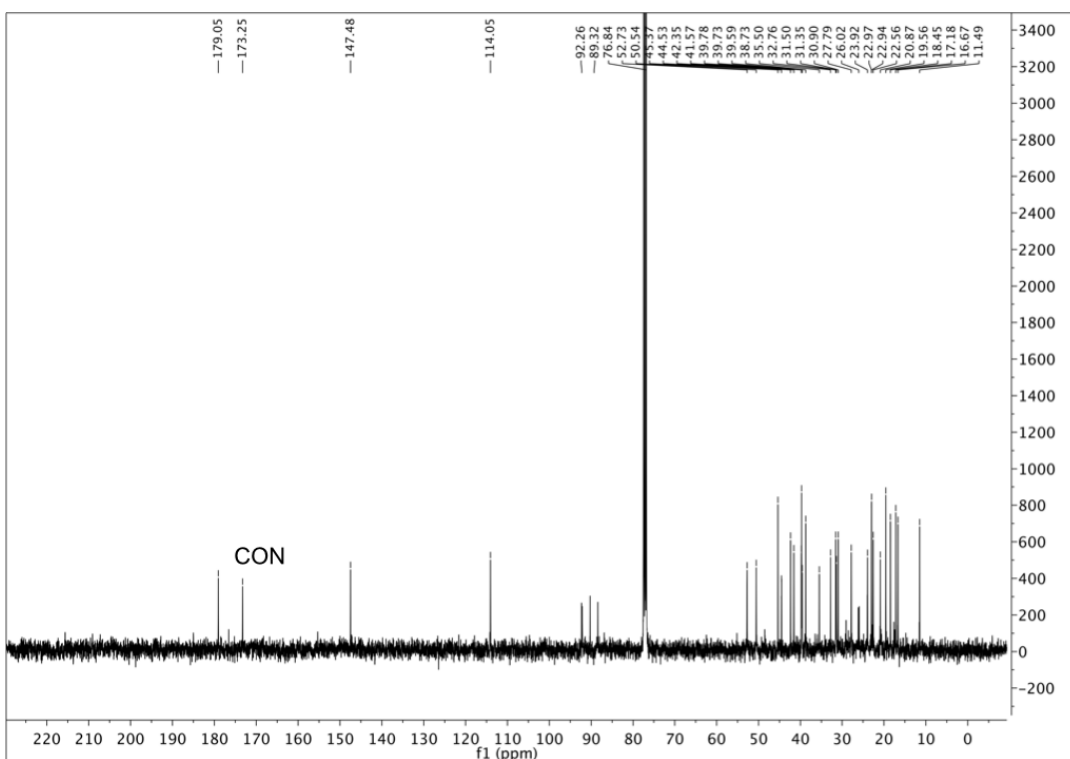


Figure 3.11. ^{13}C NMR spectrum of compound **3.17** recorded in CDCl_3 .

3.2.2. Biological studies

3.2.2.1. Evaluation of *in vitro* anticancer activity

The anticancer activities of **UA** and all the newly synthesized derivatives against NSCLC cells (H460, H322, H460 LKB1^{+/+}) were evaluated using the CellTiter-Blue[®] assay. The CellTiter-Blue[®] cell viability assay is a fluorescent and homogeneous method for estimating the number of viable cells. This assay is based on the ability of living cells to convert a redox dye (resazurin, blue color) into a fluorescent end product (resorufin, pink color). Nonviable cells lose the metabolic capacity to reduce the indicator dye, and thus the quantity of resorufin produced is proportional to the number of viable cells. The incubation period required to generate an adequate fluorescent signal above the background is usually 1 to 4 hours, and should be optimized to each cell line, because it is dependent on the metabolic activity of the cell. Cell washing, removal of medium, and multiple pipetting steps are not required, as resazurin can be dissolved directly to cells cultured in a serum-supplemented medium.^{179,180}

A culture medium containing 0.15% dimethyl sulfoxide (DMSO) served as negative control. The cell lines were treated with increasing concentrations of each compound, and the IC₅₀ values (half-maximal inhibitory concentration) were determined after 72 h of incubation. The values for IC₅₀ are summarized in Table 3.1.

Chapter 3 | Synthesis and cytotoxic activity of novel UA derivatives

Table 3.1. The inhibitory activities (IC_{50}) of **UA (3.1)** and derivatives **3.2–3.17** in the NSCLC cell lines.

Compound	Cell line ^(a) / IC_{50}		
	H460	H322	H460 LKB1 ^{+/+}
UA (3.1)	14.8±0.6	15.3±2.8	21.1±1.6
3.2	19.3±2.6	14.3±2.7	18.7±3.7
3.3	>50	>50	>50
3.4	>25	>25	13.5±0.5
3.5	ND	ND	ND
3.6	>50	>50	>50
3.7	23.0±2.3	24.1±2.5	21.8±3.2
3.8	>17	>17	>17
3.9	>50	>50	>50
3.10	>50	>50	>50
3.11	>50	>50	>50
3.12	>50	>50	>50
3.13	>50	>50	>50
3.14	>50	>50	>50
3.15	4.5±0.4	6.8±1.5	6.7±0.5
3.16	5.3±0.3	7.3±1.0	7.8±1.1
3.17	2.6±0.9	3.3±0.9	4.4±0.6

^(a)Lung cancer cell lines were treated with various concentrations of test compounds for 72 h. The inhibitory activities were determined using CellTiter-Blue[®]. IC_{50} was calculated from the results, and data are presented as means \pm SD (standard deviation) of three independent experiments. *ND*: not determined.

As shown in Table 3.1, the introduction of the fluorolactone moiety into the **UA** backbone, compound **3.2**, was not critical for the cytotoxic activity. Nevertheless, the incorporation of a fluorine atom into the **UA** structure was designed based on the desirable properties that have been attributed to the fluorine atom in several drug candidates, such as improved pharmacokinetic profile, and based on previous results from our research group.^{139,171}

The ring expansion did not contribute to the biological activity compared with the parent compound. The lactam **3.4** showed a dramatic increase in the IC_{50} values in the H460 and H322 cell lines, whereas the formation of lactone **3.5** led to a less soluble derivative for the biological assays, and so lactone **3.5** was not further tested.

The cleavage of A-ring with formation of a carboxylic acid function at C3 and an unsaturation at C4(23) (**3.6**), in order to obtain the amide derivatives, improved the solubility compared with its antecedent but did not improve the cytotoxic activity.

Chapter 3 | Synthesis and cytotoxic activity of novel UA derivatives

The primary amide **3.7** showed an improved activity compared with lactone **3.5** and carboxylic acid **3.6** derivatives but not compared with the parent compound **UA**. The introduction of a secondary amide with an aromatic substituent (**3.9–3.14**), a more bulky substituent, led to compounds with decreased activity compared with the primary amide **3.7** and parent compound **UA**. However, when a secondary amide with a short alkyl side chain was introduced (**3.15–3.17**), the cytotoxicity was improved compared with the primary amide **3.7** (×9) and the parent compound **UA** (×5).

Finally, the dehydration of the primary amide to give a nitrile function (**3.8**) led to a decreased activity.

The most active derivatives (**3.15–3.17**) were selected and their cytotoxic activity was further explored in a multicellular spheroid three-dimensional (3D) culture system.

Monolayer cultures of cells are the most commonly used model to screen for the cytotoxic activity of new drugs. Although cancer cell lines exhibit similar mutations and gene profiles as *in vivo* tumors, this model lacks the three-dimensionality, heterogeneity, dense extracellular matrix, and penetration barriers observed *in vivo*, and hence the effects observed may overestimate or underestimate the actual effects observed *in vivo* in solid tumors.^{181,182}

The use of 3D models has been proposed as an attractive approach to overcome some of the limitations of the traditional two-dimensional (2D) systems, because such models mimic more closely the complex cellular heterogeneity, cell/cell interactions, and tumor microenvironment observed *in vivo*.¹⁸¹⁻¹⁸³ One example of such a 3D system are multicellular spheroids. Multicellular spheroids are spontaneously aggregating three-dimensional cultures of tumor cells. Compared with their 2D counterparts, multicellular spheroids develop important physiological parameters of heterogeneous tumors, such as tight cell-cell interactions and mechanical tissue properties. In addition, similar to the *in vivo* microenvironment, tumor spheres are exposed to nutrients, oxygen, pH, growth factors, and anticancer drug gradients, which generate necrotic and hypoxic, quiescent, and proliferative zones from the inner spheroid core to

the outer surface (Fig. 3.12).¹⁸¹⁻¹⁸⁷ Nowadays, these models have been further developed to allow drug screening in high-throughput formats, and have become an invaluable tool for accelerating translational research and drug discovery. Importantly, not all cells adapted to growth in 2D, grow as 3D spheroids.¹⁸⁶

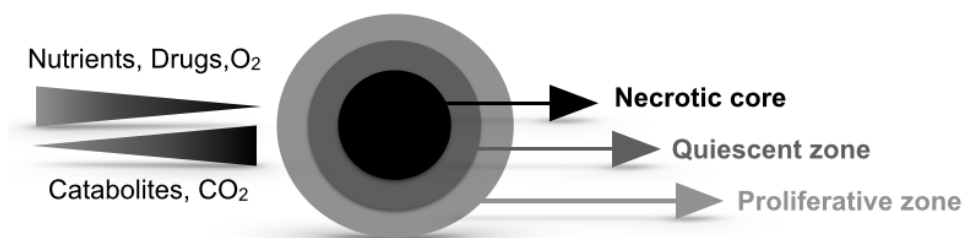


Figure 3.12. Schematic representation of the multicellular spheroid culture model.

Multicellular spheroids can be cultured by two main categories of 3D culture systems: scaffold-based and liquid-based. In the scaffold-based system, cell clusters can be embedded in 3D scaffolds that mimic the extracellular matrix *in vivo*. Hydrogels are the most frequently used cell culture scaffolds, and some examples are matrigel and collagen. A disadvantage for spheroids grown with the support of a matrix is the difficulty to temporally modify the extracellular environment to administer chemicals, such as drugs and growth factors. In this context, liquid-based cultures are advantageous, because the medium exchange allows these temporal modifications. However, careful handling in most systems is necessary due to lack of adherence of the spheroids in the liquid-based cultures. There are four main liquid-based systems available: 1) the “hanging-drop system”, where cells aggregate in a medium-drop to form one single spheroid; 2) “the growth on non-adherent surfaces”, where cells are grown in specially un(coated) plates (ultra-low attachment), or micropatterned plates that prevent attachment; 3) “rotation-based culture method”, such as spinner flasks or rotary cell culture system, which produce a high yield of multicellular spheroids, with variable sizes, by spontaneous cell

Chapter 3 | Synthesis and cytotoxic activity of novel UA derivatives

aggregation and collision; and 4) “microcarrier system”, where seeded cells attach to and aggregate on carriers or beads. All of these methods have their advantages and limitations.^{186,188}

The H460 and H322 NSCLC cell lines are able to spontaneously form spheroid aggregates, using plates with an ultra-low attachment surface that has covalently bonded hydrogel (hydrophilic and uncharged), which minimizes cell attachment, protein absorption, enzyme activation, and cellular activation. The ultra-low attachment multiwell plate selected for the anticancer screening allows the growth of one single multicellular spheroid per well with highly reproducible size. The size of the spheroid can be varied by changing the initial number of cells seeded per well.^{188,189}

The anticancer activity of **UA (3.1)**, fluorolactone derivative **3.2**, and the three most potent synthesized derivatives (**3.15–3.17**) were tested against H460 and H322 cells in a spheroid model using the CellTiter-Glo[®] assay. CellTiter-Glo[®] luminescent cell viability assay is a homogeneous method used to determine the number of viable cells in culture. This assay is based on the quantification of the ATP present, which correlates with metabolically active cells, and hence it is proportional to the number of viable cells present in culture. The reagent induces cell lysis, and simultaneously inhibits endogenous enzymes released during cell lysis (e.g., ATPases), and contains a thermostable luciferase that generates a stable “glow-type” luminescent signal proportional to the amount of ATP present. The luminescent signal reaches a steady state and stabilizes within 10 min after addition of the reagent, and typically glows with a half-life greater than 5 hours. Cell washing, removal of medium, or multiple pipetting steps are not required, as the single reagent can be add directly to cells cultured in a serum-supplemented medium.^{180,190}

A culture medium containing 0.1% DMSO served as negative control. The cell lines were treated with increasing concentrations of each compound, and the IC₅₀ values were determined after 96 h of incubation. The IC₅₀ values are summarized in Table 3.2.

Chapter 3 | Synthesis and cytotoxic activity of novel UA derivatives

Table 3.2. The inhibitory activities (IC_{50}) of **UA**, derivative **3.2**, and the most potent derivatives (**3.15–3.17**) in spheroid model of the H460 and H322 NSCLC cell lines.

Compound	Cell line ^(a) / IC_{50} , μ M			
	H460		H322	
	Monolayer	Spheroid	Monolayer	Spheroid
UA 1	14.8 \pm 0.6	30.8\pm2.8	15.3 \pm 2.8	18.2\pm10.5
3.2	19.3 \pm 2.6	19.5\pm10.4	14.3 \pm 2.7	ND
3.15	4.5 \pm 0.4	3.0\pm1.2	6.8 \pm 1.5	12.1\pm1.7
3.16	5.3 \pm 0.3	5.7\pm0.3	7.3 \pm 1.0	11.6\pm7.4
3.17	2.6 \pm 0.9	5.5\pm0.8	3.3 \pm 0.9	10.0\pm1.2

^(a)Lung cancer cell lines were treated with various concentrations of test compounds for 72 or 96 h for a 2D (monolayer) or 3D (spheroid) model, respectively. The inhibitory activities were determined using CellTiter-Blue[®] or CellTiter-Glo[®] for the 2D or 3D model, respectively. IC_{50} was calculated from the results, and data are presented as means \pm SD of three independent experiments. *ND*: not determined.

The most active derivatives (**3.15–3.17**) showed cytotoxic activity in the spheroid model, although the IC_{50} value increased in most cases, with the exception of compound **3.16**, which presented similar values of IC_{50} in the H460 cell line in both models (Table 3.2). Interestingly, the H322 cell line seemed to be more resistant than the H460 cell line in the spheroid model, as IC_{50} values were higher comparing to the monolayer system. In Figure 3.13 is shown the phenotypic effects of **UA (3.1)** and derivative **3.17** in the spheroid model for the H460 cell line at 96 h of treatment.

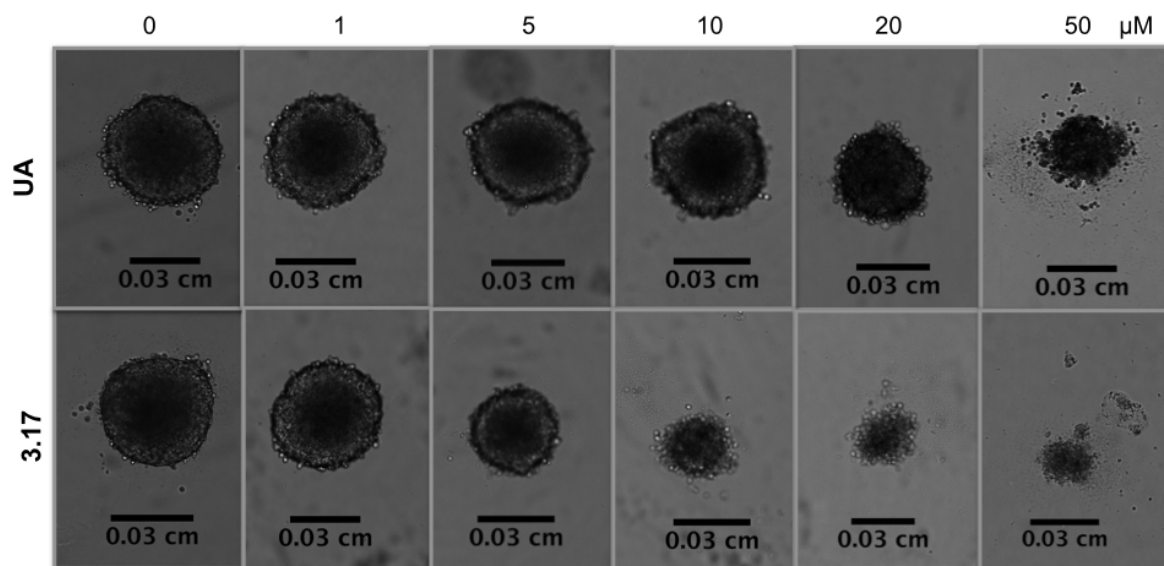


Figure 3.13. Phenotypic changes in the H460 spheroid model treated with **UA** (top panel) and **3.17** (bottom panel) for 96 h. Spheroids were treated with the indicated concentrations of **UA** and derivative **3.17**. Images were captured using a bright field phase-contrast microscope.

The molecular mechanism underlying the anticancer activity of the most active derivative **3.17** was further investigated.

3.2.2.2. Effect of compound **3.17** on cellular DNA, RNA, and protein synthesis

The [³H]thymidine, [³H]uridine, and [³H]leucine incorporation assays allow measurement of the effects of a compound in the DNA, RNA, and protein synthesis rates of cells, respectively. Although DNA and protein syntheses were not affected by treatment with compound **3.17**, as observed by the levels of thymidine and leucine, the RNA (uridine) synthesis was decreased to 65% and 60% at 24 and 48 h, respectively (Fig. 3.14).

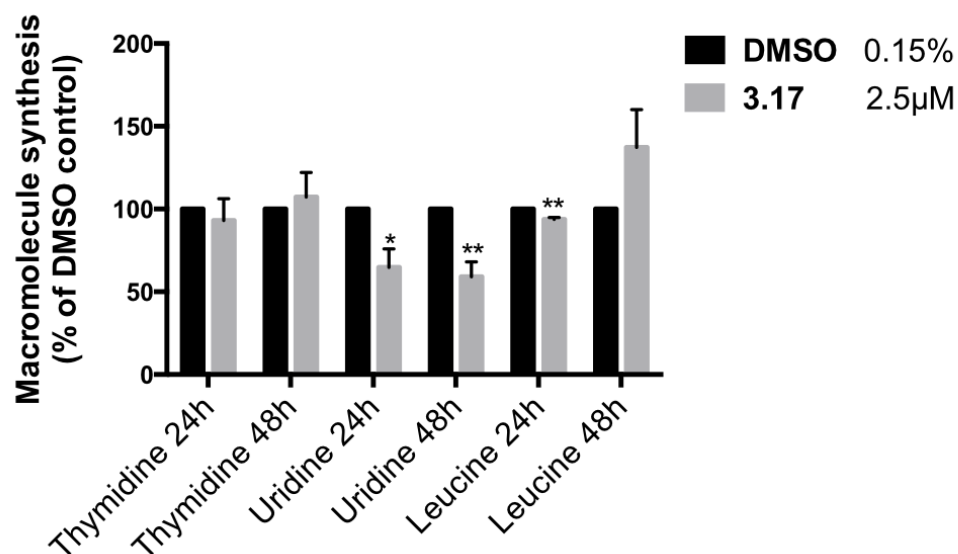


Figure 3.14. Effect of compound **3.17** treatment on the global DNA, RNA, and protein synthesis in the H460 cell line. Cells treated with vehicle or compound **3.17** at the indicated concentrations for 24 and 48 h were assessed for macromolecule synthesis. Values represent the means \pm SD of three independent experiments. p-Values obtained by comparing vehicle and treatment are presented as * <0.05 , ** <0.01 .

3.2.2.3. Effect of compound **3.17** on the cell cycle distribution

The effect of compound **3.17** on the cell cycle distribution was explored. H460 cells were treated with DMSO (0.15%), or compound **3.17** (3.5 or 4 μ M) for 24 and 72 h, and the cell cycle profile was evaluated by FACS analysis after staining cells with propidium iodide (PI). Treatment of H460 cells with compound **3.17** did not affect the population of cells at any cell cycle phase, at any concentration or time point studied (Fig. 3.15), suggesting that compound **3.17** does not affect the cell cycle profile.

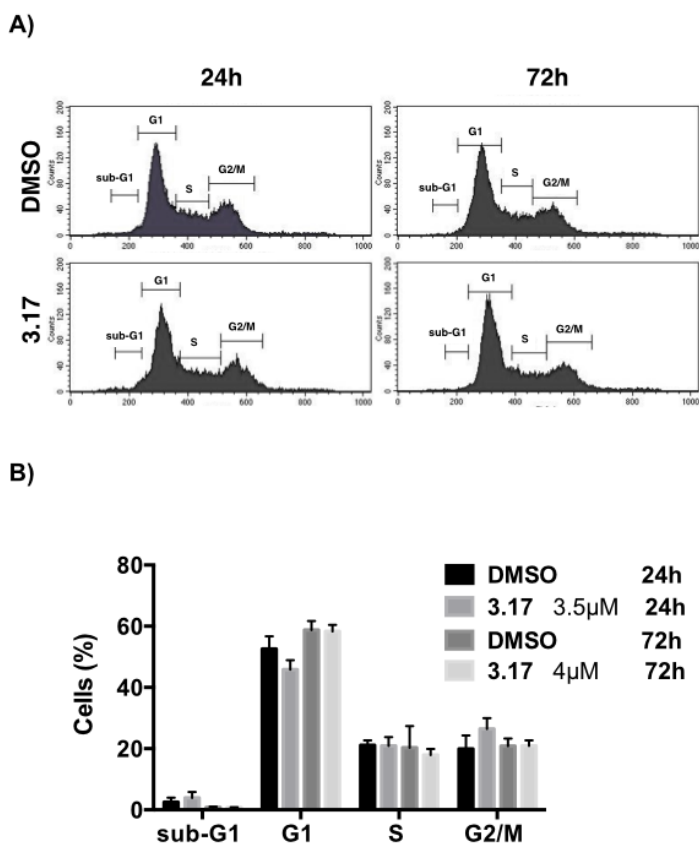


Figure 3.15. Effect of compound **3.17** on the cell cycle distribution. H460 cells treated with vehicle or compound **3.17** at the indicated concentrations for 24 and 72 h were assessed for cell cycle, using PI staining and flow cytometer analysis. A) Representative histograms of cell cycle analysis are shown. B) The bar graphic depicts the cell population (%) per cell cycle phase. The values represent the mean \pm SD of three independent experiments.

3.2.2.4. Effect of compound **3.17** on gene expression profile

The effect of compound **3.17** on the gene expression in the H460 cell line was analyzed on a genome-wide scale using Affymetrix Human Transcriptome Array 2.0 (HTA 2.0) system. This microarray platform was designed to evaluate not only differentially expressed genes but also alternative splicing events. For this purpose, H460 cells were treated with DMSO (0.15%), or compound **3.17** (3.5 μ M) for 24 h. For the gene expression analysis, Transcriptome Analysis

Console software (Affymetrix) was used to detect the differentially expressed genes, and the main pathways affected, using DMSO-treated cells as control.

Taking into account that the parent compound **UA** is considered a multifunctional agent and the derivatives described in the literature seem to preserve that property, an effort was made to identify the main pathways that could be responsible for the anticancer activity of compound **3.17**.

According to the HTA 2.0 microarray data, apoptosis and autophagy pathways were activated upon treatment of H460 cells with compound **3.17** at 24 h, and hence these two pathways were selected for further evaluation.

3.2.2.5. Apoptosis-inducing effect of compound 3.17 evaluated by annexin V-Cy5/PI assay

In the earliest stages of apoptosis, the plasma membrane loses its symmetry and the membrane phospholipid phosphatidylserine (PS) is translocated from the inner to the outer leaflet of the membrane, exposing PS to the external environment. Annexin V-Cy5 has a high affinity for PS and binds to the exposed apoptotic cell surface PS, thus allowing the quantitative assessment of apoptosis. In the late stages of apoptosis, the membrane loses its integrity and PI can enter the cell.¹⁹¹

Treatment of H460 cells with compound **3.17** at 5 μ M for 72 h led to an increased number of apoptotic cells, from 4.9% to 42.5% in treated cells (i.e., 13.4% of early apoptotic cells and 29.1% of late apoptotic cells) (Fig. 3.16). Concomitantly, the percentage of live cells decreased to 94.0% in the control and to 51.9% in treated cells. These results suggest that compound **3.17** at 5 μ M induces apoptosis in H460 cells (Fig. 3.16).

Chapter 3 | Synthesis and cytotoxic activity of novel UA derivatives

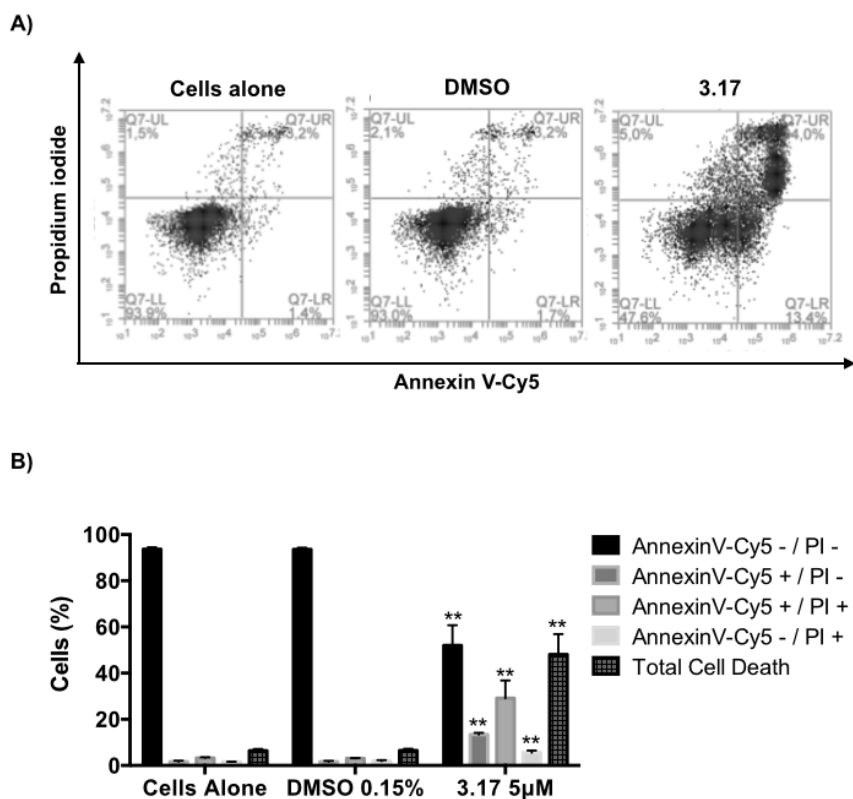


Figure 3.16. Induction of H460 cell death by compound **3.17**. Annexin V-Cy5/PI assay of H460 cells untreated, treated with vehicle, or treated with compound **3.17** at the indicated concentration for 72 h. A) Representative flow cytometric plots for the quantification of apoptosis are shown: the lower left quadrant (annexin V- and PI-) represents non-apoptotic cells, the lower right quadrant (annexin V+ and PI-) represents early apoptotic cells, the upper right quadrant (annexin V+ and PI+) represents the late apoptotic/necrotic cells, and the upper left quadrant (annexin V- and PI+) represents necrotic cells. B) The bar graph depicts the variation of the percentages of live, early apoptotic, late apoptotic, necrotic cells, and total cell death. Values represent the means \pm SD of three independent experiments. p-Values obtained by comparing vehicle and treatment are presented as * <0.05 , ** <0.01 .

3.2.2.6. Effect of compound 3.17 on the levels of apoptosis-related proteins

To gain a deeper insight into the mechanism of compound 3.17-induced apoptosis, the levels of some apoptosis-related proteins were evaluated by immunoblot analysis. Therefore, H460 and H322 cells were treated with increasing concentrations of compound 3.17 for 24 h (Fig. 3.17).

The activation of caspases is one of the fundamental mediators of apoptosis and the proteolytic cleavage of PARP, particularly by caspase-3 and caspase-7, is another characteristic event of apoptosis.¹¹ As shown in Figure 3.17, treatment of H460 cells with compound 3.17 induced cleavage of full-length PARP, as well as cleavage of procaspase-8 and procaspase-7 into their active forms (Fig. 3.17A and 3.17B). However, the level of procaspase-3 was decreased by only 29% at the higher concentration of 4.5 μ M (Fig. 3.17B). Whilst compound 3.17 did not seem to significantly alter the levels of procaspase-9 (data not shown), the significant increase in the level of activated caspase-8 suggests that compound 3.17 induces apoptosis mainly through the extrinsic pathway. Increases in the cleaved levels of PARP and procaspase-7 were also observed when the H322 cell line was treated with compound 3.17 (Fig. 3.17C).

The levels of Bcl-2 and Mcl-1, two proteins from the Bcl-2 family, were also explored. Bcl-2 protein serves as an anti-apoptotic effector, whereas Mcl-1 can occur in two alternative splicing variants, a longer (Mcl-1_L) and a shorter (Mcl-1_S) gene product, with the first one acting as an anti-apoptotic effector and the shorter as a pro-apoptotic effector.^{11,192} As depicted in Figures 3.17A and 3.17B, the treatment of H460 cells with compound 3.17 caused downregulation of Bcl-2 and both isoforms of Mcl-1 in a concentration-dependent manner.

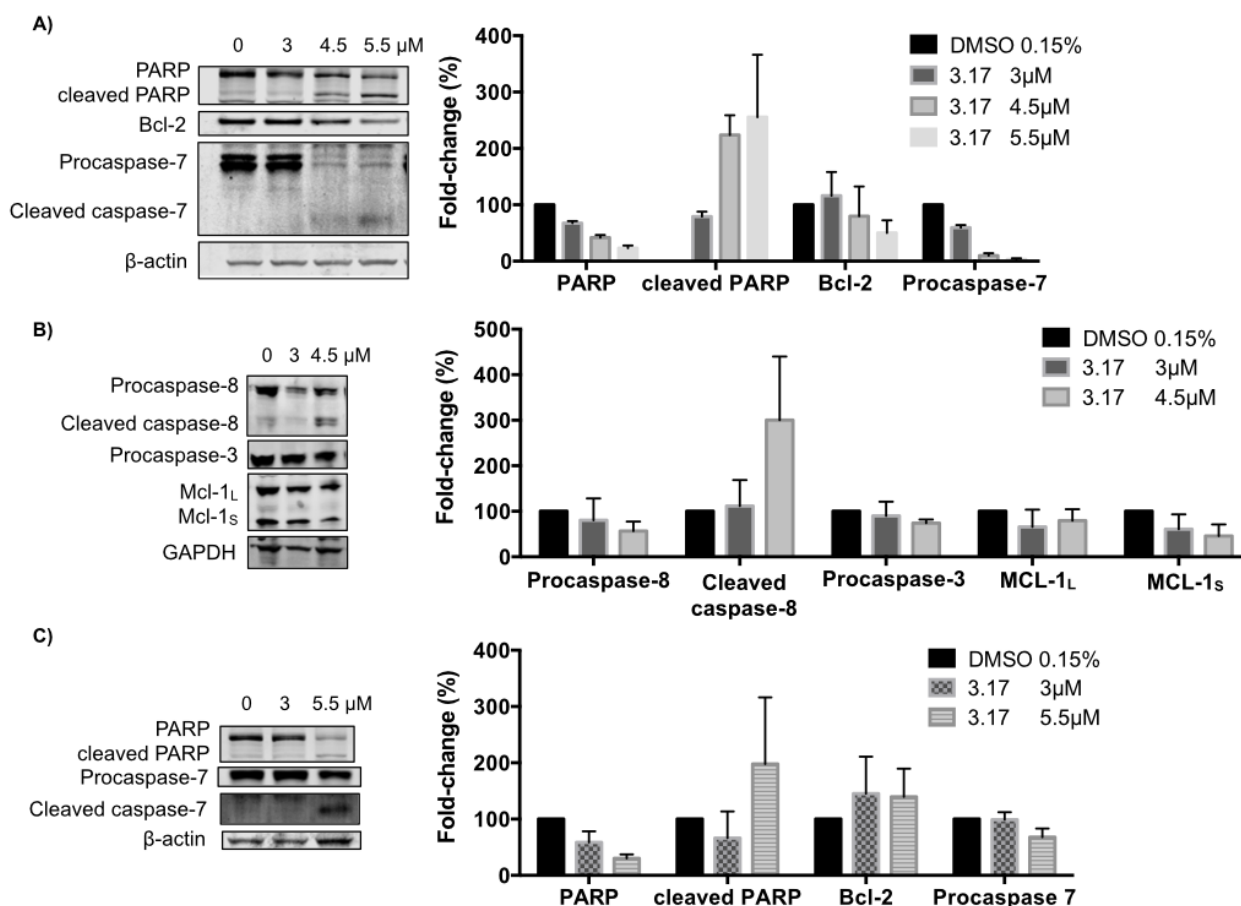


Figure 3.17. Effect of compound **3.17** on the levels of apoptosis-related proteins. H460 cells (A-B) and H322 cells (C) were treated with compound **3.17** at the indicated concentrations for 24 h. The levels of the indicated proteins were analyzed by Western blot. β -Actin or GAPDH was used as loading control. The bar graph depicts the variation of the levels of the protein expression. Values are the means \pm SD of three independent experiments.

3.2.2.7. Effect of compound 3.17 treatment on autophagy

Autophagy is characterized by the formation of acidic vesicular organelles (AVO), which can be detected by staining with acridine orange, a dye that accumulates in acidic organelles.¹⁹³ Measurement of this dye by flow cytometry was used to detect AVO formation in H460 cells treated with vehicle (0.15% DMSO), or compound **3.17** (3 μ M or 4 μ M) for 72 h. Bafilomycin A1, a known inhibitor of the late phase of autophagy, was used as a negative control to block acidic vesicular formation. Bafilomycin A1 prevents maturation of autophagic vacuoles by inhibiting

Chapter 3 | Synthesis and cytotoxic activity of novel UA derivatives

fusion between autophagosomes and lysosomes, through its inhibition of vacuolar H⁺-ATPase.^{194,195}

As depicted in Figure 3.18A, bafilomycin A1 inhibited the fusion of autophagosomes with lysosomes. Endogenous autophagy level (DMSO treatment) was less than 10% at 72 h (Fig. 3.18A and 3.18B). Treatment with compound **3.17** significantly increased the formation of AVO at 4 μ M (Fig 3.18A and 3.18B). These data suggest that compound **3.17** is able to induce autophagy in H460 cells.

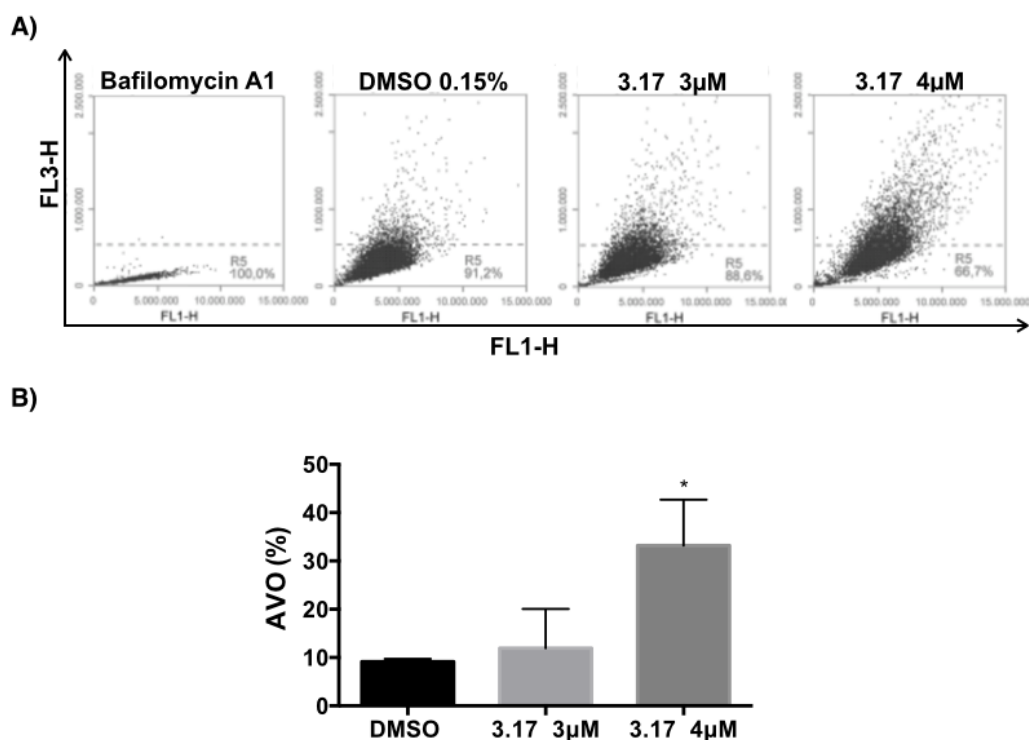


Figure 3.18. Effect of compound **3.17** treatment on induction of autophagy in the H460 cell line. A) The formation of acidic vascular organelles (AVO) was measured by acridine orange staining and flow cytometry. Representative flow cytometric plots of the percentage of AVO formation (acridine orange staining positive) of three independent experiments are shown. B) The graph bar depicts the variation of the percentage of AVO formation (acridine orange staining) and is plotted as means \pm SD of three independent experiments. p-Values obtained by comparing vehicle and treatment are presented as * <0.05 .

Chapter 3 | Synthesis and cytotoxic activity of novel UA derivatives

Under some conditions, autophagy contributes to cellular survival by providing nutrients and energy to help cells adapt to starvation or stress (such as hypoxia and anticancer drugs). However, under other conditions, activated autophagy leads to cell death.²⁹ In order to understand whether autophagy was being induced as a survival response of cells to treatment with compound **3.17**, an autophagy inhibitor, chloroquine, was used to evaluate whether the inhibition would alter the cytotoxic effect of compound **3.17**. H460 cells were treated with vehicle (0.15% DMSO), 20 μ M chloroquine (Chl), 4 μ M compound **3.17**, or a combination of Chl and compound **3.17** at the indicated doses for 72 h. As shown in Figure 3.19A and 3.19B, the inhibition of autophagy did not affect the total cell death induced by treatment with compound **3.17**. These data suggest that autophagy is not being induced as a resistance mechanism against treatment with compound **3.17** but might be induced as part of the anticancer mechanism of compound **3.17**.

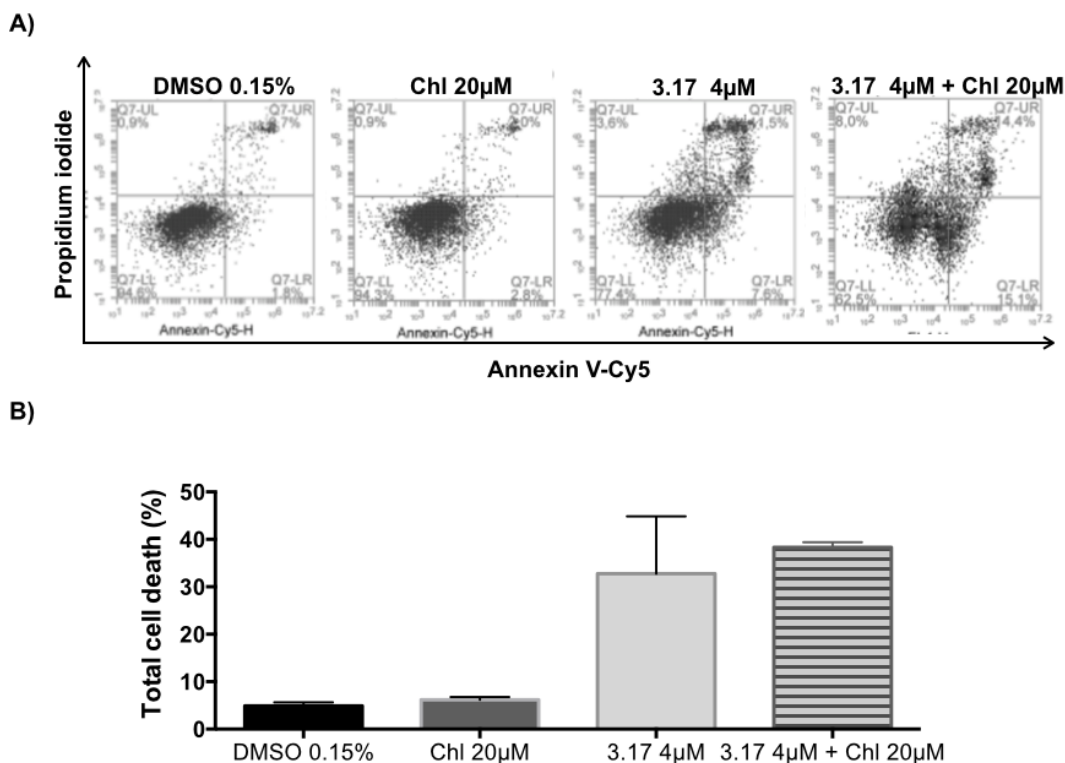


Figure 3.19. Effect of autophagy inhibition on **3.17**-induced cell death. A) Annexin V-Cy5/PI assay of H460 cells treated with vehicle, 20µM chloroquine (Chl), 4 µM compound **3.17**, or the combination of chloroquine and compound **3.17**, at the indicated concentrations for 72 h. Representative flow cytometric plots for the quantification of apoptosis are shown. B) The bar graph depicts the variation of the percentage total cell death. No statistical difference was observed comparing cells treated with compound **3.17** alone or in combination with chloroquine. Values represent the means ± SD of three independent experiments.

3.2.2.8. Effect of compound **3.17** on the levels of autophagy-related proteins

To gain a deeper insight into the mechanism of compound **3.17**-induced autophagy, the levels of some key autophagy-related proteins were evaluated by immunoblot analysis. Therefore, H460 and H322 cells were treated with increasing concentrations of compound **3.17** for 24 h (Fig. 3.20).

Chapter 3 | Synthesis and cytotoxic activity of novel UA derivatives

The mammalian target of rapamycin (mTOR) is a major negative regulator of autophagy¹⁹⁶. As shown in Figure 3.20A, mTOR was decreased upon treatment with compound **3.17**. Beclin-1 is a central regulator of autophagy that forms a complex with vacuolar protein Vps34 and serves as a platform for recruitment of other autophagy-related genes (Atgs) that are critical for phagosome formation.¹⁹⁶ As depicted in Figure 3.20A, the expression of Beclin-1 protein in H460 cells increased upon treatment with compound **3.17**. Interestingly to note, Beclin-1 activity in autophagy is inhibited by interaction with Bcl-2 protein, which was decreased upon treatment with compound **3.17** (Fig. 3.17A).

Upon autophagy initiation, LC3A/B is cleaved and lipidated to form LC3A/B-II, which is bound to autophagosomes. Consequently, LC3A/B conversion (LC3A/B-I to LC3A/B-II) is correlated with autophagosome formation and it is commonly used to monitor autophagy.¹⁹⁷ Treatment with compound **3.17** resulted in lipidation of LC3A/B-I to LC3A/B-II as shown by the increase of a lower band (around 17 kDa) in a dose-dependent manner in both cell lines (Fig. 3.20).

The p62 protein is an ubiquitin-binding protein that functions as a receptor for cargos destined to be degraded by the cellular autophagic machinery. When autophagy is induced, the p62 protein is localized to the autophagosomes and subsequently degraded.¹⁹⁶ Downregulation of the p62 protein was observed upon treatment with compound **3.17** (Fig. 3.20). Because p62 is selectively incorporated into the autophagosomes and is specifically degraded during autophagy, the total cellular expression of p62 was inversely correlated with autophagic activity.

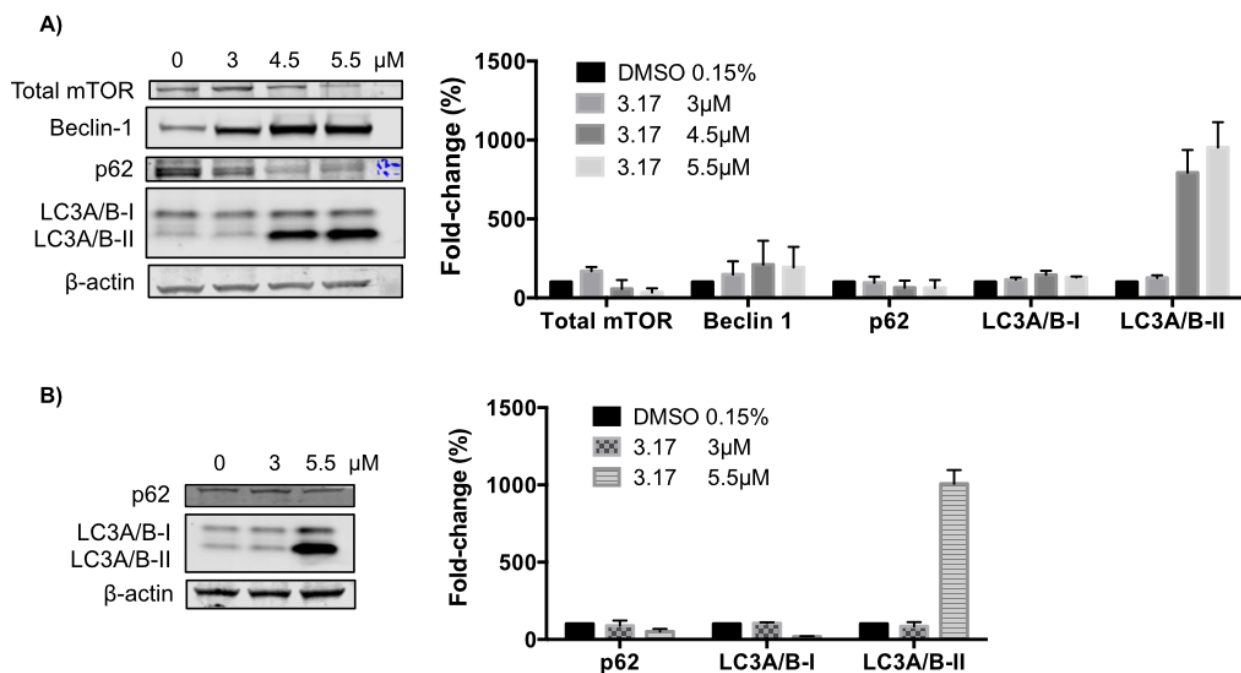


Figure 3.20. Effect of compound **3.17** on the levels of autophagy-related proteins. H460 cells (A) and H322 cells (B) were treated with compound **3.17** at the indicated concentrations for 24 h. The levels of the indicated proteins were analyzed by Western blot. β -Actin was used as loading control. The bar graph depicts the variation of the levels of the protein expression. Values represent the means \pm SD of three independent experiments.

3.2.2.9. Proposed mechanism of action

Several articles in the literature have reported the apoptosis- and autophagy-inducing properties of **UA**, in different cancer cell lines and involving different mechanisms of action.^{67,89} Moreover, the **UA** derivatives synthesized seem to preserve the ability to induce apoptosis, through different pathways.⁶⁷ Compound **3.17** appear to inherit the multitarget potential of **UA** and the ability to induce apoptosis and autophagy. Interestingly, while **UA** is able to induce both caspase-8 and caspase-9, compound **3.17** only induced the extrinsic pathway by activation of caspase-8.

Taking together, these results are in accordance with the reverse-phase protein array (RPPA) data, in which Beclin-1, LC3A/B-II, Atg7 and Atg3— proteins involved in the autophagy

Chapter 3 | Synthesis and cytotoxic activity of novel UA derivatives

pathway—were found upregulated by 5.6, 10.7, 4.5, and 5.1%, respectively, upon treatment of the H460 cell line with 3.5 μM compound **3.17** for 24 h.

mTOR regulates the level of S6 kinase, an enzyme partially responsible for ribosomal protein S6 phosphorylation and activation.^{198,199} It was also observed in the RPPA data decreases of 11.7 and 8.4% in phosphorylated levels of S6 at S235/236 and S240/S44, respectively. eIF4E is negatively regulated by mTOR.^{198,199} The phosphorylated level of eIF4E at S209 was upregulated upon treatment with compound **3.17**. These two targets of mTOR are also involved with autophagy, protein synthesis control, cell size, and ATP levels.^{198,199} H460 cells treated with compound **3.17** (2.5 μM and 4 μM) for 24, 48, and 72 h did not display significant differences in cell size between control and treatment. The cell size decrease associated with S6K activity may depend on the cell type and isoform affected.

Taking into account these cumulative results of the apoptosis and autophagy studies, a possible mechanism of action for compound **3.17** in the H460 cell line is shown in Figure 3.21.

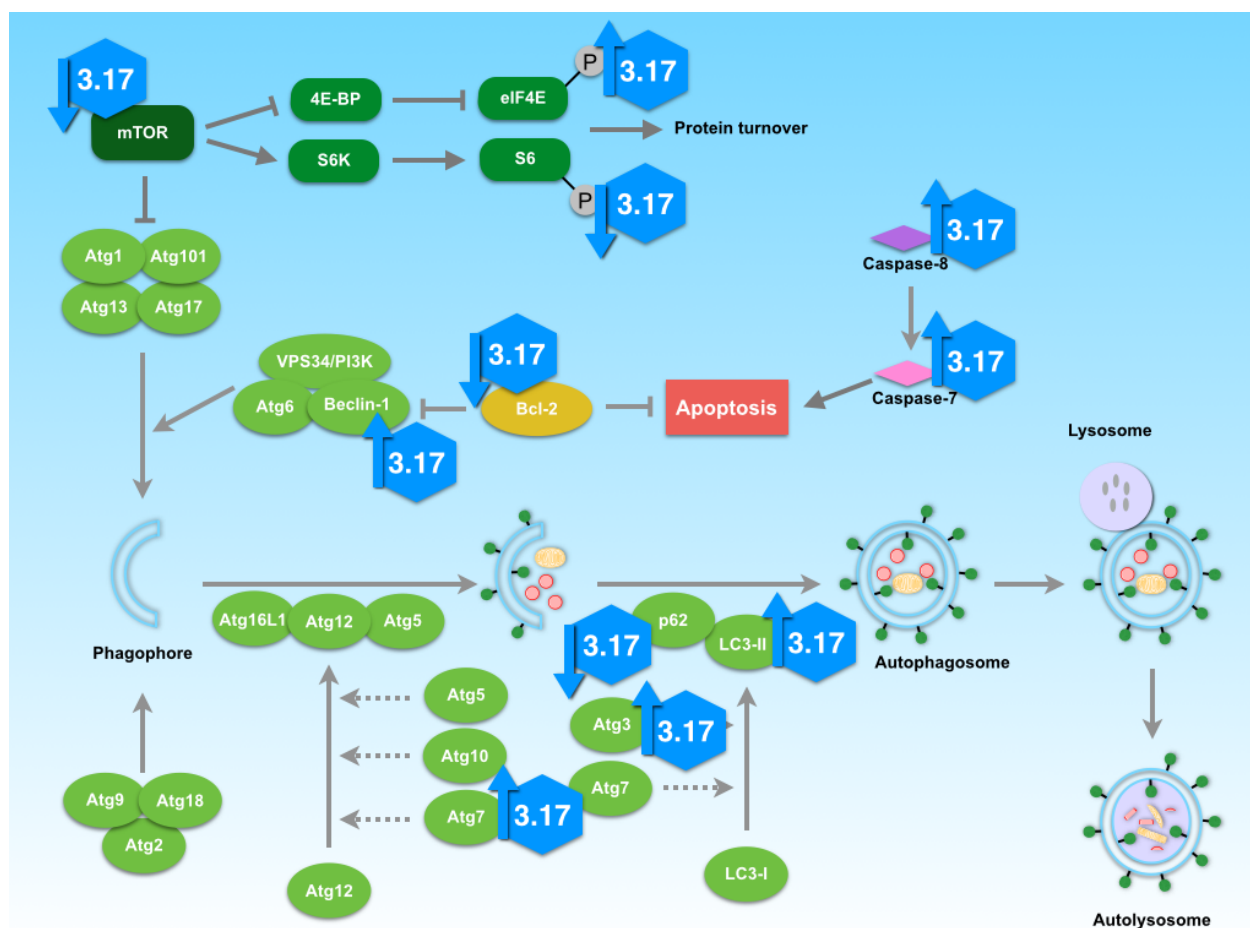


Figure 3.21. Possible anticancer mechanism of compound 3.17. Treatment of the H460 cell line with compound 3.17 showed induction of apoptosis and autophagy.

3.3. Conclusion

In this chapter, a panel of A-ring modified **UA** derivatives was synthesized and screened for anticancer activity in NSCLC cell lines using 2D and 3D culture models.

The structure-activity relationship (SAR) study based on the anticancer activity against NSCLC cell lines in the 2D model showed that the fluorolactone moiety was not critical to the cytotoxic activity of the newly synthesized derivatives, the formation of a seven-membered A-ring decreased the activity, and the cleavage of A-ring did not improved the activity. Analyzing the A-

Chapter 3 | Synthesis and cytotoxic activity of novel UA derivatives

ring cleaved derivatives, the presence of an unsaturation at C4(23) position did not seem to contribute to the cytotoxic activity, whereas the substitution at C3 had a dramatic influence on biological activity. Comparing the amide derivatives, the secondary amide with a more bulky side chain displayed a pronounced decrease in cytotoxic activity, whereas the presence of a secondary amide with a small alkyl side chain led to the most active compounds, with compound **3.17** being five times more potent than the parent compound in all cell lines.

The most active compounds (**3.15–3.17**) were active in both monolayer and spheroid culture models, with little change in their IC₅₀ value.

Compound **3.17** was selected for further mechanistic studies. The preliminary mechanism of action indicated that compound **3.17** is able to induce apoptosis via activation of caspase-8 and caspase-7, cleavage of PARP, and modulation of Bcl-2 in both NSCLC cell lines studied. Autophagy was also induced by treatment with compound **3.17** and could be a consequence of the decreased Bcl-2 levels, because this protein acts as an inhibitor of Beclin-1, an important regulator of autophagy activation. Given its activity and mechanism of action, this compound might represent a promising lead for the development of new anticancer agents for NSCLC.

3.4. Experimental section

3.4.1. Chemistry

3.4.1.1. General

Ursolic acid, Selectfluor[®], chromium(VI) oxide (CrO₃), sodium azide (NaN₃), *meta*-chloroperbenzoic acid (*m*-CPBA) 77%, *para*-toluenesulfonic acid monohydrate, aniline, phenethylamine, 4-methylbenzylamine, 4-fluorobenzylamine, 2-methoxyphenethylamine, 2-(3-

Chapter 3 | Synthesis and cytotoxic activity of novel UA derivatives

chlorophenyl)ethylamine, methylamine solution (33 wt. % in absolute ethanol), ethylamine solution (2.0 M in THF), propylamine, dioxane, nitromethane, triethylamine (Et₃N), oxalyl chloride, hydrochloric acid (HCl), sulfuric acid (H₂SO₄), and glacial acetic acid were purchased from Sigma-Aldrich Co.

T3P (50 wt. % in THF) was obtained as a free sample from Archimica GmbH, Frankfurt, Germany.

The reaction and workup solvents were purchase from VWR Portugal, and were of analytical grade. All the solvents used in the reactions were previously purified and dried according to the literature procedures.

Ammonium (25% aqueous solution), sodium chloride (NaCl), sodium sulfite (Na₂SO₃), sodium sulfate (Na₂SO₄), sodium bicarbonate (NaHCO₃), and sodium carbonate (Na₂CO₃) were purchased from Merck Co.

Thin-layer chromatography (TLC) analysis was performed in Kieselgel 60HF254/Kieselgel 60G. Separation and purification of compounds by flash column chromatography (FCC) was performed using Kieselgel 60 (230–400 mesh, Merck).

Melting points (Mp) were measured using a BUCHI melting point B-540 apparatus and are uncorrected.

IR spectra were recorded on a Fourier transform spectrometer.

¹H, ¹³C and DEPT-135 NMR spectra were recorded on a Bruker Digital NMR-Avance 400 apparatus spectrometer. The chemical shifts (δ) were reported in parts per million (ppm), using δ 7.26 (¹H NMR) and δ 77.16 (¹³C NMR) of CDCl₃ as internal standard. The coupling constants (J) were recorded in hertz (Hz).

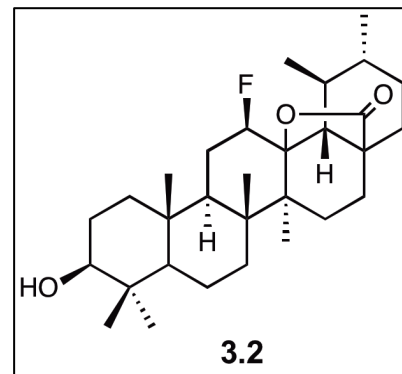
The mass spectrometry (MS) was performed using a Quadrupole/Ion Trap Mass Spectrometer (QIT-MS) (LCQ Advantage MAX, Thermo Finnigan).

Elemental analysis was performed by chromatographic combustion using an Analyser Elemental Carlo Erba 1108.

3.4.1.2. Synthetic procedures

3 β -Hydroxy-12 β -fluor-urs-13,28 β -olide (3.2): This compound was prepared from **UA (3.1)**

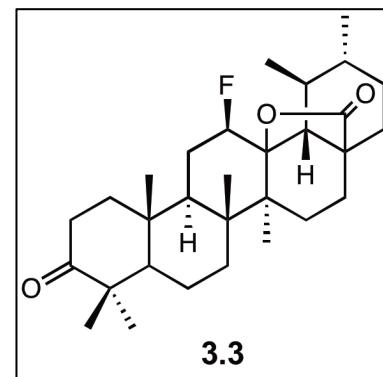
according to a previously described method¹³⁹ to give **3.2** as a white solid (80.2%). Mp 316.8 – 317.6 °C. ¹H NMR (400 MHz, CDCl₃): δ = 4.85 (dt, J = 45.6, 8.8 Hz, 1H, H-12), 3.20 (dd, J = 11.4, 4.8 Hz, 1H, H-3), 1.21 (s, 3H), 1.20 (s, 3H), 1.13 (d, J = 6.2 Hz, 3H), 0.97 (s, 3H), 0.96 (d, J = 5.5 Hz, 3H), 0.91 (s, 3H), 0.77 (s, 3H); ¹³C NMR (100 MHz, CDCl₃): δ = 178.88 (C28),



91.97 (d, J = 14.2 Hz, C13), 88.70 (d, J = 185.8 Hz, C12), 78.68 (C3), 55.32, 52.55 (d, J = 3.6 Hz), 49.18 (d, J = 9.1 Hz), 45.19, 43.90 (d, J = 2.8 Hz), 42.53, 39.53, 39.03, 38.84, 38.40, 37.12, 33.95, 31.34, 30.71, 27.92, 27.62, 27.22, 25.37 (d, J = 19.7 Hz), 22.39, 19.39, 18.50, 17.65, 17.22, 16.65, 16.46, 15.26. MS (DI-ESI) (m/z): 475.0 (100%) [$M+H$]⁺, 455.2 (17.5%).

3-Oxo-12 β -fluor-urs-13,28 β -olide (3.3): Prepared from **3.2** according to a previously described

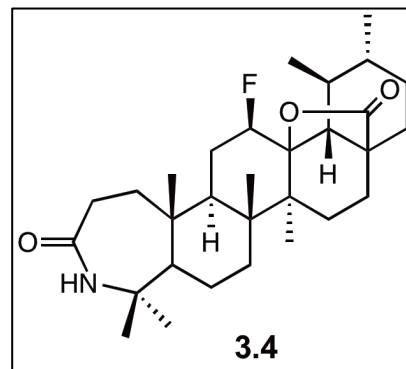
method¹³⁹ to give **3.3** as a white solid (24.4%). Mp 325.3 – 328.2 °C. ¹H NMR (400 MHz, CDCl₃): δ = 4.87 (dq, J = 46.0, 8.3 Hz, 1H, H-12), 2.60 – 2.52 (m, 1H), 2.48 – 2.41 (m, 1H), 1.26 (s, 3H), 1.21 (s, 3H), 1.14 (d, J = 6.2 Hz, 3H), 1.09 (s, 3H), 1.04 (s, 3H), 1.03 (s, 3H), 0.97 (d, J = 5.5 Hz, 3H). ¹³C NMR (100 MHz, CDCl₃): δ = 216.97 (C3), 178.75 (C28), 91.91 (d, J =14.27, C13),



89.49 (d, J = 185.77 C12), 54.83, 52.57, 48.48 (d, J = 9.33), 47.28, 45.19, 44.02 (d, J = 3.09), 42.40, 39.79, 39.55, 38.51, 36.85, 33.89, 33.37, 31.33, 30.73, 27.64, 26.58, 25.75 (d, J = 19.71), 22.39, 20.97, 19.40, 18.99, 18.17, 17.09, 16.47, 16.42. MS (DI-ESI) (m/z): 473.0 (100%) [$M+H$]⁺, 453.2 (44.3%).

Chapter 3 | Synthesis and cytotoxic activity of novel UA derivatives

3-Oxo-4-aza-A-homo-12 β -fluor-urs-13,28 β -olide (3.4): To a stirred mixture of **3.3** (250 mg, 0.53 mmol) in glacial acetic acid (7.5 ml) at 65 °C, concentrated sulfuric acid (75 μ l) was added. To this mixture, NaN₃ (125 mg, 1.92 mmol) was added in parts over 15 min, and then the temperature was stabilized at 30 °C. After 5 h, cold 5% Na₂CO₃ aqueous solution (100 ml) was added to the reaction mixture until pH 6–7. The resulting mixture was



extracted with CHCl₃ (2 × 200 ml). The subsequent organic phase was washed with water (200 ml), and 10% NaCl aqueous solution (200 ml), dried over Na₂SO₄, filtered, and evaporated to dryness. The residue was purified by flash column chromatography (petroleum ether:ethyl acetate 1:1 – 1:4) to give **3.4** as a slight yellow solid (68.6%). Mp 353.4 – 355.4 °C. IR (KBr): ν = 3220.54, 2977.55, 2931.27, 2871.48, 1774.19, 1666.2, 1457.92, 1392.35, 1184.08, 1120.44, 939.16 cm⁻¹. ¹H NMR (400 MHz, CDCl₃): δ = 5.60 (s, 1H, NH), 4.82 (dm, 1H, H-12), 2.56 – 2.50 (m, 1H, H-2), 2.39 – 2.34 (m, 1H, H-2), 1.30 (s, 3H), 1.25 (s, 3H), 1.21 (s, 3H), 1.18 (s, 3H), 1.12-1.10 (6H), 0.94 (d, J = 5.0 Hz, 3H); ¹³C NMR (100 MHz, CDCl₃): δ = 178.77 (C28), 175.94 (CON), 92.03 (d, J = 14.6 Hz, C13), 89.73 (d, J = 186.4 Hz, C12), 56.17, 52.98, 52.72 (d, J = 3.6 Hz), 49.79 (d, J = 9.5 Hz), 45.36, 44.17 (d, J = 2.9 Hz), 42.44, 40.26, 39.90, 39.65, 38.75, 33.63, 33.43, 32.06, 31.42, 30.86, 27.65, 27.42, 26.30 (d, J = 19.8 Hz), 22.47, 21.99, 19.49, 19.00, 18.01, 16.99, 16.53. MS (DI-ESI) (m/z): 488.4 (100%) [M-H]⁺. Anal. Calcd for C₃₀H₄₆FNO₃: C, 73.88; H, 9.51; N, 2.87. Found: C, 73.75; H, 9.51; N, 2.91.

Chapter 3 | Synthesis and cytotoxic activity of novel UA derivatives

3-Oxo-4-oxa-A-homo-12 β -fluor-urs-13,28 β -olide (3.5): To a stirred mixture of **3.3** (300 mg,

0.63 mmol) in CHCl₃ (10 ml), protected from light and at r.t.,

m-CPBA 77% (329 mg, 1.47 mmol) was added. Additional *m*-

CPBA 77% was added (329 mg, 1.90 mmol, e.a.) at 24 and

48 h. After 120 h, the reaction mixture was diluted with CHCl₃

(10 ml) and washed with 5% Na₂SO₃ aqueous solution (20

ml). The aqueous solution was extracted with CHCl₃ (2 × 50

ml). The resulting organic phase was washed with 10% NaHCO₃ aqueous solution (50 ml),

water (50 ml), and 10% NaCl aqueous solution (50 ml), dried over Na₂SO₄, filtered, and

evaporated to dryness. The residue was purified by flash column chromatography

(toluene:diethyl ether 2:1 – 1:3) to give **3.5** as a white solid (66.6%). Mp 240.5 – 243.5 °C. IR

(KBr): ν = 2971.77, 2931.27, 2875.34, 1764.55, 1731.76, 1457.52, 1392.35, 1280.50, 1147.44

cm⁻¹. ¹H NMR (400 MHz, CDCl₃): δ = 4.83 (dq, *J* = 45.6, 8.3 Hz, 1H, H-12), 2.70 – 2.62 (m, 1H,

H-2), 2.57 – 2.51 (m, 1H, H-2) 1.48 (s, 3H), 1.40 (s, 3H), 1.27 (s, 3H), 1.20 (s, 3H), 1.15 (s, 3H),

1.12 (d, *J* = 6.3 Hz, 3H), 0.97 (d, *J* = 5.6 Hz, 3H); ¹³C NMR (100 MHz, CDCl₃) δ = 178.74 (C28),

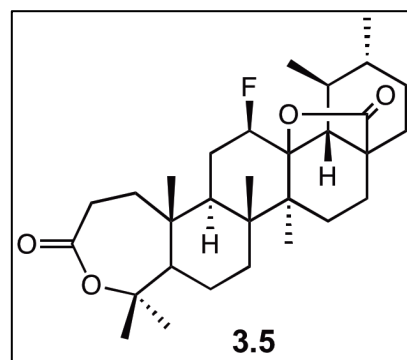
174.74 (C3), 92.02 (d, *J* = 14.1 Hz, C13), 89.51 (d, *J* = 186.5 Hz, C12), 85.80 (C4), 53.01, 52.74

(d, *J* = 3.6 Hz), 49.79 (d, *J* = 9.3 Hz), 45.38, 44.24 (d, *J* = 2.7 Hz), 42.31, 40.34, 39.68, 39.55,

38.82, 33.33, 32.33, 31.43, 31.20, 30.88, 27.68, 26.77, 26.40 (d, *J* = 19.9 Hz), 22.91, 22.48,

19.50, 19.09, 17.78, 16.98, 16.52. MS (DI-ESI) (*m/z*): 489.1 (100%) [M+H]⁺, 469.3 (26%). Anal.

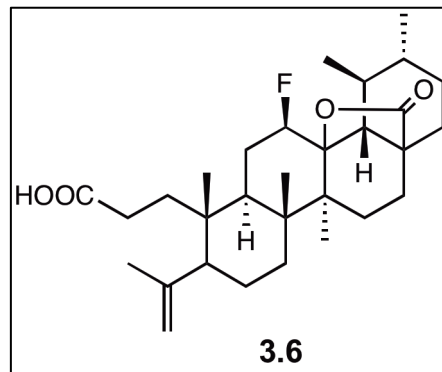
Calcd. For C₃₀H₄₅FO₄·0.2H₂O: C, 73.19; H, 9.3. Found: C, 72.99; H, 9.3.



Chapter 3 | Synthesis and cytotoxic activity of novel UA derivatives

3,4-Seco-4(23)-en-12 β -fluor-urs-13,28 β -olid-3-oic acid (3.6): To a mixture of **3.5** (475 mg,

0.97 mmol) in CH₂Cl₂ (30 ml), at r.t., *p*-toluenesulfonic acid monohydrate (1.56 g, 7.89 mmol) was added. After 24 h, the mixture was diluted with CH₂Cl₂ (20 ml) and water (20 ml). The aqueous phase was extracted twice with CH₂Cl₂ (50 ml). The organic phase was washed with 5% NaHCO₃ aqueous solution (2 × 50 ml), water (50 ml), and 10% NaCl

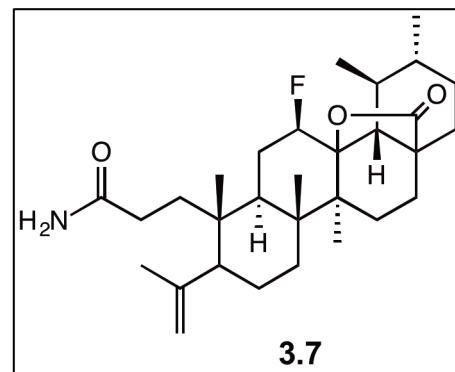


aqueous solution, dried over Na₂SO₄, filtered, and evaporated to dryness. The residue was purified by flash column chromatography (petroleum ether:ethyl acetate 5:1 – 3:1) to give **3.6** as a white solid (68.4%). Mp 230 – 234.6 °C. IR (KBr): ν = 3284.18, 3068.19, 2979.48, 2948.63, 2923.56, 2875.34, 1764.55, 1741.41, 1704.76, 1633.41 1459.85, 1392.35, 1189.86, 1143.58, 937.23 cm⁻¹. ¹H NMR (400 MHz, CDCl₃): δ = 4.88 (s, 1H, H-23), 4.83 (dm, 1H, H-12), 4.67 (s, 1H, H-23), 2.44 – 2.37 (m, 1H, H-2), 2.25 – 2.17 (m, 1H, H-2), 1.73 (3H, H-24), 1.26 (s, 3H), 1.21 (s, 3H), 1.14 (d, *J* = 6.3 Hz, 3H), 0.96 (d, *J* = 5.5 Hz, 3H), 0.92 (s, 3H); ¹³C NMR (100 MHz, CDCl₃): δ = 179.71 (COOH), 179.02 (C28), 146.85 (C=CH₂), 114.26 (C=CH₂), 92.16 (d, *J* = 14.4 Hz, C13), 89.46 (d, *J* = 186.4 Hz, C12), 52.72 (d, *J* = 3.6 Hz), 50.43, 45.37, 44.50 (d, *J* = 2.4 Hz), 42.34, 39.70, 39.71 (d, *J* = 9.3 H), 39.58, 38.71, 34.05, 32.75, 31.47, 30.88, 28.74, 27.78, 25.95 (d, *J* = 19.2 Hz), 23.90, 23.09, 22.53, 20.72, 19.55, 18.42, 17.19, 16.71. MS (DI-ESI) (*m/z*): 489.0 (100%) [M+H]⁺, 469.2 (44%). Anal. Calcd. For C₃₀H₄₅FO₄: C, 73.73; H, 9.28. Found: C, 73.55; H, 9.52.

Chapter 3 | Synthesis and cytotoxic activity of novel UA derivatives

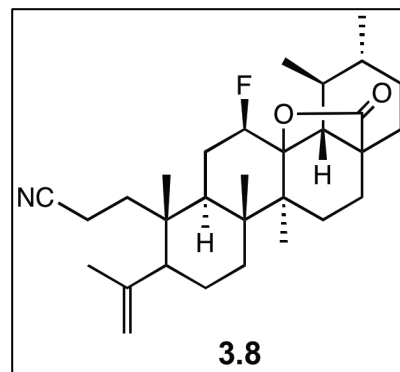
3,4-Seco-3-amide-4(23)-en-12 β -fluor-urs-13,28 β -olide (3.7): To a stirred mixture of **3.6** (140

mg, 0.29 mmol) in dry CH₂Cl₂ (3 ml), at r.t., oxalyl chloride (0.2 ml, 1.52 mmol) was added. After 15 h, the reaction mixture was evaporated and the resulting residue was dissolved in dry THF (15 ml) and cold 25% ammonium aqueous solution (12 ml) was added dropwise. After 2 h, the reaction mixture was evaporated and extracted with



ethyl acetate (3 × 60 ml). The resulting organic phase was washed with 1M HCl aqueous solution (60 ml), water (60 ml), and 10% NaCl aqueous solution (60 ml), dried over Na₂SO₄, filtered, and evaporated to dryness. The crude residue was purified by flash column chromatograph (petroleum ether:ethyl acetate 7:1 – 1:1) to give **3.7** as a white solid (74.8%). Mp 124.2 – 128.6 °C. IR (KBr): ν = 3355.53, 3075.9, 2973.7, 2929.34, 2871.49, 1772.26, 1670.05, 1616.06, 1457.92, 1390.42, 1186.01, 1141.65, 937.23 cm⁻¹. ¹H NMR (400 MHz, CDCl₃): δ = 5.79 (br s, 2H, NH₂) 4.87 (dq, J = 45.7, 8.7 Hz, 1H, H-12), 4.87 (s, 1H, H-23), 4.67 (s, 1H, H-23), 1.73 (s, 3H, H-24), 1.26 (s, 3H), 1.22 (s, 3H), 1.14 (d, J = 6.6 Hz, 3H), 0.97 (d, J = 5.2 Hz, 3H), 0.92 (s, 3H); ¹³C NMR (100 MHz, CDCl₃): δ = 179.04 (C28), 176.14 (CON), 147.33 (C=CH₂), 114.13 (C=CH₂), 92.20 (d, J = 14.2 Hz, C13), 89.39 (d, J = 185.6 Hz, C12), 52.74 (d, J = 3.4 Hz), 50.67, 45.36, 44.50 (d, J = 2.9 Hz), 42.35, 39.71 (2C), 39.71 (d, J = 9.2 Hz) 38.72, 35.17, 32.75, 31.48, 30.88, 30.47, 27.78, 26.03 (d, J = 19.2 Hz), 23.88, 22.90, 22.54, 20.81, 19.55, 18.45, 17.19, 16.73. MS (DI-ESI) (m/z): 488.24 (100%) [M-H]⁺, 487.2 (37%), 468.3 (16%). Anal. Calcd for C₃₀H₄₆FNO₃·0.8H₂O: C, 71.76; H, 9.56; N, 2.79. Found: C, 71.47; H, 9.59; N, 2.66.

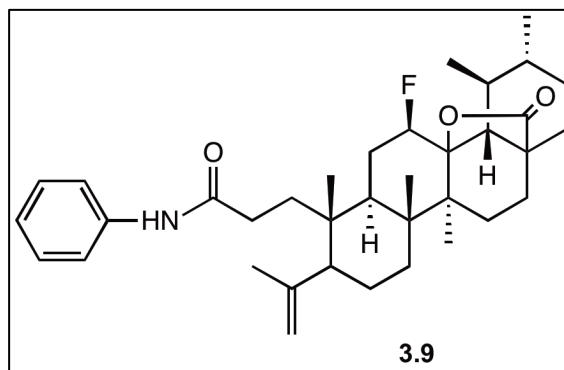
3,4-Seco-3-cyano-4(23)-en-12 β -fluor-urs-13,28 β -olide (3.8): To a stirred mixture of **3.7** (300 mg, 0.62 mmol) in ethyl acetate (3 ml), THF (1 ml), and Et₃N (0.3 ml) under N₂, T3P (50 wt. % in THF) (0.7 ml) was added dropwise. The solution was heated under reflux (77 °C). After 5 h, the reaction mixture was diluted with ethyl acetate (80 ml) and water (35 ml). The aqueous phase was extracted with ethyl acetate (2 × 70 ml). The resulting organic phase was washed



with water (70 ml), and 10% NaCl aqueous solution (70 ml), dried over Na₂SO₄, filtered, and evaporated to dryness. The residue was purified by flash column chromatography (petroleum ether:ethyl acetate 8:1 – 1:3) to give **3.8** as a slight yellow solid (50.5%). Mp 251.2 – 255.2 °C. IR (KBr): ν = 3072.05, 2979.48, 2931.27, 2867.63, 2237.02, 1768.4, 1633.41, 1452.14, 1392.35, 1238.08, 1133.94, 933.38 cm⁻¹. ¹H NMR (400 MHz, CDCl₃): δ = 5.10 (dq, J = 45.10, 8.30 Hz, 1H, H-12), 4.88 (s, 1H, H-23), 4.63 (s, 1H, H-23), 2.34 (t, J = 6.8 Hz, 2H, CNCH₂), 1.71 (s, 3H, H-24), 1.28 (s, 3H), 1.24 (s, 3H), 1.14 (d, J = 6.4 Hz, 3H), 0.96 (d, J = 5.7 Hz, 3H), 0.92 (s, 3H); ¹³C NMR (100 MHz, CDCl₃): δ = 178.97 (C28), 146.57 (C=CH₂), 120.39 (CN), 114.61 (C=CH₂), 92.01 (d, J = 14.0 Hz, C13), 88.48 (d, J = 186.0 Hz, C12), 52.75 (d, J = 3.0 Hz), 50.38, 45.29, 44.46 (d, J = 2.9 Hz), 42.34, 39.90, 39.70, 39.27 (d, J = 9.8 Hz), 38.68, 34.06, 32.55, 31.46, 30.89, 27.66, 26.21 (d, J = 19.6 Hz), 23.64, 22.67, 22.51, 20.35, 19.57, 18.47, 16.99, 16.53, 11.67. MS (DI-ESI) (m/z): 469.9 (100%) [M-H]⁺, 450.2 (16.5%). Anal. Calcd for C₃₀H₄₄FNO₂·0.6H₂O: C, 74.99; H, 9.48; N, 2.92. Found: C, 74.79; H, 9.33; N, 2.59.

3,4-Seco-3-N-phenylamide-4(23)-en-12 β -fluor-urs-13,28 β -olide (3.9): To a stirred mixture of

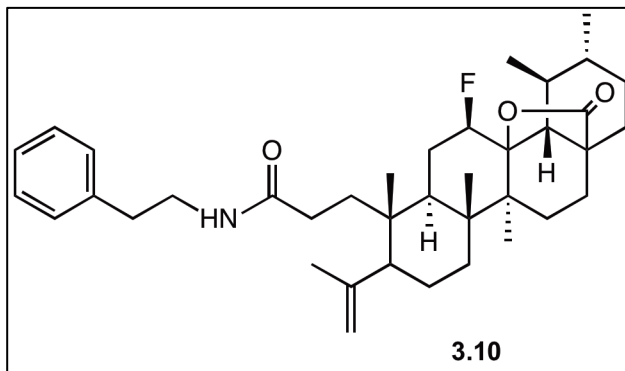
3.6 (125 mg, 0.26 mmol) in dry THF (2 ml), aniline (0.03 ml, 0.31 mmol), and Et₃N (0.07 ml) at 3–5 °C, T3P (50 wt. % in THF) (0.4 ml) was added dropwise. After 7.3 h, the reaction mixture was evaporated under reduced pressure and the residue was extracted with ethyl acetate (3 × 50



ml) from water (20 ml). The resulting organic phase was washed with 5% HCl aqueous solution (2 × 60 ml), water (60 ml), and 10% NaCl aqueous solution (60 ml), dried over Na₂SO₄, filtered, and evaporated to dryness. The residue was purified by flash column chromatography (petroleum ether:ethyl acetate 13:1 – 7:1) to give **3.9** as a white solid (74.1%). Mp 267.1 – 270.8 °C. IR (KBr): ν = 3342.03, 3289.96, 3133.76, 3072.05, 2971.77, 2931.27, 2875.34 1749.12, 1687.41, 1600.63, 1540.84, 1438.64, 1386.57, 1305.57, 1243.86, 1143.58, 937.23, 754.03, 692.32 cm⁻¹. ¹H NMR (400 MHz, CDCl₃): δ = 7.52 – 7.50 (m, 2H, H-Ar), 7.32 – 7.29 (m, 3H, H-Ar), 7.10 (t, J = 7.3 Hz, 1H, NH), 4.91 (s, 1H, H-23), 4.85 (dt, J = 43.1, 8.5 Hz, 1H, H-12), 4.73 (s, 1H, H-23), 1.76 (s, 3H, H-24), 1.26 (s, 3H), 1.21 (s, 3H), 1.04 (d, J = 6.3 Hz, 3H), 0.95 (s, 3H), 0.94 (s, 3H); ¹³C NMR (100 MHz, CDCl₃): δ = 179.09 (C28), 171.31 (CON), 147.61 (C=CH₂), 137.97 (C-Ar), 129.15 (C-Ar, 2C), 124.44 (C-Ar), 119.85 (C-Ar, 2C), 114.10 (C=CH₂), 92.6 (d, J = 14.3 Hz, C13), 89.22 (d, J = 186.0 Hz, C12), 52.73 (d, J = 3.4 Hz), 50.75, 45.35, 44.48 (d, J = 2.9 Hz), 42.40, 39.91, 39.78 (d, J = 9.8 Hz), 39.68, 38.69, 35.23, 32.79, 32.58, 31.49, 30.89, 27.77, 26.15 (d, J = 19.4 Hz), 23.92, 22.92, 22.54, 20.79, 19.54, 18.46, 17.15, 16.52. MS (DI-ESI) (m/z): 564.4 (100%) [M-H]⁺. Anal. Calcd for C₃₆H₅₀FNO₃: C, 76.69; H, 8.94; N, 2.48. Found: C, 76.66; H, 8.95; N, 2.56.

3,4-Seco-3-N-phenethylamide-4(23)-en-12 β -fluor-urs-13,28 β -olide (3.10): To a stirred

mixture of **3.6** (100 mg 0.20 mmol) in dry THF (2 ml), phenethylamine (0.03 ml, 0.25 mmol), and Et₃N (0.06 ml) at 3–5 °C, T3P (50% wt. % in THF) (0.16 ml) was added dropwise. At 2.75 h, Et₃N (0.06 ml) and T3P (50 wt. % in THF) (0.16 ml) were added. After 4 h, Et₃N

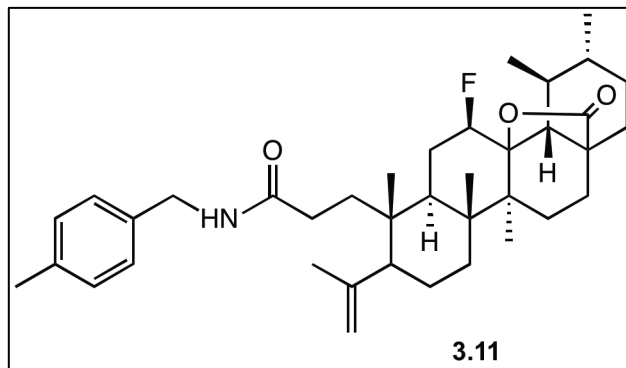


(0.06 ml) and T3P[®] (50 wt. % in THF) (0.16 ml) were added. After 6 h, the reaction mixture was evaporated under reduced pressure and the residue was extracted with ethyl acetate (3 × 50 ml) from water (20 ml). The resulting organic phase was washed with water (50 ml), and 10% NaCl aqueous solution (50 ml), dried over Na₂SO₄, filtered, and evaporated to dryness. The residue was purified by flash column chromatography (petroleum ether:ethyl acetate 8:1 – 1:1) to give **3.10** as a white solid (72.0%). Mp 101.3 – 104.0 °C. IR (KBr): ν = 3326.6, 3066.26, 3025.76, 2954.41, 2929.34, 2871.49, 1388.50, 1238.08, 1133.94, 1774.19, 1650.77, 1540.84, 1536.95, 1455.99, 937.23, 748.25, 700.03 cm⁻¹. ¹H NMR (400 MHz, CDCl₃): δ = 7.33 - 7.30 (m, 2H, H-Ar), 7.25 – 7.18 (m, 3H, H-Ar), 5.45 (t, *J* = 5.9 Hz, 1H, NH), 4.85 (dm, 1H, H-12), 4.81 (s, 1H, H-23), 4.62 (s, 1H, H-23), 3.65 – 3.36 (m, 2H, CH₂N), 2.82 (t, *J* = 6.9 Hz, 2H, ArCH₂), 1.71 (s, 3H, H-24), 1.25 (s, 3H), 1.21 (s, 3H), 1.15 (d, *J* = 6.4 Hz, 3H), 0.97 (d, *J* = 5.5 Hz, 3H), 0.89 (s, 3H); ¹³C NMR (100 MHz, CDCl₃): δ = 178.85 (C28), 172.86 (CON), 147.31 (C=CH₂), 138.79 (C-Ar), 128.78 (C-Ar, 2C), 128.67 (C-Ar, 2C), 126.57 (C-Ar), 113.85 (C=CH₂), 92.02 (d, *J* = 14.1 Hz, C13), 89.17 (d, *J* = 186.0 Hz, C12), 52.60 (d, *J* = 3.3 Hz), 50.49, 45.23, 44.37 (d, *J* = 2.9 Hz), 42.21, 40.58, 39.59 (2C), 39.53 (m), 38.60, 35.59, 35.41, 32.63, 31.37, 31.30, 30.78, 27.66, 25.85 (d, *J* = 18.5 Hz), 23.77, 22.78, 22.42, 20.71, 19.43, 18.32, 17.05, 16.55. MS (DI-ESI) (*m/z*): 592.3 (100%) [M+H]⁺. Anal. Calcd for C₃₈H₅₄FNO₃: C, 77.12; H, 9.20; N, 2.37. Found: C, 77.40; H, 9.12; N, 2.34.

Chapter 3 | Synthesis and cytotoxic activity of novel UA derivatives

3,4-Seco-3-N-(4-methylbenzamide)-4(23)-en-12 β -fluor-urs-13,28 β -olide (3.11): To a stirred

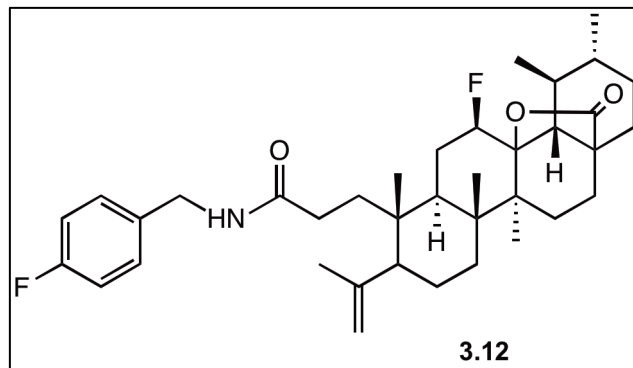
mixture of **3.6** (250 mg, 0.51 mmol) in dry THF (3.5 ml), 4-methylbenzylamine (0.08 ml, 0.61 mmol), and Et₃N (0.14 ml) at 3–5 °C, T3P (50 wt. % in THF) (0.4 ml) was added dropwise. After 5 h, the reaction mixture was evaporated under reduced pressure and the



residue was extracted with ethyl acetate (3 × 80 ml) from water (35 ml). The resulting organic phase was washed with water (80 ml), and 10% NaCl aqueous solution (80 ml), dried over Na₂SO₄, filtered, and evaporated to dryness. The residue was purified by flash column chromatography (petroleum ether:ethyl acetate 6:1 – 2:1) to give **3.11** as a white solid (46.5%). Mp 100.4 – 103.45 °C. IR (KBr): ν = 3326.60, 3070.12, 2956.34, 2927.41, 2871.49, 1774.19, 1650.77, 1540.84, 1457.92, 1388.50, 1238.08, 1133.94, 937.23, 804.17 cm⁻¹. ¹H NMR (400 MHz, CDCl₃): δ = 7.18 – 7.14 (m, 4H, H-Ar), 5.72 (t, J = 5.4 Hz, 1H, NH), 4.89 (dq, J = 45.6, 8.8 Hz, 1H, H-12), 4.86 (s, 1H, H-23), 4.67 (s, 1H, H-23), 4.38 (d, J = 5.5 Hz, 2H, CH₂N), 2.34 (s, 3H, CH₃-Ar), 1.73 (s, 3H, H-24), 1.25 (s, 3H), 1.22 (s, 3H), 1.15 (d, J = 6.7 Hz, 3H), 0.97 (d, J = 5.1 Hz, 3H), 0.91 (s, 3H); ¹³C NMR (100 MHz, CDCl₃): δ = 179.01 (C28), 172.79 (CON), 147.34 (C=CH₂), 137.51 (C-Ar), 135.25 (C-Ar), 129.57 (C-Ar, 2C), 128.07 (C-Ar, 2C), 114.12 (C=CH₂), 92.20 (d, J = 14.3 Hz, C13), 89.30 (d, J = 186.5 Hz, C12), 52.74 (d, J = 3.6 Hz), 50.52, 45.36, 44.51 (d, J = 2.9 Hz), 43.68, 42.34, 39.72 (2C), 39.63, 38.73, 35.37, 32.77, 31.49, 31.37, 30.90, 27.78, 26.03 (d, J = 19.2 Hz), 23.92, 23.02, 22.55, 21.23, 20.82, 19.55, 18.44, 17.17, 16.69. MS (DI-ESI) (m/z): 592.4 (100%) [M+H]⁺. Anal. Calcd for C₃₈H₅₄FNO₃·0.85H₂O: C, 75.17; H, 9.25; N, 2.31. Found: C, 74.87; H, 8.98; N, 2.13.

3,4-Seco-3-N-(4-fluorobenzamide)-4(23)-en-12 β -fluor-urs-13,28 β -olide (3.12): To a stirred

mixture of **3.6** (150 mg, 0.31 mmol) in dry THF (2 ml), 4-fluorobenzylamine (0.04 ml, 0.37 mmol), and Et₃N (0.05 ml) at 3–5 °C, T3P (50 wt. % in THF) (0.24 ml) was added dropwise. After 4 h, the reaction mixture was evaporated under reduced pressure and the



residue was extracted with ethyl acetate (3 × 50 ml) from water (10 ml). The resulting organic phase was washed with 5% HCl aqueous solution (50 ml), water (50 ml), and 10% NaCl aqueous solution (50 ml), dried over Na₂SO₄, filtered, and evaporated to dryness to give **3.12** as

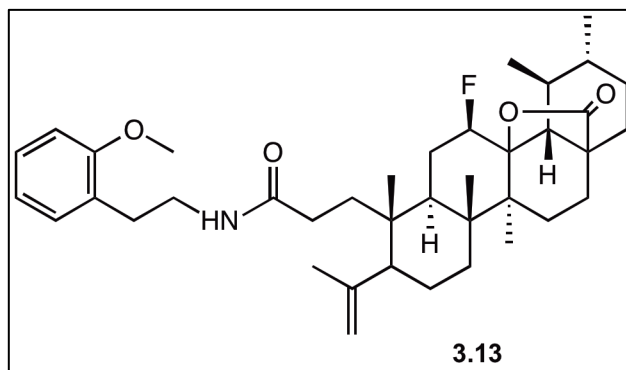
a white solid (87.5%). Mp 119.2 – 123.1 °C. IR (KBr): ν = 3342.03, 3072.05, 2956.34, 2929.34, 2871.49, 1174.19, 1650.77, 1509.99, 1457.92, 1390.42, 1222.65, 1133.94, 937.23, 823.46 cm⁻¹.

¹H NMR (400 MHz, CDCl₃): δ = 7.26 - 7.23 (m, 2H, H-Ar), 7.02 (t, *J* = 8.5 Hz, 2H, H-Ar), 5.82 (br s, 1H, NH), 4.88 (dq, *J* = 45.9, 8.4 Hz, 1H, H-12), 4.85 (s, 1H, H-23), 4.67 (s, 1H, H-23), 4.39 (d, *J* = 4.3 Hz, CH₂N), 1.73 (s, 3H, H-24), 1.25 (s, 3H), 1.16 (s, 3H), 1.15 (d, *J* = 6.1 Hz, 3H), 0.96 (d, *J* = 4.5 Hz, 3H), 0.91 (s, 3H); ¹³C NMR (100 MHz, CDCl₃): δ = 179.01 (C28), 173.01 (CON), 162.25 (d, *J* = 246.7 Hz, CF-Ar), 147.38 (C=CH₂), 134.13 (d, *J* = 3.03 Hz, C-Ar), 129.70 (d, *J* = 8.13 Hz, 2C, C-Ar), 115.74 (d, *J* = 21.32 Hz, 2C, C-Ar), 114.10 (C=CH₂), 92.18 (d, *J* = 14.3 Hz, C13), 89.31 (d, *J* = 186.1 Hz, C12), 52.74 (d, *J* = 3.5 Hz), 50.58, 45.36, 44.51 (d, *J* = 2.8 Hz), 43.16, 42.35, 39.77, 39.72, 39.66, 38.73, 35.42, 32.76, 31.49, 31.34, 30.89, 27.78, 26.04 (d, *J* = 19.0 Hz), 23.90, 22.97, 22.54, 20.82, 19.55, 18.43, 17.18, 16.69. MS (DI-ESI) (*m/z*): 596.3 (100%) [M+H]⁺. Anal. Calcd for C₃₇H₅₁F₂NO₃: C, 74.59; H, 8.63; N, 2.35. Found: C, 74.69; H, 8.58; N, 2.16.

Chapter 3 | Synthesis and cytotoxic activity of novel UA derivatives

3,4-Seco-3-N-(2-methoxyphenethylamide)-4(23)-en-12 β -fluor-urs-13,28 β -olide (3.13):

To a stirred mixture of **3.6** (335 mg, 0.69 mmol) in dry THF (4 ml), 2-methoxyphenethylamine (0.12 ml, 0.82 mmol), and Et₃N (0.19 ml) at 3–5 °C, T3P (50 wt. % in THF) (0.5 ml) was added dropwise. At 2 h, Et₃N (0.19 ml) and T3P (50% wt.% in THF) (0.5 ml) were added.



After 5 h, the reaction mixture was evaporated under reduced pressure and the residue was extracted with ethyl acetate (3 × 80 ml) from water (35 ml). The resulting organic phase was washed with 5% HCl aqueous solution (80 ml), water (80 ml), and 10% NaCl aqueous solution (80 ml), dried over Na₂SO₄, filtered, and evaporated to dryness. The residue was purified by flash column chromatography (petroleum ether:ethyl acetate 7:1 – 2:1) to give **3.13** as a white solid (46.8%). Mp 100.4 – 103.45 °C. IR (KBr): ν = 3318.89, 3072.05, 2954.41, 2929.34, 2871.49, 1774.19, 1646.91, 1540.84, 1494.56, 1457.92, 1388.50, 1243.86, 1133.94, 937.23, 754.03 cm⁻¹. ¹H NMR (400 MHz, CDCl₃): δ = 7.23 (td, J = 7.9, 1.7 Hz, 1H, H-Ar), 7.12 (dd, J = 7.4, 1.8 Hz, 1H, H-Ar), 6.94 - 6.85 (m, 2H, H-Ar), 5.78 (t, J = 5.5 Hz, 1H, NH), 4.86 (dq, J = 45.5, 8.8 Hz, 1H, H-12), 4.83 (s, 1H, H-23), 4.63 (s, 1H, H-23), 3.84 (s, 3H, CH₃O-Ar), 3.50 - 3.46 (m, 2H, CH₂N), 2.84 (t, J = 6.6 Hz, 2H, Ar-CH₂), 1.71 (s, 3H, H-24), 1.25 (s, 3H), 1.20 (s, 3H), 1.15 (d, J = 6.2 Hz, 3H), 0.97 (d, J = 4.7 Hz, 3H), 0.89 (s, 3H); ¹³C NMR (100 MHz, CDCl₃): δ = 179.03 (C28), 173.35 (CON), 157.54 (C-Ar), 147.29 (C=CH₂), 130.86 (C-Ar), 128.15 (C-Ar), 127.42 (C-Ar), 121.05 (C-Ar), 114.07 (C=CH₂), 110.70 (C-Ar), 92.22 (d, J = 14.2 Hz, C13), 89.22 (d, J = 185.9 Hz, C12), 55.59, 52.74 (d, J = 3.5 Hz), 50.42, 45.36, 44.51 (d, J = 2.8 Hz), 42.32, 40.36, 39.72 (2C), 39.55 (d, J = 9.8 Hz), 38.73, 35.23, 32.74, 31.50, 31.16, 30.91, 29.98, 27.78, 25.95 (d, J = 19.4 Hz), 23.92, 23.06, 22.55, 20.89, 19.56, 18.44, 17.17, 16.65. MS (DI-ESI)

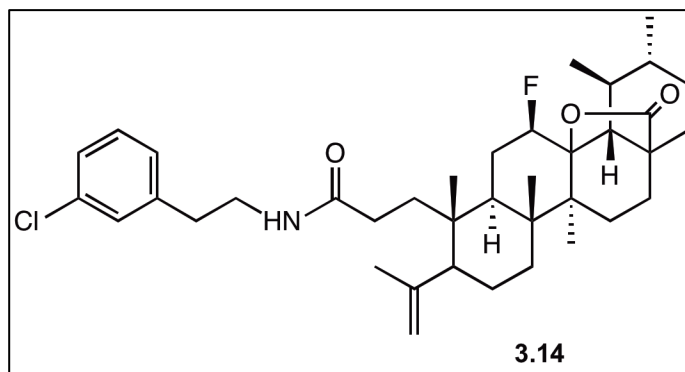
Chapter 3 | Synthesis and cytotoxic activity of novel UA derivatives

(m/z): 622.4 (100%) [M+H]⁺. Anal. Calcd for C₃₉H₅₆FNO₄·0.2H₂O: C, 74.89; H, 9.09; N, 2.24.

Found: C, 74.70; H, 9.06; N, 2.30.

3,4-Seco-3-N-(3-chlorophenylethylamide)-4(23)-en-12β-fluor-urs-13,28β-olide (3.14):

To a stirred mixture of **3.6** (125 mg, 0.26 mmol) in dry THF (2 ml), 2-(3-chlorophenyl)ethylamine (0.04 ml, 0.31 mmol), and Et₃N (0.14 ml) at 3–5 °C, T3P (50 wt. % in THF) (0.4 ml) was added dropwise. After 5 h, the reaction mixture



was evaporated under reduced pressure and the residue was extracted with ethyl acetate (3 × 60 ml) from water (25 ml). The resulting organic phase was washed with 5% HCl aqueous solution (60 ml), water (60 ml), and 10% NaCl aqueous solution (60 ml), dried over Na₂SO₄, filtered, and evaporated to dryness. The residue was purified by flash column chromatography (petroleum ether:ethyl acetate 7:1 – 2:1) to give **3.14** as a white solid (88.8%). Mp 101.7 – 105.0 °C. IR (KBr): ν = 3330.46, 3070.12, 2954.41, 2929.34, 2871.49, 1774.19, 1650.77, 1598.70, 1540.84, 1457.92, 1390.42, 1238.08, 1133.94, 937.22, 782.96, 698.10, 664.61 cm⁻¹. ¹H NMR (400 MHz, CDCl₃): δ = 7.25 - 7.22 (m, 2H, H-Ar), 7.17 (s, 1H, H-2'-Ar), 7.07 (d, *J* = 6.8 Hz, 1H, H-Ar), 5.47 (t, *J* = 5.6 Hz, 1H, NH), 4.86 (dm, 1H, H-12), 4.82 (s, 1H, H-23), 4.62 (s, 1H, H-23), 3.60 - 3.41 (m, 2H, CH₂N), 2.80 (t, *J* = 6.9 Hz, 2H, Ar-CH₂), 1.71 (s, 3H, H-24), 1.25 (s, 3H), 1.21 (s, 3H), 1.15 (d, *J* = 6.4 Hz, 3H), 0.97 (d, *J* = 5.6 Hz, 3H), 0.90 (s, 3H); ¹³C NMR (100 MHz, CDCl₃): δ = 178.84 (C28), 172.95 (CON), 147.37 (C=CH₂), 140.89 (C-Ar), 134.40 (C-Ar), 129.91 (C-Ar), 128.93 (C-Ar), 126.96 (C-Ar), 126.77 (C-Ar), 113.84 (C=CH₂), 92.03 (d, *J* = 14.3 Hz, C13), 89.18 (d, *J* = 186.0 Hz, C12), 53.86, 52.60 (d, *J* = 3.4 Hz), 50.53, 45.22, 44.37 (d, *J* = 3.0 Hz), 42.22, 40.41, 39.72, 39.68 (d, *J* = 8.5 Hz), 38.60, 35.45, 35.30, 32.63, 31.37, 31.30, 30.77, 27.66, 25.86 (d, *J* = 19.7 Hz), 23.75, 22.73, 22.42, 20.69, 19.43, 18.32, 17.05, 16.56. MS (DI-

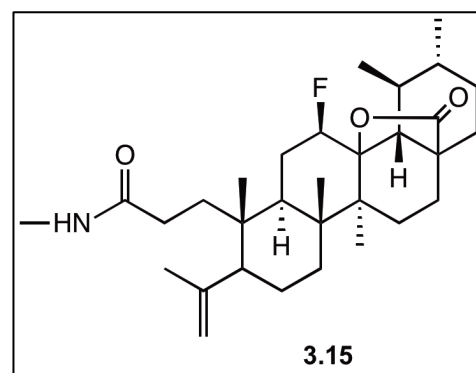
Chapter 3 | Synthesis and cytotoxic activity of novel UA derivatives

ESI) (m/z): 626.2 (100%) [M+H]⁺. Anal. Calcd for C₃₈H₅₃ClFNO₃: C, 72.88; H, 8.53; N, 2.24.

Found: C, 72.86; H, 8.53; N, 2.25.

3,4-Seco-3-N-methylamide-4(23)-en-12β-fluor-urs-13,28β-olide (3.15): To a stirred mixture of

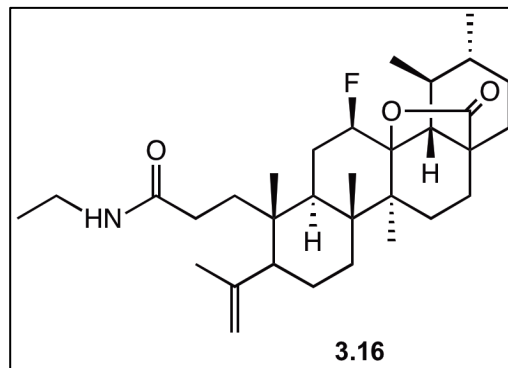
3.6 (250 mg, 0.51 mmol) in dry THF (3 ml), methylamine solution (33 wt. % in absolute ethanol) (0.07 ml, 0.56 mmol), and Et₃N (0.14 ml) at 3–5 °C, T3P (50 wt. % in THF) (0.4 ml) was added dropwise. After 5 h, the reaction mixture was evaporated under reduced pressure and the residue was extracted with ethyl acetate (3 × 80 ml) from



water (35 ml). The resulting organic phase was washed with water (45 ml), and 10% NaCl aqueous solution, dried over Na₂SO₄, filtered, and evaporated to dryness. The residue was purified by flash column chromatography (petroleum ether:ethyl acetate 6:1 – 2:1) to give **3.15** as a white solid (52.4%). Mp 151.2 – 155.3 °C. IR (KBr): ν = 3278.39, 3085.55, 2956.34, 2929.34, 2871.49, 1774.19, 1639.20, 1563.99, 1457.92, 1390.42, 1236.15, 1133.94, 937.23 cm⁻¹. ¹H NMR (400 MHz, CDCl₃): δ = 5.65 (br s, 1H, NH), 4.86 (s, 1H, H-23), 4.85 (dq, J = 44.8, 8.4 Hz, 1H, H-12), 4.68 (s, 1H, H-23), 2.81 (d, J = 3.1 Hz, 3H, NCH₃), 1.73 (s, 3H, H-24), 1.25 (s, 3H), 1.22 (s, 3H), 1.15 (d, J = 6.2 Hz, 3H), 0.96 (d, J = 4.9 Hz, 3H), 0.91 (s, 3H); ¹³C NMR (100 MHz, CDCl₃): δ 179.06 (C28), 173.97 (CON), 147.34 (C=CH₂), 114.10 (C=CH₂), 92.24 (d, J = 14.4 Hz, C13), 89.30 (d, J = 186.3 Hz, C12), 52.75 (d, J = 3.4 Hz), 50.50, 45.37, 44.52 (d, J = 2.7 Hz), 42.35, 39.79, 39.73, 39.62 (d, J = 9.5 Hz), 38.73, 35.37, 32.76, 31.50, 31.08, 30.89, 27.78, 26.63, 26.03 (d, J = 19.3 Hz), 23.92, 23.00, 22.55, 20.86, 19.55, 18.44, 17.17, 16.65. MS (DI-ESI) (m/z): 502.3 (100%) [M+H]⁺. Anal. Calcd for C₃₁H₄₈FNO₃·0.2H₂O: C, 73.68; H, 9.65; N, 2.77. Found: C, 73.35; H, 10.02; N, 2.60.

3,4-Seco-3-N-ethylamide-4(23)-en-12 β -fluor-urs-13,28 β -olide (3.16): To a stirred solution of

3.6 (250 mg, 0.51 mmol) in dry THF (3.5 ml), ethylamine solution (2.0 M in THF) (0.3 ml, 0.60 mmol) and Et₃N (0.14 ml) at 3–5 °C, T3P (50 wt. % in THF) (0.4 ml) was added dropwise. After 3 h, the reaction mixture was evaporated under reduced pressure and the residue was extracted with ethyl acetate (3 × 80

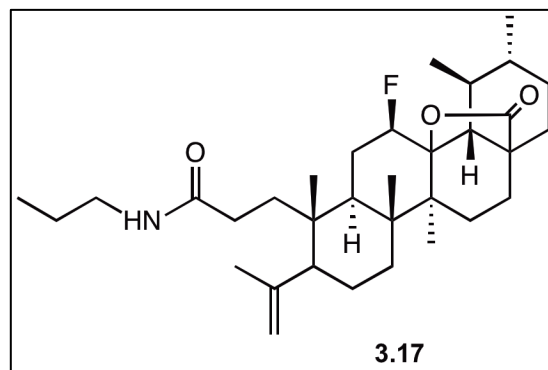


ml) from water (35 ml). The resulting organic phase was washed with water (2 × 90 ml), and 10% NaCl aqueous solution (90 ml), dried over Na₂SO₄, filtered, and evaporated to dryness. The residue was purified by flash column chromatography (petroleum ether:ethyl acetate 6:1 – 1:3) to give **3.16** as a white solid (51.7%). Mp 108.5 – 112.5 °C. IR (KBr): ν = 3268.11, 3081.69, 2971.77, 2931.27, 2873.42, 1774.19, 1635.34, 1556.27, 1457.92, 1390.42, 1238.08, 1133.94, 937.23. ¹H NMR (400 MHz, CDCl₃): δ 5.53 (m, 1H, NH), 4.86 (s, 1H, H-23), 4.84 (dq, J = 45.8, 8.1 Hz, 1H, H-12), 4.67 (s, 1H, H-23), 3.32 - 3.22 (m, 2H, CH₂N), 1.73 (s, 3H, H-24), 1.25 (s, 3H), 1.21 (s, 3H), 1.15 – 1.12 (m, 6H), 0.96 (d, J = 5.6 Hz, 3H), 0.91 (s, 3H); ¹³C NMR (100 MHz, CDCl₃): δ = 179.05 (C28), 172.92 (CON), 147.40 (C=CH₂), 114.05 (C=CH₂), 92.23 (d, J = 14.0 Hz, C13), 89.28 (d, J = 185.6 Hz, C12), 52.73 (d, J = 3.1 Hz), 50.49, 45.36, 44.50 (d, J = 2.9 Hz), 42.33, 39.76, 39.72, 39.62 (d, J = 9.7 Hz), 38.72, 35.42, 34.61, 32.76, 31.49, 31.39, 30.89, 27.77, 26.02 (d, J = 19.2 Hz), 23.96, 23.93, 23.02, 22.54, 20.84, 19.54, 18.43, 17.16, 16.64, 14.96. MS (DI-ESI) (m/z): 516.3 (100%) [M+H]⁺. Anal. Calcd for C₃₂H₅₀FNO₃·0.8H₂O: C, 72.50; H, 9.81; N, 2.64. Found: C, 72.20; H, 9.86; N, 2.37.

Chapter 3 | Synthesis and cytotoxic activity of novel UA derivatives

3,4-Seco-3-N-propylamide-4(23)-en-12 β -fluor-urs-13,28 β -olide (3.17): To a stirred mixture of

3.6 (250 mg, 0.51 mmol) in dry THF (4 ml), propylamine (0.05 ml, 0.61 mmol), and Et₃N (0.14 ml) at 3–5 °C, T3P (50 wt. % in THF) (0.4 ml) was added dropwise. After 5 h, the reaction mixture was evaporated under reduced pressure and the residue was extracted with ethyl acetate (3 × 80 ml)



from water (35 ml). The resulting organic phase was washed with water (45 ml), and 10% NaCl aqueous solution, dried over Na₂SO₄, filtered, and evaporated to dryness. The residue was purified by flash column chromatography (petroleum ether:ethyl acetate 6:1 – 1:2) to give **3.17** as a white solid (62.1%). Mp 110.3 – 116.1 °C. IR (KBr): ν = 3270.68, 3079.76, 2962.12, 2931.27, 2873.42, 1774.19, 1641.13, 1544.70, 1457.92, 1388.50, 1238.08, 1133.94, 937.23 cm⁻¹. ¹H NMR (400 MHz, CDCl₃): δ = 5.59 (br s, 1H, NH), 4.87 (s, 1H, H-23), 4.86 (dq, J = 45.5, 8.3 Hz, 1H, H-12), 4.68 (s, 1H, H-23), 3.23 - 3.19 (m, 2H, CH₂N), 1.74 (s, 3H, H-24), 1.25 (s, 3H), 1.22 (s, 3H), 1.15 (d, J = 5.6 Hz, 3H), 0.97 (d, J = 5.2 Hz, 3H), 0.94 - 0.89 (m, 6H); ¹³C NMR (100 MHz, CDCl₃): δ = 179.05 (C28), 173.25 (CON), 147.48 (C=CH₂), 114.05 (C=CH₂), 92.23 (d, J = 14.1 Hz, C13), 89.32 (d, J = 186.1 Hz, C12), 52.74 (d, J = 3.6 Hz), 50.54, 45.37, 44.51 (d, J = 2.9 Hz), 42.35, 41.57, 39.78, 39.73, 39.63 (d, J = 9.7 Hz), 38.73, 35.50, 32.76, 31.50, 31.35, 30.90, 27.79, 26.02 (d, J = 19.4 Hz), 23.92, 22.97, 22.94, 22.56, 20.87, 19.56, 18.45, 17.18, 16.67, 11.49. MS (DI-ESI) (m/z): 530.3 (100%) [M+H]⁺. Anal. Calcd for C₃₃H₅₂FNO₃·0.2EtOAc: C, 74.16; H, 9.87; N, 2.56. Found: C, 74.00; H, 10.15; N, 2.19.

3.4.2. Biology

3.4.2.1. Cell lines and culture

H460 CTR5, H460 LKB1/5^{+/+}, and H322 (NSCLC) cell lines were obtained from Dr. John Heymach at MD Anderson Cancer Center. H460 CTR5, H460 LKB1^{+/+}, and H322 cell lines were maintained in RPMI-1640 medium (Corning Cellgro) supplemented with 10% FBS (Invitrogen) and were cultured at 37 °C in CO₂ incubators. These cell lines were authenticated using an AmpF/STR Identification Kit (Applied Biosystems) and routinely tested for *Mycoplasma* contamination using a MycoTect kit (Invitrogen). Experiments were conducted in cells with fewer than 18 passages and maintained at a logarithmic growth concentration between 10⁵ cells/ml and 10⁶ cells/ml as determined by a Coulter Channelyzer (Beckman Coulter) with less than 10% endogenous cell death confirmed by flow cytometry.

3.4.2.2. Materials

UA derivatives were dissolved in DMSO at a concentration of 20 mM and stored at -80 °C. To obtain final assay concentrations, the stock solutions were diluted in culture medium. The final concentration of DMSO in working solution was 0.15%.

[Methyl-³H]thymidine, [5,6-³H]uridine, and [4,5-³H]L-leucine (1.0 mCi/ml) were purchased from Moravek Biochemicals, Brea, CA.

Bafilomycin A1 (B1793) and chloroquine (C6628) were purchased from Sigma-Aldrich. Annexin V-Cy5 and PI were obtained from BD Biosciences Pharmingen.

Primary antibodies against caspase-8 (1C12), caspase-3 (8G10), caspase-7 (#9492), LC3A/B (D3U4C) XP, and total mTOR (4517) were obtained from Cell Signaling. Primary antibody against Bcl-2 (clone 124) was obtained from Dako. Beclin-1 (NB500-266SS) and

Chapter 3 | Synthesis and cytotoxic activity of novel UA derivatives

GAPDH (NB600-502) were purchased from Novus Biologicals. Antibody against β -actin (AC-15) was obtained from Sigma-Aldrich. Primary antibody against Mcl-1 (s-19) was obtained from Santa Cruz Biotechnology. Primary antibody against PARP (4C10-5) was purchased from BD Pharmingen. Primary antibody against p62 (BML-PW9860) was purchased from Enzo Life Sciences. Secondary antibodies goat anti-mouse (926-68070) and goat anti-rabbit (926-32211) were obtained from LI-COR Biosciences.

3.4.2.3. Viability assay

For the monolayer culture model, cells were seeded in a 384-well black polystyrene Greiner plate at densities of 850 cells/well for H460 CTR5, 660 cells/well for H460 LKB1/5^{+/+}, and 1780 cells/well for H322 in RPMI-1640 (10% FBS). The cell density was determined based on the size and cell growth characteristics of each cell line, in order for the cell density at the end point to be 70-80% of the well surface. Cells were treated with 0.15% DMSO or different concentrations of each drug. After 72 h of treatment, 5 μ l of CellTiter-Blue® Viability assay (Promega) was added to each well and incubated until color change was observed (50–60 min for H460 CTR5, 80–90 min for H460 LKB1/5, and 100–120 min for H322). The fluorescence was measured at 590 nm using a PHERAstar plate reader. Concentrations that inhibited cell growth by 50% (IC_{50}) were determined by nonlinear regression with GraphPad Prism software 6.2 (GraphPad Software, San Diego, CA).

For the spheroid culture model, H460 CTR5 and H322 cells were grown at 495 cells/well and 650 cells/well, respectively, using a round-bottom, ultra-low attachment 96-well plate (Corning® Costar® Ultra-low attachment multiwell plates, Sigma-Aldrich). Cells were treated with 0.1% DMSO or different concentrations of each drug. After 96 h of treatment, volumes were adjusted to the same level, 100 μ l of CellTiter-Glo® Luminescence Viability assay (Promega) was added, plates were sealed and shaken for 20 min at speed 10, and then incubated for 10

Chapter 3 | Synthesis and cytotoxic activity of novel UA derivatives

min before luminescence was measured using a PHERAstar plate reader at 560 nm. Concentrations that inhibited cell growth by 50% (IC_{50}) were determined by nonlinear regression with GraphPad Prism software 6.2.

3.4.2.4. Macromolecule synthesis assay

Global DNA, RNA, and protein syntheses were measured using [3H]thymidine, [3H]uridine, and [3H]leucine incorporation assays, respectively. Cells were plated in a six-well plate (0.55×10^5 cells/well, 24 h treatment, and 0.15×10^5 cells/well, 48 h treatment, H460 CTR5 cell line, 1 ml RPMI-1640–10% FBS) and after 24 h, cells were treated with DMSO alone or with drugs (in 1 ml of RPMI-1640–10% FBS, total volume 2 ml) for 24 and 48 h. Afterwards, 20 μ l of [methyl- 3H]thymidine, 10 μ l of [5,6- 3H]uridine, or 20 μ l of [4,5- 3H]L-leucine (each isotope was diluted 1:10 times from the original concentration stock (1.0 mCi/ml), in water) per well was added and incubated for an additional 60 min at 37 °C. Cultures were treated with 2 ml of cold PBS, supernatant was collected, and cells were harvested by trypsinization. Each sample was poured into a filter (glass fiber filters, 2.7 cm, wet with 1% (m/v) $Na_4P_2O_4 \cdot 10H_2O$) in a manifold, washed with cold 0.4N perchloric acid aqueous solution (5 ml), and rinsed with 70% EtOH and 100% EtOH. Each dried filter was added to a scintillation vial and 7 ml of scintillation fluid was added. Radioactivity (dpm) was counted using a liquid scintillation counter (instrument series 1900CA, Packard).

3.4.2.5. Cell cycle assay

The cell cycle was assessed by the PI flow cytometric assay. H460 cells were plated in a 100 mm \times 20 mm dish for 24 and 72 h of treatment (3×10^5 and 0.8×10^5 cells/dish, respectively, H460 CTR5 cell line, 10 ml RPMI-1640–10% FBS) and after 24 h, cells were treated with DMSO alone or drugs (in 5 ml RPMI-1640–10% FBS, total volume 15 ml) for 24 and

Chapter 3 | Synthesis and cytotoxic activity of novel UA derivatives

72 h. DMSO or drug-treated cells (1×10^6 cells per experiment) were harvested by trypsinization, collected by centrifugation, washed with PBS, and collected as a pellet. Cells were fixed overnight at 4 °C by adding 70% ethanol and vortexing. Cells were then removed from the ethanol by centrifugation and washed twice with PBS, followed by 15 min of incubation at r.t. with cold PI solution (PBS, 25 µg/ml PI, and 2.5 µg/ml DNase-free RNase). Cell cycle analysis was assessed by flow cytometry using a fluorescence-activated cell sorter (FACS) (BD Accuri™ C6 flow cytometer; BD Biosciences).

3.4.2.6. RNA isolation and array hybridization

Total RNA was extracted with TRIzol® reagent (Life Technologies) according to the manufacturer's protocol. Briefly, cells were plated in a six-well plate (0.55×10^5 cells/well, H460 CTR5 cell line, 1 ml RPMI-10% FBS) and, after 24 h cells were treated with 0.15% DMSO alone or drug (in 1 ml RPMI-10% FBS, total volume 2 ml). After 24 h treatment, medium was removed and 1 ml of TRIzol® reagent was directly add to each well, and the resulting suspension was transferred to an eppendorf, vortex and incubated for 5 min at r.t.. After adding 200 µL of chloroform, samples were vortex for 1 min, incubated for 3 min at r.t., and centrifuged at $12,000 \times g$ for 15 min at 4 °C. After isolation of the aqueous phase, 500 µL 100% isopropanol was added, and samples were incubated for 10 min at r.t., and centrifuged at $12,000 \times g$ for 10 min at 4 °C. Samples were washed twice with 75% ethanol, air dried, and re-suspended in nuclease-free water. RNA concentration was quantified using Thermo Scientific NanoDrop™ 1000 Spectrophotometer, and the RNA integrity was evaluated using Agilent RNA 6000 Nano Kit and Agilent 2100 Bioanalyzer (Agilent Technologies). The total integrity number varied between 7.2 and 7.9. An aliquot of 100 ng of total RNA was amplified using Genechip® WT PLUS Reagent Kit (Affimetrix), according to the manufacturer's instructions. Subsequently, 5.5 µg of single-stranded cDNA was fragmented and terminally labeled, and then was hybridized to Affimetrix

Chapter 3 | Synthesis and cytotoxic activity of novel UA derivatives

GeneChip® HTA 2.0 for 16 h at 45 °C, and washed according to Affimetrix standard protocol. Raw data, transcript data, and exon data were normalized, quality control tested, and analyzed with Expression Console Software (Affymetrix Inc) at the The Sequencing and Non-coding RNA Program, Center for Targeted Therapy at MD Anderson Cancer Center, Houston, TX, USA. For the gene expression analysis, Transcriptome Analysis Console (TAC) software (Affimetrix) was used to detect the differentially expressed genes, using DMSO-treated cells as control.

3.4.2.7. Annexin V-Cy5/PI flow cytometric assay

Apoptosis was measured by using the annexin V/PI flow cytometric assay. Cells were plated in a six-well plate (0.095×10^5 cells/well, H460 CTR5 cell line, 2 ml of RPMI-1640–10% FBS), and after 24 h, cells were treated with DMSO alone or with drugs (in 1 ml of RPMI-1640–10% FBS, total volume 3 ml) for 72 h. Cells were harvested by trypsinization, collected by centrifuge, washed with PBS, and collected as a pellet. The pellet was re-suspended in annexin V-Cy5/buffer solution (5 μ l of annexin V-Cy5 in annexin binding buffer $\times 10$) and incubated at room temperature in the dark for 15 min. PI solution (10 μ l PI (50 μ g/ml) + 300 μ l annexin binding buffer) was added just before analysis using a BD Accuri™ C6 flow cytometer (BD Biosciences). Data from 1×10^4 cells per sample were collected and analyzed.

3.4.2.8. Acridine orange staining

As a marker of autophagy, acidic vesicular organelles were quantified by acridine orange staining. Cells were plated onto six-well plates (0.095×10^5 cells/well, H460 CTR5 cell line, 2 ml of RPMI-1640–10% FBS) and after 24 h, cells were treated with DMSO alone, drugs, or medium alone (in 1 ml of RPMI-1640–10% FBS, total volume 3 ml) for 72 h. 30 min prior to staining, 1 μ l of 160 μ M bafilomycin A1 was added to the untreated well (medium only) as a negative control,

Chapter 3 | Synthesis and cytotoxic activity of novel UA derivatives

and samples were incubated at 37 °C. Afterwards, 3 µl of acridine orange stain (10 mg/ml stock) (Invitrogen Life Technologies) was added to each sample and incubated at 37 °C for 15 min in the dark. The medium was collected, and cells were harvested using Accumax cell dissociation solution in DPBS, using RPMI-1640 with no phenol red (Gibco Life Technologies) to stop the reaction, and centrifuged. The pellet was washed with PBS, centrifuged, and re-suspended in RPMI-1640 without phenol red. Accumulation of acidic vesicles was quantified as the red/green (FL3/FL1) fluorescence ratio using a BD Accuri C6 flow cytometer.

3.4.2.9. Protein extraction and immunoblot assay

To prepare the total protein extracts, H460 CTR5 cells (3×10^5) and H322 cells (4.2×10^5) were seeded in a 100 mm × 20 mm dish (10 ml of RPMI-1640–10% FBS) and incubated at 37 °C. After 24 h, cells were treated with DMSO or different concentrations of drug (in 5 ml of RPMI-1640–10% FBS, total volume 15 ml) for 24 h. After treatment, medium was collected and cells were harvested by trypsinization, washed twice with PBS, centrifuged, lysed using cold 1× RIPA buffer (1 ml of 10× RIPA lysis buffer, one tablet of PhosStop phosphatase inhibitor cocktail, and one tablet of cOmplete mini protease inhibitor cocktail), and sonicated for 4 min with 30-second intervals at 4 °C. Lysed cells were centrifuged for 10 min at 13,000 rpm, and supernatant was carefully removed. All steps were performed on ice. Protein concentration of the lysate was determined using a DCTM protein assay kit (Bio-Rad Laboratories). 5 µl of lysate was added to a 96-well plate followed by the addition of 25 µl of working solution A-S (20 µl reagent S to each milliliter of reagent A needed for the assay) plus the addition of 200 µl of reagent B. The plate reading was taken at 750 nm (Powerwave XS, Bio-Tek Instruments, Inc.) using known standards; unknown concentrations of protein lysates were determined using Gen5TM software (BioTek). 30 µg of protein lysates was boiled with loading buffer SDS-PAGE with 10% 2-mercaptoethanol at 95 °C for 10 min. Prepared lysate buffer solutions were

Chapter 3 | Synthesis and cytotoxic activity of novel UA derivatives

electrophoresed on Criterion Bis-Tris gel (4-10% or 12%) using 1× MOPS or 1× MES running buffer. Afterwards, proteins were transferred from the gel to membrane nitrocellulose (LI-COR Biosciences) or polyvinylidene difluoride (PVDF, RMD Millipore) (this membrane was pre-treated with methanol), using a transfer buffer solution (800 ml Millipore water, 100 ml methanol, 100 ml 10× transfer buffer (30 g Tris-base, 144 g glycine for 1 liter of Millipore water)) at 75V for 50 min on ice. After transfer, PVDF membrane was dried for 1h, wet with methanol, and washed with PBS. PVDF and nitrocellulose membranes were first blocked with Odyssey® blocking buffer solution for 1 h at room temperature and then probed with primary antibodies overnight at 3–8 °C. Membranes were washed twice for 10 min with 0.1% Tween 20 (in PBS) and then one time with PBS, and probed with infrared-labeled secondary antibody (1:10000 dilution, LI-COR Inc.) for 1 h at room temperature. Membranes were again washed as before and scanned using the LI-COR Odyssey CLx Infrared Imager.

3.4.2.10. Reverse Phase-Protein Array (RPPA)

H460 CTR5 cells (3×10^5) were seeded in a dish 100 mm x 20 mm (10 ml RPMI-1640-10% FBS) and incubated at 37 °C. After 24 h, cells were treated with DMSO or different concentration of drug (in 5 ml RPMI-1640-10% FBS, total volume 15 ml) for 24 h. After treatment, medium was collected and cells were harvested by trypsinization, washed twice with PBS, centrifuged, and the cells lysates were prepared according to the instructions of the Functional Proteomics Core facility at MDACC, Houston, TX, USA. In brief, cells were lysed in RPPA lysis buffer (1% Triton X-100, 50 mM HEPES, pH 7.4, 150 mM NaCl, 1.5 mM MgCl₂, 1 mM EGTA, 100 mM NaF, 10 mM Na pyrophosphate, 1 mM Na₃VO₄, 10% glycerol, one tablet of PhosStop (phosphatase inhibitor cocktail) and one tablet of cOmplete™, Mini (protease inhibitor cocktail)). The cell lysates were sonicated for 4 min with 30-second intervals at 4 °C. Lysed cells were centrifuged for 10 min at 13,000 rpm at 4 °C, and supernatant was carefully removed. All

Chapter 3 | Synthesis and cytotoxic activity of novel UA derivatives

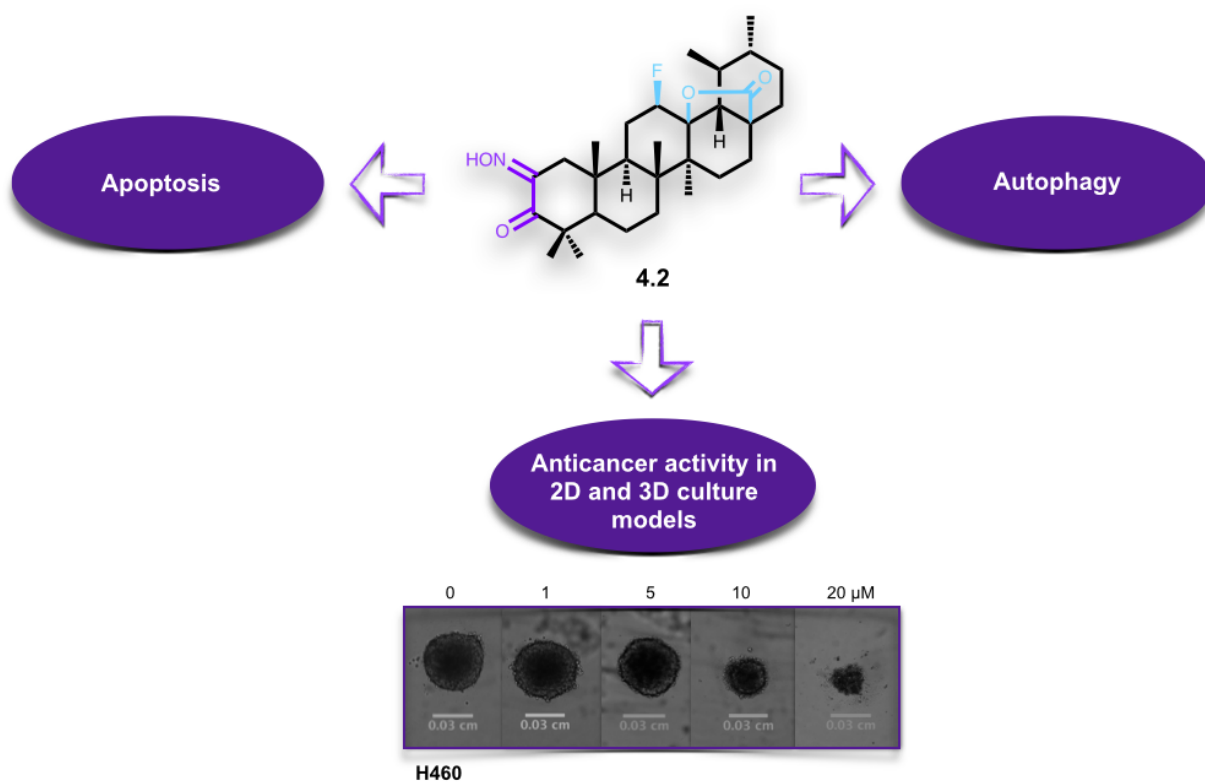
steps were performed on ice. Protein concentration was determined as described in section 3.4.2.9. The protein concentration was adjusted to 1.5 μ l, and the cell lysate was mixed with 4X SDS sample buffer (40 % glycerol, 8 % SDS, 0.25 M Tris-HCl, pH 6.8) with 10% 2-mercaptoethanol, boiled for 10 min at 95 °C. Protein samples were serially diluted and arrayed on nitrocellulose-coated glass slides. The slides were probed with 298 primary antibodies against critical nodes in the cancer cell signaling pathways, and scanned with ImageQuant (Molecular Dynamics). Signal intensity was quantified using MicroVigene automated RPPA module software (VigeneTech Inc.), relative protein abundance was estimated by supercurve fitting, and normalized for protein loading. The RPPA data were normalized to control, log₁₀ transformed, statistically analyzed (unpaired *t*-test), and the overall fold-change was analyzed.

3.4.2.11. Data and statistical analysis

All cell line data were analyzed in triplicate and are presented as mean values \pm standard deviation (SD). All data were analyzed and plotted using GraphPad Prism 6.2 software. Protein levels were quantified using Odyssey software for the Odyssey Infrared Imaging System (LI-COR Inc.) and then normalized to DMSO control using GraphPad Prism software. The ratio of protein to GAPDH or to β -actin was calculated for the immunoblot analyses. For statistical analysis, most data were analyzed by the Student's unpaired *t* test, as described in the respective figure legends.

Chapter 4

Synthesis and cytotoxic activity of new oxime and nitrile ursolic acid derivatives in NSCLC



Vanessa I. S. Mendes, Geoffrey A. Bartholomeusz, Varsha Gandhi, and Jorge A. R. Salvador, *Synthesis and anti-lung cancer activity of new oxime and nitrile ursolic acid derivatives in 2D and 3D models*, in preparation.

4.1. Introduction

The introduction of a nitrile group into pharmaceutical compounds has been attracting interest, because its presence in key positions of a biologically active molecule can modulate the physicochemical and pharmacokinetic properties.^{200,201} In fact, structurally diverse nitrile-containing drugs are currently prescribed for a variety of diseases, including cancer, and several of nitrile-containing leads are currently in clinical trials.²⁰⁰ A survey of a range of pharmaceuticals and clinical candidates has identified several effects of the introduction of a nitrile function into bioactive molecules.²⁰⁰ This functional group can act not only as a hydroxyl and carboxyl surrogate, due to its strong hydrogen bond interactions, but also as a carbonyl and halogen bioisostere.^{200,202-204}

The introduction of an oxime function into an appropriate scaffold is also a rational approach for the preparation of potent cytotoxic agents, as illustrated in diverse examples where its introduction into different backbones has led to derivatives with potent antiproliferative activities against human cancers.²⁰⁵⁻²⁰⁷

Furthermore, in previous studies, our research group has reported that the introduction of *N*-acylimidazole moiety in pentacyclic triterpene structures could improve the *in vitro* anticancer activity of the parent compound.^{138,208-211} Hence, the introduction of *N*-acylimidazole moiety was further explored using the commercial available reagents 1,1'-carbonyldiimidazol (CDI), 1,1'-carbonyl-di-(1,2,4-triazole) (CDT), and 1,1'-carbonylbis(2-methylimidazole) (CBMI).

This chapter describes the design and preparation of a panel of derivatives with a modified A-ring. The introduction of oxime and nitrile functions, as well as *N*-acylimidazole moieties was explored. The structures of the newly synthesized compounds were fully elucidated by IR, MS and NMR techniques. The *in vitro* anticancer activity was tested against

NSCLC cell lines, in monolayer and spheroid culture models, and the preliminary mechanism of action of the most potent derivative was explored.

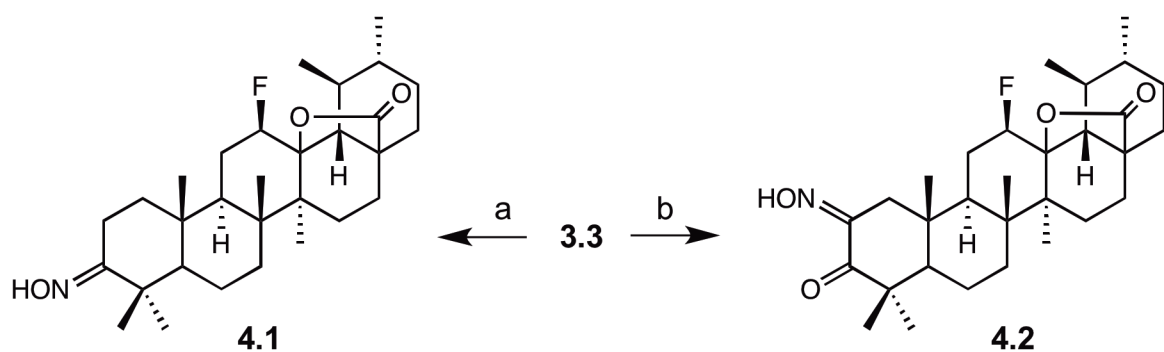
4.2. Results and discussion

4.2.1. Chemistry

The synthetic route began with the formation of 12 β -fluoro-13,28 β -lactone (**3.2**) and 3-oxo (**3.3**) derivatives as described in chapter 3.

To study the effect of the introduction of an oxime group on the anticancer activity, several **UA** derivatives were prepared bearing an oxime group at positions C3, C2, or C2 and C3.

Treatment of 3-oxo-derivative **3.3** with $\text{NH}_2\text{OH}\cdot\text{HCl}$ in pyridine at 50 °C afforded oxime derivative **4.1**, while treatment with butyl nitrite in a mixture of *t*-BuOK in *t*-BuOH, under N_2 at 25 °C, afforded compound **4.2** (Scheme 4.1).

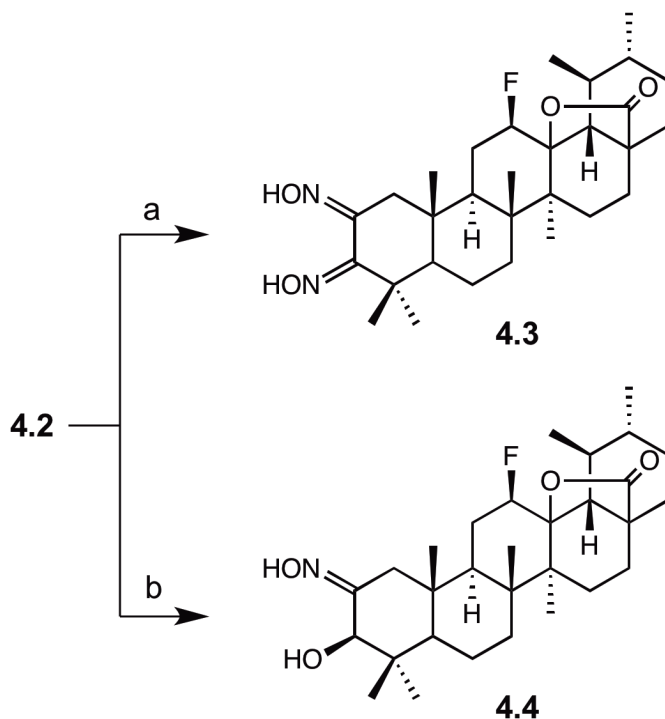


Scheme 4.1. Synthesis of derivatives **4.1** and **4.2**.

Reagents and conditions: a) $\text{NH}_2\text{OH}\cdot\text{HCl}$, pyridine, 50 °C, 2 h; b) *n*-BuONO, *t*-BuOK, *t*-BuOH, N_2 , 25 °C, 2 h.

Chapter 4 | Synthesis and cytotoxic activity of novel UA derivatives

Compound **4.2** was treated with $\text{NH}_2\text{OH}\cdot\text{HCl}$, as before, to obtain the double oxime derivative **4.3**. Moreover, the carbonyl function at C3 of compound **4.2** was reduced with NaBH_4 , in a mixture of dry methanol and THF under N_2 at room temperature to obtain compound **4.4** (Scheme 4.2).



Scheme 4.2. Synthesis of derivatives **4.3** and **4.4**.

Reagents and conditions: a) $\text{NH}_2\text{OH}\cdot\text{HCl}$, pyridine, 50 °C, 7 h; b) NaBH_4 , dry methanol/THF, N_2 , r.t., 3 h.

The presence of an oxime group was confirmed in the ^1H NMR spectra by a broad singlet at 9.00, 7.55, and 6.71 ppm for compounds **4.1**, **4.2**, and **4.3**, respectively. For compounds **4.2** and **4.3**, the protons at position C1 were identified as a double doublet around 3.10 and 2.20 ppm, with a coupling constant of around 18.5 Hz. Figure 4.1 represents the ^1H NMR spectrum of compound **4.2**.

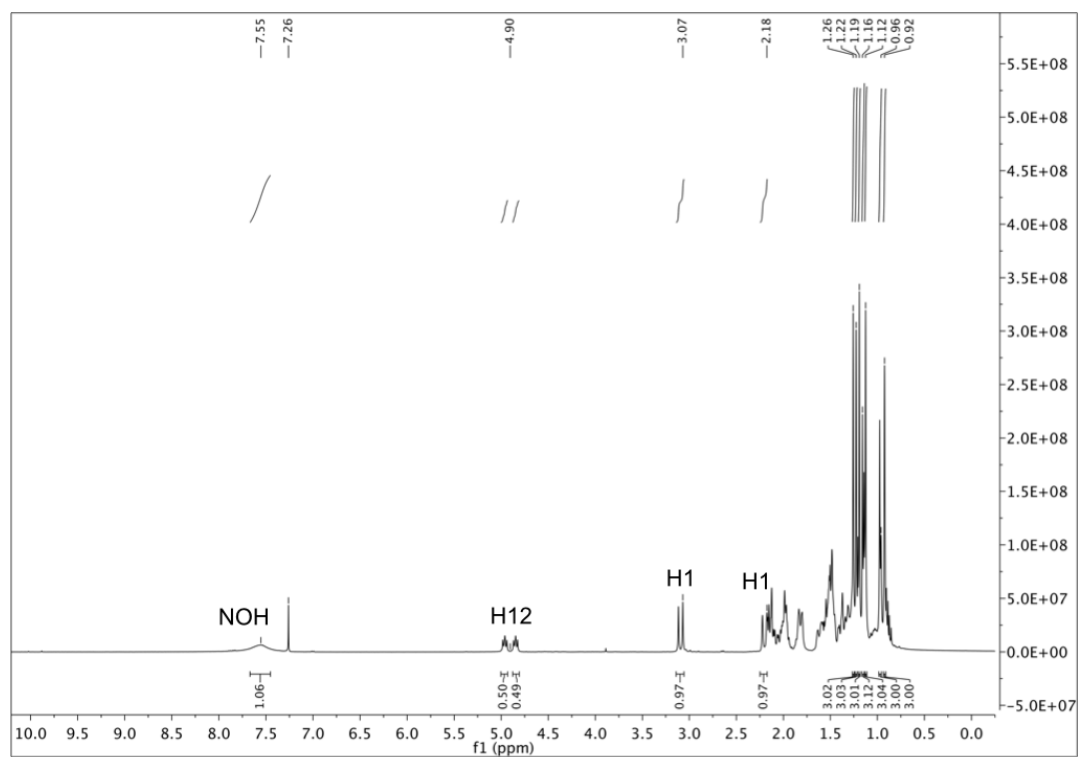


Figure 4.1. ^1H NMR spectrum of compound **4.2** recorded in CDCl_3 .

In the ^{13}C NMR spectra, the carbon of the oxime was identified at 166.47 ppm for **4.1**, 153.53 ppm for **4.2**, and 153.32 and 153.20 ppm for **4.3**. For compound **4.2**, the carbonyl carbon at C3 was identified at 203.08 ppm (Fig. 4.2).

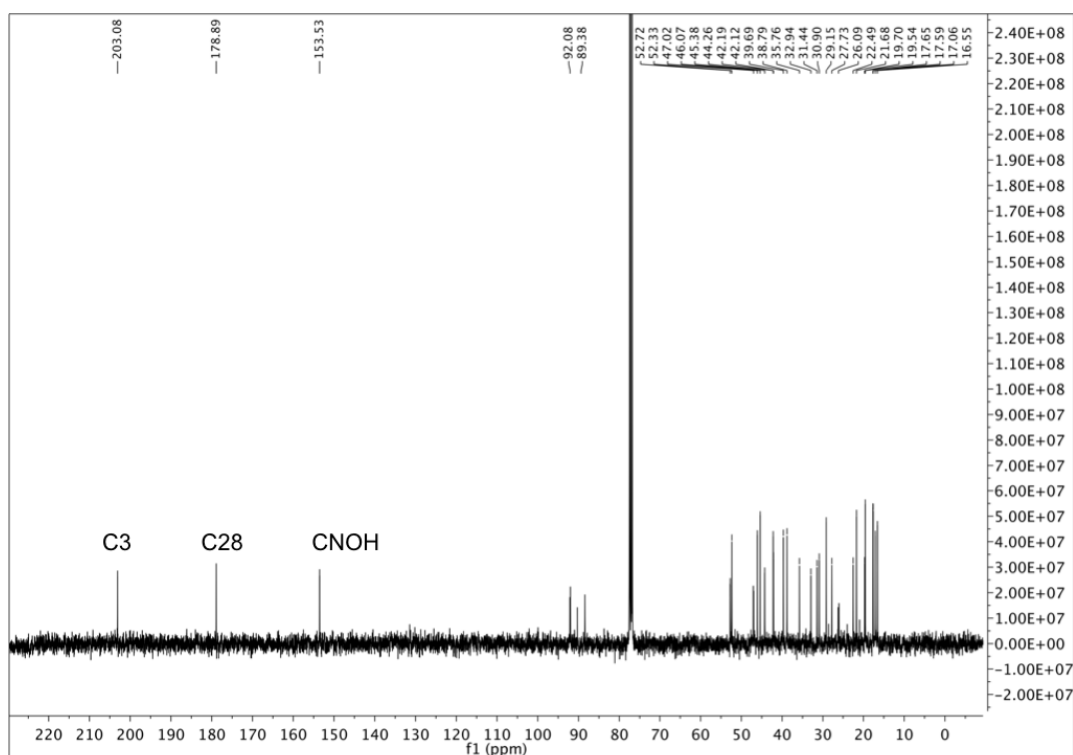


Figure 4.2. ^{13}C NMR spectrum of compound **4.2** recorded in CDCl_3 .

The characteristic IR bands for OH (oxime) and for C=N (oxime) were observed around $3359\text{--}3214\text{ cm}^{-1}$ and $1656\text{--}1606\text{ cm}^{-1}$, respectively. For compound **4.2**, the band for C=O (C3) was identified at 1703 cm^{-1} (Fig. 4.3).

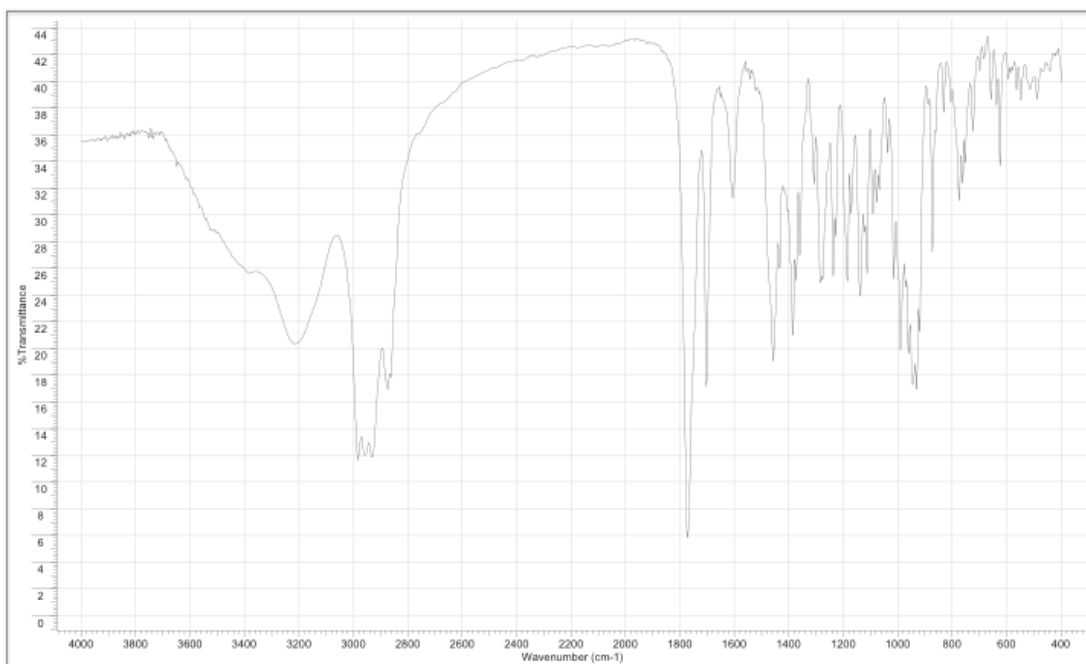


Figure 4.3. IR spectrum of compound 4.2.

Previous studies reported in the literature under similar chemical conditions and using similar triterpenoid substrates indicated that oximes **4.1**²¹², **4.2**^{213,214} and **4.3**²¹⁴ prepared by the indicated methods display an *E*-configuration. The configuration of compound **4.3** was confirmed via X-ray crystallography, which established compound **4.3** as an *E*-isomer (Fig. 4.4).

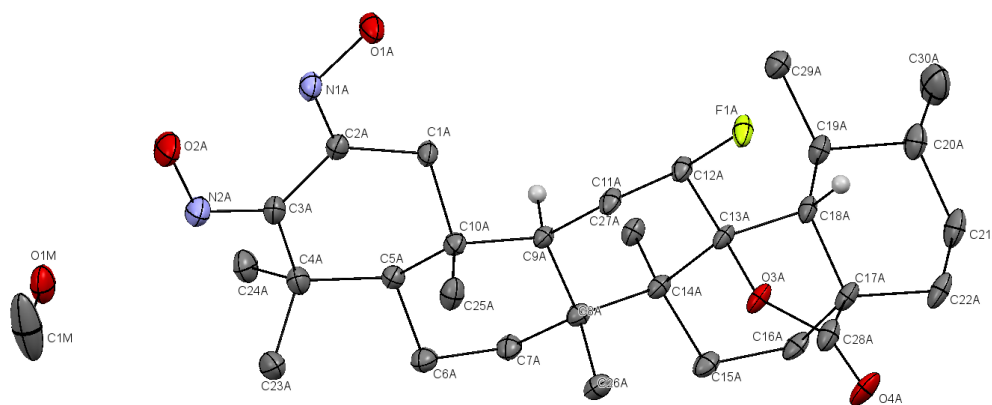


Figure 4.4. ORTEP diagram of compound 4.3 crystallized from methanol.

Chapter 4 | Synthesis and cytotoxic activity of novel UA derivatives

The reduction of the carbonyl function to obtain derivative **4.4** was identified in the ^1H NMR spectrum by a signal of a singlet at 3.85 ppm for the proton at position 3 (Fig. 4.5), and in the ^{13}C NMR spectrum by the substitution of the signal at 203.08 ppm (compound **4.2**) with a signal at 78.51 ppm for the C3 (Fig. 4.6).

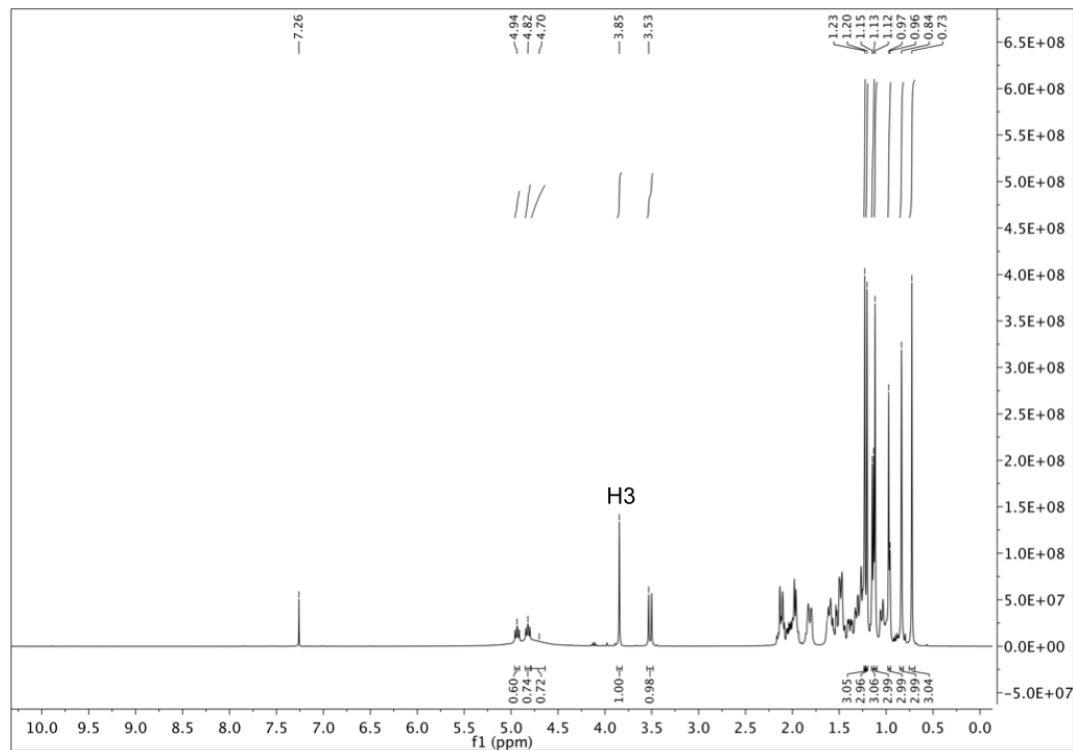


Figure 4.5. ^1H NMR spectrum of compound **4.4** recorded in CDCl_3 .

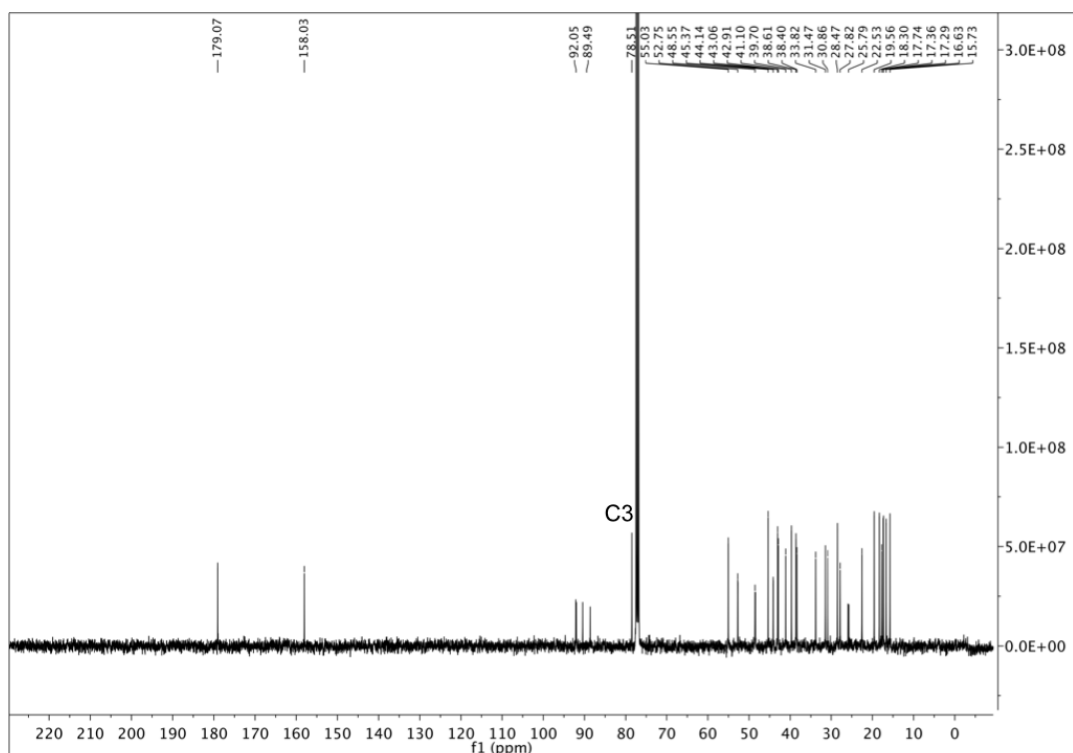


Figure 4.6. ^{13}C NMR spectrum of compound **4.4** recorded in CDCl_3 .

NOESY NMR experiments correlate protons that are close to each other in space, allowing the identification of protons with the same space orientation. Accordingly, for compound **4.4**, the proton at position 3, in the NOESY NMR spectrum, correlated with the two methyl groups at positions 23 and 24, and with the proton at position 5 (Fig. 4.7 and 4.8). This profile indicates that the proton at position 3 has an alpha-configuration, as a beta-configuration would not be able to correlate with the proton at position 5 (Fig. 4.8). These data are in accordance with previous studies reported in the literature under similar chemical conditions and using similar triterpenoid substrates.^{215,216}

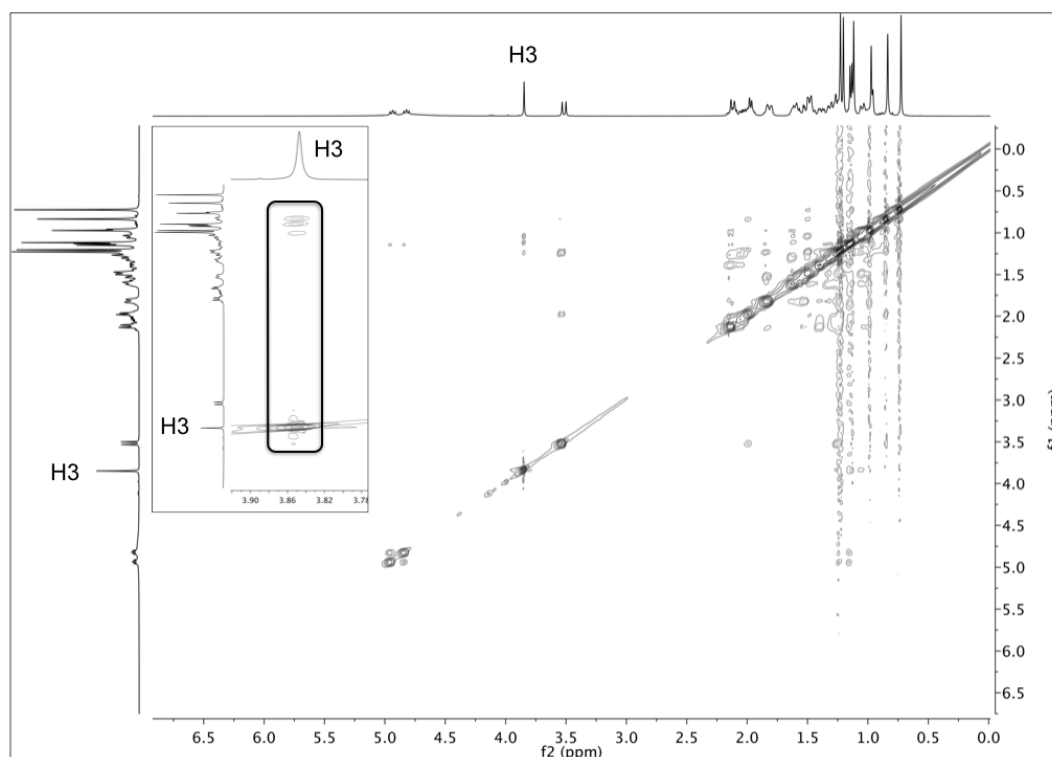


Figure 4.7. NOESY NMR spectrum of compound **4.4** recorded in CDCl_3 .

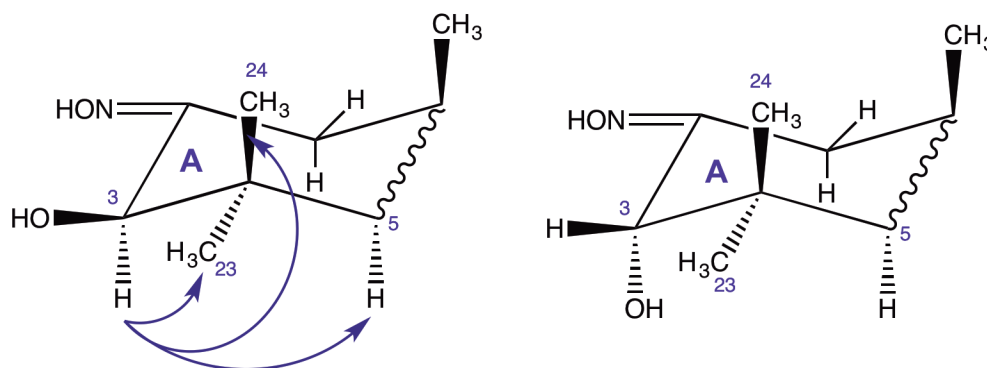


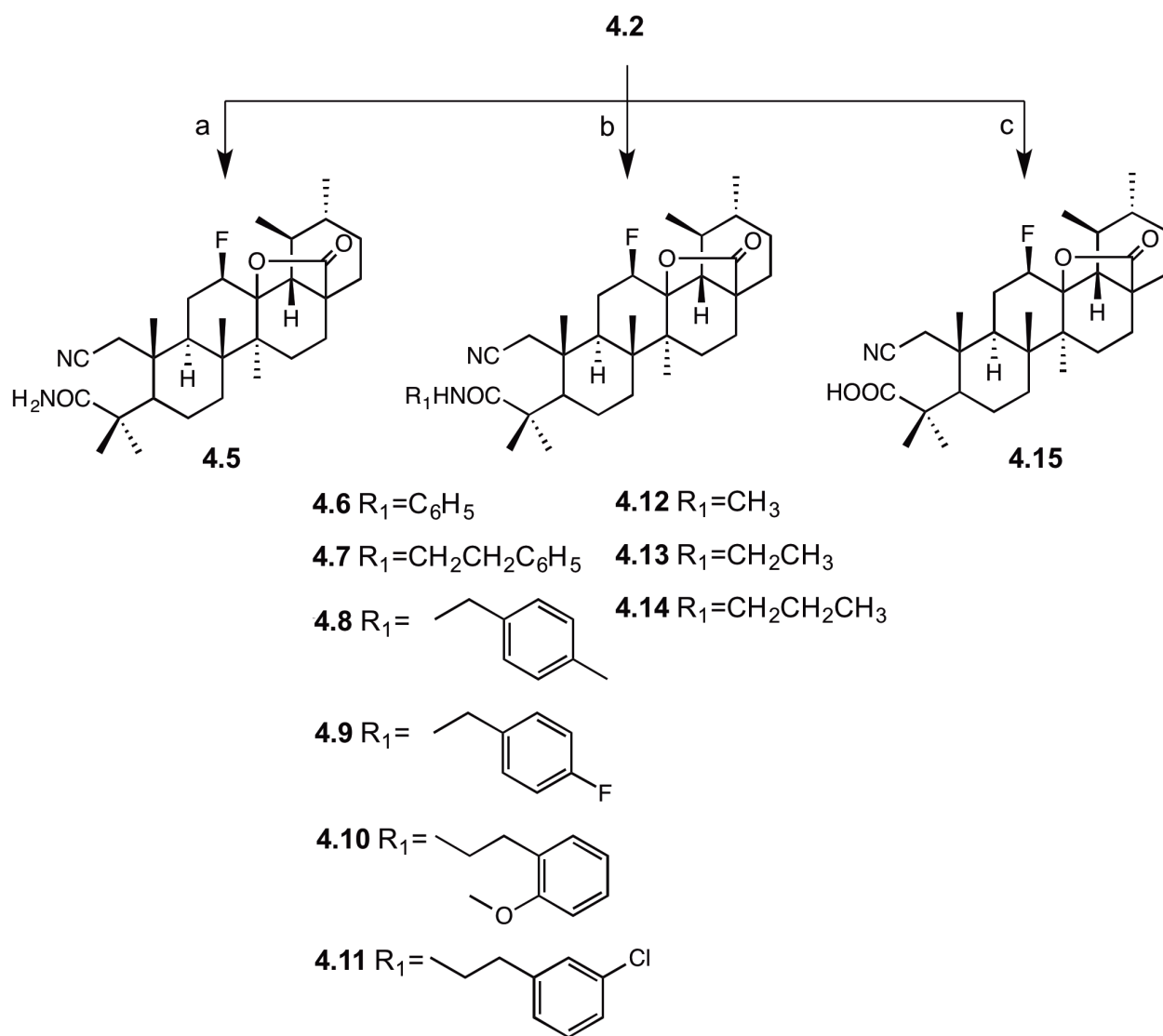
Figure 4.8. NOESY correlation for compound **4.4**. The proton at position 3 is shown with an alpha- (left image) or beta-configuration (right image).

Taking into account the ability of the nitrile group to modulate the physicochemical and pharmacokinetic properties, a panel of **UA** nitrile derivatives was synthesized (**4.5–4.20**) (Schemes 4.3–4.5).

Chapter 4 | Synthesis and cytotoxic activity of novel UA derivatives

As mentioned previously, amide bonds play a major role in the elaboration and composition of biological systems, representing the main chemical bonds that link amino acid building blocks together to provide proteins.³⁸⁻⁴⁰ Therefore, a series of cleaved A-ring derivatives bearing a nitrile group at C2 and an amide function at C3 (**4.5–4.14**) were prepared.

Firstly, compound **4.2** was treated with thionyl chloride (SOCl₂) in dry THF/benzene at 80 °C for 3 h to form an intermediate with a cleaved A-ring and bearing a nitrile function at position 2. Then, the reaction solvents were evaporated, and the residue was dissolved with dry THF and treated with cold ammonium solution 25% to afford compound **4.5**, or dissolved with dry CH₂Cl₂, pH-adjusted with Et₃N to 8–9, and treated with several amines to afford the respective amide derivatives (**4.6–4.14**). Compound **4.15** was isolated by reacting compound **4.2** with SOCl₂, as describe above (Scheme 4.3).



Scheme 4.3. Synthesis of derivatives **4.5–4.15**.

Reagents and conditions: a) i - $SOCl_2$, dry THF/benzene, 80 °C, 3 h; ii - cold ammonium solution 25%, THF, 1 h; b) i - $SOCl_2$, dry THF/benzene, 80 °C; ii – R_1NH_2 , dry CH_2Cl_2 , Et_3N , r.t., **4.6–4.9**, **4.11**: 2 h; **4.10**: 3 h; **4.12**, **4.13**: 1.5 h; **4.14**: 3.5 h; c) $SOCl_2$, dry THF/benzene, 80 °C, 3.5 h.

This cleavage reaction with formation of nitrile and carboxylic acid groups has been designated as “abnormal” Beckmann rearrangement or Beckmann rearrangement of second order, in which α -oximino ketones possessing an anti- or α -configuration when treated with acid chlorides, strong acids, or an acylating agent and base, are cleaved to a nitrile and a carboxylic

Chapter 4 | Synthesis and cytotoxic activity of novel UA derivatives

acid instead of the amide product of the Beckmann rearrangement.²¹⁷ According to the proposed mechanism, the reaction involves the conversion of the hydroxyl group of the oxime into a leaving group by SOCl_2 , accompanied by a shift of a electron pair forming the carbon-nitrogen triple bond, and hence the nitrile. The intermediate cation then combines with a hydroxide anion or water to form the carboxylic acid group (Fig. 4.9).

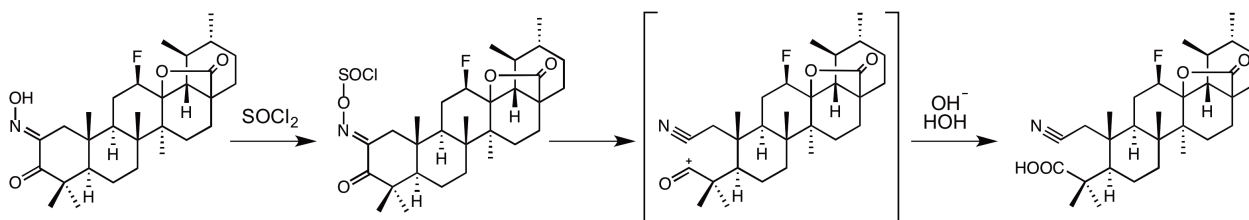


Figure 4.9. Proposed reaction mechanism of the “abnormal” Beckmann rearrangement for the formation of compound **4.15**.

In the ^1H NMR spectrum, the typical signal for the NH proton (compounds **4.5–4.14**) was observed around 6.09–5.75 ppm, which varied between singlet, triplet, and double doublet, according to the type of amide derivative. The protons at position 1 were observed by two doublets around 2.81–2.39 and 2.51–2.30 ppm, with a coupling constant of 18.3 Hz. Figure 4.10 represents the ^1H NMR spectrum of the primary amide derivative **4.5**.

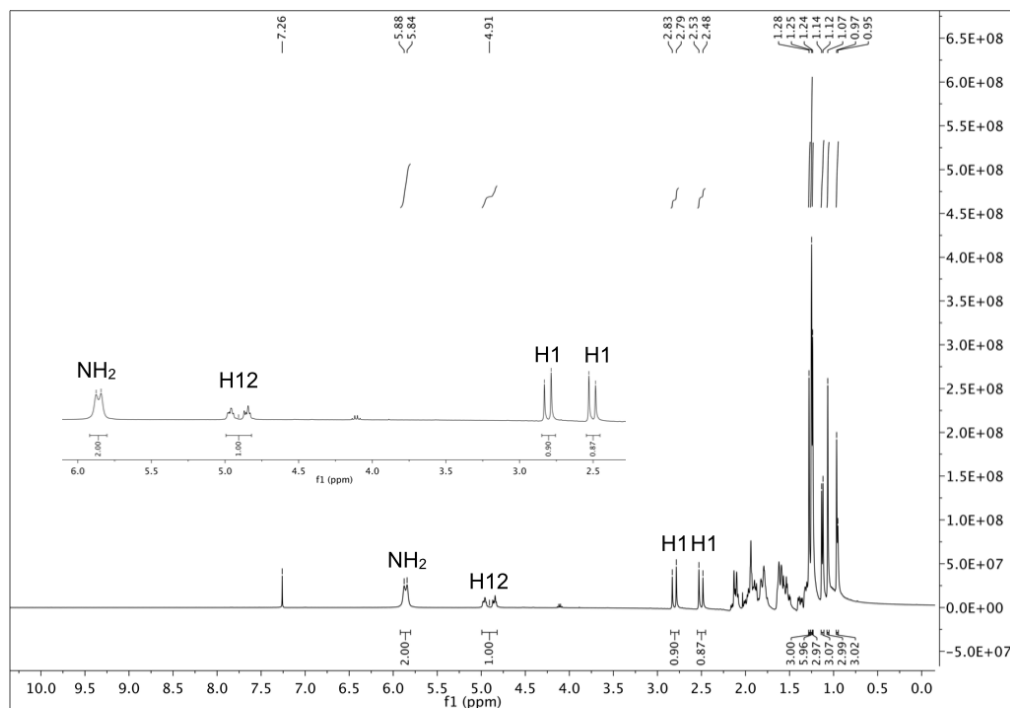


Figure 4.10. ¹H NMR spectrum of compound 4.5 recorded in CDCl₃.

The carbonyl carbon of the amide was observed in the ¹³C NMR spectra at 181.67 ppm for the primary amide 4.5 (Fig. 4.11), and around 179–176 ppm for the secondary amide derivatives (4.6–4.14). The carbon of the nitrile group was identified at around 119–118 ppm (Fig. 4.11).

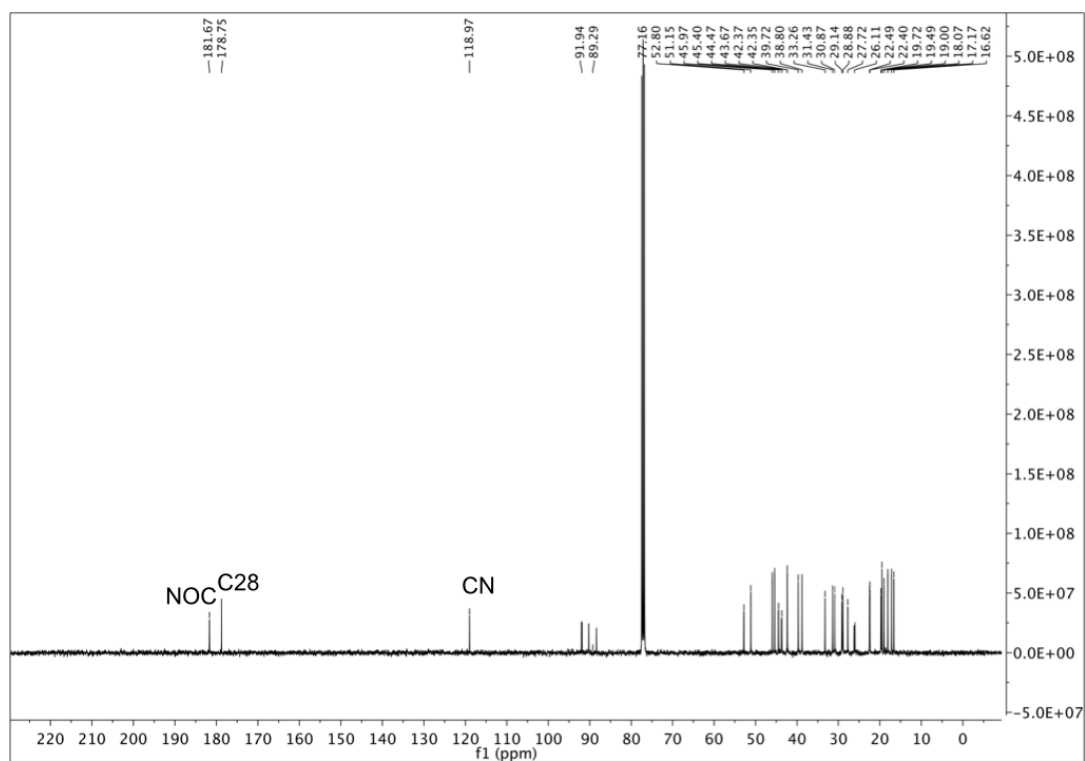


Figure 4.11. ^{13}C NMR spectrum of compound **4.5** recorded in CDCl_3 .

The carbon of the carboxylic acid of derivative **4.15** displayed a signal at 184.40 ppm in the ^{13}C NMR spectrum. Figures 4.12 and 4.13 represent the ^1H and ^{13}C NMR spectra of compound **4.15**, respectively.

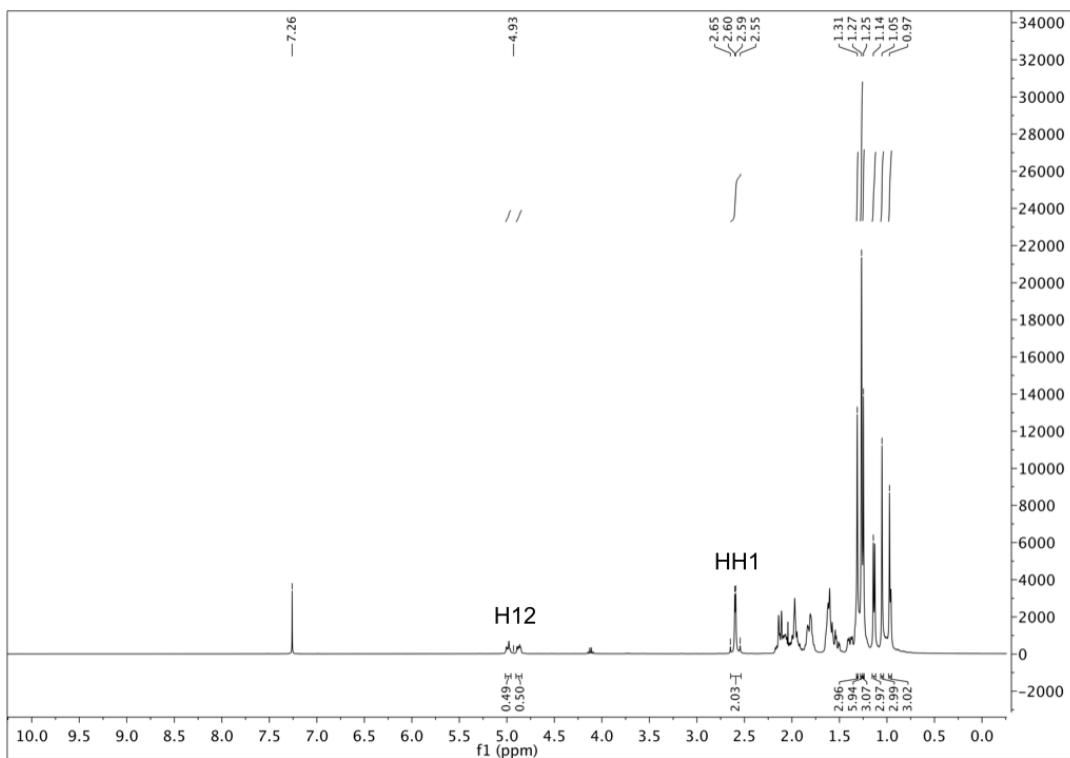


Figure 4.12. ^1H NMR spectrum of compound **4.15** recorded in CDCl_3 .

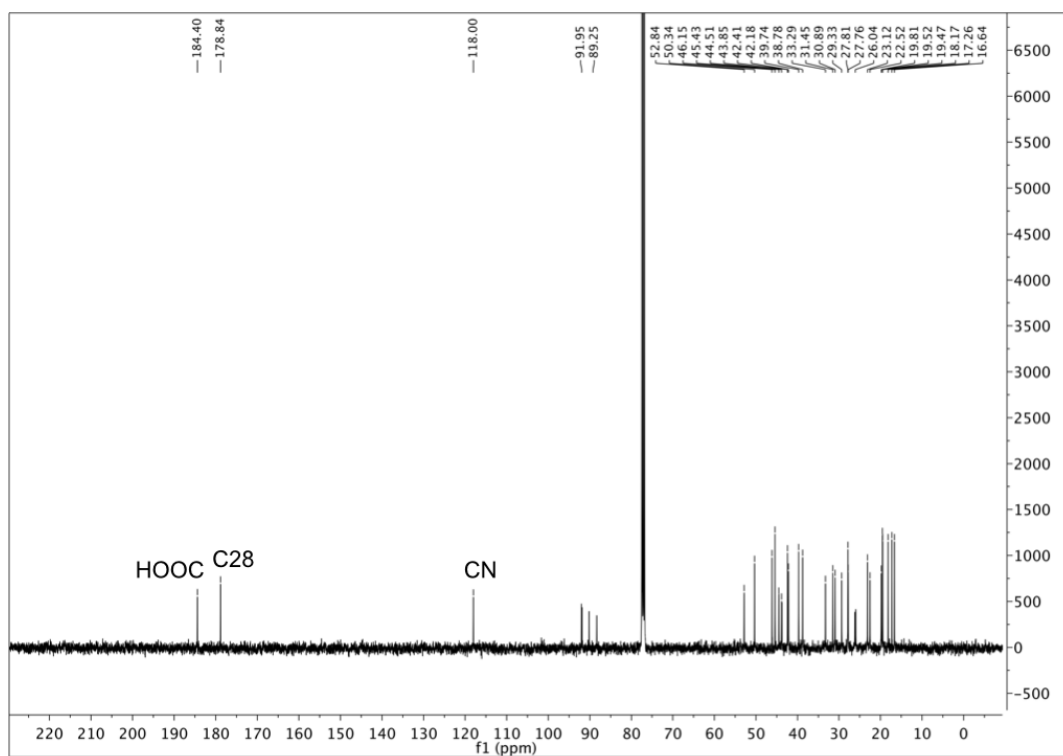


Figure 4.13. ^{13}C NMR spectrum of compound **4.15** recorded in CDCl_3 .

Chapter 4 | Synthesis and cytotoxic activity of novel UA derivatives

In the IR spectra, a band at 2243–2231 cm^{-1} identified the presence of a CN group. For the amide function, two stretching bands at 3508 and 3371 cm^{-1} were observed for the primary amide **4.5** (Fig 4.14), while the stretching bands for the secondary amides (**4.6–4.14**) were identified at 3464–3363 cm^{-1} .

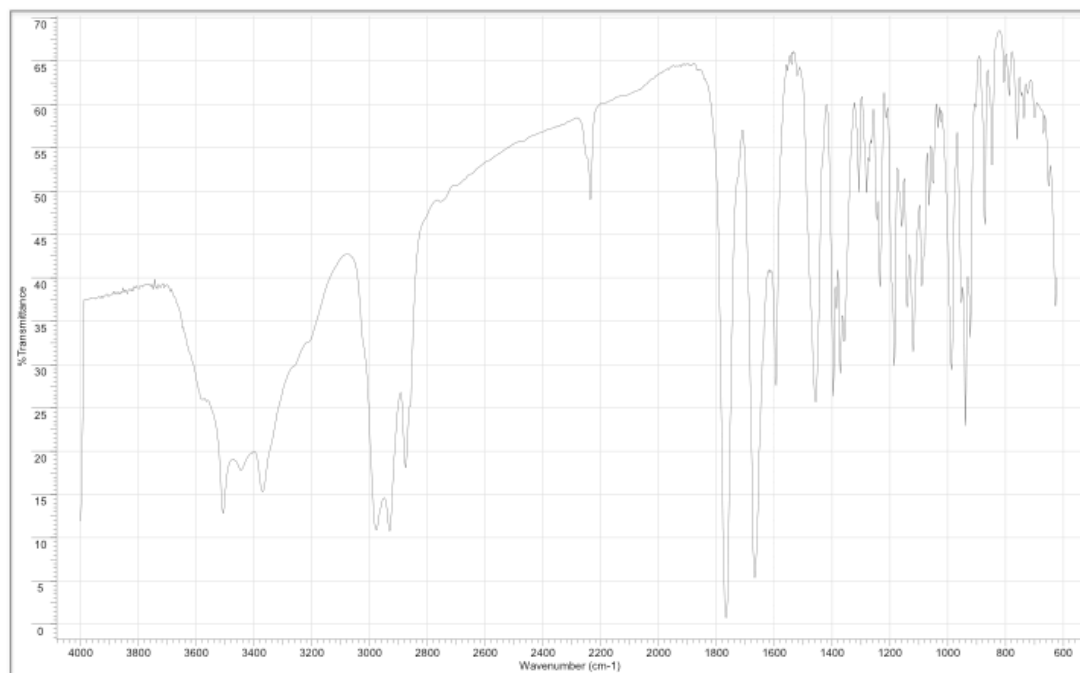
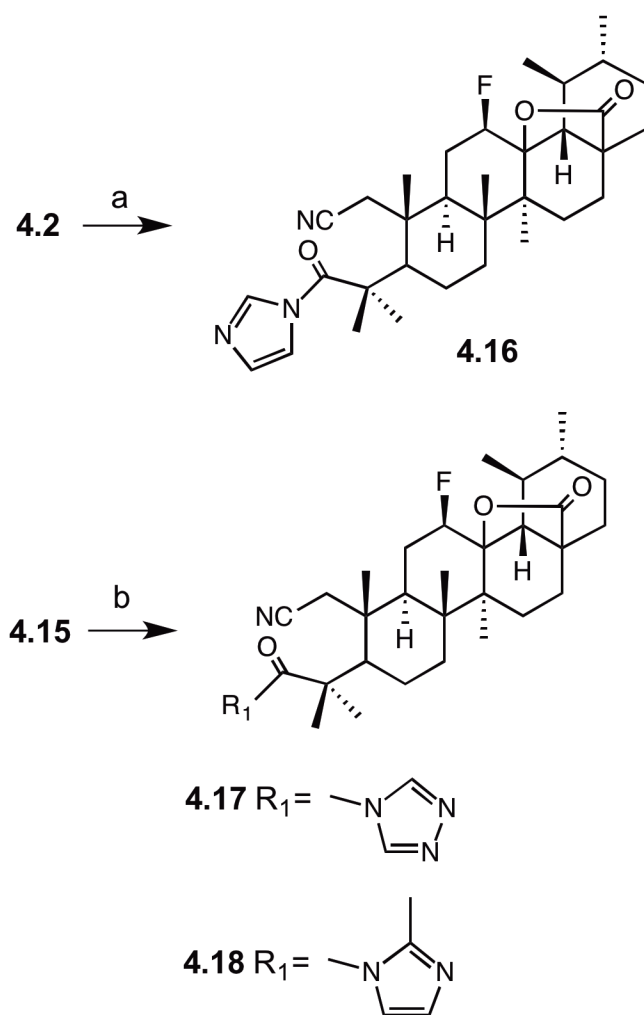


Figure 4.14. IR spectrum of compound **4.5**.

In previous studies, our research group has reported that the introduction of *N*-acylimidazole moiety in pentacyclic triterpene structures often improves the *in vitro* anticancer activity of the parent compound.^{138,208-211} Therefore, *N*-acylimidazole derivatives were prepared (**4.16–4.18**) by reacting compound **4.2** with CDI, in THF at 50 °C under N₂ to obtain **4.16**, or by reacting compound **4.15** with CDT or CBMI in dry THF at 70 °C under N₂ to afford compounds **4.17** and **4.18**, respectively (Scheme 4.4).



Scheme 4.4. Synthesis of derivatives **4.16–4.18**.

Reagents and conditions: a) CDI, dry THF, N₂, 50 °C, 3 h; b) CDT (for **4.17**) or CBMI (for **4.18**), dry THF, 70 °C, **4.17**: 4.25 h, **4.18**: 2.25 h.

The formation of the imidazole derivative **4.16** was confirmed by the presence of three proton signals at 8.40, 7.75, and 7.12 ppm in the ¹H NMR spectrum (Fig. 4.15). The triazole derivative **4.17** was confirmed, in the ¹H NMR spectrum, by the presence of two signals at 8.96 and 8.09 ppm that correspond to the two protons in the triazole ring. In the case of the 2-methylimidazole derivative **4.18**, the two characteristic proton signals appeared at 7.72 and 6.96 ppm, and an additional methyl signal was observed at 2.61 ppm.^{209,210}

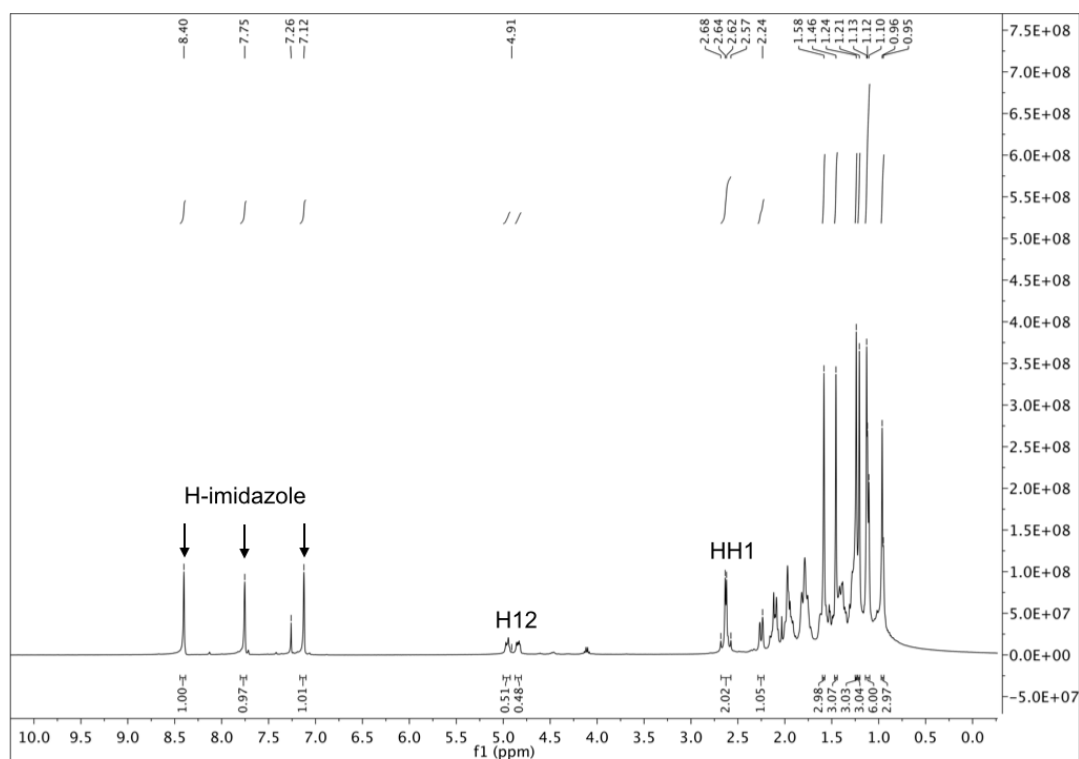


Figure 4.15. ^1H NMR spectrum of compound **4.16** recorded in CDCl_3 .

In the ^{13}C NMR spectrum, the formation of the imidazole derivative **4.16** was confirmed by the presence of three carbon signals at 138.07, 130.90 and 117.80 ppm that correspond to the imidazole ring, and by the signal of the carbon of the amide function at 175.64 ppm (Fig. 4.16). The signal of the carbon of the nitrile appeared at the same chemical shift as one of the imidazole carbons (117.80 ppm) (Fig. 4.16). The structure of compound **4.16** was confirmed by X-ray crystallography (Fig 4.17). In the case of the triazole derivative **4.17**, the two signals of the carbons of the triazole moiety were identified at 153.01 and 145.76 ppm. Similarly, the 2-methylimidazole derivative **4.18** was confirmed by the presence of three carbon signals at 149.65, 128.24 and 117.88 ppm.

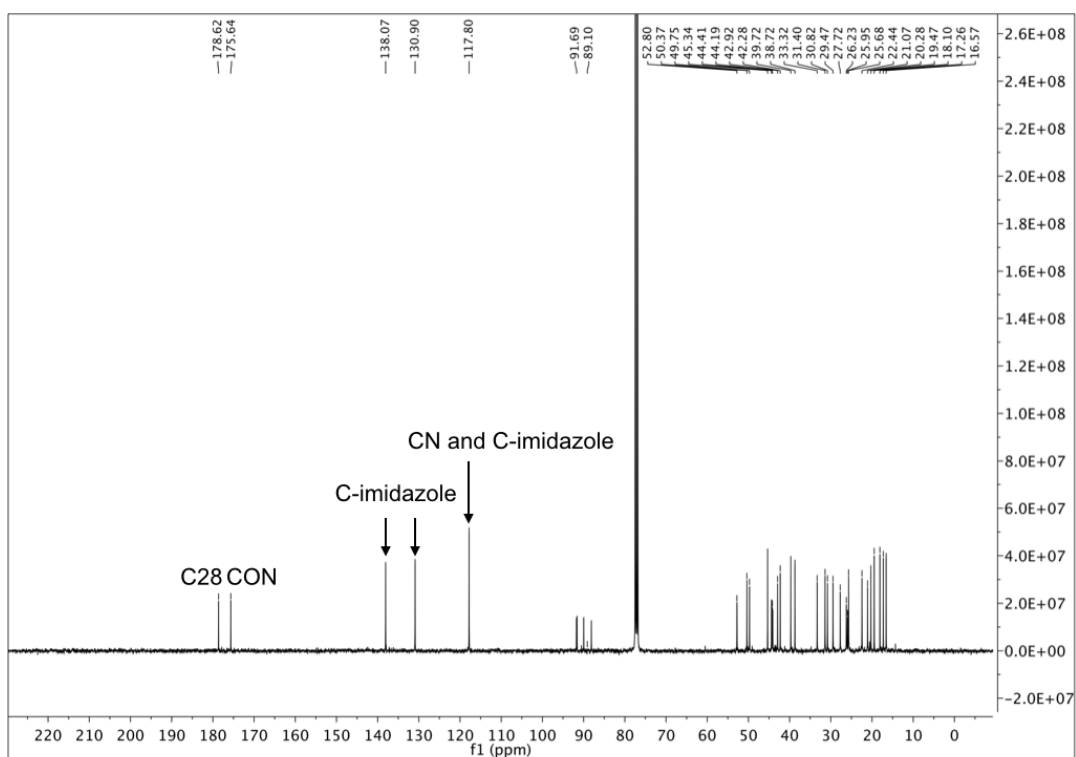


Figure 4.16. ^{13}C NMR spectrum of compound **4.16** recorded in CDCl_3 .

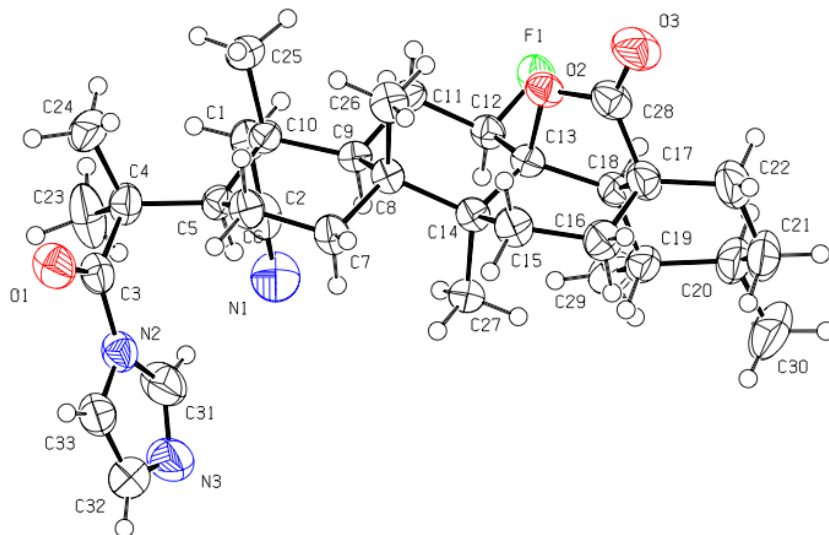
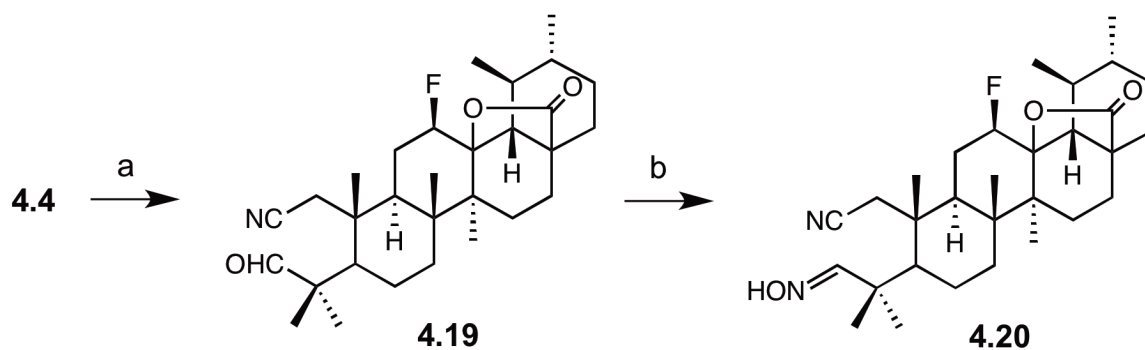


Figure 4.17. ORTEP diagram of compound **4.16** crystallized from acetonitrile.

Chapter 4 | Synthesis and cytotoxic activity of novel UA derivatives

To further study the presence of different functional groups at position C3 coupled with a nitrile group at C2, an aldehyde (**4.19**) and an aldoxime (**4.20**) derivatives were synthesized. Compound **4.19** was prepared by reaction of compound **4.4** with *p*-toluenesulfonyl chloride (*p*-TsCl) in pyridine, and compound **4.20** was prepared by reaction of **4.19** with $\text{NH}_2\text{OH}\cdot\text{HCl}$ in pyridine at 50 °C (Scheme 4.5).



Scheme 4.5. Synthesis of derivatives **4.19** and **4.20**.

Reagents and conditions: a) *p*-TsCl, pyridine, r.t, 2 h; b) $\text{NH}_2\text{OH}\cdot\text{HCl}$, pyridine, 50 °C, 1.50 h.

The proton of the aldehyde group of derivative **4.19** appeared as a singlet at 9.66 ppm in the ^1H NMR spectrum (Fig. 4.18), whereas the signal for the carbonyl carbon of CHO was observed at 205.66 ppm in the ^{13}C NMR spectrum (Fig. 4.19). In the IR spectrum, stretching bands for C-H and C=O of aldehyde were observed at 2723 and 1716 cm^{-1} , respectively (Fig. 4.20).

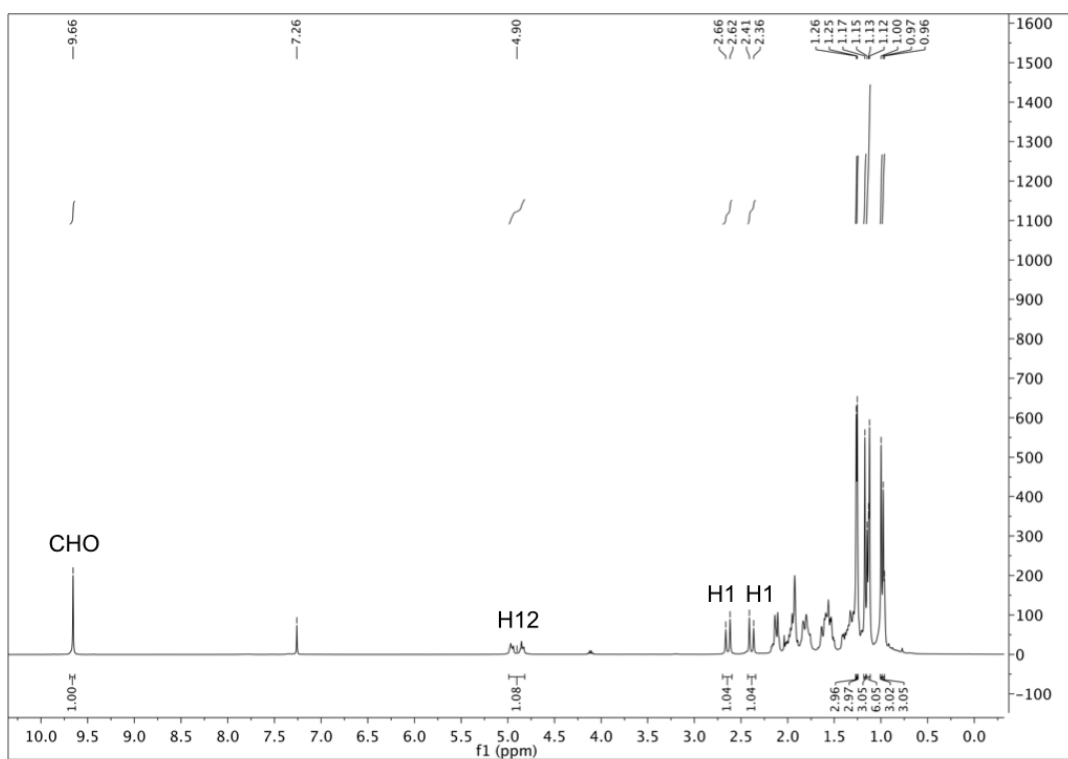


Figure 4.18. ^1H NMR spectrum of compound 4.19 recorded in CDCl_3 .

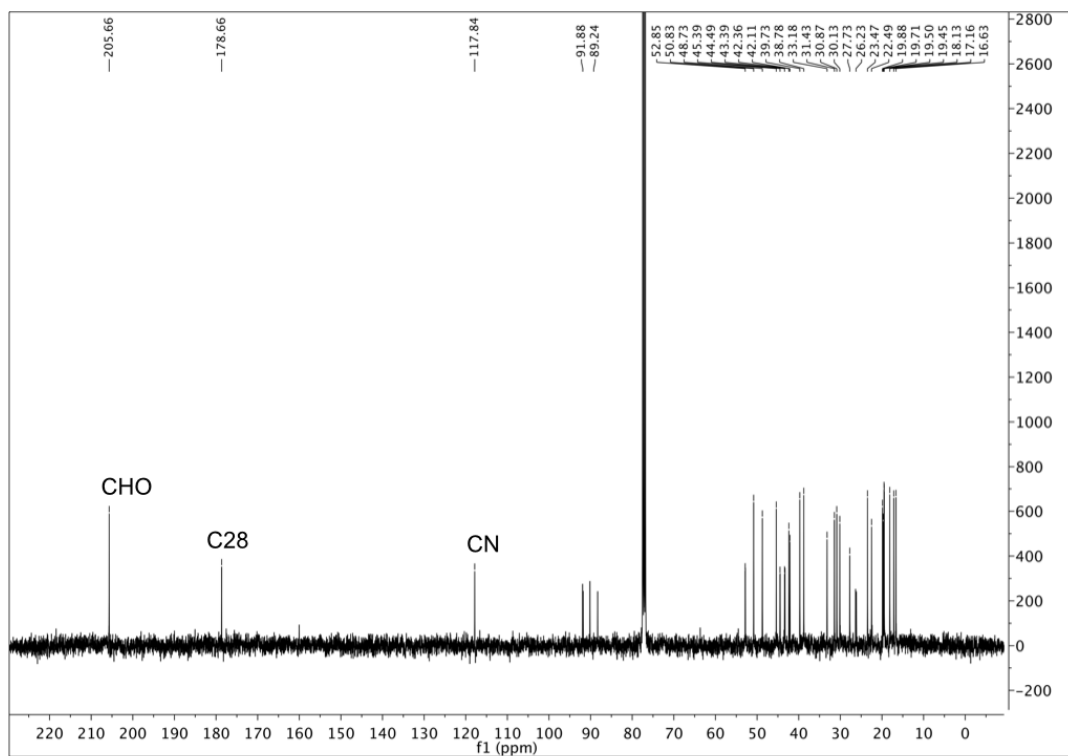


Figure 4.19. ^{13}C NMR spectrum of compound 4.19 recorded in CDCl_3 .



Figure 4.20. IR spectrum of compound 4.19.

The proton at position 3 in derivative **4.20** appeared as a singlet at 7.53 ppm in ¹H NMR spectrum (Fig. 4.21), whereas the signal of the carbon of the aldoxime group was observed at 159.83 ppm in the ¹³C NMR spectrum (Fig 4.22).

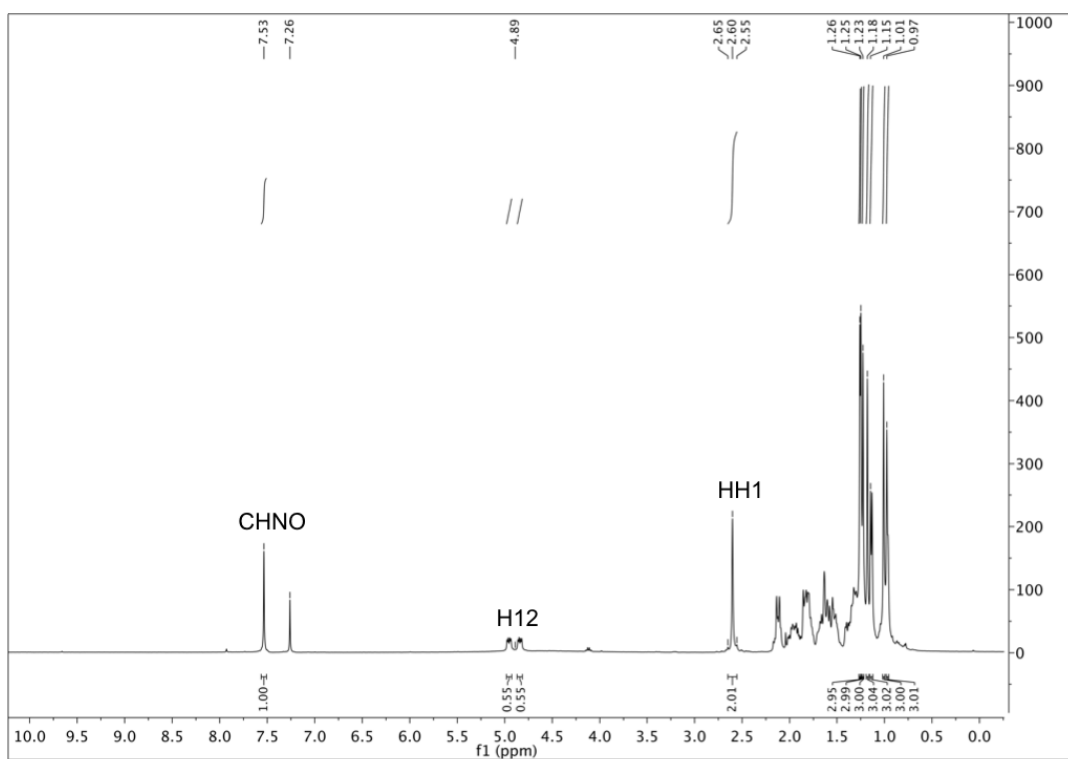


Figure 4.21. ^1H NMR spectrum of compound 4.20 recorded in CDCl_3 .

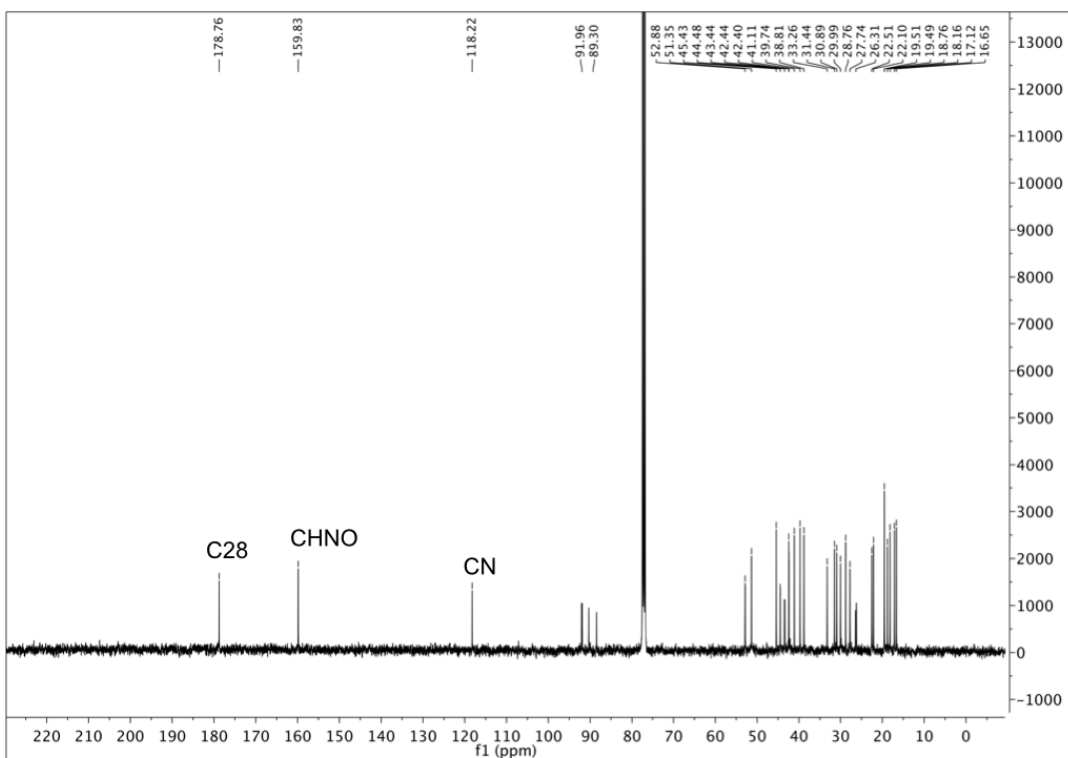


Figure 4.22. ^{13}C NMR spectrum of compound 4.20 recorded in CDCl_3 .

4.2.2. Biological studies

4.2.2.1. Evaluation of *in vitro* anticancer activity

The anticancer activities of **UA** and of the newly synthesized derivatives (**4.1–4.20**) against NSCLC cells (H460, H322, H460 LKB1^{+/+}) were evaluated by using the CellTiter-Blue[®] cell viability assay. Culture medium containing 0.15% DMSO served as negative control. The cell lines were treated with increasing concentrations of each compound, and the IC₅₀ values were determined after 72 h of incubation. The IC₅₀ values are summarized in Table 4.1.

Table 4.1. The inhibitory activities (IC₅₀) of **UA** and derivatives **4.1–4.20** in the NSCLC cell lines.

Compound	Cell line ^a /IC ₅₀ , μ M		
	H460	H322	H460 LKB1 ^{+/+}
UA	14.8 \pm 0.6	15.3 \pm 2.8	21.1 \pm 1.6
4.1	7.5 \pm 0.9	6.8 \pm 4.0	7.9 \pm 0.5
4.2	5.9 \pm 0.2	1.5 \pm 0.1	11.6 \pm 1.6
4.3	27.1 \pm 0.2	28.7 \pm 4.2	32.6 \pm 0.7
4.4	11.6 \pm 0.8	12.7 \pm 0.8	16.8 \pm 2.1
4.5	>50	>50	11.9 \pm 0.5
4.6	>50	>50	>50
4.7	>50	>50	>50
4.8	>50	>50	>50
4.9	>50	>50	>50
4.10	>50	>50	>50
4.11	>50	>50	19.5 \pm 1.3
4.12	>50	>50	18.7 \pm 0.4
4.13	>30	>30	>30
4.14	>25	>25	>25
4.15	>50	>50	>50
4.16	4.5 \pm 0.4	6.8 \pm 0.6	4.6 \pm 0.1
4.17	ND	ND	ND
4.18	8.7 \pm 0.1	8.4 \pm 1.5	6.3 \pm 1.0
4.19	ND	ND	ND
4.20	>50	>50	8.0 \pm 0.09

^aLung cancer cell lines were treated with various concentrations of test compounds for 72 h. The inhibitory activities were determined using the CellTiter-Blue cell viability assay. IC₅₀ was calculated from the results, and data are presented as means \pm SD of three independent experiments. *ND*: not determined.

Chapter 4 | Synthesis and cytotoxic activity of novel UA derivatives

As shown in Table 4.1, compared with **UA**, most of the oxime derivatives (**4.1–4.4**) displayed an improved cytotoxic activity, with compounds **4.1** and **4.2** being the most active ones. Interesting to note, while compound **4.1** had similar IC_{50} values among all cell lines, derivative **4.2** showed different potencies according to cell line, being 2.5, 10.2, and 1.8 times more active than **UA** in H460, H322, and H460 LKB1^{+/+} cells, respectively. Compound **4.3**, with two oxime functions at the C2 and C3 positions, displayed a decreased activity compared with its mono-oxime counterparts (**4.1** and **4.2**), but it was slightly more active than **UA** in the H460 LKB1^{+/+} cells. Reduction of the carbonyl at C3 of **4.2** to obtain compound **4.4** led to a decrease in the anticancer activity, which might have been due to the loss of the α,β -unsaturated system present in compound **4.2**. Indeed, it has been shown that the presence of an α,β -unsaturated carbonyl group in the A-ring of pentacyclic triterpenoids significantly enhanced their biological activities.^{67,218,219}

Comparison of the nitrile derivatives (**4.5–4.20**) indicated that the nitrile group at C2 did not seem to be critical for the cytotoxic activity. Nevertheless, the inclusion of a nitrile group into the **UA** backbone was designed based on the desirable properties that have been attributed to this function, such as improved pharmacokinetic profile.²⁰⁰ On the other hand, the substitution at C3 had a dramatic influence on the biological activity of the derivatives.

The set of C3-amide derivatives, bearing a primary amide (**4.5**), different aromatic substituents (more bulky side chains) (**4.6–4.11**), or a secondary amide with a short alkyl side chain (**4.12–4.14**), had a higher IC_{50} value than did the parent compound.

The introduction of a heterocyclic substituent at position C3 (**4.16** and **4.18**) significantly increased the cytotoxicity compared with the parent compound, by approximately 3 times and 2 times, respectively. The triazole derivative **4.17** was not soluble in the experimental conditions of the biological assay, and so **4.17** was not further tested.

Finally, the introduction of an aldehyde group at C3 led to a less soluble compound **4.19** under these experimental conditions, which was not further studied. The introduction of an

Chapter 4 | Synthesis and cytotoxic activity of novel UA derivatives

aldoxime at C3 generated a derivative **4.20** that seemed to be specifically active in the H460 LKB1^{+/+} cell line. The H460 NSCLC cell line is LKB1 deficient, while H460 LKB1^{+/+} was reconstituted with LKB1 by Heymach group at MD Anderson Cancer Center.²²⁰

The most active compounds, **4.2** and **4.16**, were selected and their cytotoxic activity was further explored in a multicellular spheroid 3D culture system. Using the CellTiter-Glo[®] assay, the anticancer activity of **UA**, and the two most active derivatives (**4.2** and **4.16**) were tested against H460 and H322 spheroid models. Culture medium containing 0.1% DMSO served as negative control. The cell lines were treated with increasing concentrations of each compound, and the IC₅₀ values were determined after 96 h of incubation. The IC₅₀ values are summarized in Table 4.2.

Table 4.2. The inhibitory activities (IC₅₀) of **UA**, and the most potent derivatives (**4.2** and **4.16**) in the spheroid model of the NSCLC cell lines H460 and H322.

Compound	Cell line ^a / IC ₅₀ , μM			
	H460		H322	
	Monolayer	Spheroid	Monolayer	Spheroid
UA	14.8 ± 0.6	30.8 ± 2.8	15.3 ± 2.8	18.2 ± 10.5
4.2	5.9 ± 0.2	8.4 ± 1.0	1.5 ± 0.1	3.9 ± 0.6
4.16	4.5 ± 0.4	6.3 ± 0.7	6.8 ± 0.6	>15

^aLung cancer cell lines were treated with various concentrations of test compounds for 72 or 96 h for a 2D (monolayer) or 3D (spheroid) model, respectively. The inhibitory activities were determined using CellTiter-Blue[®] or CellTiter-Glo[®] for the 2D or 3D model, respectively. IC₅₀ was calculated from the results, and data are presented as means ± SD of three independent experiments.

Although derivative **4.2** was active in spheroid models of both cell lines, derivative **4.16** had a much higher IC₅₀ value in the H322 spheroid culture model, compared with its two-dimensional counterpart (Table 4.2). Noteworthy, the IC₅₀ values for compound **4.2** increased slightly compared with values obtained using the two-dimensional culture model. In Figure 4.23

Chapter 4 | Synthesis and cytotoxic activity of novel UA derivatives

is shown the phenotypic effect of **UA**, compound **4.2**, and compound **4.16** in the spheroid model for the H460 cell line after 96 h of treatment.

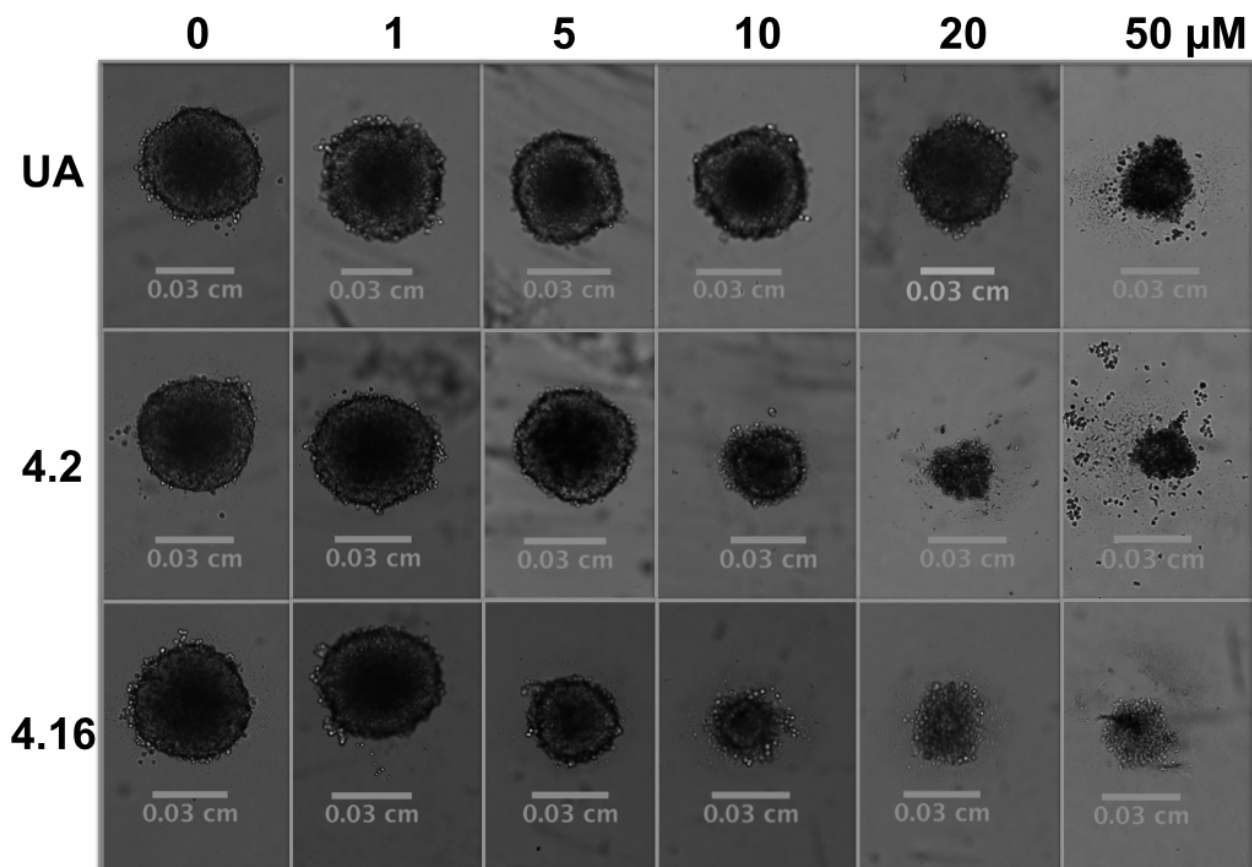


Figure 4.23. Phenotypic changes in the H460 spheroid model treated with **UA** (top panel), compound **4.2** (middle panel), and compound **4.16** (bottom panel) for 96 h. Spheroids were treated with the indicated concentrations of the compounds tested. Images were captured using bright field phase-contrast microscopy.

Taking into account these results, compound **4.2** was selected for further studies in order to explore its possible mechanism of action.

4.2.2.2. Effect of compound 4.2 on cellular DNA, RNA, and protein synthesis

The [³H]thymidine, [³H]uridine, and [³H]leucine incorporation assays allow measurement of the drug effect in the DNA, RNA, and protein synthesis rates of cells, respectively. Although DNA synthesis was not significantly affected at 24 h, an increase of 50.7% was observed at 48 h with treatment using compound **4.2** (Fig. 4.24A). Conversely, the RNA synthesis rate was decreased by treatment with this compound at 24 h (5.8%) and at 48 h (6.3%) (Fig. 4.24B). Incorporation of leucine (protein synthesis rate) at 24 h was also lower by 17.7% following treatment with compound **4.2** (Fig. 4.24C).

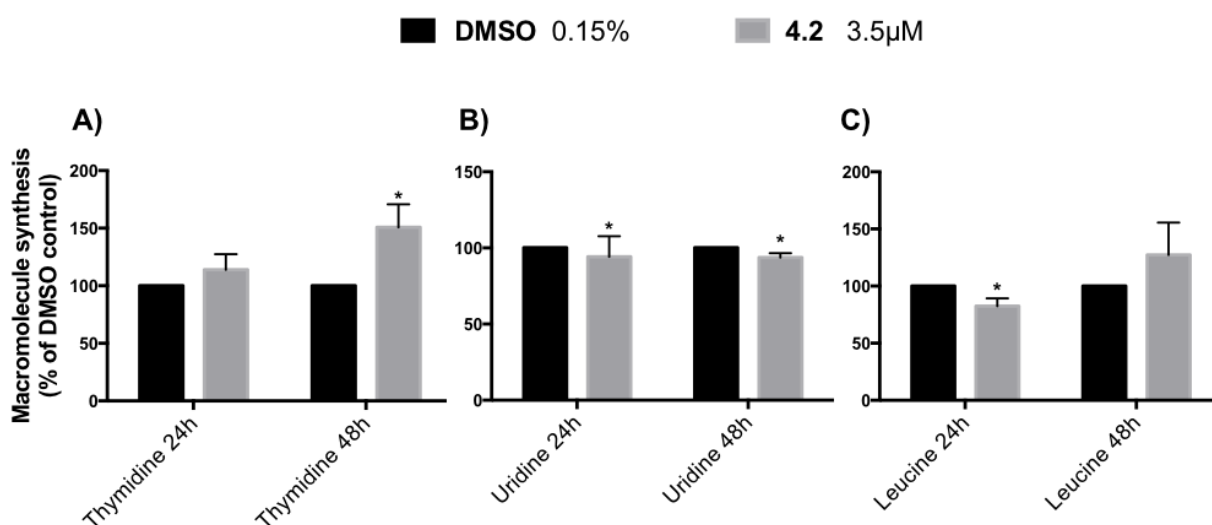


Figure 4.24. The effect of treatment with compound **4.2** on the global DNA (A), RNA (B), and protein (C) synthesis in the H460 cell line. Cells treated with vehicle or compound **4.2** at the indicated concentrations for 24 and 48 h were assessed for macromolecular synthesis. Values represent the means \pm SD of three independent experiments. p-Values obtained by comparing vehicle and treatment are presented as * < 0.05.

4.2.2.3. Effect of compound 4.2 on the cell cycle distribution

The effect of compound **4.2** on the cell cycle distribution was explored. Cells were treated with DMSO (0.15%), or compound **4.2** (4 μ M) for 24 and 72 h, and the cell cycle profile was evaluated by FACS analysis after staining cells with PI.

Treatment of H460 cells with compound **4.2** did not affect the population of cells of any of the cell cycle phases (Fig. 4.25). However, increases in the sub-G1 population at 24 h (7.6%) and 72 h (4.5%) were observed (Fig. 4.25). These findings suggest DNA fragmentation by apoptosis.

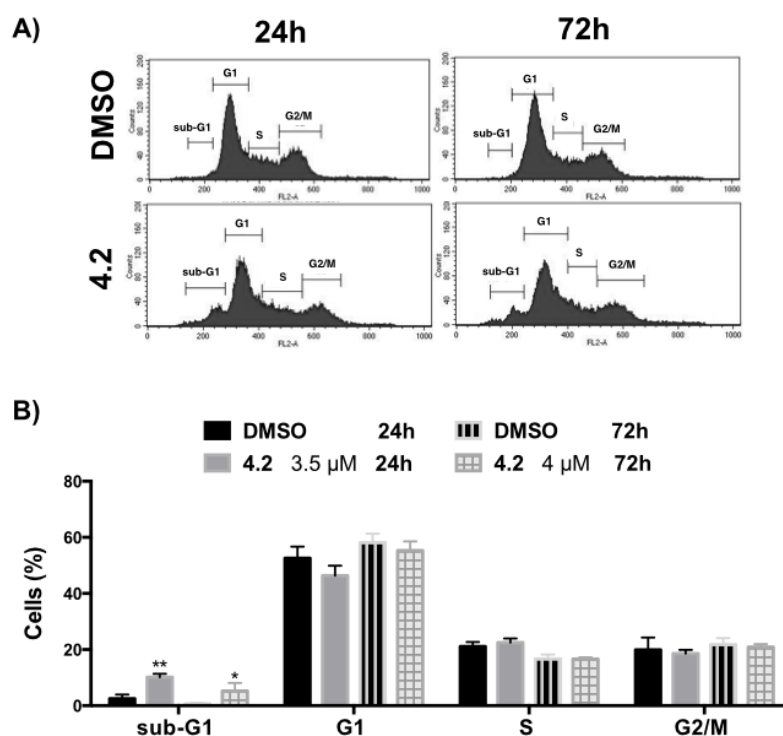


Figure 4.25. Effect of compound **4.2** on the cell cycle distribution. H460 cells treated with vehicle, or compound **4.2** at the indicated concentrations for 24 and 72 h were assessed for cell cycle, using PI staining and flow cytometric analysis. A) Representative histograms of cell cycle analysis are shown. B) The bar graphic depicts the cell population (%) per cell cycle phase. Values represent the means \pm SD of three independent experiments. p-Values obtained by comparing vehicle and treatment are presented as * < 0.05, ** < 0.01.

4.2.2.4. Effect of compound 4.2 on gene expression profile

The effect of compound **4.2** on the gene expression in the H460 cell line was analyzed on a genome-wide scale using Affymetrix HTA 2.0 system. For this purpose, H460 cells were treated with DMSO (0.15%) or compound **4.2** (4 μ M) for 24 h. For the gene expression analysis, Transcriptome Analysis Console software (Affymetrix) was used to detect the differentially expressed genes and the main pathways affected, using DMSO-treated cells as control.

Taking into account that the parent compound **UA** is considered a multifunctional agent and the derivatives described in literature seem to preserve that property, an effort was made to identify the main pathways that could be responsible for the anticancer activity of compound **4.2**, in order to plan the biological assays to study the possible anticancer mechanism.

According to HTA 2.0 microarray data, apoptosis and autophagy pathways were activated upon treatment of H460 cells with compound **4.2** at 24 h, and thus these two pathways were selected for further evaluation.

4.2.2.5. Apoptosis-inducing effect of compound 4.2 evaluated by annexin V-Cy5/PI assay

To evaluate whether the loss of cell viability induced by compound **4.2** was associated with apoptosis, the annexin V-Cy5/PI binding assay was performed. FACS analysis of annexin V-Cy5/PI double staining was used to differentiate live, early apoptotic, late apoptotic, and necrotic cells. Accordingly, H460 cells were treated with derivative **4.2** at 4.5 μ M for 72 h, and apoptosis was quantified by flow cytometry after double staining with annexin V-Cy5/PI.

As shown in Figure 4.26, in comparison with control (0.15% DMSO-treated cells), treatment with derivative **4.2** decreased the percentage of live cells from 94% in the control to 56.2% in treated cells. Simultaneously, the percentage of apoptotic cells increased from 4.5% to

Chapter 4 | Synthesis and cytotoxic activity of novel UA derivatives

38.3% in treated cells, being 11.7% early apoptotic cells and 26.5% late apoptotic cells. These results suggest that compound **4.2** at 4.5 μM induces apoptosis in H460 cells, which could explain the sub-G1 population increase observed in Fig. 4.25.

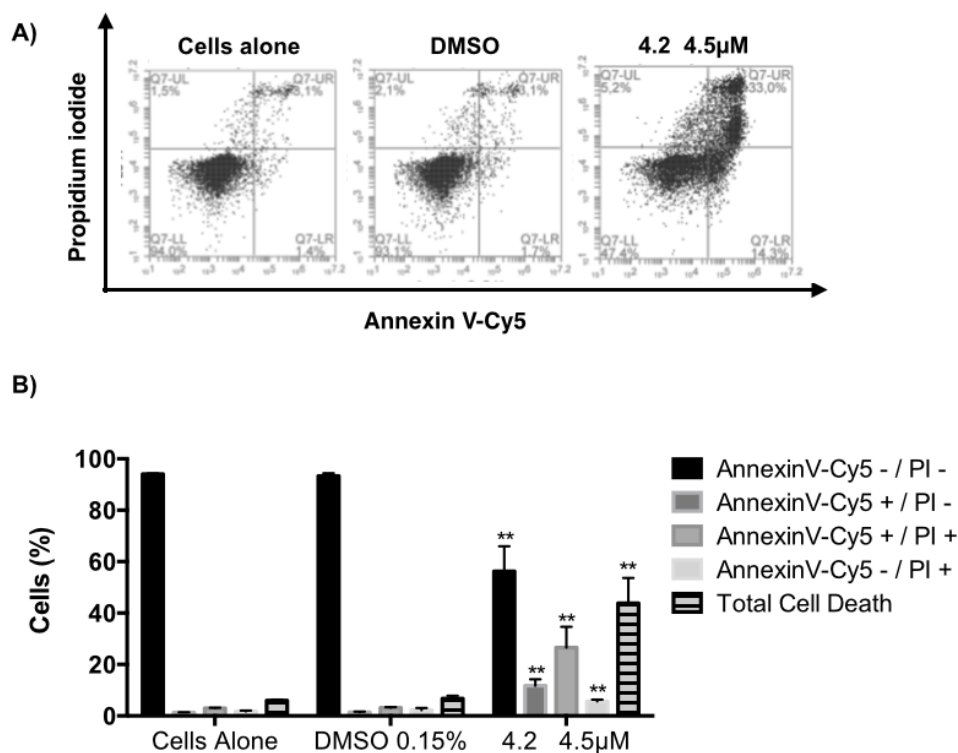


Figure 4.26. Induction of H460 cell death by compound **4.2**. Annexin V-Cy5/PI assay of H460 cells that were untreated, treated with vehicle, or treated with compound **4.2** at the indicated concentrations for 72 h. A) Representative flow cytometric plots for the quantification of apoptosis are shown: the lower left quadrant (annexin V- and PI-) represents non-apoptotic cells, the lower right quadrant (annexin V+ and PI-) represents early apoptotic cells, the upper right quadrant (annexin V+ and PI+) represents the late apoptotic/necrotic cells, and the upper left quadrant (annexin V- and PI+) represents necrotic cells. B) The bar graph depicts the variation of the percentage of live, early apoptotic, late apoptotic cells, necrotic cells, and total cell death. Values represent the means \pm SD of three independent experiments. p-Values obtained by comparing vehicle and treatment are presented as $** < 0.01$.

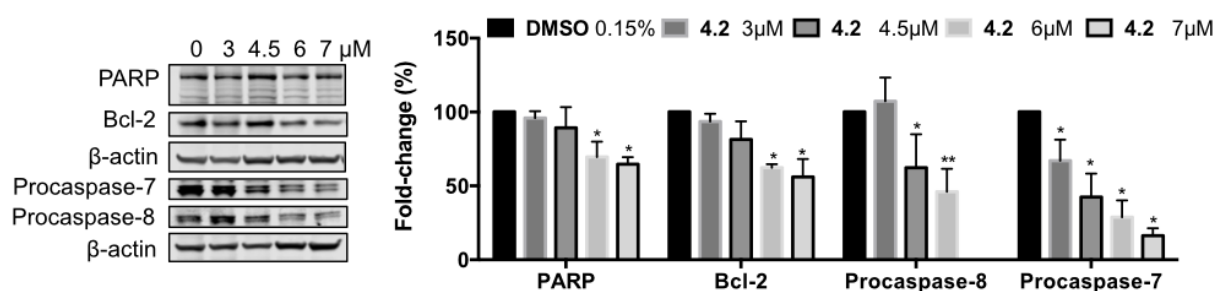
4.2.2.6. Effect of compound 4.2 on the levels of apoptosis-related proteins

To further investigate the mechanism of compound 4.2-induced apoptosis, the levels of some apoptosis-related proteins were assessed by immunoblot analysis. H460 and H322 cells were treated with increasing concentrations of compound 4.2 for 24 h (Fig. 4.27).

The treatment of H460 cells with compound 4.2 led to a decrease of the levels of the full-length PARP, which was associated with decreased levels of procaspases-8 and -7 (Fig. 4.27A). These findings suggest that compound 4.2 is able to induce apoptosis via the extrinsic pathway. Similar results were found when H322 cells were treated with compound 4.2 (Fig. 4.27B).

The levels of Bcl-2, an anti-apoptotic member of the Bcl-2 family, were also investigated.¹¹ Treatment of H460 cells with compound 4.2 downregulated Bcl-2 in a concentration-dependent manner (Fig. 4.27).

A)



B)

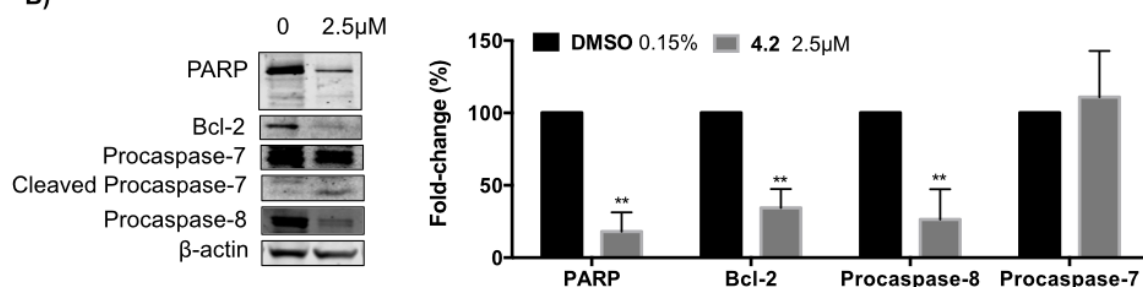


Figure 4.27. Effect of compound **4.2** on the levels of apoptosis-related proteins. H460 (A) and H322 (B) cells were treated with compound **4.2** at the indicated concentrations for 24 h. The levels of the indicated proteins were analyzed by Western blot. β -Actin was used as loading control. The bar graph depicts the variation in the levels of the protein expression. Values represent the means \pm SD of three independent experiments. p-Values obtained by comparing vehicle and treatment are presented as * <0.05 , ** <0.01 .

4.2.2.7. Effect of compound 4.2 treatment on autophagy

Autophagy is a catabolic process involved in the degradation of cellular organelles and proteins through the lysosomal machinery.²⁹ As mentioned before, autophagy is characterized by the formation of acidic vesicular organelles (AVO), which can be detected by staining with acridine orange, a dye that accumulates in acidic organelles.¹⁹³ Measurement of this dye by flow cytometry was used to detect AVO formation in H460 cells treated with vehicle (0.15% DMSO) or compound **4.2** (3 or 5 μ M) for 72 h. Bafilomycin A1 was used as a negative control to block acidic vesicular formation.

Chapter 4 | Synthesis and cytotoxic activity of novel UA derivatives

As shown in Figure 4.28A, bafilomycin A1 inhibited the fusion of autophagosomes with lysosomes. The endogenous autophagy level (DMSO treatment) was less than 10% at 72 h (Fig. 4.28). Treatment with compound **4.2** significantly increased the formation of AVO at 3 and 5 μM , by 5.2 and 11.1%, respectively (Fig. 4.28). These data suggest that compound **4.2** is able to induce autophagy in H460 cells.

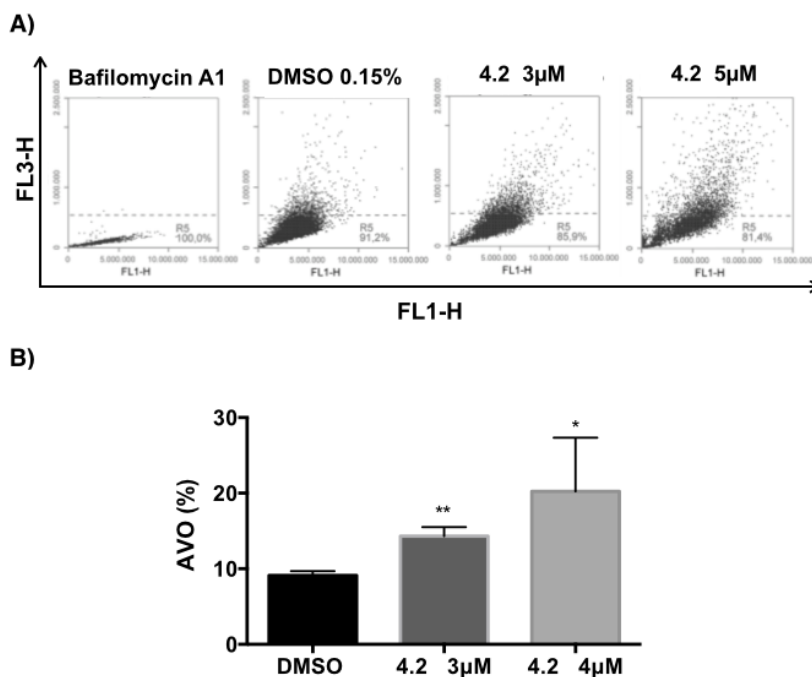


Figure 4.28. Effect of compound **4.2** treatment on induction of autophagy in the H460 cell. A) The formation of AVO was measured by acridine orange staining and flow cytometry. Representative flow cytometric plots of the percentage of AVO formation (acridine orange staining positive) of three independent experiments are shown. B) The graph bar depicts the variation of the percentage of AVO formation and is plotted as means \pm SD of three independent experiments. p-Values obtained by comparing vehicle and treatment are presented as * <0.05 , ** <0.01 .

On the one hand, autophagy may contribute to cell survival, and on the other hand activation of autophagy may also lead to cell death.²⁹ Because autophagy may be induced as a survival response of cells to treatment with derivative **4.2**, an autophagy inhibitor (chloroquine) was used, as in chapter 3, to evaluate whether the inhibition of autophagy would affect the

Chapter 4 | Synthesis and cytotoxic activity of novel UA derivatives

cytotoxic activity of compound **4.2**. H460 cells were treated for 72 h with vehicle (0.15% DMSO), 20 μ M chloroquine (Chl), compound **4.2** (3 or 4.5 μ M), or combination of chloroquine and compound **4.2** at the indicated concentrations. Inhibition of autophagy did not affect the total cell death induced by treatment with compound **4.2** (Fig. 7.29A and B). These data suggest that autophagy had not been induced as a resistance mechanism against treatment with compound **4.2** but might be induced as part of the anticancer mechanism of compound **4.2**.

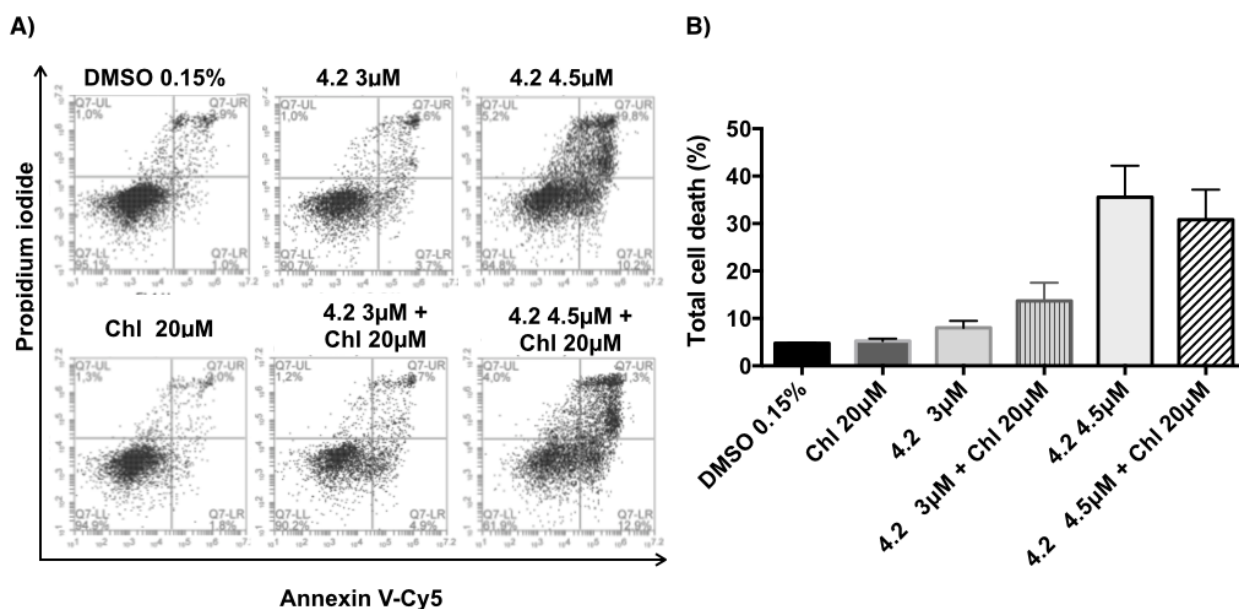


Figure 4.29. Effect of autophagy inhibition on **4.2**-induced cell death. A) Annexin V-Cy5/PI assay of H460 cells treated with vehicle, 20 μ M of chloroquine (Chl), compound **4.2** (3 or 4.5 μ M), or the combination of chloroquine and compound **4.2** at the indicated concentrations for 72 h. Representative flow cytometric plots for the quantification of apoptosis are shown. B) The bar graph depicts the variation of the percentage of total cell death. No statistical difference was observed comparing cells treated with compound **4.2** alone or in combination with chloroquine. Values represent the means \pm SD of three independent experiments.

4.2.2.8. Effect of compound 4.2 on the levels of autophagy-related proteins

To gain deeper insight into the mechanism via which compound **4.2** induces autophagy, its effect on the levels of some autophagy-related proteins was explored by immunoblot analysis. H460 and H322 cells were treated with increasing concentrations of compound **4.2** for 24 h (Fig. 4.30).

The level of total mTOR, a major negative regulator of autophagy,¹⁹⁶ was investigated. Treatment of H460 cells with compound **4.2** did not seem to affect the mTOR levels (Fig. 4.30A).

The conversion of LC3A/B-I into LC3A/B-II is commonly used to monitor autophagy.¹⁹⁷ Treatment of H460 and H322 cells with compound **4.2** resulted in lipidation of LC3A/B-I to LC3A/B-II, as shown by the increase of a lower band around 17 KDa (Fig. 4.30A and B).

The p62 protein is an ubiquitin-binding protein that upon activation of autophagy is localized to the autophagosomes and is subsequently degraded.¹⁹⁶ The p62 levels were appreciably lower at higher concentrations of compound **4.2** tested (Fig 4.30A).

As shown in Figures 4.30A and B, the expression of Beclin-1 protein, a central regulator of autophagy, in H460 and H322 cells decreased upon treatment with compound **4.2**. This finding was unexpected, because one would predict an increase in the levels of Beclin-1, as the levels of Bcl-2 protein were decreased (Fig. 4.27A), and autophagy was detected by acridine orange staining. Beclin-1 activity in autophagy is inhibited by interaction with Bcl-2 protein.

Overall, these results indicate that compound **4.2** is able to induce autophagy in H460 and H322 cell lines.

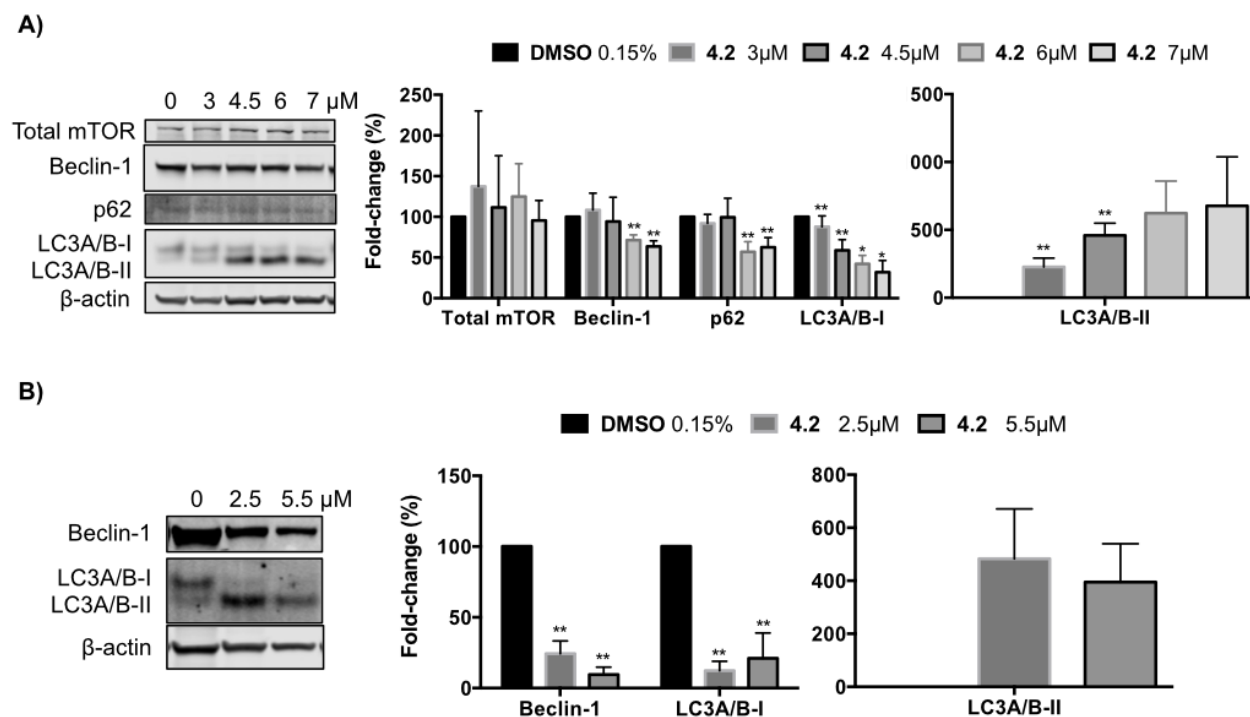


Figure 4.30. Effect of compound **4.2** on the levels of autophagy-related proteins. H460 (A) and H322 (B) cells were treated with compound **4.2** at the indicated concentrations for 24 h. The levels of the indicated proteins were analyzed by Western blot. β -Actin was used as loading control. The bar graph depicts the variation in the levels of the protein expression. Values represent the means \pm SD of three independent experiments. p-Values obtained by comparing vehicle and treatment are presented as * < 0.05 , ** < 0.01 .

4.3. Conclusion

In the current chapter, several derivatives of **UA** were successfully synthesized and their anticancer activity was screened against NSCLC cell lines, using monolayer and spheroid culture models.

The structure-activity relationship (SAR) study based on the anticancer activity against NSCLC cell lines in the monolayer culture model showed that the oxime substitution at C3, or at C2 in conjunction with a carbonyl function, improved the cytotoxicity compared with the parent compound. Moreover, analysis of the nitrile derivatives indicated that the presence of a nitrile

Chapter 4 | Synthesis and cytotoxic activity of novel UA derivatives

group at C2 was not critical for the anticancer activity, whereas the substitution at C3 had a dramatic influence on the overall activity. In the nitrile derivatives with a cleaved A-ring, the presence of the heterocyclic imidazolyl (**4.16**) and 2'-methylimidazolyl (**4.18**) moieties at C3 improved the activity compared with the parent compound.

The most active derivatives displayed an oxime group conjugated with a carbonyl function at the A-ring (**4.2**), and a cleaved A-ring bearing nitrile and heterocycle groups (**4.16**).

While derivative **4.2** was active in both monolayer and spheroid culture models, with little change in its IC₅₀ value, compound **4.16** seems to lose potency in the H322 spheroid model. For this reason, derivative **4.2** was selected for further mechanistic studies.

The preliminary studies on the mechanism of action revealed that compound **4.2** does not induce cell cycle arrest but is able to modulate the RNA synthesis rate and to promote apoptosis via activation of caspase-8 and -7, cleavage of PARP, and modulation of Bcl-2 in both NSCLC cell lines studied. Moreover, autophagy was also induced by treatment with compound **4.2**. Taken together, these results suggest that compound **4.2** is a promising candidate for the development of new anti-NSCLC agents.

4.4 Experimental section

4.4.1. Chemistry

4.4.1.1. General

Ursolic acid, hydroxylamine hydrochloride (NH₂OH·HCl), potassium *tert*-butoxide (*t*-BuOK), butyl nitrite (*n*-BuONO), sodium borohydride (NaBH₄), thionyl chloride (SOCl₂), aniline, phenethylamine, 4-methylbenzylamine, 4-fluorobenzylamine, 2-methoxyphenethylamine, 2-(3-chlorophenyl)ethylamine, methylamine solution (33 wt. % in absolute ethanol), ethylamine

Chapter 4 | Synthesis and cytotoxic activity of novel UA derivatives

solution (2.0 M in THF), propylamine, 1,1'-carbonyldiimidazole (CDI), 1,1'-carbonyl-di-(1,2,4-triazole) (CDT), 1,1'-carbonylbis(2-methylimidazole) (CBMI), *para*-toluenesulfonyl chloride (*p*-TsCl), *tert*-butanol (*t*-BuOH), triethylamine (Et₃N), pyridine, benzene, hydrochloric acid (HCl), were purchased from Sigma-Aldrich Co.

The reaction and workup solvents were purchase from VWR Portugal, and were of analytical grade. All the solvents used in the reactions were previously purified and dried according to the literature procedures.

Ammonium (25% aqueous solution), sodium chloride (NaCl), sodium sulfite (Na₂SO₃), and sodium sulfate (Na₂SO₄) were purchased from Merck Co.

TLC analysis was performed using Kieselgel 60HF₂₅₄/Kieselgel 60G TLC plates.

Separation and purification of compounds was performed by flash column chromatography using Kieselgel 60 (230–400 mesh, Merck), or by TLC Preparative, using Kieselgel 60 HF254 and Kieselgel 60G (Merck).

Melting points (Mp) were measured using a BUCHI melting point B-540 apparatus and are uncorrected.

IR spectra were obtained on a Fourier transform spectrometer.

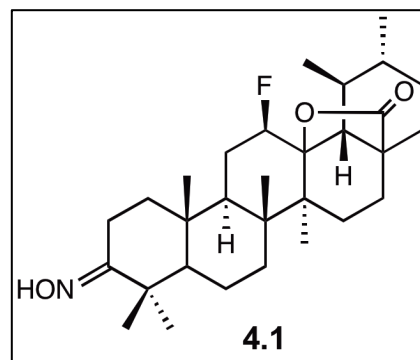
NMR spectra were recorded on a Bruker NMR Avance 400 digital spectrometer, using CDCl₃ as internal standard. The chemical shifts (δ) are reported in parts per million (ppm) and coupling constants (*J*) in hertz (Hz).

The mass spectrometry (MS) was performed using a Quadrupole/Ion Trap Mass Spectrometer (QIT-MS) (LCQ Advantage MAX, Thermo Finnigan).

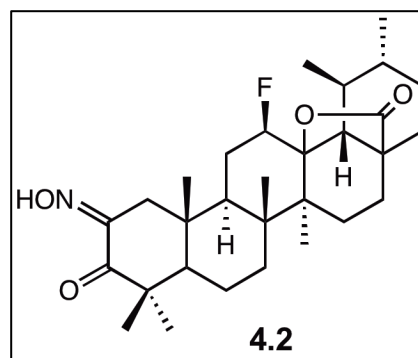
Elemental analysis was performed in an Analyzer Elemental Carlo Erba 1108 by chromatographic combustion.

4.4.1.2. Synthetic procedures

(E)-3-Hydroxyimino-12 β -fluor-urs-13,28 β -olide (4.1): To a stirred mixture of **3.3** (300 mg, 0.63 mmol) in pyridine (3.7 ml) at 50 °C, NH₂OH·HCl (230 mg, 3.31 mmol) was added. After 2 h, the reaction mixture was evaporated under vacuum, and the residue was treated with water (30 ml) and extracted with ethyl acetate (3 × 70 ml). The resulting organic phase was washed with 10% Na₂SO₃ aqueous solution (70 ml), water (70 ml), and 10% NaCl aqueous solution (70 ml), dried over Na₂SO₄, filtered, and concentrated to dryness. The residue was purified by flash column chromatography (petroleum ether:ethyl acetate 6:1–4:1) to give **4.1** as a white solid (90.5%). Mp 275.9 – 279.8 °C. IR (KBr): ν = 3270.68, 2975.62, 2923.56, 2873.42, 1774.19, 1656.55, 1463.71, 1388.50, 1236.15, 1122.37, 937.23 cm⁻¹. ¹H NMR (400 MHz, CDCl₃): δ = 9.00 (br s, 1H, NOH), 4.84 (dq, J = 45.5 Hz, 1H, H-12), 3.05–2.98 (m, 1H, H-2), 2.35–2.27 (m, 1H, H-2), 1.24 (s, 3H), 1.18 (s, 3H), 1.15 (s, 3H), 1.12 (d, J = 6.3 Hz, 3H), 1.06 (s, 3H), 1.01 (s, 3H), 0.96 (d, J = 5.5 Hz, 3H). ¹³C NMR (100 MHz, CDCl₃): δ = 178.96 (C28), 166.47 (CNOH), 92.07 (d, J = 14.5 Hz, C13), 89.74 (d, J = 185.9 Hz, C12), 55.63, 52.71 (d, J = 3.7 Hz), 48.91 (d, J = 9.5 Hz), 45.34, 44.11 (d, J = 3.0 Hz), 42.65, 40.41, 39.67, 39.15, 38.59, 37.34, 33.73, 31.47, 30.87, 27.75, 27.49, 25.76 (d, J = 19.6 Hz), 22.98, 22.52, 19.55, 18.54, 18.51, 17.24, 17.17, 16.64, 16.46. MS (DI-ESI) (m/z): 488.4 (100%) [M+H]⁺. Anal. Calcd for C₃₀H₄₆FNO₃: C, 73.88; H, 9.51; N, 2.87. Found: C, 74.13; H, 9.59; N, 2.92.



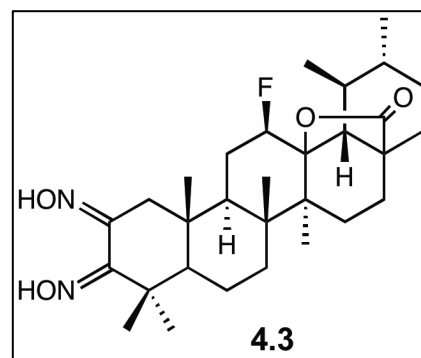
(E)-2-Hydroxyimino-3-oxo-12 β -fluor-urs-13,28 β -olide (4.2): To a stirred solution of **3.3** (500 mg, 1.06 mmol) and *t*-BuOK (395 mg, 3.52 mmol) in *t*-BuOH (30 ml) under N₂ at 25 °C, *n*-BuONO (302 mg, 2.93 mmol) was added. After 2 h, the reaction mixture was neutralized with 1M HCl and extracted with diethyl ether (3 × 70 ml). The resulting organic phase was washed with water (70 ml), and 10% NaCl aqueous solution (70 ml), dried over Na₂SO₄,



filtered, and concentrated to dryness. The residue was purified by flash column chromatography (petroleum ether:ethyl acetate 5:1–1:5) to give **4.2** as a slightly yellow solid (83.2%). Mp 275.7 – 277.3 °C. IR (KBr): ν = 3214.75, 2983.34, 2931.27, 2873.42, 1772.26, 1702.84, 1606.41, 1457.92, 1384.64, 1282.43, 1137.80, 989.30, 931.45 cm⁻¹. ¹H NMR (400 MHz, CDCl₃): δ = 7.55 (br s, 1H, NOH), 4.90 (dt, *J* = 45.8, 8.5 Hz, 1H, H-12), 3.09 (d, *J* = 18.5 Hz, 1H, H-1), 2.20 (d, *J* = 18.5 Hz, 1H, H-1), 1.26 (s, 3H), 1.22 (s, 3H), 1.19 (s, 3H), 1.15 (d, *J* = 6.2 Hz, 3H), 1.12 (s, 3H), 0.97 (d, *J* = 5.9 Hz, 3H), 0.92 (s, 3H). ¹³C NMR (100 MHz, CDCl₃): δ = 203.08 (C3), 178.89 (C28), 153.53 (CNOH), 92.08 (d, *J* = 14.3 Hz, C13), 89.38 (d, *J* = 186.6 Hz, C12), 52.74 (d, *J* = 3.6 Hz), 52.33, 47.02 (d, *J* = 9.3 Hz), 46.07, 45.38, 44.27 (d, *J* = 2.9 Hz), 42.19, 42.12, 39.69, 38.79, 35.76, 32.94, 31.44, 30.90, 29.15, 27.73, 26.10 (d, *J* = 20.0 Hz), 22.49, 21.68, 19.70, 19.54, 17.65, 17.59, 17.06, 16.55. MS (DI-ESI) (*m/z*): 502.0 (100%) [M+H]⁺, 105.6 (13.6%), 96.5 (23.7%). Anal. Calcd for C₃₀H₄₄FNO₄: C, 71.82; H, 8.84; N, 2.79. Found: C, 71.52; H, 9.17; N, 2.81.

Chapter 4 | Synthesis and cytotoxic activity of novel UA derivatives

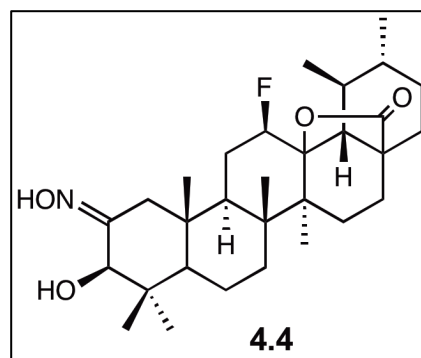
(*E,E*)-2,3-Dihydroxyimino-12 β -fluor-urs-13,28 β -olide (4.3): To a stirred mixture of **4.2** (259 mg, 0.52 mmol) in pyridine (3 ml) at 50 °C, NH₂OH·HCl (285.48 mg, 4.11 mmol) was added. After 7 h, the reaction mixture was evaporated under vacuum, and the residue was treated with water (30 ml) and extracted with ethyl acetate (3 × 70 ml). The resulting organic phase was washed with 5% HCl aqueous solution (60 ml), water (60 ml), and 10% NaCl



aqueous solution (60 ml), dried over Na₂SO₄, filtered, and concentrated to dryness. The residue was purified by flash column chromatography (petroleum ether:ethyl acetate 10:1–2:1) to give **4.3** as a white solid (44.9%). Mp 259.7 – 263.2 °C. IR (KBr): ν = 3359.39, 2983.34, 2927.41, 2873.42, 1770.33, 1625.7, 1455.99, 1386.57, 1238.08, 1120.44, 999.30, 941.09 cm⁻¹. ¹H NMR (400 MHz, CDCl₃): δ = 6.71 (br s, 2H, NOH), 4.89 (dt, J = 45.3, 8.42 Hz, 1H, H-12) 3.21 (d, J = 18.0 Hz, 1H, H-1), 1.28 (s, 3H), 1.24 (s, 3H), 1.23 (s, 3H), 1.21 (s, 3H), 1.14 (d, J = 6.3 Hz, 3H), 0.97 (d, J = 5.7 Hz, 3H), 0.93 (s, 3H). ¹³C NMR (100 MHz, CDCl₃): δ = 179.13 (C28), 153.32 (CNOH), 153.21 (CNOH), 92.21 (d, J = 14.3 Hz, C13), 89.44 (d, J = 186.4 Hz, C12), 52.76 (d, J = 5.6 Hz), 47.48 (d, J = 9.4 Hz), 45.43, 44.24 (d, J = 2.7 Hz), 42.21, 40.78, 39.82, 39.69, 38.78, 36.11, 33.07, 32.55, 31.44, 30.88, 27.73, 26.09 (d, J = 19.0 Hz), 23.81, 22.50, 19.53 (2C), 17.68, 17.20, 17.07, 16.55. MS (DI-ESI) (m/z): 517.3 (100%) [M+H]⁺, Anal. Calcd for C₃₀H₄₅FN₂O₄·0.7H₂O: C, 68.08; H, 8.84; N, 5.29. Found: C, 67.70; H, 8.58; N, 5.10.

(E)-2-Hydroxyimino-3 β -hydroxy-12 β -fluor-urs-13,28 β -olide (4.4): To a stirred mixture of **4.2**

(250 mg, 0.50 mmol) in dry methanol (4 ml) and THF (4 ml) under N₂ at r.t., NaBH₄ (207 mg, 5.47 mmol) was added slowly. After 3 h, acetone (3 ml) was added, and stirring continued for 10 min. The reaction mixture was evaporated under reduced pressure, and the residue was extracted with ethyl acetate (3 × 70 ml) from water (30 ml). The resulting

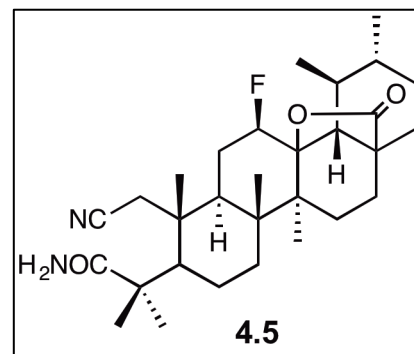


organic phase was washed with water (70 ml), and 10% NaCl aqueous solution (70 ml), dried over Na₂SO₄, filtered, and concentrated to dryness. The crude residue was purified by flash column chromatography (petroleum ether:ethyl acetate 7:1–1:1) to give **4.4** as a white solid (59.1%). Mp 328.2 – 331.9 °C. IR (KBr): ν = 3523.31, 3390.24, 2973.70, 2931.27, 2875.34, 1770.33, 1459.85, 1392.35, 1236.15 1120.44, 1052.94, 991.23, 943.02 cm⁻¹. ¹H NMR (400 MHz, CDCl₃): δ = 4.88 (dm, 1H, H-12), 4.70 (br s, 1H, NOH), 3.85 (s, 1H, H-3), 3.52 (d, J = 12.6 Hz, 1H, H-1), 1.23 (s, 3H), 1.20 (s, 3H), 1.14 (d, J = 6.3 Hz, 3H), 1.12 (s, 3H), 0.97 (d, J = 5.6 Hz, 3H), 0.84 (s, 3H), 0.73 (s, 3H). ¹³C NMR (100 MHz, CDCl₃): δ = 179.07 (C28), 158.03 (CNOH), 92.05 (d, J = 14.1 Hz, C13), 89.49 (d, J = 186.0 Hz, C12), 78.51 (C3), 55.03, 52.73 (d, J = 3.7 Hz), 48.50 (d, J = 9.5 Hz), 45.37, 44.13 (d, J = 3.0 Hz), 43.06, 42.91, 41.10, 39.70, 38.61, 38.40, 33.82, 31.47, 30.86, 28.47, 27.82, 25.79 (d, J = 19.5 Hz), 22.53, 19.56, 18.30, 17.74, 17.36, 17.29, 16.63, 15.73. MS (DI-ESI) (m/z): 504.3 (100%) [M+H]⁺, 466.4 (15.7%). Anal. Calcd for C₃₀H₄₆FNO₄: C, 71.54; H, 9.21; N, 2.78. Found: C, 71.52; H, 9.17; N, 2.93.

Chapter 4 | Synthesis and cytotoxic activity of novel UA derivatives

2,3-Seco-2-cyano-3-amide-12 β -fluor-urs-13,28 β -olide (4.5): To a stirred mixture of **4.2** (200

mg, 0.40 mmol) in dry THF (3 ml) and benzene (3 ml) at 80 °C, SOCl₂ (0.1 ml, 1.39 mmol) was added. After 3.5 h, the reaction mixture was evaporated under reduced pressure, and the residue was dissolved in dry THF (30 ml) and treated with cold 25% ammonium solution (33 ml). After 1 h, the reaction mixture was evaporated under reduced pressure, and

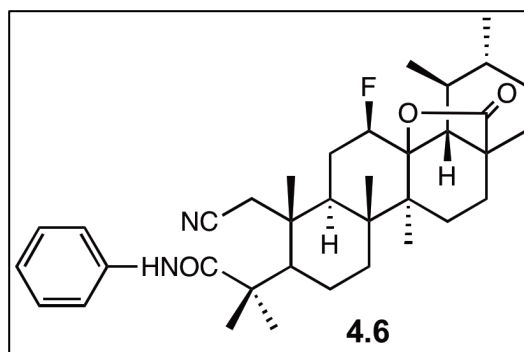


extracted with ethyl acetate (3 × 60 ml). The resulting organic phase was washed with 5% HCl aqueous solution (2 × 60 ml), water (60 ml), and 10% NaCl aqueous solution (60 ml), dried over Na₂SO₄, filtered, and concentrated to dryness. The crude residue was purified by flash column chromatography (petroleum ether:ethyl acetate 3:1–1:3) to give **4.5** as a white solid (58.6%). Mp 338.6 – 340.9 °C. IR (KBr): ν = 3507.88, 3370.96, 2977.55, 2931.27, 2875.34, 2237.02, 1766.48, 1668.12, 1594.84, 1457.92, 1396.21, 1236.15, 1186.01, 1120.44, 939.16 cm⁻¹. ¹H NMR (400 MHz, CDCl₃): δ = 5.88 (s, 1H, NH), 5.84 (s, 1H, NH), 4.91 (dm, 1H, H-12), 2.81 (d, *J* = 18.3 Hz, 1H, H-1), 2.51 (d, *J* = 18.2 Hz, 1H, H-1), 1.28 (s, 3H), 1.25 (s, 6H), 1.24 (s, 3H), 1.13 (d, *J* = 6.3 Hz, 3H), 1.07 (s, 3H), 0.97 (d, *J* = 5.8 Hz, 3H). ¹³C NMR (100 MHz, CDCl₃): δ = 181.67 (CON), 178.75 (C28), 118.97 (CN), 91.94 (d, *J* = 14.4 Hz, C13), 89.29 (d, *J* = 186.4 Hz, C12), 52.81 (d, *J* = 3.6 Hz), 51.15, 45.97, 45.40, 44.48 (d, *J* = 3.0 Hz), 43.72 (d, *J* = 9.7 Hz), 42.37, 42.35, 39.72, 38.80, 33.26, 31.43, 30.87, 29.14, 28.88, 27.72, 26.09 (d, *J* = 19.9 Hz), 22.49, 22.42, 19.72, 19.50, 19.00, 18.07, 17.17, 16.62. MS (DI-ESI) (*m/z*): 501.5 (100%) [M+H]⁺, 481.7 (15.6%). Anal. Calcd for C₃₀H₄₅FN₂O₃: C, 71.97; H, 9.06; N, 5.59. Found: C, 71.65; H, 8.81; N, 5.63.

Chapter 4 | Synthesis and cytotoxic activity of novel UA derivatives

2,3-Seco-2-cyano-3-N-phenylamide-12 β -fluor-urs-13,28 β -olide (4.6): To a stirred mixture of

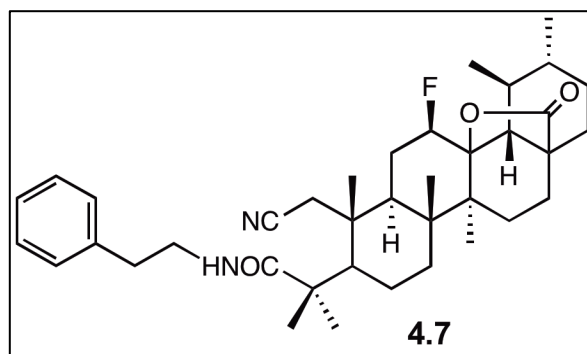
4.2 (200 mg, 0.40 mmol) in dry THF (4 ml) and benzene (4 ml) at 80 °C, SOCl₂ (0.1 ml, 1.39 mmol) was added. After 3 h, the reaction mixture was evaporated under reduced pressure, and the residue was dissolved in dry CH₂Cl₂ (4 ml) and basified to pH 8–9 with Et₃N (1.5 ml). Then aniline



(0.15 ml, 1.65 mmol) was added, and the resultant mixture was stirred at r.t. for 1 h. The reaction mixture was evaporated under reduced pressure, and the resultant residue was extracted with ethyl acetate (3 × 50 ml) from water (20 ml). The resulting organic phase was washed with 5% HCl aqueous solution (50 ml), water (50 ml), and 10% NaCl aqueous solution (50 ml), dried over Na₂SO₄, filtered, and concentrated to dryness. The crude residue was purified by flash column chromatography (petroleum ether:ethyl acetate 7:1–3:1) to give **4.6** as a yellow solid (45.4%). Mp 305.4 – 307.5 °C. IR (KBr): ν = 3442.31, 2960.20, 2931.27, 2875.34, 2231.24, 1774.19, 1671.98, 1596.77, 1523.49, 1434.78, 1311.36, 1236.15, 1110.80, 987.37, 937.23, 752.10, 686.53 cm⁻¹. ¹H NMR (400 MHz, CDCl₃): δ = 7.60 (d, *J* = 7.9 Hz, 2H, H₂'₆'-Ar), 7.49 (s, 1H, NH), 7.34 (t, *J* = 7.8 Hz, 2H, H₃'₅'-Ar), 7.14 (t, *J* = 7.3 Hz, 1H, H₄'-Ar), 4.89 (dm, *J* = 42.7 Hz, 1H, H-12), 2.62 (d, *J* = 18.4 Hz, 1H, H-1), 2.47 (d, *J* = 18.3 Hz, 1H, H-1), 1.41 (s, 3H), 1.35 (s, 3H), 1.27 (s, 3H), 1.26 (s, 3H), 1.13 (d, *J* = 6.3 Hz, 3H), 1.10 (s, 3H), 0.96 (d, *J* = 5.3 Hz, 3H). ¹³C NMR (100 MHz, CDCl₃): δ = 178.71 (C₂₈), 176.72 (CON), 137.69 (C-Ar), 129.20 (C-Ar, 2C), 124.72 (C-Ar), 120.11 (C-Ar, 2C), 118.95 (CN), 91.94 (d, *J* = 14.2 Hz, C₁₃), 89.38 (d, *J* = 186.7 Hz, C₁₂), 52.84 (d, *J* = 3.4 Hz), 51.56, 46.98, 45.41, 44.51 (d, *J* = 2.9 Hz), 43.56 (d, *J* = 9.6 Hz), 42.43, 42.38, 39.73, 38.83, 33.26, 31.44, 30.88, 29.19, 28.77, 27.73, 26.19 (d, *J* = 20.0 Hz), 22.53, 22.50, 20.03, 19.50, 18.56, 18.08, 17.16, 16.63. MS (DI-ESI) (*m/z*): 577.3 (100%) [M+H]⁺. Anal. Calcd for C₃₆H₄₉FN₂O₃: C, 74.96; H, 8.56; N, 4.86. Found: C, 74.59; H, 8.65; N, 4.81.

2,3-Seco-2-cyano-3-N-phenethylamide-12 β -fluor-urs-13,28 β -olide (4.7): To a stirred mixture

of **4.2** (200 mg, 0.40 mmol) in dry THF (4 ml) and benzene (4 ml) at 80 °C, SOCl₂ (0.1 ml, 1.39 mmol) was added. After 3.5 h, the reaction mixture was evaporated under reduced pressure, and the residue was dissolved in dry CH₂Cl₂ (4 ml) and basified to pH 8–9 with Et₃N



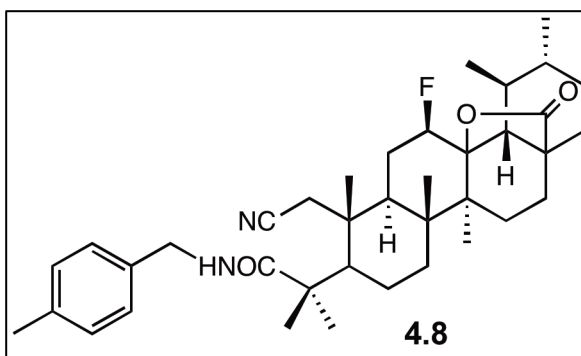
(1.5 ml). Then phenethylamine (0.2 ml, 1.59 mmol) was added, and the resultant mixture was stirred at r.t. for 2 h. The reaction mixture was evaporated under reduced pressure, and the resultant residue was extracted with ethyl acetate (3 × 50 ml) from water (20 ml). The resulting organic phase was washed with 5% HCl aqueous solution (50 ml), water (50 ml), and 10% NaCl aqueous solution (50 ml), dried over Na₂SO₄, filtered, and concentrated to dryness. The crude residue was purified by flash column chromatography (petroleum ether:ethyl acetate 7:1–2:1) to give **4.7** as a slightly yellow solid (45.5%). Mp 229.8 – 233.6 °C. IR (KBr): ν = 3363.25, 3025.76, 2977.55, 2927.41, 2875.34, 2235.09, 1766.48, 1639.20, 1529.27, 1455.99, 1375.00, 1193.72, 989.3, 937.23, 755.97, 701.96 cm⁻¹. ¹H NMR (400 MHz, CDCl₃): δ = 7.32–7.29 (m, 2H, H-Ar), 7.24–7.20 (m, 3H, H-Ar) 5.78 (t, *J* = 5.0 Hz, 1H, NH), 4.89 (dm, *J* = 45.9 Hz, 1H, H-12), 3.77–3.69 (m, 1H, CHHN), 3.40–3.32 (m, 1H, CHHN), 2.87 (t, *J* = 6.9 Hz, 2H, Ar-CH₂), 2.59 (d, *J* = 18.3 Hz, 1H, H-1), 2.39 (d, *J* = 18.3 Hz, 1H, H-1), 1.23 (6H), 1.16 (6H), 1.13 (d, *J* = 6.3 Hz, 3H), 1.01 (s, 3H), 0.97 (d, *J* = 5.1 Hz, 3H). ¹³C NMR (100 MHz, CDCl₃): δ = 178.62 (C28), 178.50 (CON), 138.77 (C-Ar), 128.80 (C-Ar, 2C), 128.66 (C-Ar, 2C), 126.59 (C-Ar), 118.76 (CN), 91.80 (d *J* = 14.3 Hz, C13), 89.18 (d, *J* = 186.3 Hz, C12), 52.69 (d, *J* = 3.2 Hz), 51.42, 45.62, 45.27, 44.34 (d, *J* = 3.0 Hz), 43.49 (d, *J* = 9.4 Hz), 42.23, 42.12, 40.97, 39.60, 38.68, 35.27, 33.12, 31.32, 30.76, 29.00, 28.47, 27.59, 25.97 (d, *J* = 19.9 Hz), 22.38, 21.94, 19.55, 19.38, 18.61,

Chapter 4 | Synthesis and cytotoxic activity of novel UA derivatives

17.94, 17.05, 16.51. MS (DI-ESI) (m/z): 605.6 (100%) [M+H]⁺. Anal. Calcd for C₃₈H₅₃FN₂O₃·0.8H₂O: C, 73.70; H, 8.89; N, 4.52. Found: C, 73.49; H, 8.86; N, 4.53.

2,3-Seco-2-cyano-3-N-(4-methylbenzylamide)-12β-fluor-urs-13,28β-olide (4.8): To a stirred

mixture of **4.2** (200 mg, 0.40 mmol) in dry THF (4 ml) and benzene (4 ml) at 80 °C, SOCl₂ (0.1 ml, 1.39 mmol) was added. After 3.5 h, the reaction mixture was evaporated under reduced pressure, and the residue was dissolved in dry CH₂Cl₂ (4 ml) and basified to pH 8–9 with Et₃N (1.5 ml).



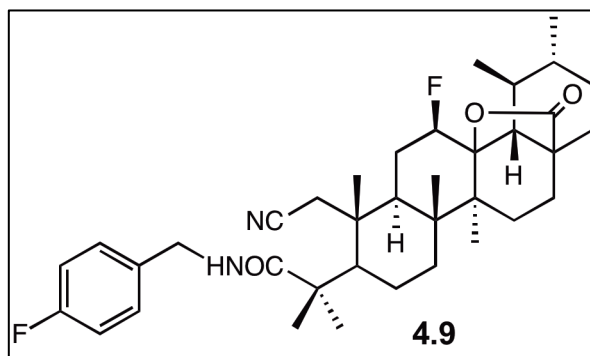
Then 4-methylbenzylamine (0.2 ml, 1.57 mmol) was added, and the resultant mixture was stirred at r.t. for 2 h. The reaction mixture was evaporated under reduced pressure, and the resultant residue was extracted with ethyl acetate (3 × 50 ml) from water (20 ml). The resulting organic phase was washed with 5% HCl aqueous solution (50 ml), water (50 ml), and 10% NaCl aqueous solution (50 ml), dried over Na₂SO₄, filtered, and concentrated to dryness. The crude residue was purified by flash column chromatography (petroleum ether:ethyl acetate 7:1–2:1) to give **4.8** as a slightly yellow solid (45.1%). Mp 239.5 – 243.4 °C. IR (KBr): ν = 3463.53, 3016.12, 2977.55, 2929.34, 2873.42, 2235.09, 1772.26, 1658.48, 1517.70, 1459.85, 1394.28, 1186.01, 1114.65, 989.30, 939.16, 806.10 cm⁻¹. ¹H NMR (400 MHz, CDCl₃): δ = 7.20 (d, J = 8.02 Hz, 2H, H-Ar), 7.14 (d, J = 8.02 Hz, 2H, H-Ar), 6.04 (dd, J = 6.3, 4.1 Hz, 1H, NH), 4.90 (dm, 1H, H-12) 4.65 (dd, J = 14.3, 6.8 Hz, 1H, CHHN), 4.17 (dd, J = 14.3, 3.9 Hz, 1H, CHHN), 2.65 (d, J = 18.4 Hz, 1H, H-1), 2.43 (d, J = 18.3 Hz, 1H, H-1), 2.33 (s, 3H, CH₃-Ar), 1.26 (s, 3H), 1.24 (6H), 1.23 (s, 3H), 1.13 (d, J = 6.3 Hz, 3H), 1.05 (s, 3H), 0.96 (d, J = 5.6 Hz, 3H). ¹³C NMR (100 MHz, CDCl₃): δ = 178.74 (C28), 178.40 (CONH), 137.46 (C-Ar), 134.97 (C-Ar), 129.54 (2C, C-Ar), 128.26 (2C, C-Ar), 118.86 (CN), 91.93 (d, J = 14.5 Hz, C13), 89.35 (d, J = 186.2 Hz, C12), 52.81 (d, J = 3.4 Hz), 51.62, 45.77, 45.39, 44.46 (d, J = 2.9 Hz), 43.94, 43.65 (d, J = 9.6 Hz), 42.36,

Chapter 4 | Synthesis and cytotoxic activity of novel UA derivatives

42.29, 39.72, 38.79, 33.25, 31.43, 30.87, 29.26, 28.69, 27.71, 26.08 (d, $J = 20.0$ Hz), 22.49, 22.13, 21.24, 19.68, 19.49, 18.82, 18.07, 17.15, 16.61. MS (DI-ESI) (m/z): 605.6 (100%) $[M+H]^+$. Anal. Calcd for $C_{38}H_{53}FN_2O_3 \cdot 0.4H_2O$: C, 74.57; H, 8.86; N, 4.58. Found: C, 74.31; H, 8.68; N, 4.62.

2,3-Seco-2-cyano-3-N-(4-fluorobenzamide)-12 β -fluor-urs-13,28 β -olide (4.9): To a stirred

mixture of **4.2** (200 mg, 0.40 mmol) in dry THF (4 ml) and benzene (4 ml) at 80 °C, $SOCl_2$ (0.1 ml, 1.39 mmol) was added. After 3.5 h, the reaction mixture was evaporated under reduced pressure, and the residue was dissolved in dry CH_2Cl_2 (4 ml) and basified to pH 8–9 with Et_3N (1.5 ml).

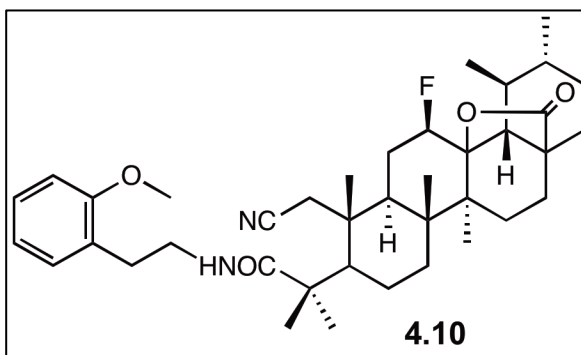


Then 4-fluorobenzylamine (0.19 ml, 1.66 mmol) was added and the resultant mixture was stirred at r.t. for 2 h. The reaction mixture was evaporated under reduced pressure, and the resultant residue was extracted with ethyl acetate (3 × 50 ml) from water (20 ml). The resulting organic phase was washed with 5% HCl aqueous solution (50 ml), water (50 ml), and 10% NaCl aqueous solution (50 ml), dried over Na_2SO_4 , filtered, and concentrated to dryness. The crude residue was purified by flash column chromatography (petroleum ether:ethyl acetate 7:1–2:1) to give **4.9** as a light yellow solid (44.2%). Mp 145.4 – 149.4 °C. IR (KBr): $\nu = 3407.60, 2977.55, 2931.27, 2873.42, 2288.95, 1774.19, 1650.77, 1509.99, 1459.85, 1220.72, 1157.08, 987.34, 937.23, 846.60$ cm^{-1} . 1H NMR (400 MHz, $CDCl_3$): $\delta = 7.31$ – 7.26 (m, 2H, H-Ar), 7.01 (t, $J = 8.6$ Hz, 2H, H-Ar), 6.08 (t, $J = 5.4$ Hz, 1H, NH), 4.90 (dm, $J = 45.5$ Hz, 1H, H-12), 4.66 (dd, $J = 14.4, 6.8$ Hz, 1H, CHHN), 4.18 (dd, $J = 14.4, 3.9$ Hz, 1H, CHHN), 2.62 (d, $J = 18.4$ Hz, 1H, H-1), 2.44 (d, $J = 18.3$ Hz, 1H, H-1), 1.26 (s, 3H), 1.24 (9H), 1.13 (d, $J = 6.2$ Hz, 3H), 1.06 (s, 3H), 0.96 (d, $J = 5.6$ Hz, 3H). ^{13}C NMR (100 MHz, $CDCl_3$): $\delta = 178.73$ (C28), 178.58 (CON), 162.35 (d, $J = 254.9$ Hz, CF-Ar), 133.87 (d, $J = 3.2$ Hz, C-Ar), 130.06 (C-Ar), 129.98 (C-Ar), 118.95 (CN),

115.84 (C-Ar), 115.63 (C-Ar), 91.91 (d, $J = 14.5$ Hz, C13), 89.31 (d, $J = 186.4$ Hz, C12), 52.82 (d, $J = 3.2$ Hz), 51.69, 45.83, 45.40, 44.47 (d, $J = 2.8$ Hz), 43.69 (d, $J = 9.5$ Hz), 43.47, 42.37, 42.34, 39.73, 38.81, 33.25, 31.44, 30.88, 29.20, 28.71, 27.72, 26.13 (d, $J = 20.1$ Hz), 22.49, 22.14, 19.70, 19.50, 18.84, 18.09, 17.16, 16.63. MS (DI-ESI) (m/z): 609.6 (100%) $[M+H]^+$. Anal. Calcd for $C_{37}H_{50}F_2N_2O_3 \cdot 0.2H_2O$: C, 72.57; H, 8.29; N, 4.57. Found: C, 72.57; H, 7.96; N, 4.61.

2,3-Seco-2-cyano-3-N-(2-methoxyphenethylamide)-12 β -fluor-urs-13,28 β -olide (4.10): To a

stirred mixture of **4.2** (200 mg, 0.40 mmol) in dry THF (4 ml) and benzene (4 ml) at 80 °C, $SOCl_2$ (0.1 ml, 1.39 mmol) was added. After 3.5 h, the reaction mixture was evaporated under reduced pressure, and the residue was dissolved in dry CH_2Cl_2 (4 ml) and basified to pH 8–9 with Et_3N



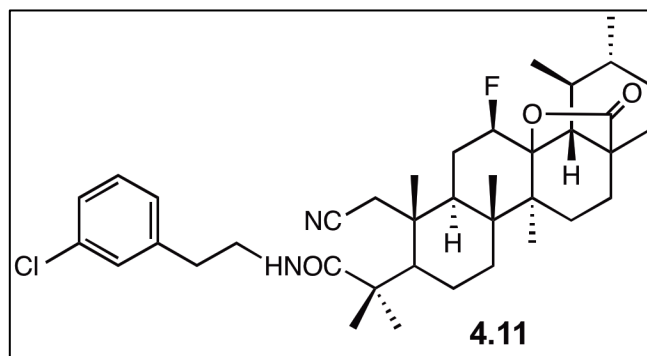
(1.5 ml). Then 2-methoxyphenethylamine (0.23 ml, 1.57 mmol) was added, and the resultant mixture was stirred at r.t. for 3 h. The reaction mixture was evaporated under reduced pressure, and the resultant residue was extracted with ethyl acetate (3 × 50 ml) from water (20 ml). The resulting organic phase was washed with 5% HCl aqueous solution (50 ml), water (50 ml), and 10% NaCl aqueous solution (50 ml), dried over Na_2SO_4 , filtered, and concentrated to dryness. The crude residue was purified by flash column chromatography (petroleum ether:ethyl acetate 7:1–3:1) to give **4.10** as a light yellow solid (41.5%). Mp 210.7 – 213.0 °C. IR (KBr): $\nu = 3421.10, 2969.84, 2927.41, 2871.49, 2231.24, 1774.19, 1627.63, 1521.56, 1457.92, 1375.00, 1243.86, 1122.37, 989.3, 937.23, 754.03$ cm^{-1} . 1H NMR (400 MHz, $CDCl_3$): $\delta = 7.21$ (t, $J = 7.5$ Hz, 1H, H-Ar), 7.14 (d, $J = 7.0$ Hz, 1H, H-Ar), 6.90 (t, $J = 7.6$ Hz, 1H, H-Ar), 6.86 (d, $J = 8.2$ Hz, 1H, H-Ar), 6.09 (t, $J = 4.8$ Hz, 1H, NH), 4.89 (dm, $J = 45.6$ Hz, 1H, H-12), 3.84 (s, 3H, CH_3O -Ar), 3.68–3.60 (m, 1H, $CHHN$), 3.40–3.32 (m, 1H, $CHHN$), 2.98–2.92 (m, 1H, $CHHCH_2N$), 2.87–2.80 (m, 1H, $CHHCH_2N$), 2.49 (d, $J = 18.3$ Hz, 1H, H-1), 2.30 (d, $J = 18.2$ Hz, 1H, H-1), 1.24 (s, 3H), 1.22 (s,

Chapter 4 | Synthesis and cytotoxic activity of novel UA derivatives

3H), 1.16 (s, 3H), 1.14 (s, 3H), 1.12 (d, $J = 6.4$ Hz, 3H), 0.96 (3H), 0.95 (3H). ^{13}C NMR (100 MHz, CDCl_3): $\delta = 178.79$ (C28), 178.44 (CON), 157.52 (C-Ar), 130.84 (C-Ar), 128.10 (C-Ar), 127.61 (C-Ar), 121.01 (C-Ar), 118.69 (CN), 110.66 (C-Ar), 91.97 (d, $J = 14.3$ Hz, C13), 89.34 (d, $J = 186.2$ Hz, C12), 55.59, 52.80 (d, $J = 3.2$ Hz), 51.39, 45.53, 45.40, 44.46 (d, $J = 3.0$ Hz), 43.56 (d, $J = 9.3$ Hz), 42.33, 42.10, 40.69, 39.72, 38.79, 33.27, 31.44, 30.87, 29.60, 29.24, 28.44, 27.71, 26.04 (d, $J = 19.9$ Hz), 22.50, 21.93, 19.57, 19.49, 18.69, 18.05, 17.18, 16.61. MS (DI-ESI) (m/z): 635.6 (100%) $[\text{M}+\text{H}]^+$. Anal. Calcd for $\text{C}_{39}\text{H}_{55}\text{FN}_2\text{O}_4 \cdot 0.5\text{H}_2\text{O}$: C, 72.75; H, 8.77; N, 4.35. Found: C, 72.74; H, 8.50; N, 4.43.

2,3-Seco-2-cyano-3-N-(3-chlorophenylethylamide)-12 β -fluor-urs-13,28 β -olide (4.11): To a

stirred mixture of **4.2** (200 mg, 0.40 mmol) in dry THF (4 ml) and benzene (4 ml) at 80 °C, SOCl_2 (0.1 ml, 1.39 mmol) was added. After 3.5 h, the reaction mixture was evaporated under reduced pressure, and the residue was dissolved in dry CH_2Cl_2 (4



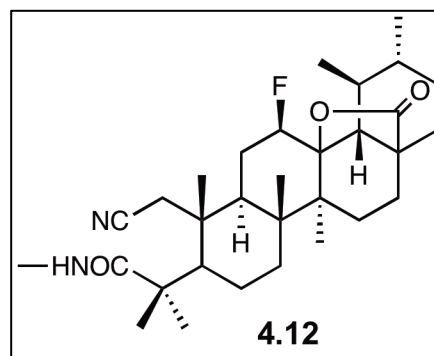
ml) and basified to pH 8–9 with Et_3N (1.5 ml). Then 2-(3-chlorophenyl)ethylamine (0.2 ml, 1.44 mmol) was added, and the resultant mixture was stirred at r.t. for 2 h. The reaction mixture was evaporated under reduced pressure, and the resultant residue was extracted with ethyl acetate (3 × 50 ml) from water (20 ml). The resulting organic phase was washed with 5% HCl aqueous solution (50 ml), water (50 ml), and 10% NaCl aqueous solution (50 ml), dried over Na_2SO_4 , filtered, and concentrated to dryness. The crude residue was purified by flash column chromatography (petroleum ether:ethyl acetate 7:1–2:1) to give **4.11** as a slightly yellow solid (49.9%). Mp 212.0 – 214.5 °C. IR (KBr): $\nu = 3405.67, 2977.55, 2931.27, 2875.34, 2237.02, 1770.33, 1639.20, 1521.56, 1457.92, 1375.00, 1186.01, 1116.58, 987.37, 937.23, 871.67,$

Chapter 4 | Synthesis and cytotoxic activity of novel UA derivatives

782.96, 700.03 cm^{-1} . ^1H NMR (400 MHz, CDCl_3): δ = 7.24–7.21 (m, 2H, H-Ar), 7.19 (s, 1H, H2'-Ar), 7.09 (d, J = 6.9 Hz, 1H, H-Ar), 5.80 (t, J = 5.4 Hz, 1H, NH), 4.89 (dm, J = 45.4 Hz, 1H, H-12), 3.76–3.68 (m, 1H, CHHN), 3.38–3.30 (m, 1H, CHHN), 2.85 (t, J = 6.9 Hz, 2H, Ar-CH₂CH₂N), 2.60 (d, J = 18.3 Hz, 1H, H-1), 2.42 (d, J = 18.2 Hz, 1H, H-1), 1.23 (6H), 1.18 (6H), 1.13 (d, J = 6.0 Hz, 3H), 1.02 (s, 3H), 0.96 (d, J = 5.3 Hz, 3H). ^{13}C NMR (100 MHz, CDCl_3): δ = 178.79 (CON), 178.75 (C28), 140.98 (C1-Ar), 134.49 (CCI-Ar), 130.04 (C-Ar), 129.13 (C-Ar), 127.09 (C-Ar), 126.91 (C-Ar), 118.92 (CN), 91.93 (d, J = 14.4 Hz, C13), 89.28 (d, J = 186.3 Hz, C12), 52.82 (d, J = 3.3 Hz), 51.59, 45.82, 45.40, 44.46 (d, J = 2.9 Hz), 43.65 (d, J = 9.5 Hz), 42.36, 42.28, 40.93, 39.73, 38.80, 35.09, 33.24, 31.44, 30.87, 29.07, 28.61, 27.71, 26.08 (d, J = 20.0 Hz), 22.49, 22.11, 19.70, 19.50, 18.76, 18.07, 17.16, 16.64. MS (DI-ESI) (m/z): 639.5 (100%) $[\text{M}+\text{H}]^+$. Anal. Calcd for $\text{C}_{38}\text{H}_{52}\text{ClFN}_2\text{O}_3 \cdot 0.3\text{H}_2\text{O}$: C, 70.80; H, 8.22; N, 4.35. Found: C, 70.66; H, 8.08; N, 4.29.

2,3-Seco-2-cyano-3-N-methylamide-12 β -fluor-urs-13,28 β -olide (4.12): To a stirred mixture of

4.2 (200 mg, 0.40 mmol) in dry THF (3 ml) and benzene (3 ml) at 80 °C, SOCl_2 (0.1 ml, 1.39 mmol) was added. After 3.25 h, the reaction mixture was evaporated under reduced pressure, and the residue was dissolved in dry CH_2Cl_2 (4 ml) and basified to pH 8–9 with Et_3N (1.5 ml). Then methylamine solution (33 wt. % in absolute ethanol) (0.15 ml, 1.20 mmol)



was added, and the resultant mixture was stirred at r.t. for 1.5 h. The reaction mixture was evaporated under reduced pressure, and the resultant residue was extracted with ethyl acetate (3 × 50 ml) from water (20 ml). The resulting organic phase was washed with 5% HCl aqueous solution (50 ml), water (50 ml), and 10% NaCl aqueous solution (50 ml), dried over Na_2SO_4 , filtered, and concentrated to dryness. The crude residue was purified by flash column chromatography (petroleum ether:ethyl acetate 7:1–1:1) to give **4.12** as a slightly yellow solid

Chapter 4 | Synthesis and cytotoxic activity of novel UA derivatives

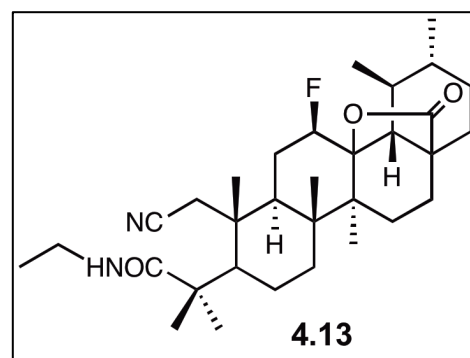
(48.2%). Mp 282 – 285.4 °C. IR (KBr): ν = 3403.74, 2977.55, 2931.27, 2875.34, 2233.16, 1774.19, 1627.63, 1533.13, 1459.85, 1375.00, 1236.15, 1186.01, 1114.65, 937.23 cm^{-1} . ^1H NMR (400 MHz, CDCl_3): δ = 5.88–5.84 (m, 1H, NH), 4.88 (dm, 1H, H-12), 2.85 (d, J = 4.5 Hz, 3H, CH_3N), 2.61 (d, J = 18.4 Hz, 1H, H-1), 2.44 (d, J = 18.3 Hz, 1H, H-1), 1.26 (s, 3H), 1.25 (6H), 1.20 (s, 3H), 1.13 (d, J = 6.3 Hz, 3H), 1.06 (s, 3H), 0.96 (d, J = 5.3 Hz, 3H). ^{13}C NMR (100 MHz, CDCl_3): δ = 179.35 (CON), 178.74 (C28), 118.91 (CN), 91.93 (d, J = 14.4 Hz, C13), 89.34 (d, J = 186.7 Hz, C12), 52.83 (d, J = 3.3 Hz), 52.05, 45.55, 45.40, 44.47 (d, J = 2.9 Hz), 43.61 (d, J = 9.4 Hz), 42.39, 42.31, 39.72, 38.81, 33.30, 31.43, 30.87, 29.62, 28.31, 27.72, 26.85, 26.12 (d, J = 20.3 Hz), 22.49, 21.69, 19.59, 19.50, 18.58, 18.08, 17.16, 16.64. MS (DI-ESI) (m/z): 515.6 (100%) $[\text{M}+\text{H}]^+$. Anal. Calcd for $\text{C}_{31}\text{H}_{47}\text{FN}_2\text{O}_3 \cdot 0.5\text{H}_2\text{O}$: C, 71.09; H, 9.24; N, 5.35. Found: C, 70.81; H, 8.90; N, 5.32.

2,3-Seco-2-cyano-3-N-ethylamide-12 β -fluor-urs-13,28 β -olide (4.13): To a stirred mixture of

4.2 (200 mg, 0.40 mmol) in dry THF (3 ml) and benzene (3 ml) at 80 °C, SOCl_2 (0.1 ml, 1.39 mmol) was added.

After 3 h, the reaction mixture was evaporated under reduced pressure, and the residue was dissolved in dry CH_2Cl_2 (4 ml) and basified to pH 8–9 with Et_3N (1.5 ml).

Then ethylamine solution (2.0 M in THF) (0.1 ml) was



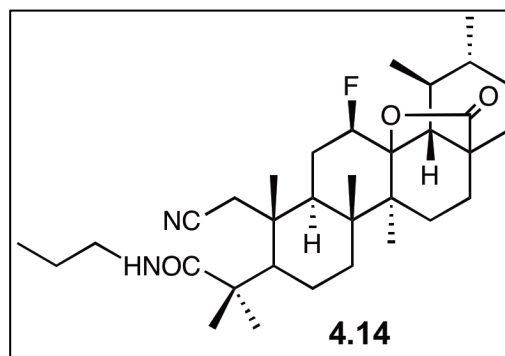
added, and the resultant mixture was stirred at r.t. for 1.5 h. The reaction mixture was evaporated under reduced pressure, and the resultant residue was extracted with ethyl acetate (3 × 50 ml) from water (20 ml). The resulting organic phase was washed with 5% HCl aqueous solution (50 ml), water (50 ml), and 10% NaCl aqueous solution (50 ml), dried over Na_2SO_4 , filtered, and concentrated to dryness. The crude residue was purified by flash column chromatography (petroleum ether:ethyl acetate 7:1–2:1) to give **4.13** as a slightly yellow solid (47.6%). Mp 322.5 – 326.1 °C. IR (KBr): ν = 3455.81, 2975.62, 2929.34, 2875.34, 2235.09,

Chapter 4 | Synthesis and cytotoxic activity of novel UA derivatives

1774.19, 1650.77, 1504.20, 1457.92, 1388.50, 1234.22, 1193.72, 937.23 cm^{-1} . ^1H NMR (400 MHz, CDCl_3): δ = 5.75 (t, J = 4.7 Hz, 1H, NH), 4.89 (dm, 1H, H-12), 3.48–3.38 (m, 1H, CHHN), 3.22–3.13 (m, 1H, CHHN), 2.65 (d, J = 18.3 Hz, 1H, H-1), 2.44 (d, J = 18.3 Hz, 1H, H-1), 1.26 (s, 3H), 1.25 (6H), 1.21–1.19 (m, 6H), 1.13 (d, J = 6.3 Hz, 3H), 1.06 (s, 3H), 0.96 (d, J = 5.3 Hz, 3H). ^{13}C NMR (100 MHz, CDCl_3): δ = 178.73 (C28), 178.60 (CON), 119.00 (CN), 91.95 (d, J = 14.8 Hz, C13), 89.28 (d, J = 186.6 Hz, C12), 52.81 (d, J = 3.3 Hz), 51.76, 45.56, 45.39, 44.47 (d, J = 3.0 Hz), 43.61 (d, J = 9.5 Hz), 42.36, 42.30, 39.72, 38.80, 35.08, 33.28, 31.44, 30.87, 29.49, 28.57, 27.71, 26.11 (d, J = 19.9 Hz), 22.49, 21.91, 19.67, 19.49, 18.65, 18.06, 17.16, 16.63, 14.47. MS (DI-ESI) (m/z): 529.6 (100%) $[\text{M}+\text{H}]^+$, 509.7 (18.8%). Anal. Calcd for $\text{C}_{32}\text{H}_{49}\text{FN}_2\text{O}_3 \cdot 0.2\text{H}_2\text{O}$: C, 72.20; H, 9.35; N, 5.26. Found: C, 72.37; H, 9.28; N, 5.21.

2,3-Seco-2-cyano-3-N-propylamide-12 β -fluor-urs-13,28 β -olide (4.14): To a stirred mixture of

4.2 (200 mg, 0.40 mmol) in dry THF (3 ml) and benzene (3 ml) at 80 $^\circ\text{C}$, SOCl_2 (0.1 ml, 1.39 mmol) was added. After 3.5 h, the reaction mixture was evaporated under reduced pressure, and the residue was dissolved in dry CH_2Cl_2 (4 ml) and basified to pH 8–9 with Et_3N (1.5 ml). Then propylamine (0.13 ml,

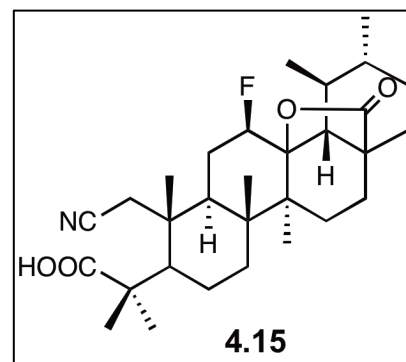


1.58 mmol) was added, and the resultant mixture was stirred at r.t. for 3 h. The reaction mixture was evaporated under reduced pressure, and the resultant residue was extracted with ethyl acetate (3 \times 50 ml) from water (20 ml). The resulting organic phase was washed with 5% HCl aqueous solution (50 ml), water (50 ml), and 10% NaCl aqueous solution (50 ml), dried over Na_2SO_4 , filtered, and concentrated to dryness. The crude residue was purified by flash column chromatography (petroleum ether:ethyl acetate 7:1–2:1) to give **4.14** as a yellow solid (47.4%). Mp 255.9 – 259.8 $^\circ\text{C}$. IR (KBr): ν = 3424.96, 2969.84, 2923.56, 2871.49, 2242.81, 1760.69, 1660.41, 1513.85, 1459.85, 1384.64, 1265.07, 1184.08, 989.30, 935.31 cm^{-1} . ^1H NMR (400

Chapter 4 | Synthesis and cytotoxic activity of novel UA derivatives

MHz, CDCl₃): δ = 5.80 (t, J = 5.07 Hz, 1H, NH), 4.89 (dm, 1H, H-12), 3.44–3.36 (m, 1H, CHHN), 3.09–3.01 (m, 1H, CHHN), 2.65 (d, J = 18.3 Hz, 1H, H-1), 2.44 (d, J = 18.3 Hz, 1H, H-1), 1.26 (s, 3H), 1.25 (6H), 1.21 (s, 3H), 1.13 (d, J = 6.2 Hz, 3H), 1.05 (s, 3H), 0.96–0.91 (m, 6H). ¹³C NMR (100 MHz, CDCl₃): δ = 178.71 (C28), 178.61 (CON), 118.95 (CN), 91.93 (d, J = 14.6 Hz, C13), 89.31 (d, J = 186.9 Hz, C12), 52.81 (d, J = 3.3 Hz), 51.69, 45.73, 45.39, 44.47 (d, J = 3.0 Hz), 43.61 (d, J = 9.5 Hz), 42.36, 42.30, 41.79, 39.72, 38.80, 33.27, 31.44, 30.87, 29.33, 28.63, 27.71, 26.12 (d, J = 19.9 Hz), 22.61, 22.49, 22.07, 19.72, 19.49, 18.67, 18.06, 17.15, 16.63, 11.56. MS (DI-ESI) (m/z): 543.5 (100%) [M+H]⁺, 523.7 (13.1%). Anal. Calcd for C₃₃H₅₁FN₂O₃·0.2H₂O: C, 72.54; H, 9.48; N, 5.13. Found: C, 72.26; H, 9.59; N, 4.98.

2,3-Seco-2-cyano-12 β -fluor-urs-13,28 β -olid-3-oic acid (4.15): To a stirred mixture of **4.2** (200 mg, 0.40 mmol) in dry THF (4 ml) and benzene (4 ml) at 80 °C, SOCl₂ (0.1 ml, 1.37 mmol) was added. After 3.5 h, the reaction mixture was evaporated under reduced pressure, and the resultant residue was extracted with ethyl acetate (3 × 60 ml) from water (30 ml). The resulting organic phase was washed with water (60 ml), and 10% NaCl aqueous solution (60 ml),



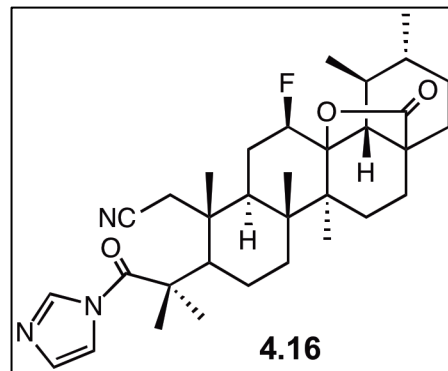
dried over Na₂SO₄, filtered, and concentrated to dryness. The crude residue was purified by preparative TLC (petroleum ether:chloroform 130:1) to give **4.15** as a slightly yellow solid (35.7%). Mp 327.1 – 331.7 °C. IR (KBr): ν = 3461.6, 2985.27, 2937.05, 2877.27, 2240.88, 1766.48, 1700.91, 1459.85, 1398.14, 1286.29, 1186.01, 1120.44, 939.16 cm⁻¹. ¹H NMR (400 MHz, CDCl₃): δ = 4.93 (dm, 1H, H-12), 2.60 (dd, J = 18.5 Hz, 2H, H-1), 1.31 (s, 3H), 1.27 (6H), 1.25 (3H), 1.14 (d, J = 6.3 Hz, 3H), 1.05 (s, 3H), 0.97 (d, J = 5.7 Hz, 3H). ¹³C NMR (100 MHz, CDCl₃): δ = 184.44 (COOH), 178.84 (C28), 118.00 (CN), 91.98 (d, J = 14.3 Hz, C13), 89.25 (d, J = 186.4 Hz, C12), 52.82 (d, J = 3.2 Hz), 50.34, 46.15, 45.43, 44.49 (d, J = 3.1 Hz), 43.80 (d, J = 9.4 Hz), 42.41, 42.18, 39.74, 38.78, 33.29, 31.45, 30.89, 29.33, 27.81, 27.76, 26.04 (d, J = 20.0

Chapter 4 | Synthesis and cytotoxic activity of novel UA derivatives

Hz), 23.12, 22.52, 19.81, 19.52, 19.47, 18.17, 17.26, 16.64. MS (DI-ESI) (m/z): 502.8 (100%) [M+H]⁺, 483.40 (16.60%), 482.38 (54.52%). Anal. Calcd for C₃₀H₄₄FNO₄: C, 71.82; H, 8.84; N, 2.79. Found: C, 71.65; H, 8.81; N, 2.93.

2,3-Seco-2-cyano-3-oxo-(1H-imidazol-1-yl)-12 β -fluor-urs-13,28 β -olide (4.16): To a stirred

mixture of **4.2** (300 mg, 0.60 mmol) in dry THF (3.7 ml) under N₂ at 50 °C, CDI (194 mg, 1.20 mmol) was added. After 3 h, additional CDI (194 mg, 1.20 mmol) was added. After 24 h, the solvent was evaporated under reduced pressure, and the residue was extracted with ethyl acetate (3 × 70 ml) from water (30 ml). The resulting organic phase



was washed with water (80 ml), and 10% NaCl aqueous solution (80 ml), dried over Na₂SO₄, filtered, and concentrated to dryness. The crude residue was purified by flash column chromatography (petroleum ether:ethyl acetate 4:1–1:5) to give **4.16** as a slightly yellow solid (45.2%). Mp 285.9 – 288.7 °C. IR (KBr): ν = 3160.76, 3143.4, 3124.12, 2971.77, 2933.20, 2879.20, 2238.95, 1770.33, 1716.34, 1533.13, 1459.85, 1398.14, 1270.86, 1232.29, 1072.23, 919.88 cm⁻¹. ¹H NMR (400 MHz, CDCl₃): δ = 8.40 (s, 1H, H-imidazole), 7.75 (s, 1H, H-imidazole), 7.12 (s, 1H, H-imidazole), 4.90 (dm, J = 45.9 Hz, 1H, H-12), 2.63 (dd, J = 18.3 Hz, 2H, H-1), 1.58 (s, 3H), 1.46 (s, 3H), 1.24 (s, 3H), 1.21 (s, 3H), 1.13 (s, 3H), 1.11 (d, J = 6.5 Hz, 3H), 0.96 (d, J = 5.0 Hz, 3H). ¹³C NMR (100 MHz, CDCl₃): δ = 178.62 (C28), 175.64 (CON), 138.07 (C-imidazole), 130.90 (C-imidazole), 117.80 (C-imidazole and CN), 91.67 (d, J = 14.4 Hz, C13), 89.10 (d, J = 186.6 Hz, C12), 52.78 (d, J = 3.6 Hz), 50.37, 49.75, 45.34, 44.39 (d, J = 3.10 Hz), 44.14 (d, J = 9.7 Hz), 42.92, 42.28, 39.72, 38.72, 33.32, 31.40, 30.82, 29.47 (C1), 27.72, 26.23, 25.84 (d, J = 20.9 Hz), 25.68, 22.44, 21.07, 20.28, 19.47, 18.10, 17.26, 16.57. MS (DI-ESI) (m/z): 552.3 (100%) [M+H]⁺, 456.5 (17.8%). Anal. Calcd for C₃₃H₄₆FN₃O₃: C, 71.84; H, 8.40; N, 7.62. Found: C, 71.98; H, 8.39; N, 7.46.

Chapter 4 | Synthesis and cytotoxic activity of novel UA derivatives

2,3-Seco-2-cyano-3-oxo-(4H-triazol-4-yl)-12 β -fluor-urs-13,28 β -olide (4.17): To a stirred

solution of **4.15** (239 mg, 0.48 mmol) in dry THF (5 ml)

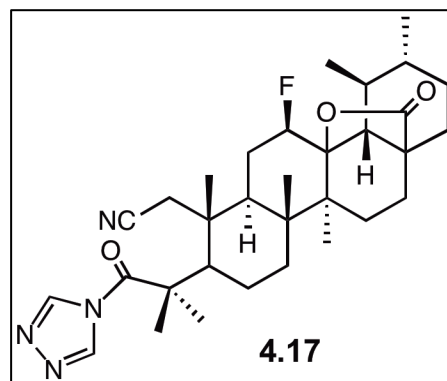
under N₂ at 70 °C, CDT (156.4 mg, 0.95 mmol) was added.

After 4.25 h, the reaction mixture was evaporated under

reduced pressure, and the resultant residue was extracted

with ethyl acetate (3 × 50 ml) from water (20 ml). The

resulting organic phase was washed with water (50 ml),



and 10% NaCl aqueous solution (50 ml), dried over Na₂SO₄, filtered, and concentrated to

dryness. The crude residue was purified by flash column chromatography (petroleum ether:ethyl

acetate 7:1–2:1) to give **4.17** as a white solid (38.2%). Mp 285.4 – 288.3 °C. IR (KBr): ν =

3156.90, 3145.33, 2975.62, 2925.48, 2869.56, 2235.09, 1770.33, 1725.98, 1540.84, 1459.85,

1355.71, 1280.50, 1186.01, 1120.44, 939.16 cm⁻¹. ¹H NMR (400 MHz, CDCl₃): δ = 8.96 (s, 1H,

H-triazole), 8.09 (s, 1H, H-triazole), 4.90 (dq, J = 45.31, 8.1 Hz, 1H, H-12), 2.96 (d, J = 10.2 Hz,

1H), 2.58–2.49 (m, 2H, H-1), 1.55 (s, 3H), 1.52 (s, 3H), 1.24 (s, 6H), 1.11 (d, J = 6.4 Hz, 3H),

1.10 (s, 3H), 0.96 (d, J = 4.9 Hz, 3H). ¹³C NMR (100 MHz, CDCl₃): δ = 178.76 (C28), 176.44

(CON), 153.01 (C-triazole), 145.76 (C-triazole), 116.77 (CN), 91.83 (d, J = 14.6 Hz, C13), 89.13

(d, J = 186.2 Hz, C12), 52.78 (d, J = 3.4 Hz), 49.93, 48.08, 45.39, 44.46 (d, J = 3.0 Hz), 44.08

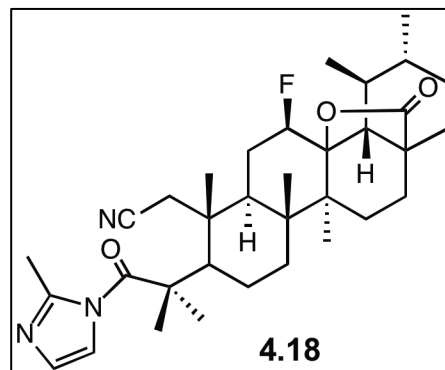
(d, J = 9.5 Hz), 42.56, 42.31, 39.74, 38.76, 33.27, 31.45, 30.87, 28.97, 27.78, 26.63, 25.87 (d, J

= 20.4 Hz), 24.45, 22.51, 20.31 (2C), 19.51, 18.10, 17.35, 16.59. MS (DI-ESI) (m/z): 553.4

(100%) [M+H]⁺, 533.7 (27.8%), 456.7 (33.4%).

2,3-Seco-2-cyano-3-oxo-(2-methyl-1H-imidazol-1-yl)-12 β -fluor-urs-13,28 β -olide (4.18): To a

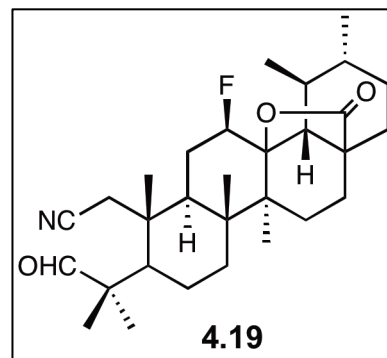
stirred solution of **4.15** (284 mg, 0.57 mmol) in dry THF (5 ml) under N₂ at 70 °C, CBMI (216 mg, 0.95 mmol) was added. After 2.25 h, the reaction mixture was evaporated under reduced pressure, and the resultant residue was extracted with ethyl acetate (3 × 50 ml) from water (20 ml). The resulting organic phase was washed with water (50 ml),



and 10% NaCl aqueous solution (50 ml), dried over Na₂SO₄, filtered, and concentrated to dryness. The crude residue was purified by flash column chromatography (petroleum ether:ethyl acetate 7:1–2:1) to give **4.18** as a white solid (39.3%). Mp 284.0 – 285.3 °C. IR (KBr): ν = 3158.83, 3041.19, 2989.12, 2923.56, 2867.63, 2237.02, 1768.4, 1710.55, 1558.20, 1459.85, 1365.35, 1265.35, 1105.01, 939.16 cm⁻¹. ¹H NMR (400 MHz, CDCl₃): δ = 7.72 (s, 1H, H-imidazole), 6.96 (s, 1H, H-imidazole), 4.91 (dm, *J* = 46.1 Hz, 1H, H-12), 2.67–2.66 (m, 2H, H-1), 2.61 (s, 3H, CH₃-imidazole), 2.30 (d, *J* = 11.5 Hz, 1H), 1.61 (s, 3H), 1.42 (s, 3H), 1.23 (s, 3H), 1.19 (3H), 1.13 (s, 3H), 1.12 (d, *J* = 6.4 Hz, 3H), 0.96 (d, *J* = 4.9 Hz, 3H). ¹³C NMR (100 MHz, CDCl₃): δ = 178.63 (C28), 177.61 (CON), 149.65 (CCH₃-imidazole), 128.24 (C-imidazole), 118.12 (CN), 117.88 (C-imizadole), 91.68 (d, *J* = 14.4 Hz, C13), 89.03 (d, *J* = 186.3 Hz, C12), 52.79 (d, *J* = 3.2 Hz), 51.50, 48.99, 45.35, 44.38 (d, *J* = 3.1 Hz), 44.21 (d, *J* = 9.5 Hz), 42.85, 42.32, 39.72, 38.70, 33.25, 31.41, 30.81, 29.69, 27.71, 26.31, 25.88 (d, *J* = 20.4 Hz), 25.69, 22.45, 21.67, 20.27, 19.48, 18.26, 18.12, 17.21, 16.61. MS (DI-ESI) (*m/z*): 566.3 (100%) [M+H]⁺, 456.4 (19.3%). Anal. Calcd for C₃₄H₄₈FN₃O₃: C, 72.18; H, 8.55; N, 7.43. Found: C, 71.82; H, 8.40; N, 7.09.

Chapter 4 | Synthesis and cytotoxic activity of novel UA derivatives

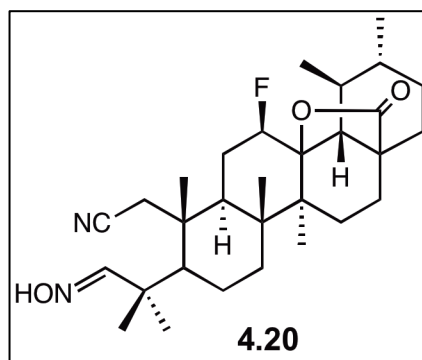
2,3-Seco-2-cyano-3-formyl-12 β -fluor-urs-13,28 β -olide (4.19): To a stirred mixture of **4.4** (200 mg, 0.40 mmol) in dry pyridine (9 ml) at r.t., *p*-TsCl (335 mg, 1.76 mmol) was added. After 2 h, the reaction mixture was evaporated under reduced pressure, and the residue was extracted with ethyl acetate (3 \times 70 ml) from water (30 ml). The resulting organic phase was washed with water (70 ml), and 10% NaCl aqueous solution (70 ml), dried over Na₂SO₄, filtered,



and concentrated to dryness. The crude residue was purified by flash column chromatography (petroleum ether:ethyl acetate 7:1–1:4) to give **4.19** as a white solid (39.1%). Mp 305.6 – 309.0 °C. IR (KBr): ν = 2979.48, 2933.20, 2875.34, 2722.99, 2237.02, 1768.40, 1716.34, 1457.92, 1375.00, 1236.15, 1120.44, 939.16 cm⁻¹. ¹H NMR (400 MHz, CDCl₃): δ = 9.66 (s, 1H, CHO), 4.90 (dm, 1H, H-12), 2.64 (d, *J* = 18.5 Hz, 1H, H-1), 2.39 (d, *J* = 18.5 Hz, 1H, H-1), 1.26 (s, 3H), 1.25 (s, 3H), 1.17 (s, 3H), 1.14 (d, *J* = 6.6 Hz, 3H), 1.12 (s, 3H), 1.00 (s, 3H), 0.97 (d, *J* = 5.2, 4 Hz, 3H). ¹³C NMR (100 MHz, CDCl₃): δ = 205.66 (CHO), 178.66 (C28), 117.84 (CN), 91.88 (d, *J* = 14.2 Hz, C13), 89.24 (d, *J* = 186.3 Hz, C12), 52.84 (d, *J* = 3.3 Hz), 50.83, 48.73, 45.39, 44.48 (d, *J* = 3.0 Hz), 43.34 (d, *J* = 9.6 Hz), 42.36, 42.11, 39.73, 38.78, 33.18, 31.43, 30.87, 30.13, 27.73, 26.23 (d, *J* = 20.0 Hz), 23.47, 22.49, 19.88, 19.71, 19.50, 19.45, 18.13, 17.16, 16.63. MS (DI-ESI) (*m/z*): 485.9 (100%) [M+H]⁺, 466.2 (10.5%), 458.4 (13.0%). Anal. Calcd for C₃₀H₄₄FNO₃·0.1H₂O: C, 73.92; H, 9.14; N, 2.87. Found: C, 73.76; H, 9.01; N, 2.86.

2,3-Seco-2-cyano-3-hydroxyimino-12 β -fluor-urs-13,28 β -olide (4.20): To a stirred mixture of

4.19 (190 mg, 0.39 mmol) in pyridine (3.5 ml), $\text{NH}_2\text{OH}\cdot\text{HCl}$ (147 mg, 2.12 mmol) was added. After stirring for 1.5 h at 50 °C, the reaction mixture was evaporated under reduced pressure, and the resultant residue was extracted with ethyl acetate (3 \times 50 ml) from water (20 ml). The resulting organic phase was washed with 5% HCl aqueous solution (50 ml),



water (50 ml), and 10% NaCl aqueous solution (50 ml), dried over Na_2SO_4 , filtered, and concentrated to dryness. The crude residue was purified by flash column chromatography (petroleum ether:ethyl acetate 7:1–1:2) to give **4.20** as a white solid (39.6%). Mp 286.1 – 289.6 °C. IR (KBr): $\nu = 3392.17, 2977.55, 2927.41, 2875.34, 2237.02, 1768.40, 1635.34, 1459.85, 1392.35, 1236.15, 1186.01, 1112.73, 987.37, 941.09 \text{ cm}^{-1}$. ^1H NMR (400 MHz, CDCl_3): $\delta = 7.53$ (s, 1H, HCNOH), 4.90 (dq, $J = 45.4, 8.2$ Hz, 1H, H-12), 2.65–2.56 (m, 2H, H-1), 1.26 (s, 3H), 1.25 (s, 3H), 1.23 (s, 3H), 1.18 (s, 3H), 1.14 (d, $J = 6.2$ Hz, 3H), 1.01 (s, 3H), 0.97 (d, $J = 4.8$ Hz, 3H). ^{13}C NMR (100 MHz, CDCl_3): $\delta = 178.76$ (C28), 159.83 (CNOH), 118.22 (CN), 91.97 (d, $J = 14.3$ Hz, C13), 89.30 (d, $J = 186.6$ Hz, C12), 52.87 (d, $J = 3.3$ Hz), 51.35, 45.43, 44.46 (d, $J = 2.8$ Hz), 43.43 (d, $J = 9.4$ Hz), 42.44, 42.40, 41.11, 39.74, 38.81, 33.26, 31.44, 30.89, 29.99, 28.76, 27.74, 26.31 (d, $J = 20.1$ Hz), 22.51, 22.10, 19.51, 19.49, 18.76, 18.16, 17.12, 16.65. MS (DI-ESI) (m/z): 501.1 (100%) $[\text{M}+\text{H}]^+$, 481.3 (66.4%), 456.4 (36.3%), 453.4 (15.1%), 436.4 (18.7%), 262.9 (13.4%), 246.8 (13.8%), 244.8 (24.8%). Anal. Calcd for $\text{C}_{30}\text{H}_{45}\text{FN}_2\text{O}_3$: C, 71.97; H, 9.06; N, 5.59. Found: C, 71.88; H, 8.81; N, 5.32.

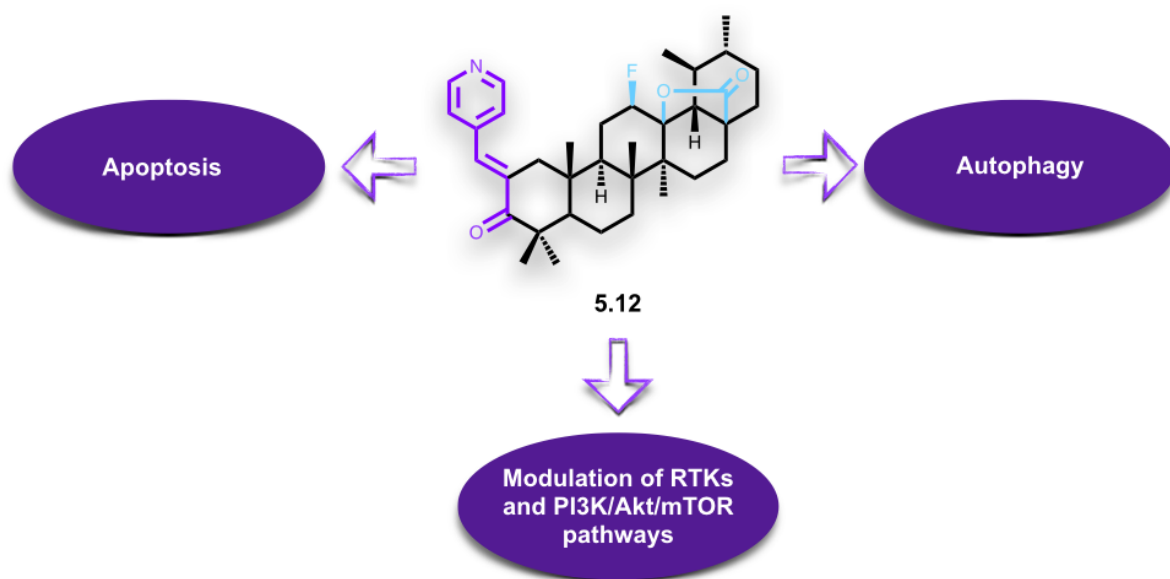
4.4.2. Biology

4.4.2.1. Cell lines and culture, materials and assays

All cell lines, materials and assays were used and performed according to the procedures described in chapter 3.

Chapter 5

Synthesis and cytotoxic activity of new esters and α,β -unsaturated carbonyl derivatives of ursolic acid in NSCLC



Vanessa I. S. Mendes, Geoffrey A. Bartholomeusz, Varsha Gandhi, and Jorge A. R. Salvador, *Synthesis and cytotoxic activity of new esters and α,β -unsaturated carbonyl derivatives of ursolic acid in NSCLC*, in preparation.

5.1. Introduction

Structural modifications of the A-ring of **UA** were further explored in this chapter, by the introduction of esters (saturated or unsaturated), and of an α,β -unsaturated carbonyl system.

The presence of an α,β -unsaturated carbonyl unit in natural products, such as chalcone and curcumin, has been shown to contribute to their cytotoxicity and mechanism of action. Their mechanism of action has been postulated to involve a reaction known as Michael addition, in which there is a nucleophilic attack of a thiol (-SH), or other nucleophiles, to the double bond of the α,β -unsaturated carbonyl system.²²¹⁻²²⁴ The fact that compounds bearing an α,β -unsaturated carbonyl system react preferentially with thiol groups, present for example on cysteine residues, may eliminate the side effects of mutagenicity and carcinogenicity associated with the alkylating agents used in chemotherapy. This type of drugs alkylate cellular nucleophiles by interaction with nucleic acids, which do not contain thiol groups.²²⁴ It has been shown previously that the presence of an α,β -unsaturated carbonyl unit in the A-ring of pentacyclic triterpenoids significantly enhanced their biological activities.^{67,139,218,219,225}

The aldol condensation is one of the most versatile organic reactions, with more than 25,000 entries in SciFinder.²²⁶ The aldol condensation involves the reaction of two carbonyl compounds, one as electrophile and the other as nucleophile, with formation of a new carbon-carbon double bond.²²⁶ Although acid-catalyzed aldol reaction has been described, the base-catalyzed reaction is the most commonly used. The first part of the aldol condensation is an aldol reaction, which involves the formation of the enolate ion through a basic catalysis (Fig. 5.1, step 1), followed by nucleophilic attack of the enolate ion to the aldehyde at the electrophilic carbonyl, resulting in an intermediate alkoxide, with formation of a C-C bond (Fig. 5.1, step 2), which is followed by proton equilibration (Fig. 5.1, step 3). The second part of the reaction

Chapter 5 | Synthesis and cytotoxic activity of novel UA derivatives

consists in the dehydration of the aldol product, with a second enolization by a basic catalysis (Fig. 5.1, step 4), followed by hydroxide elimination and double bond formation (Fig. 5.1, step 5).^{226,227}

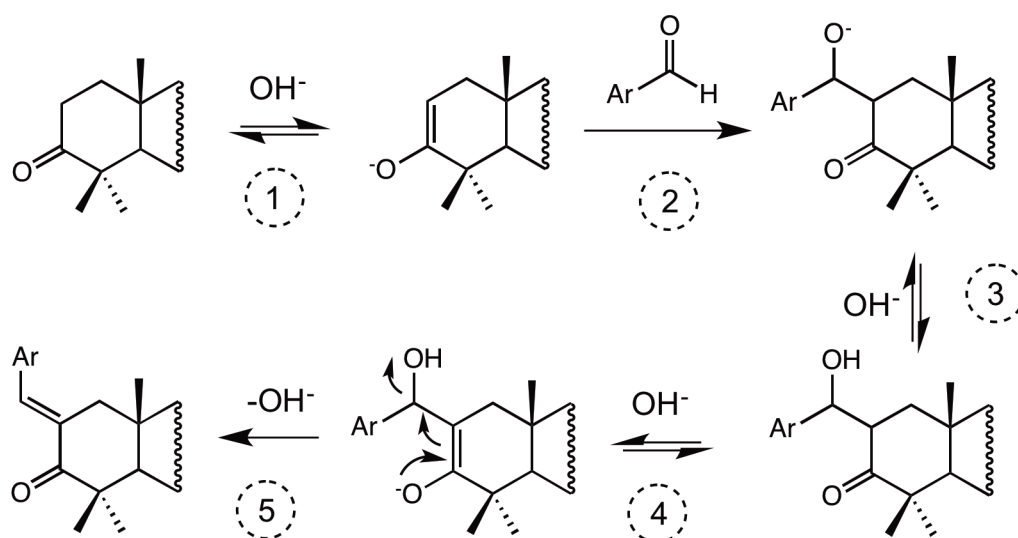


Figure 5.1. Mechanism of the base-catalyzed aldol condensation reaction.

The Claisen-Schmidt condensation – condensation of an aromatic aldehyde with an aliphatic aldehyde or ketone, in the presence of a base or acid to form an α,β -unsaturated aldehyde or ketone²²⁸ – was selected to explore the introduction of an arylidene function conjugated with a carbonyl group at A-ring, in order to investigate the effect of the presence of an α,β -unsaturated carbonyl system with an exocyclic double bond on the anticancer activity. Whereas, the introduction of a diosphenol was used to explore the effect of the presence of an α,β -unsaturated carbonyl system with an endocyclic double bond on the anticancer activity.

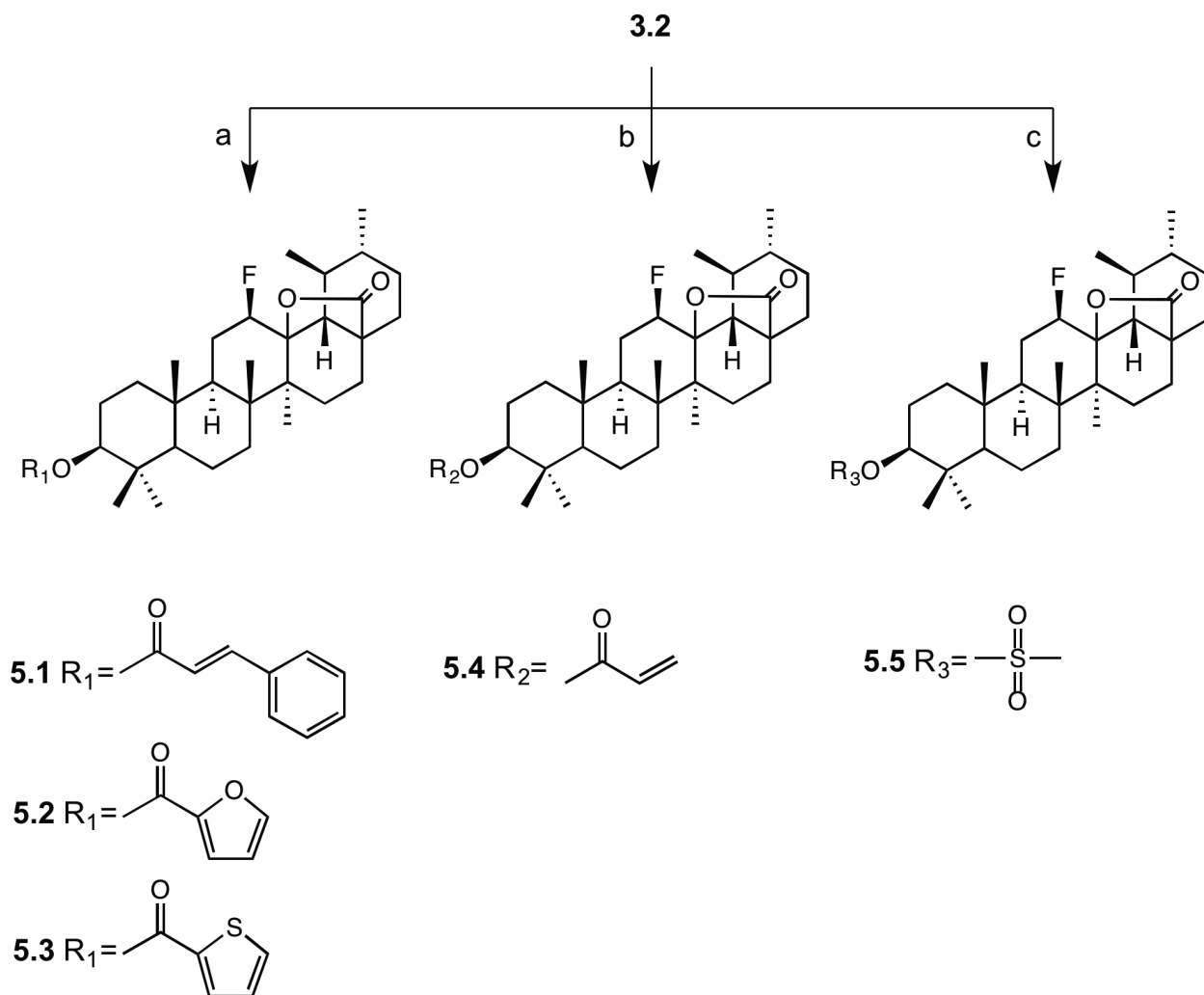
This chapter describes the design and preparation of a series UA derivatives with a modified A-ring at positions C1, C2 and C3. The introduction of esters and α,β -unsaturated carbonyl system was explored. The structures of the newly synthesized compounds were fully elucidated by IR, MS and NMR techniques. The *in vitro* anticancer activity was tested against

NSCLC cell lines, in monolayer and spheroid cultures models, and the preliminary mechanism of action of the most potent derivative was explored.

5.2. Results and discussion

5.2.1. Chemistry

The synthetic route began with the formation of 12 β -fluoro-13,28 β -lactone (**3.2**), as described in chapter 3, which was followed by the synthesis of a series of esters derivatives (Scheme 5.1). Compound **3.2**, in a mixture of dry benzene/THF, Et₃N and 4-(dimethylamino)pyridine (DMAP), under N₂ at 80 °C, was treated with different acyl chlorides to afford compounds **5.1–5.3**. Compounds **5.4** and **5.5** were obtained through reaction of compound **3.2** with acryloyl chloride or methanesulfonyl chloride, respectively, under similar conditions as above, but using dry CH₂Cl₂ as the solvent, and at room temperature. These reaction conditions were optimized in order to obtain a better yield in each reaction.



Scheme 5.1. Synthesis of derivatives **5.1–5.5**.

Reagents and conditions: a) dry benzene/THF or dry benzene, Et₃N, DMAP, R₁Cl, N₂, 80 °C, **5.1**: 4 h; **5.2**: 12.5 h; **5.3**: 11.5 h; b) dry CH₂Cl₂, Et₃N, DMAP, acryloyl chloride, N₂, 25 °C, 2 h; c) dry CH₂Cl₂, Et₃N, DMAP, methanesulfonyl chloride, N₂, r.t., 2 h.

The introduction of the *trans*-cinnamoyloxy group in compound **5.1** was confirmed by the presence in the ¹H NMR spectrum of two doublets at 7.67 and 6.44 ppm with a coupling constant of around 16 Hz, for the vinylic protons of the unsaturated side chain (Fig. 5.2). The coupling constant observed is characteristic of a *trans*-configuration, which was expected taking into account the reaction mechanism, and the configuration of the acyl chloride used. Additionally, the protons of the aromatic ring were observed as two multiplets at 7.54–7.52 and

7.39–7.37 ppm, and the proton at position 3 was observed at 4.63 ppm as a double doublet with a coupling constant of 10.8, 5.5 Hz, in the ^1H NMR spectrum (Fig. 5.2).

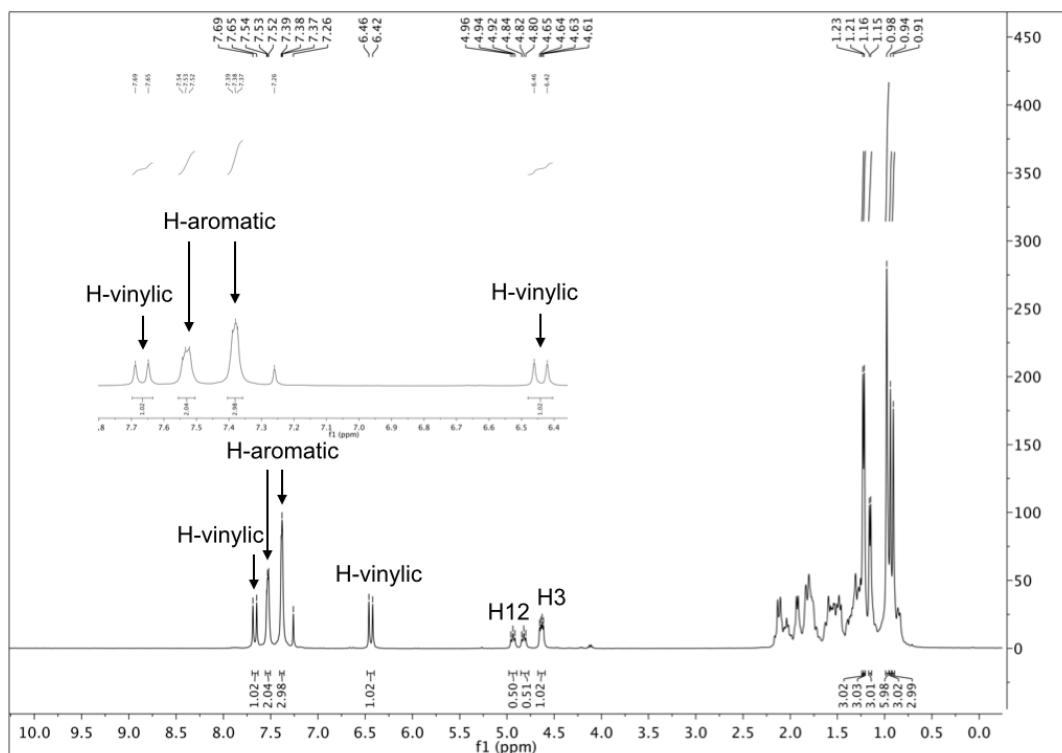


Figure 5.2. ^1H NMR spectrum of compound 5.1 recorded in CDCl_3 .

The presence of a furoyl group in compound 5.2 was confirmed in the ^1H NMR spectrum by three double doublets at 7.58 ($J = 1.7, 0.7$ Hz), 7.14 ($J = 3.4, 0.6$ Hz), and 6.50 ($J = 3.4, 1.7$ Hz) ppm that correspond to the three protons of the heterocyclic ring (Fig. 5.3). In the case of compound 5.3, the introduction of a thiophenecarbonyl group was confirmed in the ^1H NMR spectrum by two doublets at 7.78 ($J = 3.0$ Hz) and 7.54 ($J = 4.6$ Hz) ppm, and one multiplet at 7.11–7.09 ppm that correspond to the three protons of the thiophene group.

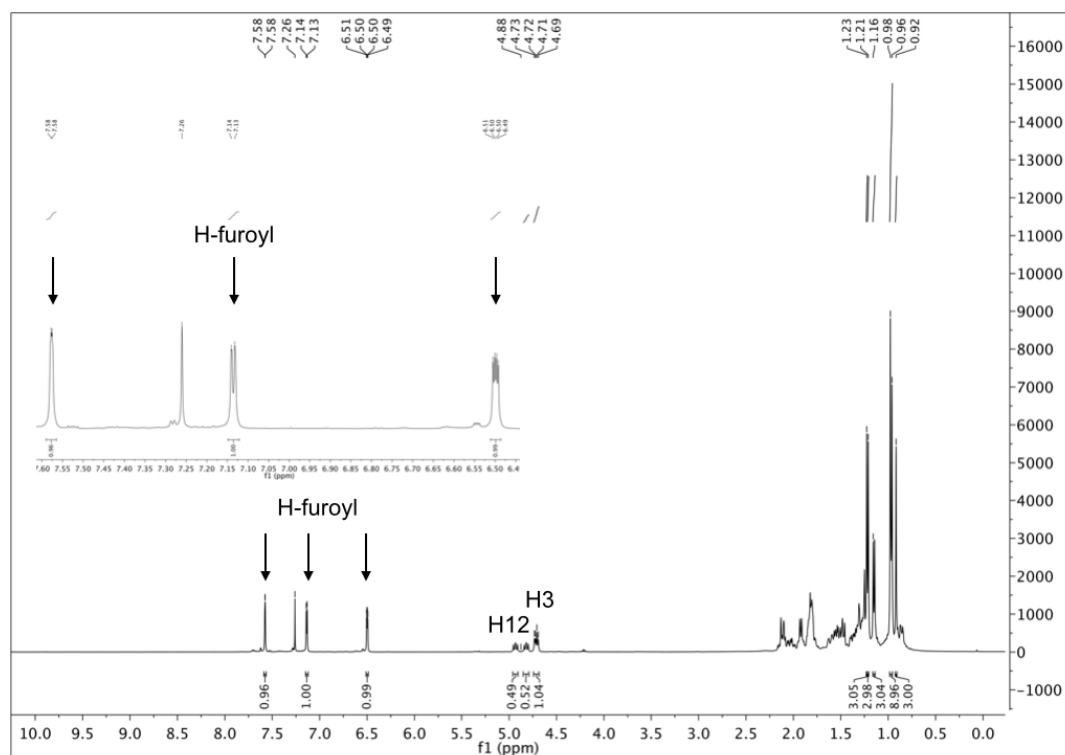


Figure 5.3. ^1H NMR spectrum of compound **5.2** recorded in CDCl_3 .

The introduction of an exocyclic double bond to obtain compound **5.4** was identified by the presence of two doublets at 6.38 ($J = 17.2$ Hz) and 5.81 ($J = 10.6$ Hz) ppm, and by the presence of a double doublet at 6.11 ($J = 17.3, 10.4$ Hz) ppm that correspond to the three protons of the double bond (Fig. 5.4). According to the coupling constants, the protons at 6.11 and 5.81 ppm are geminal to each other, while the protons at 6.38 and 6.11 ppm are vicinal, and have a *trans*-configuration.

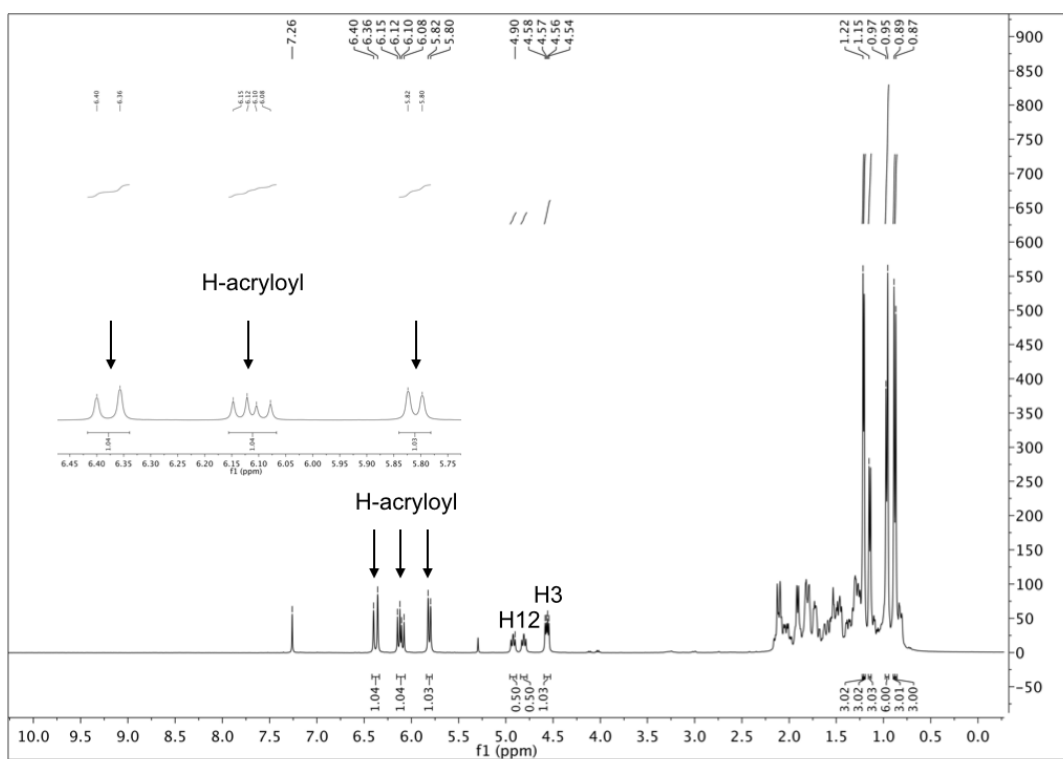


Figure 5.4. ^1H NMR spectrum of compound **5.4** recorded in CDCl_3 .

In the ^1H NMR spectrum of compound **5.5**, the methyl group of the methanesulfonyl function was observed as a singlet at 3.02 ppm, whereas the proton at position 3 was identified as a double doublet at 4.34 ($J = 10.9, 5.7$ Hz) ppm (Fig. 5.5).

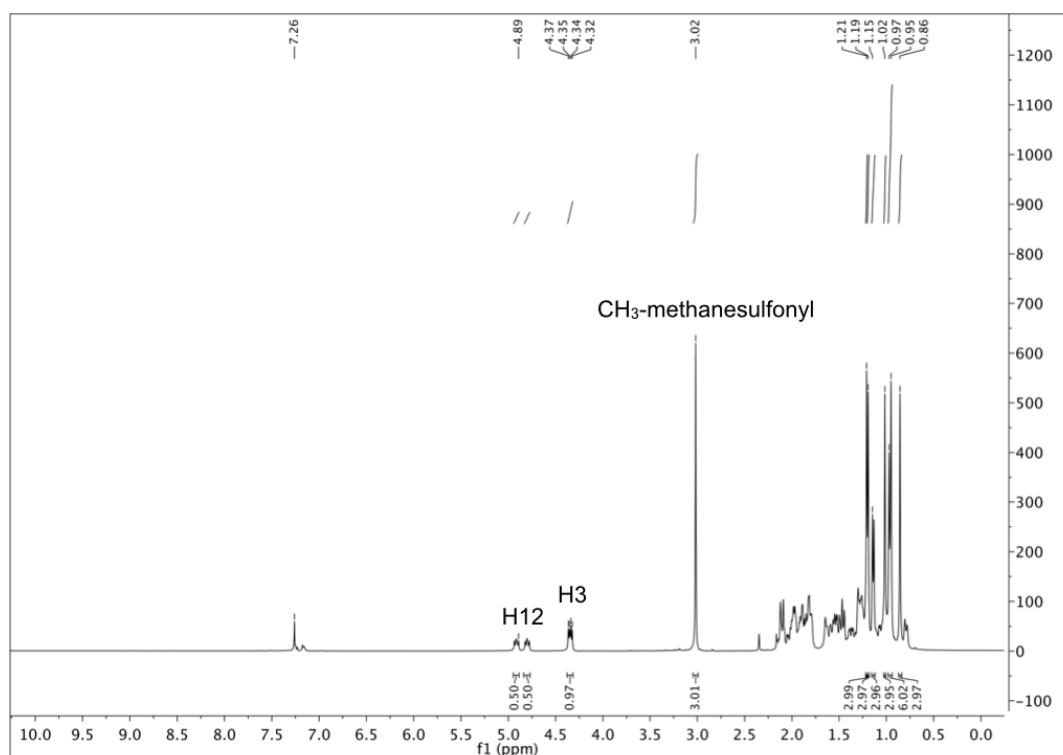


Figure 5.5. ^1H NMR spectrum of compound **5.5** recorded in CDCl_3 .

In the ^{13}C NMR spectra, the carbon of the ester function for compounds **5.1–5.4** was identified around 167–158 ppm, and the carbon at position 3 was identified around 82–80 ppm. For compound **5.1**, four signals at 134.61, 130.36, 129.01 (2C) and 128.18 (2C) ppm were observed for the aromatic carbons, while the carbons of the unsaturated side chain were observed at 144.29 and 118.67 ppm (Fig. 5.6). In the ^{13}C NMR spectra, the carbons of the heterocyclic furoyl (**5.2**) and thiophenecarbonyl (**5.3**) groups were identified by the presence of 4 signals at the region of 146.4–111.7 ppm. As for compound **5.4**, the carbons of the double bond were identified at 130.43 and 129.14 ppm, as a carbon with two protons ($\text{CH}_2=\text{CH}$) and carbon with one proton ($\text{CH}_2=\text{CH}$) by ^{13}C and DEPT-135 NMR spectra (Fig. 5.7 and 5.8).

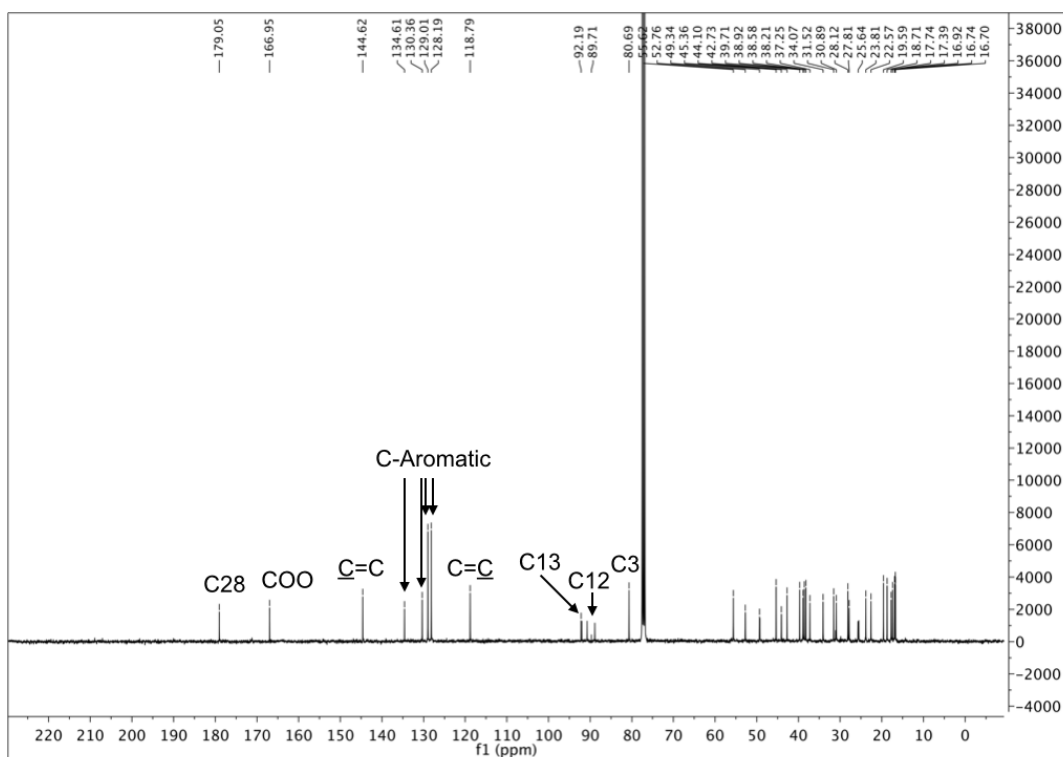


Figure 5.6. ^{13}C NMR spectrum of compound 5.1 recorded in CDCl_3 .

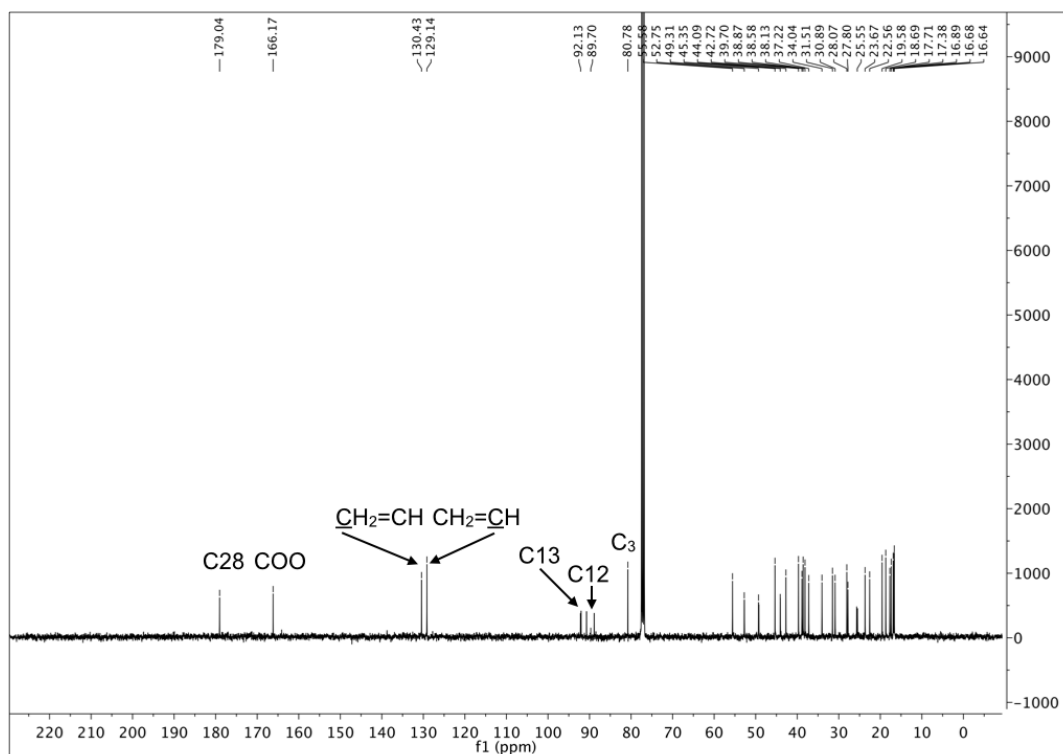


Figure 5.7. ^{13}C NMR spectrum of compound 5.4 recorded in CDCl_3 .

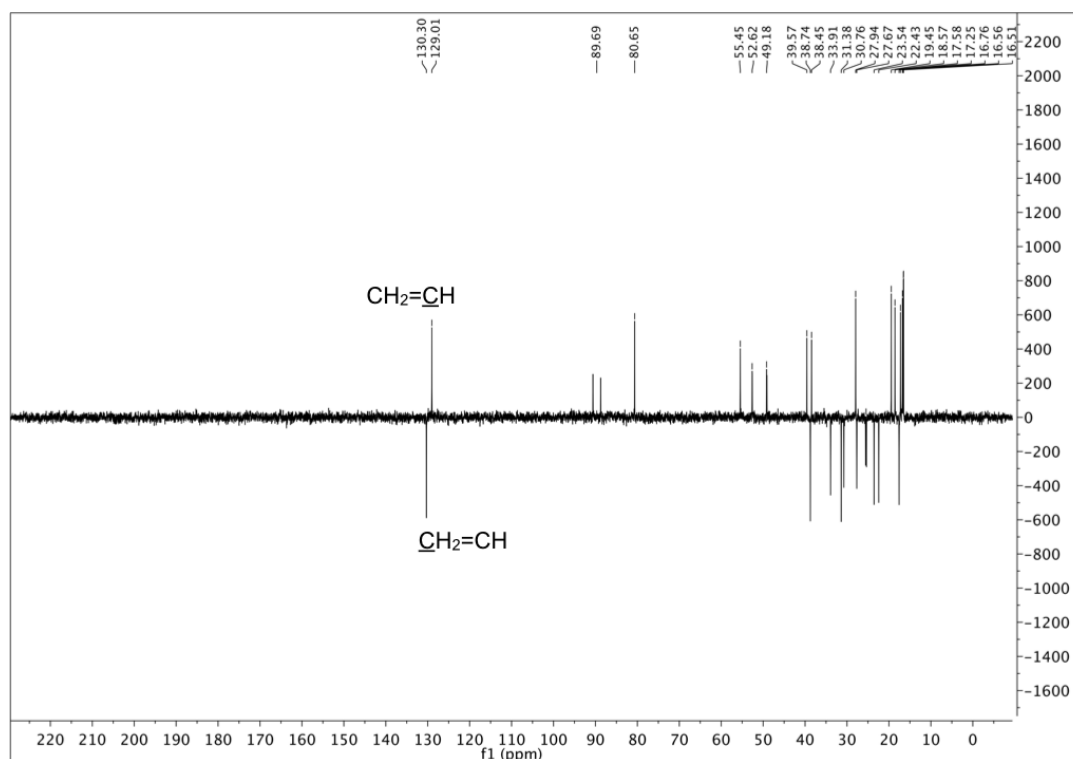
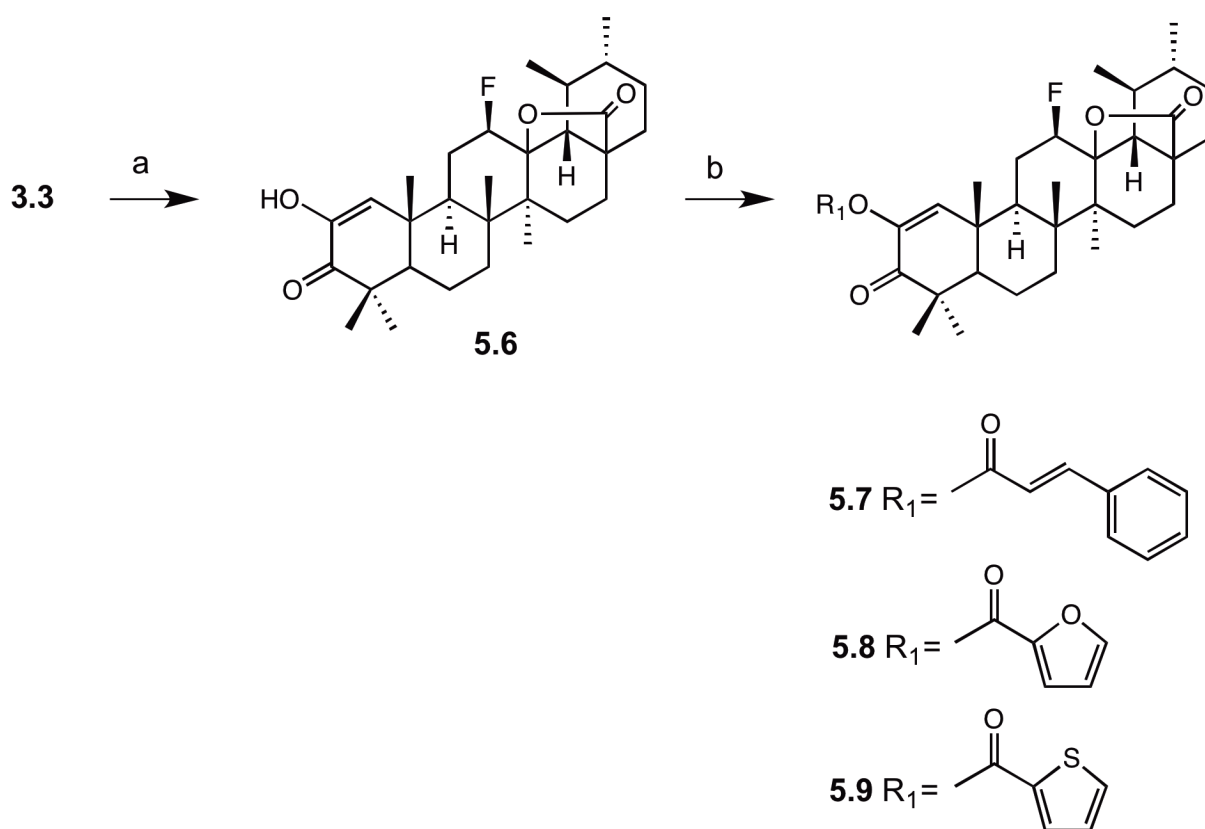


Figure 5.8. DEPT-135 NMR spectrum of compound **5.4** recorded in CDCl_3 .

In order to study the effect of the presence of an α,β -unsaturated carbonyl unit in the anticancer activity, compounds **5.6–5.14** were prepared (Schemes 5.2 and 5.3).

Firstly, the diosphenol derivative (**5.6**) was prepared through oxidation of compound **3.3** (described in chapter 3) with a constant flux of air, in a mixture of *t*-BuOH and *t*-BuOK, at 25–30 °C, as described previously²²⁹ (Scheme 5.2). Esterification of the diosphenol **5.6** was performed using different acyl chlorides in a mixture of dry benzene/THF, Et_3N and DMAP, under N_2 at 80 °C, to afford compounds **5.7–5.9** (Scheme 5.2).



Scheme 5.2. Synthesis of derivatives **5.6–5.9**.

Reagents and conditions: a) *t*-BuOH, *t*-BuOK, constant flux of air, 25–30 °C, 6 h; b) dry benzene/THF or dry benzene, Et₃N, DMAP, R₁Cl, N₂, 80 °C., **5.7**: 2h; **5.8**: 4 h; **5.9**: 2.5 h.

In the ¹H NMR spectrum, the formation of the diosphenol derivative **5.6** was confirmed by the presence of a singlet at 6.43 ppm for proton at position 1, and by a singlet at 5.95 ppm for the proton of the hydroxyl group (Fig. 5.9). In the ¹³C NMR spectrum, the carbons of the double bond at positions 1 and 2 were identified at 127.56 and 144.31 ppm, respectively, and the carbonyl carbon at position 3 was observed at 200.89 ppm (Fig. 5.10).

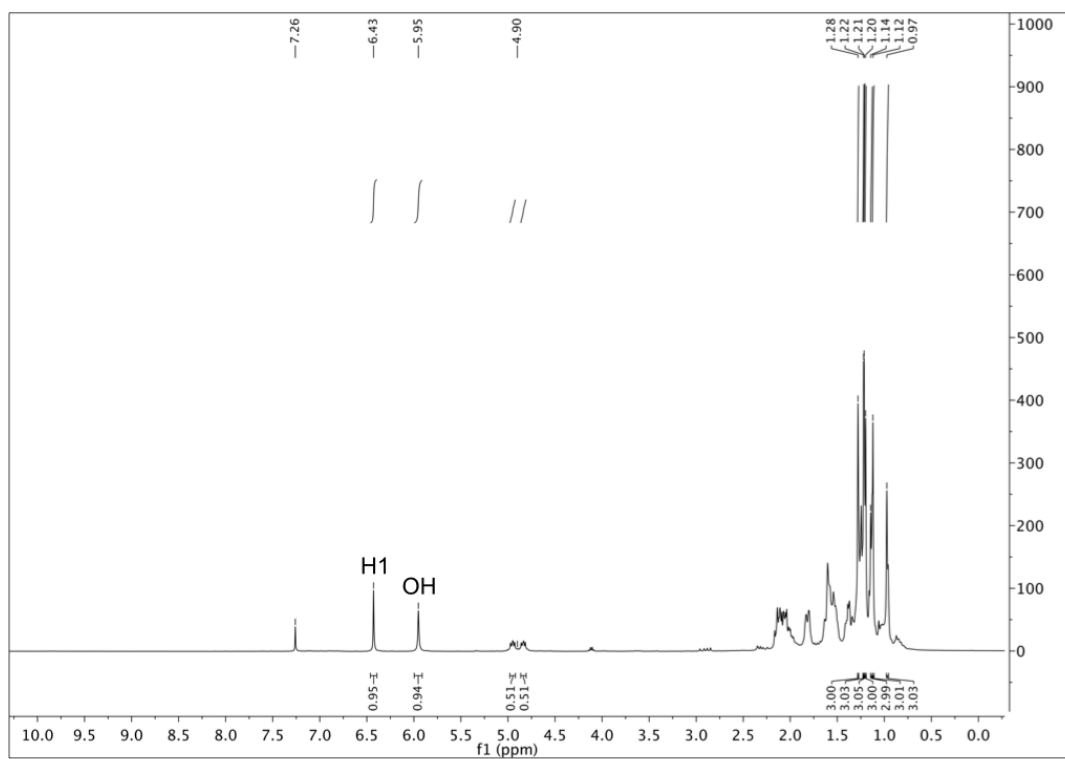


Figure 5.9. ^1H NMR spectrum of compound **5.6** recorded in CDCl_3 .

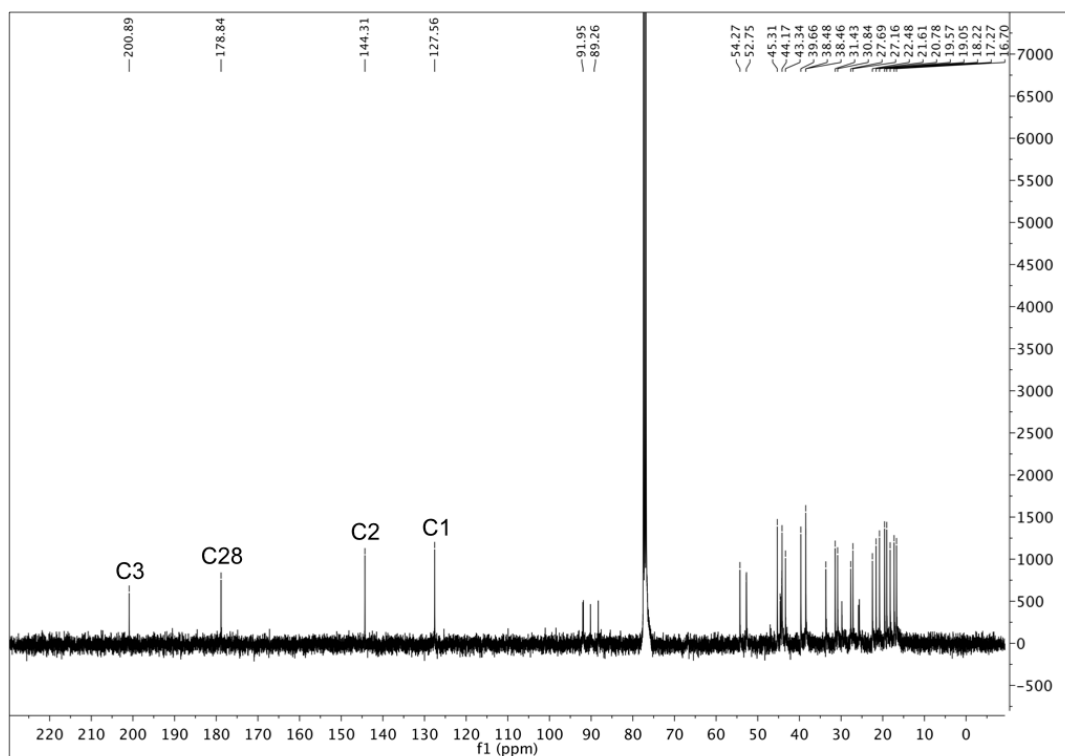


Figure 5.10. ^{13}C NMR spectrum of compound **5.6** recorded in CDCl_3 .

Chapter 5 | Synthesis and cytotoxic activity of novel UA derivatives

In the ^1H NMR spectrum, the introduction of the *trans*-cinnamoyloxy group in compound **5.7** was confirmed by the presence of two doublets at 7.80 and 6.54 ppm with a coupling constant of around 16 Hz, for the vinylic protons of the unsaturated side chain. Additionally, the protons of the aromatic ring were observed as two multiplets at 7.55–7.53 and 7.41–7.40 ppm, and the proton at position 1 was observed as a singlet at 6.84 ppm (Fig. 5.11).

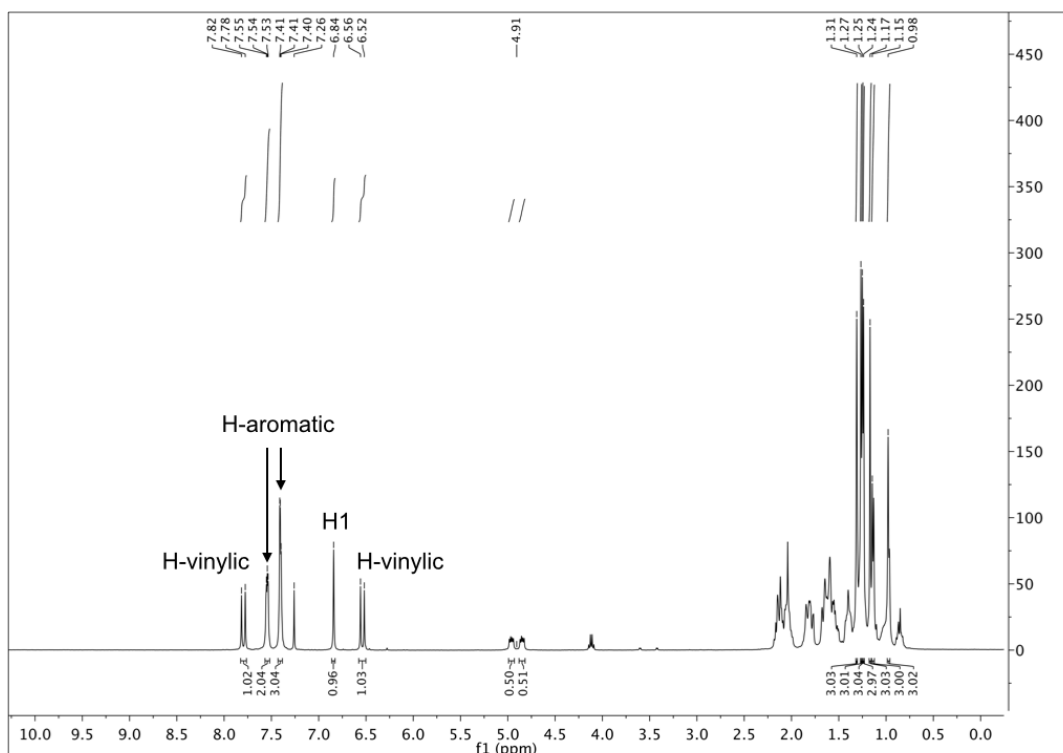


Figure 5.11. ^1H NMR spectrum of compound **5.7** recorded in CDCl_3 .

In the ^{13}C NMR spectrum, the introduction of the *trans*-cinnamoyloxy group in compound **5.7** was confirmed by the presence of four signals at 134.24, 130.88 (2C), 129.10 (2C) and 128.47 ppm for the aromatic carbons, as well as by two signals at 147.18 and 116.50 ppm for the carbons of the unsaturated side chain. Moreover, the carbon at position 2 was identified at 143.46 ppm, while the carbon at position 1 was observed at 143.41 ppm, in the ^{13}C NMR spectrum (Fig. 5.12). These data were correlated and confirmed by DEPT-135 NMR spectrum and by 2D NMR experiments (COSY, NOESY, HMQC and HMBC).

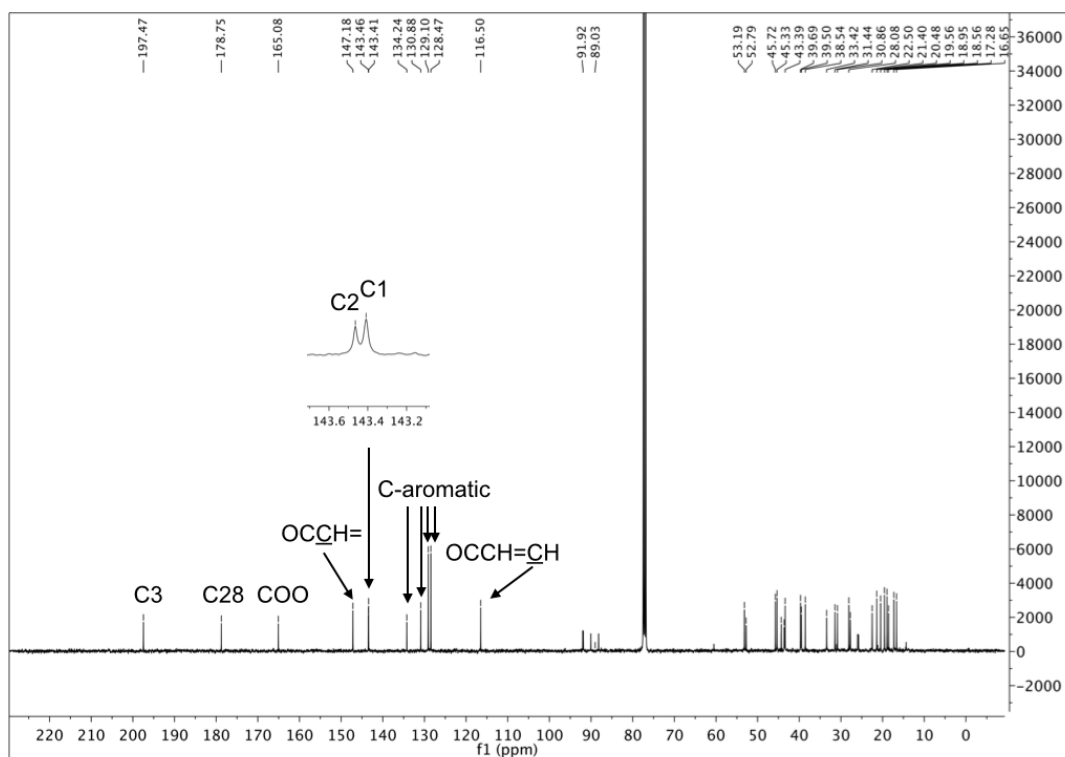
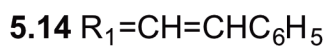
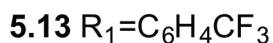
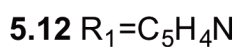
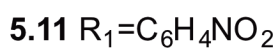
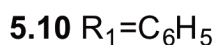
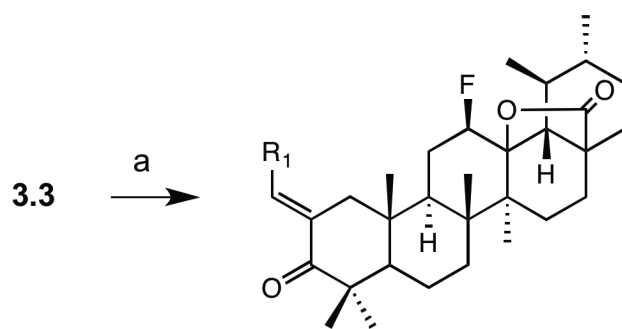


Figure 5.12. ^{13}C NMR spectrum of compound **5.7** recorded in CDCl_3 .

The 2-arylidene derivatives (**5.10–5.14**) were prepared by the Claisen-Schmidt condensation reaction of compound **3.3** with several aromatic aldehydes, in the presence of methanolic potassium hydroxide (5% w/v) (Scheme 5.3).



Scheme 5.3. Synthesis of derivatives **5.10–5.14**.

Reagents and conditions: a) i – KOH/CH₃OH (5% w/v), R₁CHO, 40 °C; ii – r.t., **5.10** and **5.11**: 2.5 h; **5.12**: 4.5 h; **5.13**: 10 h; **5.14**: 17 h.

In the ¹H NMR spectra, the introduction of the 2-arylidene (**5.10–5.14**) function was confirmed by the presence of the olefinic proton around 7.60–6.90 ppm (Fig. 5.13). In the ¹³C NMR spectra, the methine carbon was identified around 139–134 ppm, and the carbon at position 2 at 138–132 ppm (Fig. 5.14).

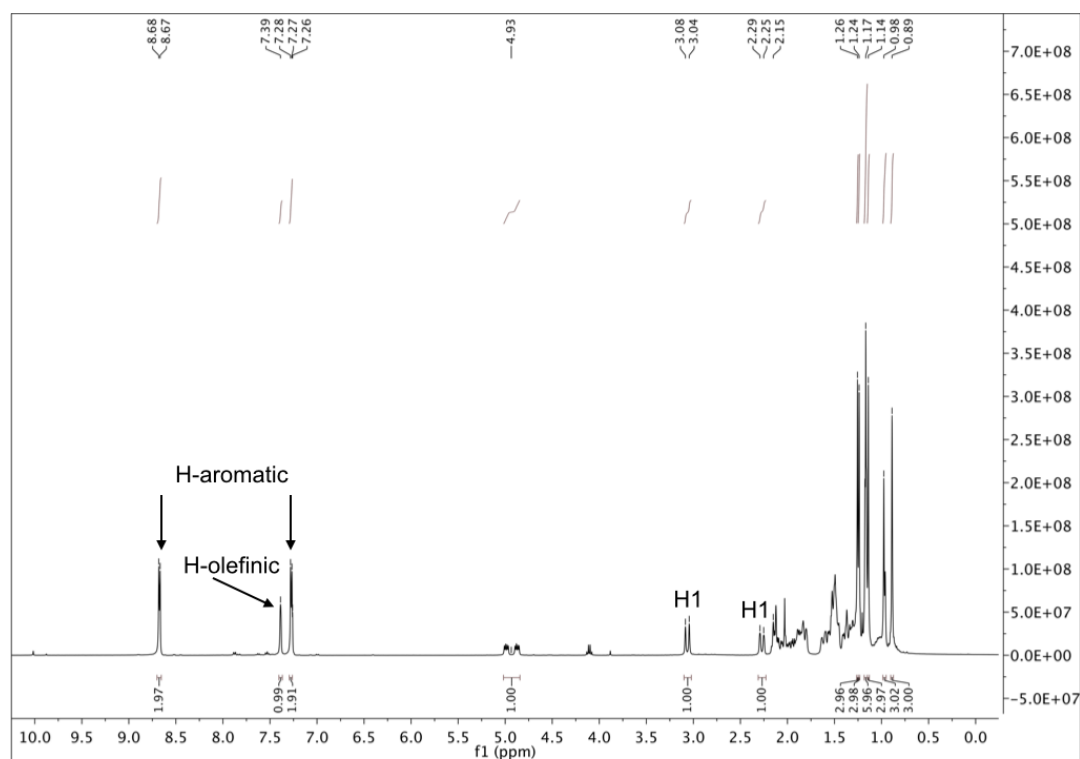


Figure 5.13. ^1H NMR spectrum of compound **5.12** recorded in CDCl_3 .

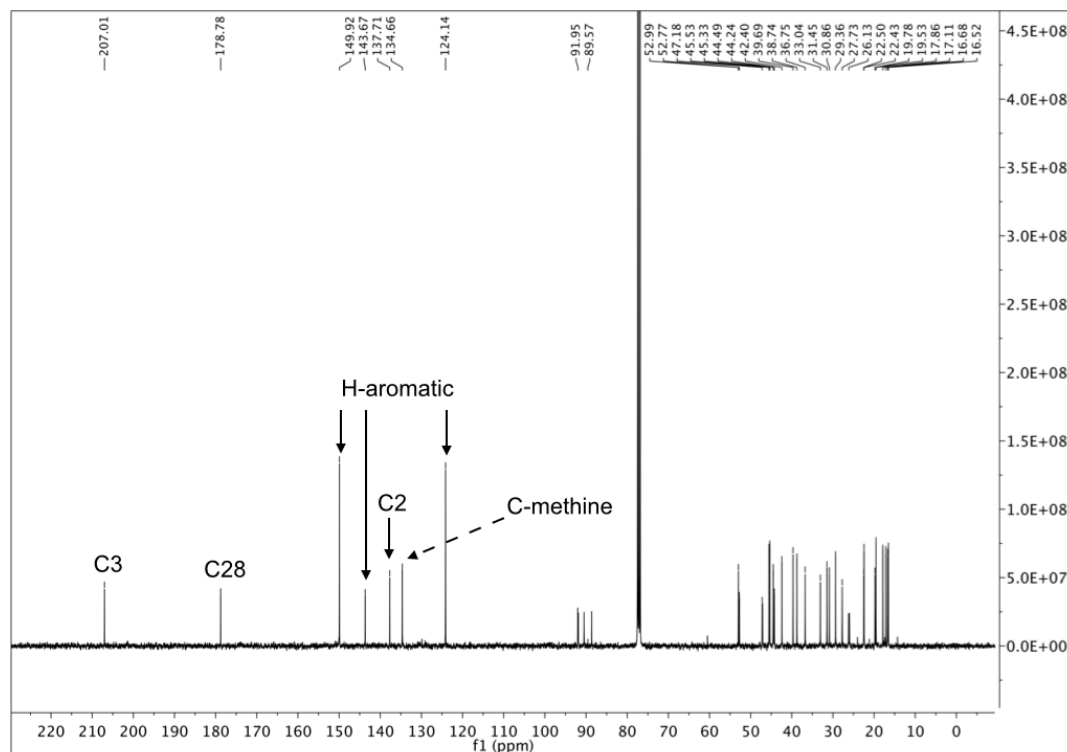


Figure 5.14. ^{13}C NMR spectrum of compound **5.12** recorded in CDCl_3 .

Chapter 5 | Synthesis and cytotoxic activity of novel UA derivatives

According to the NOESY NMR spectra, there is a spatial correlation between the two protons of aromatic ring closest to the olefinic proton (**5.10–5.13**), and the protons at position 1, suggesting that these derivatives, prepared by the Claisen-Schmidt method, have an *E*-configuration (Fig. 5.15 and 5.16). In contrast, if these derivatives had displayed a *Z*-configuration, the protons of the aromatic ring would have not been able to correlate with the protons at position 1 (Fig. 5.15 and 5.16). In the case of compound **5.14**, the spatial correlation is observed between the olefinic proton of the cinnamoyl side chain and the protons at position 1.

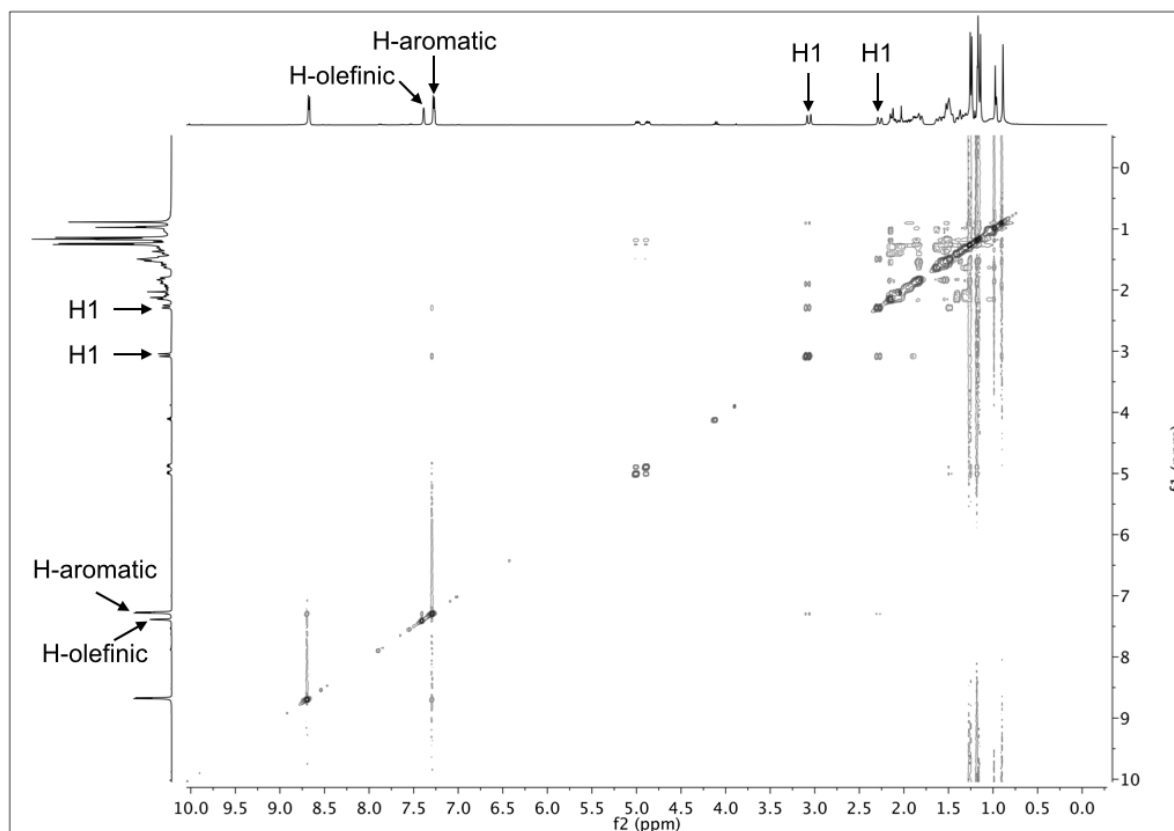


Figure 5.15. NOESY NMR spectrum of compound **5.12** recorded in CDCl_3 .

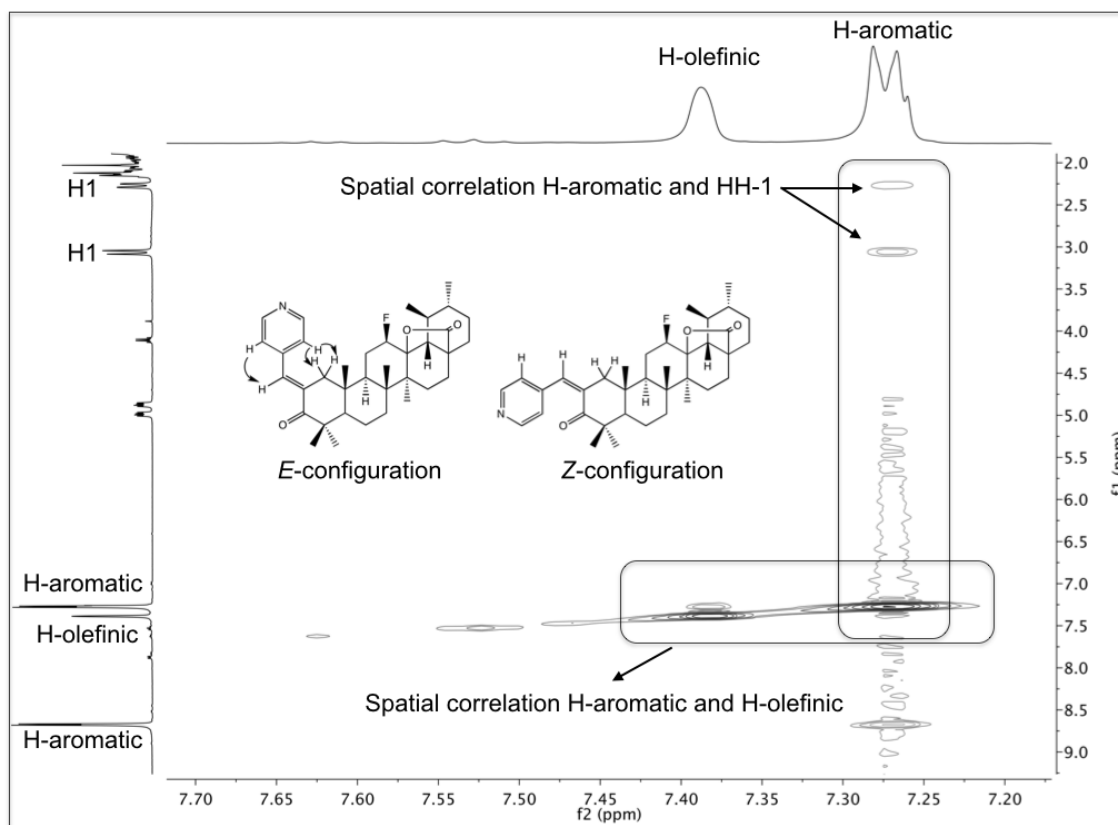


Figure 5.16. Detailed NOESY NMR spectrum of compound **5.12**. The spatial correlation of the aromatic protons with the olefinic proton (horizontal box), and the spatial correlation of the aromatic protons with the protons at position 1 (vertical box) are shown. The chemical structures of an *E*- and *Z*-configurations are also included.

5.2.2. Biological studies

5.2.2.1. Evaluation of *in vitro* anticancer activity

The anticancer activities of **UA** and of the newly synthesized derivatives (**5.1–5.14**) against NSCLC cells (H460, H322, H460 LKB1^{+/+}) were evaluated by using the CellTiter-Blue[®] cell viability assay. Culture medium containing 0.15% DMSO served as negative control. The cell lines were treated with increasing concentrations of each compound, and the IC₅₀ values were determined after 72 h of incubation. The IC₅₀ values are summarized in Table 5.1.

Chapter 5 | Synthesis and cytotoxic activity of novel UA derivatives

Table 5.1. The inhibitory activities (IC₅₀) of **UA** and derivatives **5.1–5.14** in the NSCLC cell lines.

Compound	Cell line ^a /IC ₅₀ , μM		
	H460	H322	H460 LKB1 ^{+/+}
UA	14.8 ± 0.6	15.3 ± 2.8	21.1 ± 1.6
5.1	ND	ND	ND
5.2	24.9±7.6	31.5±2.39	12.3±1.59
5.3	>30	>30	>30
5.4	ND	ND	ND
5.5	ND	ND	ND
5.6	8.3±0.41	11.3±0.95	13.1±1.89
5.7	>50	>50	>50
5.8	>50	>50	>50
5.9	>50	>50	>50
5.10	>50	>50	>50
5.11	>50	>50	>50
5.12	6.4±0.97	9.8±0.61	7.5±0.79
5.13	ND	ND	ND
5.14	>50	>50	>50

^aLung cancer cell lines were treated with various concentrations of test compounds for 72 h. The inhibitory activities were determined using the CellTiter-Blue cell viability assay. IC₅₀ was calculated from the results, and data are presented as means ± SD of three independent experiments. *ND*: not determined.

As shown in Table 5.1, the introduction of esters at position 3 of the ursane scaffold (**5.1–5.5**) did not contribute to the anticancer activity compared with the parent compound. Nevertheless, the furoyl derivative **5.2** displayed the best activity among the esters derivatives, and it seemed to be specifically more active on the H460 LKB1^{+/+} cell line, being 1.7 times more active than the parent compound.

The diosphenol compound (**5.6**), with an α,β-unsaturated system bearing an endocyclic double bond, showed an improved anticancer activity compared with the parent compound **UA**, specially in the H460 cell line, with an 1.8 times lower IC₅₀ value than **UA**.

Analysis of the diosphenol derivatives (**5.7–5.9**) indicated that the esterification of the hydroxyl function at position 2 led to a decreased anticancer activity, with IC₅₀ values greater than 50 μM. These results suggest that the hydroxyl function in the diosphenol moiety is important for the cytotoxic activity, as it may contribute not only to the solubility of the compound, but also participate in interactions with different cancer molecular targets.

Chapter 5 | Synthesis and cytotoxic activity of novel UA derivatives

The introduction of an arylidene moiety at position 2, conjugated with a ketone function at position 3 (**5.10–5.14**), was designed to explore the effect of an α,β -unsaturated system bearing an exocyclic double bond on the anticancer activity. As shown in Table 5.1, most derivatives were less active than the parent compound, with exception of compound **5.12** that was 2.3, 1.6, and 2.8 times more active than the parent compound in the H460, H322 and H460 LKB1^{+/+} cell lines, respectively. It is interesting to note that in this group of aromatic derivatives, the heteroaromatic derivative (**5.12**) was able to potentiate the cytotoxicity, while the aromatic (**5.10**), or substituted aromatic (**5.11**, **5.13** and **5.14**) derivatives showed a decreased anticancer activity.

The most active compound **5.12** was selected and its cytotoxic activity was further explored in a multicellular spheroid 3D culture system. Using the CellTiter-Glo[®] assay, the anticancer activity of **UA**, and the 2-arylidene derivative **5.12** were tested against H460 spheroid culture model. Culture medium containing 0.1% DMSO served as negative control. The cell line was treated with increasing concentrations of each compound, and the IC₅₀ values were determined after 96 h of incubation. The IC₅₀ values are summarized in Table 5.2.

Table 5.2. The inhibitory activities (IC₅₀) of **UA**, and the most potent derivative **5.12** in the spheroid model of the NSCLC cell line H460.

Compound	Cell line ^a /IC ₅₀ , μ M	
	H460	
	Monolayer	Spheroid
UA	14.8 \pm 0.6	30.8 \pm 2.8
5.12	6.4 \pm 0.97	>20

^aLung cancer cell line H460 was treated with various concentrations of test compounds for 72 or 96 h for a 2D (monolayer) or 3D (spheroid) model, respectively. The inhibitory activities were determined using CellTiter-Blue[®] or CellTiter-Glo[®] for the 2D or 3D model, respectively. IC₅₀ was calculated from the results, and data are presented as means \pm SD of three independent experiments.

Chapter 5 | Synthesis and cytotoxic activity of novel UA derivatives

As shown in Table 5.2, albeit being active in the monolayer culture model, compound **5.12** lost potency in the H460 spheroid culture model, with an IC_{50} value greater than 20 μ M. In Figure 5.17 is shown the phenotypic effect of **UA** and compound **5.12** in the spheroid model for the H460 cell line after 96 h of treatment.

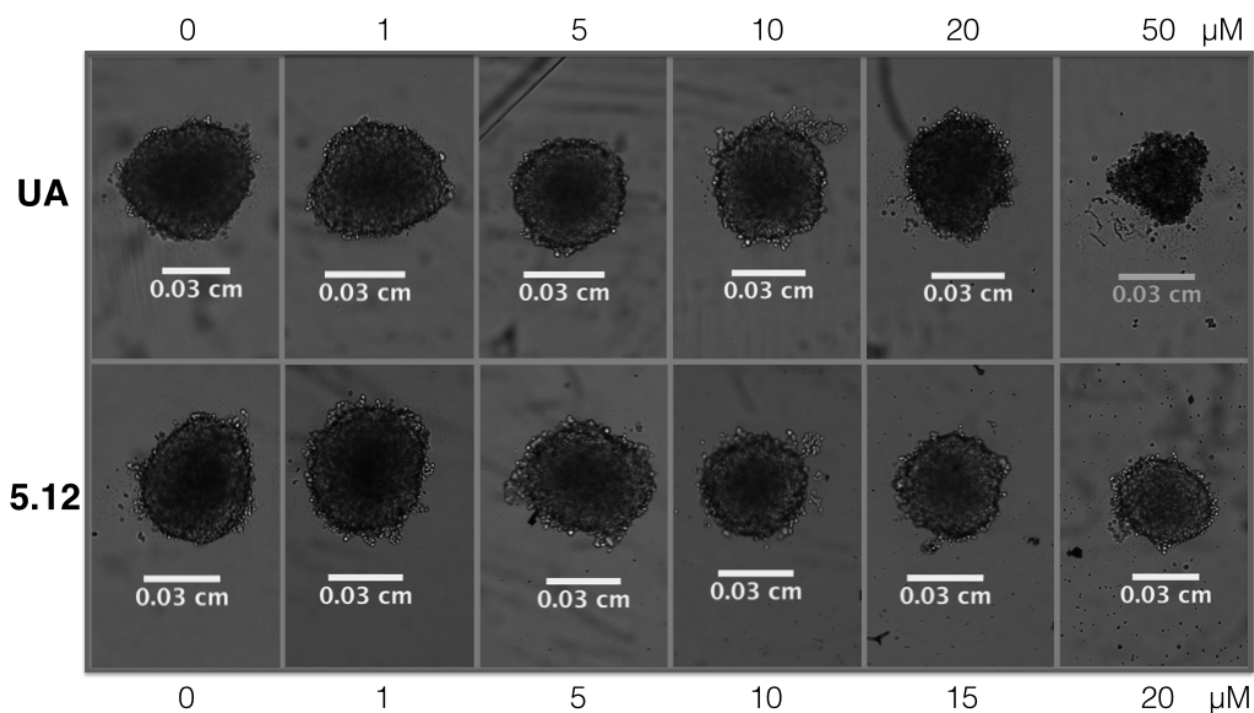


Figure 5.17. Phenotypic changes in the H460 spheroid model treated with **UA** (top panel), and compound **5.12** (bottom panel) for 96 h. Spheroids were treated with the indicated concentrations of the compounds. Images were captured using bright field phase-contrast microscopy.

5.2.2.2. Effect of compound 5.12 on cellular DNA, RNA, and protein synthesis

The [^3H]thymidine, [^3H]uridine, and [^3H]leucine incorporation assays allow the measurement of the effect of a drug in the DNA, RNA, and protein synthesis rates of cells, respectively. Although DNA and protein syntheses were not significantly affected at 24 and 48 h, the RNA synthesis rate was decreased by treatment with compound **5.12** at 24 h (23.4%) and at 48 h (15.1%) (Fig. 5.18).

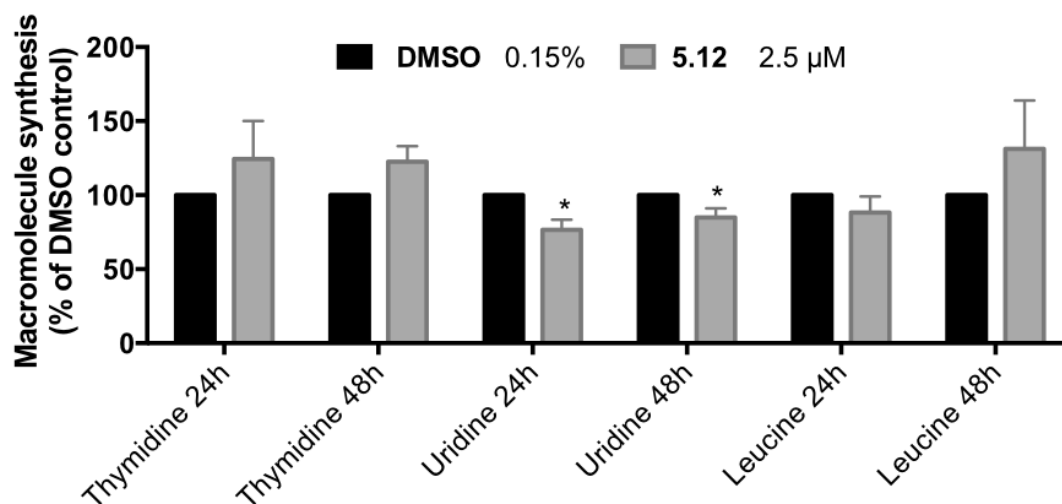


Figure 5.18. The effect of treatment with compound **5.12** on the global DNA, RNA, and protein synthesis in the H460 cell line. Cells treated with vehicle or compound **5.12** at the indicated concentrations for 24 and 48 h were assessed for macromolecular synthesis. Values represent the means \pm SD of three independent experiments. p-Values obtained by comparing vehicle and treatment are presented as $* < 0.05$.

5.2.2.3. Effect of compound 5.12 on the cell cycle distribution

The effect of compound **5.12** on the cell cycle distribution was explored. Cells were treated with DMSO (0.15%), or compound **5.12** (4 μ M) for 24 and 72 h, and the cell cycle profile was evaluated by FACS analysis after staining cells with PI (Fig. 5.19).

Treatment of H460 cells with compound **5.12** induced a slight increase in the G1-phase population of cells (6.1%), which was accompanied by a slight decrease in the G2/M-phase population of cells (6.4%) at 72 h (Fig. 5.19). These results suggest that compound **5.12** is able to induce a G1-phase arrest at 72 h in H460 cells.

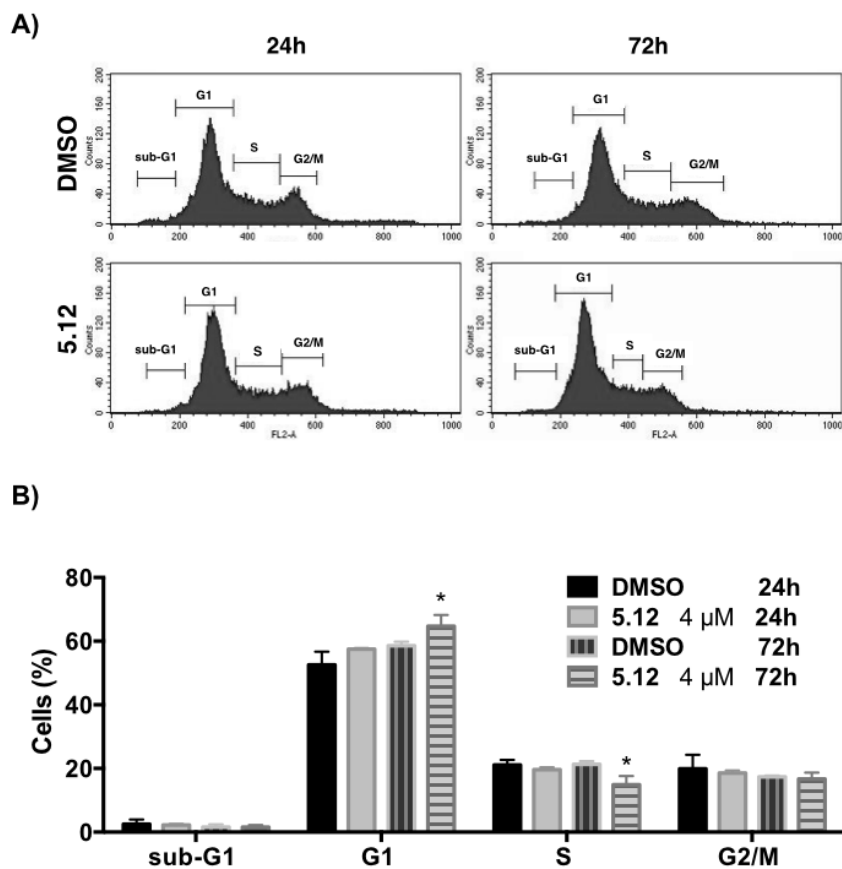


Figure 5.19. Effect of compound **5.12** on the cell cycle distribution. H460 cells treated with vehicle or compound **5.12** at the indicated concentrations for 24 and 72 h were assessed for cell cycle, using PI staining and flow cytometric analysis. A) Representative histograms of cell cycle analysis are shown. B) The bar graphic depicts the cell population (%) per cell cycle phase. Values represent the means \pm SD of three independent experiments. p-Values obtained by comparing vehicle and treatment are presented as * < 0.05 .

5.2.2.4. Apoptosis-inducing effect of compound **5.12** evaluated by annexin V-Cy5/PI assay

To evaluate whether the loss of cell viability induced by compound **5.12** was associated with apoptosis, the annexin V-Cy5/PI binding assay was performed. FACS analysis of annexin V-Cy5/PI double staining was used to differentiate live, early apoptotic, late apoptotic, and necrotic cells, as described previously.

As shown in Figure 5.20, in comparison with control (0.15% DMSO-treated cells), treatment with derivative **5.12** at 4.5 μ M for 72 h decreased the percentage of live cells from 94.2% in the control to 80.6% in treated cells. Simultaneously, the percentage of apoptotic cells increased from 3.9% to 14.7% in treated cells (i.e., 5.8% early apoptotic cells and 8.9% late apoptotic cells). These results suggest that compound **5.12** at 4.5 μ M induces apoptosis in H460 cells at 72 h.

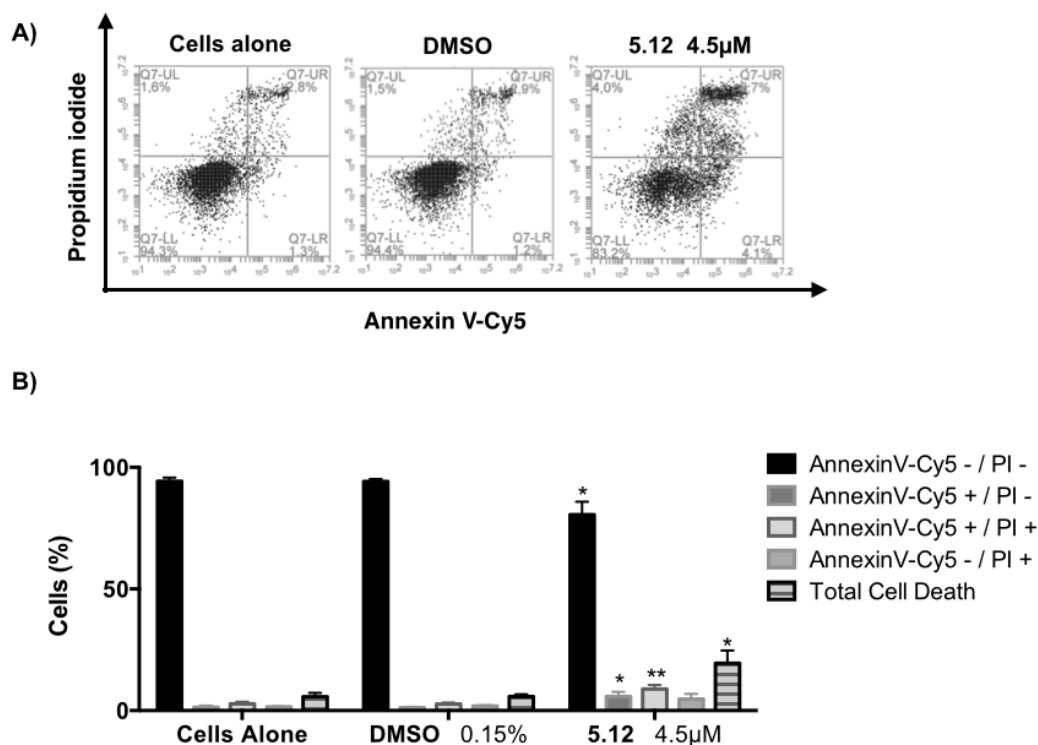


Figure 5.20. Induction of H460 cell death by compound **5.12**. Annexin V-Cy5/PI assay of H460 cells that were untreated, treated with vehicle, or treated with compound **5.12** at the indicated concentrations for 72 h. A) Representative flow cytometric plots for the quantification of apoptosis are shown: the lower left quadrant (annexin V- and PI-) represents non-apoptotic cells, the lower right quadrant (annexin V+ and PI-) represents early apoptotic cells, the upper right quadrant (annexin V+ and PI+) represents the late apoptotic/necrotic cells, and the upper left quadrant (annexin V- and PI+) represents necrotic cells. B) The bar graph depicts the variation of the percentage of live, early apoptotic, late apoptotic cells, necrotic cells, and total cell death. Values represent the means \pm SD of three independent experiments. p-Values obtained by comparing vehicle and treatment are presented as * < 0.05, **<0.01.

5.2.2.5. Effect of compound **5.12** treatment on autophagy

Autophagy is characterized by the formation of acidic vesicular organelles (AVO), which can be detected by staining with acridine orange.¹⁹³ This dye that accumulates in acidic organelles, was measured by flow cytometer to detect AVO formation in H460 cells treated with vehicle (0.15% DMSO) or compound **5.12** (5 μ M) for 72 h. Bafilomycin A1 was used as a negative control to block acidic vesicular formation.

Chapter 5 | Synthesis and cytotoxic activity of novel UA derivatives

As shown in Figure 5.21A, bafilomycin A1 inhibited the fusion of autophagosomes with lysosomes. Endogenous autophagy level (DMSO treatment) was less than 10% at 72 h (Fig. 5.21). Treatment of H460 cells with compound **5.12** significantly increased the formation of AVO (5.2%) at 5 μ M (Fig. 5.21). These data suggest that compound **5.12** is able to induce autophagy in H460 cells at 72 h.

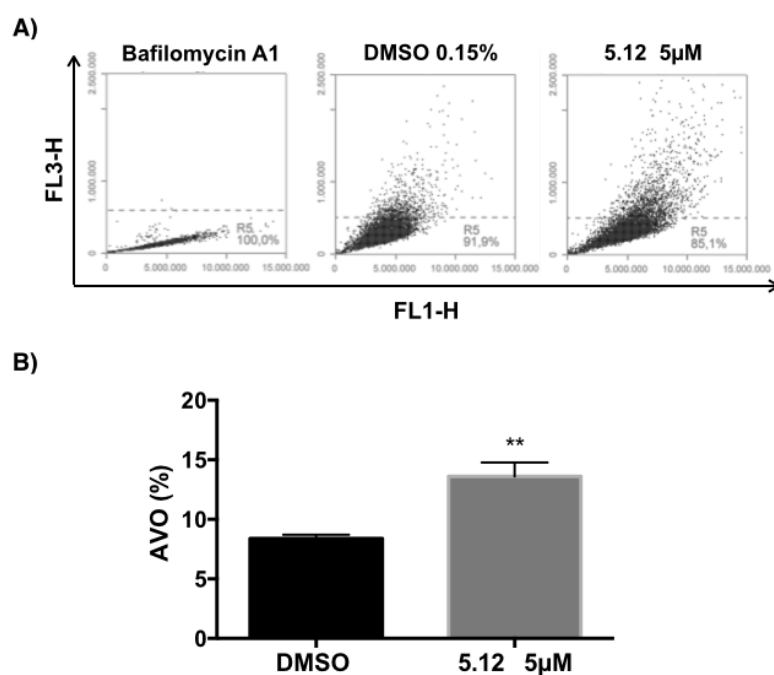


Figure 5.21. Effect of compound **5.12** treatment on induction of autophagy in the H460 cell line. A) The formation of acidic vascular organelles (AVO) was measured by acridine orange staining and flow cytometry. Representative flow cytometric plots of the percentage of AVO formation of three independent experiments are shown. B) The graph bar depicts the variation of the percentage of AVO formation and is plotted as means \pm SD of three independent experiments. p-Values obtained by comparing vehicle and treatment are presented as **<0.01.

5.2.2.6. Effect of compound 5.12 on protein expression profile

To investigate the effect of compound **5.12** on the cellular protein levels across a broad set of pathways, RPPA analysis was used to evaluate changes in the level of 298 proteins. RPPA is a high-throughput antibody-based technique with a similar procedure to Western blots, in which proteins are extracted from the cultured cells, denatured, printed on nitrocellulose-coated slides, and probed with different antibodies. Accordingly, H460 cells were treated with DMSO (0.15%), or compound **5.12** (5.5 μ M) for 24 h. The protein level changes were compared to the control, and statistically analyzed in order to identify the main pathways affected by compound **5.12**.

Components of the PI3K/Akt/mTOR pathway emerged as key molecules affected by compound **5.12** in the H460 cell line at 24 h. The PI3K/Akt/mTOR pathway is a prototypic survival pathway that is constitutively activated in many types of cancer, including lung cancer. Once activated, the signaling cascade can be propagated through Akt to several substrates, including mTOR, a key regulator of protein translation and autophagy.^{230,231}

The levels of total Akt, total mTOR, and phosphorylated level of mTOR at S2448 were decreased by 3.5, 10.7 and 9.7%, respectively, upon treatment of H460 cell line with 5.5 μ M of compound **5.12** for 24 h (Fig. 5.22). Likewise, Rictor, a subunit of the mTOR complex,²³² was decreased by 7.5%. mTOR regulates the level of the S6 kinase, an enzyme partially responsible for S6 phosphorylation and activation.^{198,199} Accordingly, p70S6K, and the phosphorylated level of S6 at S235/236 and S240/244, were decreased by 7.1, 41.5 and 24.9%, respectively (Fig. 5.22). Moreover, the total level of eIF4E, a protein that is negatively regulated by mTOR^{198,199}, was decreased by 7.6%, while its phosphorylated level at S209 was increased by 17.1% upon treatment with compound **5.12**. The X-linked inhibitor of apoptosis protein (XIAP), a substrate of Akt,²³³ was also decreased by 12.2%. Akt has also been shown to inhibit MYT1 and WEE1 proteins,²³⁴ which are key G2/M checkpoint regulators that negatively regulate the entry into

Chapter 5 | Synthesis and cytotoxic activity of novel UA derivatives

mitosis by inhibition of CDK1, with inactivation of the cyclin B/CDK1 complex, and arrest at the G2/M phase.²³⁵⁻²³⁷ MYT1 and WEE1 were found upregulated by 6.2 and 21.7%, respectively, by treatment with compound **5.12**. In contrast to the overall results, the level of PI3K-p110, a catalytic subunit of PI3K²³⁸, was found increased by 17.2% (Fig. 5.22).

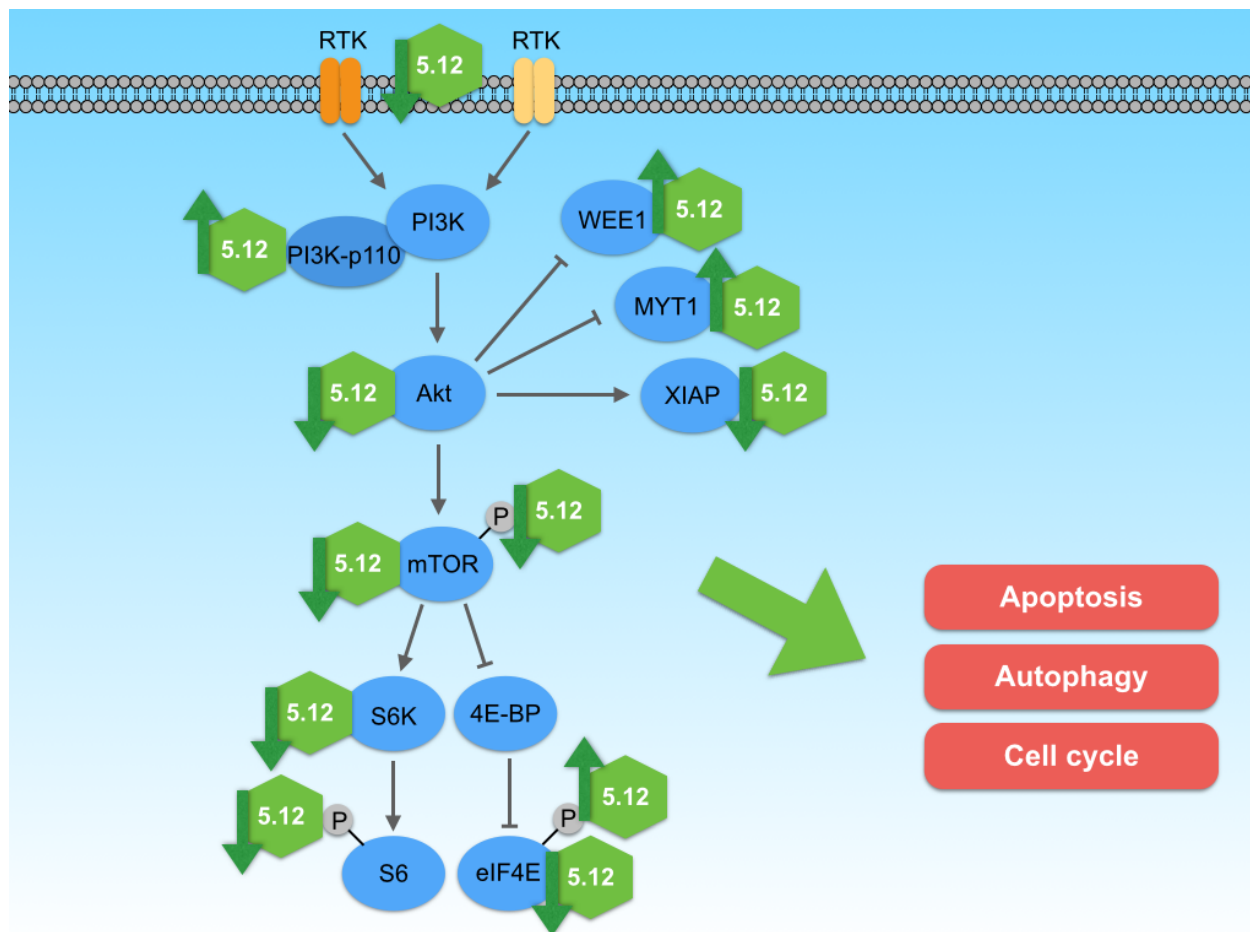


Figure 5.22. Effect of compound **5.12** on the RTKs and PI3K/Akt/mTOR pathway. According to the RPPA data, treatment of the H460 cell line with compound **5.12** was able to modulate different RTKs and the PI3K/Akt/mTOR pathway.

Receptor tyrosine kinases (RTKs) are the main mediators of the signaling network that transmit extracellular signals into the cell, and control fundamental cellular processes, such as cell cycle, proliferation, differentiation, motility, and cell death or survival. In normal cells, the

Chapter 5 | Synthesis and cytotoxic activity of novel UA derivatives

RTK activity is strictly regulated; however deregulation or constitutive activation of RTKs has been found in a wide range of cancers. The RTKs control several signaling pathways including the PI3K/Akt/mTOR and the Ras/MAPK pathways.²³⁹⁻²⁴¹ The insulin-like growth factor receptor (IGFR), tyrosine-protein kinase receptor UFO (AXL), vascular endothelial growth factor receptor-2 (VEGFR-2), human epidermal growth factor receptor 3 (HER3) (phosphorylated level at T1289), epidermal growth factor receptor (EGFR), and KIT proto-oncogene receptor tyrosine kinase (c-Kit) RTKs were found decreased by 12.6, 10.6, 8.4, 7.2, 6.3, and 5.8%, respectively, upon treatment with compound **5.12**, which could explain the effects observed on the PI3K/Akt/mTOR pathway (Fig. 5.22). In addition, while the phosphorylated level of c-MET RTK at T1234/1235 was decreased by 11.9%, the total level of this RTK was increased by 10.9%

The RTKs and PI3K/Akt/mTOR pathway are an attractive therapeutic target in cancer, as it is a convergence point for different growth stimuli, and its downstream substrates are involved in cellular processes that contribute to the initiation and maintenance of cancer. Additionally, the activation of this pathway has been shown to confer resistance to several anticancer drugs, and it is considered a poor prognostic factor in different types of cancers.

The RPPA data also show different apoptosis- and autophagy-related proteins affected by treatment with compound **5.12**. For example, the levels of the active forms of caspase-8 and caspase-7 were increased by 8.6 and 23.0%, respectively, which suggest that compound **5.12** is able to induce the extrinsic pathway of apoptosis. Moreover, Beclin-1, LC3A/B-II, and Atg3 — proteins involved in the autophagy pathway — were found increased by 13.4, 3.2, and 7.8%, respectively, upon treatment of the H460 cell line with 5.5 μ M compound **5.12** for 24 h.

The cell cycle regulation was also found altered by treatment with compound **5.12**. The cell cycle comprises four main successive phases: G1 phase (first gap), S phase (DNA synthesis), G2 phase (second gap), and M phase (mitosis). The progression of the cell cycle is regulated by cyclins and cyclin-dependent kinases (CDKs). Certain signals stimulate the activation of D-type cyclins and their connection with CDK4 or CDK6. These complexes then

Chapter 5 | Synthesis and cytotoxic activity of novel UA derivatives

phosphorylate the retinoblastoma protein (Rb), and inhibit its affinity to bind the transcription factor E2F, which is critical for the expression of specific genes involved in the DNA replication. Additionally, the cyclin E/CDK2 complex fully inactivates Rb by hyperphosphorylation, ensuring the progression from G1 to S phase. Cyclin A then binds to CDK2, forming a complex that phosphorylates several substrates important for DNA replication. After completion of the S phase, the cyclin A/CDK1 complex plays a critical role in the transition from the S to the G2/M phase of the cell cycle. The cyclin B/CDK1, which appears in the late G2 phase, regulates the mitosis phase and triggers the G2/M transition. After a complete cell cycle, cells can undergo a new cell cycle or enter the G0 phase, which is a quiescent state (Fig. 5.23).^{242,243} According to the RPPA data, cyclin D3 (6.5%), total Rb (12.5%), and cyclin E1 (15.0%) were upregulated, whereas cyclin B1 was decreased by 20.5% (Fig. 5.23). These results suggest that compound **5.12** at 5.5 μ M is able to induce a G2/M-phase arrest at 24 h, which may indicate a concentration- and time-dependent effect, as at 4 μ M no change in any cell cycle phase was detected by FACS analysis after staining cells with PI at 24 h, and at 72 h it was detected a G1-phase arrest (Fig. 5.19).

During cell cycle, two important checkpoints (G1/S and G2/M) coordinate the CDK activity and ensure that each stage of the cell cycle is correctly completed before allowing its further progress. As mention previously, MYT1 and WEE1 were found upregulated by 6.2 and 21.7%, respectively, by treatment with compound **5.12**. Moreover, the polo-like kinase 1 (PLK1) was found decreased by 20.7%. This kinase activates the cyclin B/CDK1 complex by activating CDC25, and by inhibiting both MYT1 and WEE1 proteins (Fig. 5.23). PLK1 has shown to be overexpressed in several human cancers.²⁴⁴ The mammalian transcription factor forkhead box protein M1 (FOXM1) has an important role in the regulation of the mitotic entry, and subsequent execution of the mitotic program by controlling the expression of a cluster of G2/M target genes. PLK1 regulates FOXM1 transcriptional activity by direct phosphorylation.^{244,245} The expression of FOXM1 was found decreased by 10.3% upon treatment with compound **5.12**.

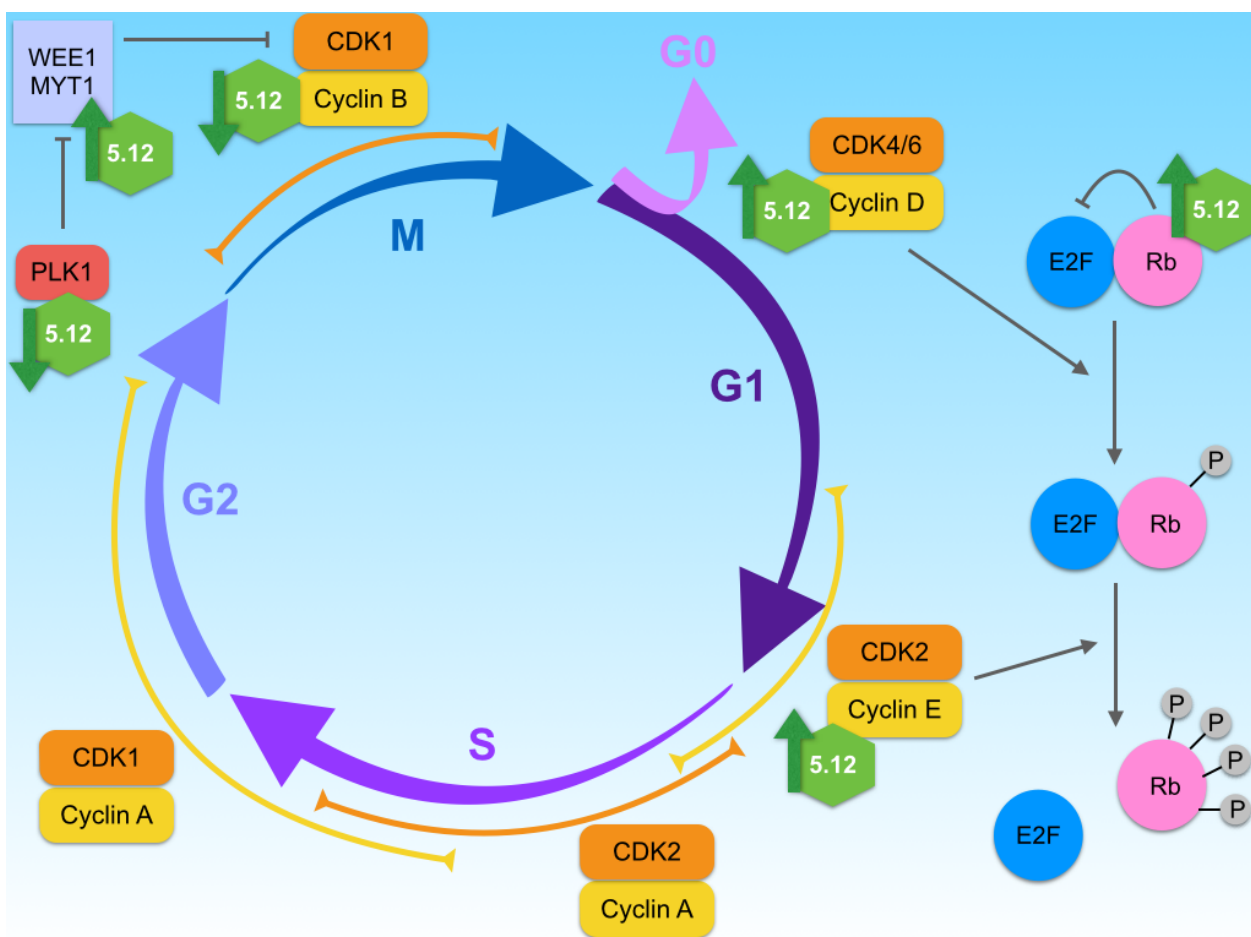


Figure 5.23. Simplified scheme of the cell cycle, its regulation, and the effect of compound **5.12** on the cell cycle.

These RPPA results should be validated by immunoblot analysis to confirm the potential involvement of these pathways in the anticancer mechanism of compound **5.12**.

5.3. Conclusion

In the current chapter, several derivatives of ursolic acid were successfully synthesized and their anticancer activity was screened against NSCLC cell lines, using monolayer and spheroid culture models.

The most active compound (**5.12**) displayed an α,β -unsaturated carbonyl system, with an exocyclic double bond, conjugated with an heteroaromatic ring (pyridine).

The preliminary studies on the mechanism of action demonstrated that compound **5.12** is able to modulate the RNA synthesis rate, to affect the cell cycle, and to promote apoptosis via activation of caspase-8 and caspase-7, as well as autophagy. Moreover, the analysis of the RPPA data demonstrated that compound **5.12** is able to modulate several RTKs and the PI3K/Akt/mTOR pathway.

Despite being active in the monolayer culture model, compound **5.12** seems to lose potency in the spheroid culture model.

Overall, additional studies will be needed in order to validate the RPPA data, and to understand the difference in the anticancer activity between the monolayer and the spheroid culture models with compound **5.12**.

5.4 Experimental section

5.4.1. Chemistry

5.4.1.1. General

Ursolic acid, 4-(dimethylamino)pyridine (DMAP), cinnamoyl chloride (*trans*-3-phenylacryloyl chloride), 2-furoyl chloride, 2-thiophenecarbonyl chloride, acryloyl chloride, methanesulfonyl chloride, potassium *tert*-butoxide (*t*-BuOK), benzaldehyde, 4-nitrobenzaldehyde, 4-pyridinecarboxaldehyde, 4-(trifluoromethyl)benzaldehyde, cinnamaldehyde, triethylamine (Et₃N), *tert*-butanol (*t*-BuOH), benzene, hydrochloric acid (HCl), were purchased from Sigma-Aldrich Co.

The reaction and workup solvents were purchase from VWR Portugal, and were of analytical grade. All the solvents used in the reactions were previously purified and dried according to the literature procedures.

Potassium hydroxide (KOH), sodium chloride (NaCl), and sodium sulfate (Na₂SO₄) were purchased from Merck Co.

TLC analysis was performed using Kieselgel 60HF₂₅₄/Kieselgel 60G TLC plates.

Separation and purification of compounds was performed by flash column chromatography using Kieselgel 60 (230–400 mesh, Merck), or by TLC Preparative, using Kieselgel 60 HF254 and Kieselgel 60G (Merck).

Melting points (Mp) were measured using a BUCHI melting point B-540 apparatus and are uncorrected.

IR spectra were obtained on a Fourier transform spectrometer.

Chapter 5 | Synthesis and cytotoxic activity of novel UA derivatives

NMR spectra were recorded on a Bruker NMR Avance 400 digital spectrometer, using CDCl_3 as internal standard. The chemical shifts (δ) are reported in parts per million (ppm) and coupling constants (J) in hertz (Hz).

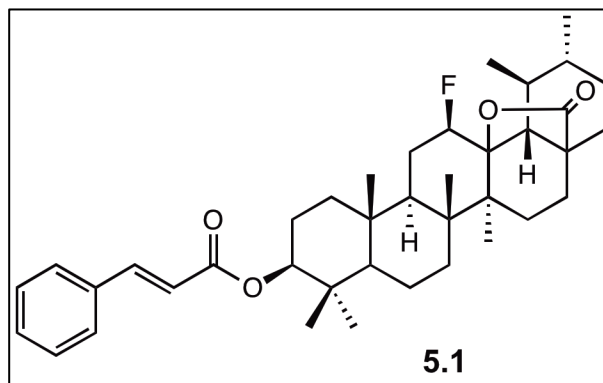
The mass spectrometry (MS) was performed using a Quadrupole/Ion Trap Mass Spectrometer (QIT-MS) (LCQ Advantage MAX, Thermo Finnigan).

Elemental analysis was performed in an Analyzer Elemental Carlo Erba 1108 by chromatographic combustion.

5.4.1.2. Synthetic procedures

3 β -(*trans*-Cinnamoyloxy)-12 β -fluor-urs-13,28 β -olide (5.1): To a stirred mixture of **3.2** (120

mg, 0.25 mmol) in dry benzene (3 ml), THF (1 ml), Et_3N (0.1 ml) and DMAP (100 mg, 0.82 mmol), under N_2 at r.t., cinnamoyl chloride (96.7 mg, 0.58 mmol) was added. After stirring for 4 h at 80 °C, the reaction solvents were removed under reduced pressure, and the



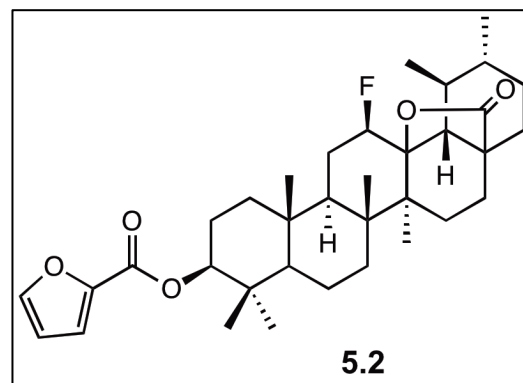
resultant residue was extracted with ethyl acetate (3 × 50 ml) from water (20 ml). The resulting organic phase was washed with 5% HCl aqueous solution (50 ml), water (50 ml), and 10% NaCl aqueous solution (50 ml), dried over Na_2SO_4 , filtered, and concentrated to dryness. The crude residue was purified by two preparative TLC (petroleum ether:ethyl acetate 7:1, and chloroform:ethanol 75:1) to give **5.1** as a light yellow solid (57.9%). Mp 274.7 – 278.3 °C. IR (KBr): $\nu = 3080.62, 3027.69, 2975.62, 2923.56, 2875.34, 1764.55, 1706.69, 1631.48, 1448.28, 1270.86, 1235.50, 1022.09, 977.73, 767.53, 705.82 \text{ cm}^{-1}$. ^1H NMR (400 MHz, CDCl_3): $\delta = 7.67$ (d, $J = 16.0$ Hz, 1H, H-vinyl), 7.54–7.52 (m, 2H, H-Ar), 7.39–7.37 (m, 3H, H-Ar), 6.44 (d, $J = 16.0$

Chapter 5 | Synthesis and cytotoxic activity of novel UA derivatives

Hz, 1H, H-vinyl), 4.88 (dt, $J = 45.6, 8.6$ Hz, 1H, H-12), 4.63 (dd, $J = 10.8, 5.5$ Hz, 1H, H-3), 1.23 (s, 3H), 1.21 (s, 3H), 1.15 (d, $J = 6.2$ Hz, 3H), 0.98 (6H), 0.94 (s, 3H), 0.91 (s, 3H). ^{13}C NMR (100 MHz, CDCl_3): $\delta = 179.05$ (C28), 166.95 (OCO), 144.62 (C-vinyl), 134.61 (C-Ar), 130.36 (C-Ar), 129.01 (2C, C-Ar), 128.19 (2C, C-Ar), 118.79 (C-vinyl), 92.13 (d, $J = 14.3$ Hz, C13), 89.71 (d, $J = 186.1$ Hz, C12), 80.69 (C3), 55.52, 52.74 (d, $J = 3.4$ Hz), 49.29 (d, $J = 9.2$ Hz), 45.36, 44.09 (d, $J = 2.9$ Hz), 42.73, 39.71, 38.92, 38.58, 38.21, 37.25, 34.07, 31.52, 30.89, 28.12, 27.81, 25.60 (d, $J = 19.4$ Hz), 23.81, 22.57, 19.59, 18.71, 17.74, 17.39, 16.92, 16.74, 16.70. MS (DI-ESI) (m/z): 604.9 (100%) $[\text{M}+\text{H}]^+$. Anal. Calcd for $\text{C}_{39}\text{H}_{53}\text{FO}_4$: C, 77.45; H, 8.83. Found: C, 77.23; H, 8.82.

3 β -(2-Furoyloxy)-12 β -fluor-urs-13,28 β -olide (5.2): To a stirred mixture of **3.2** (120 mg, 0.25

mmol) in dry benzene (6 ml), Et_3N (0.1 ml) and DMAP (100 mg, 0.82 mmol), under N_2 at r.t., 2-furoyl chloride (0.05 ml, 0.51 mmol) was added. After stirring for 12.5 h at 80 $^\circ\text{C}$, the reaction solvent was removed under reduced pressure, and the resultant residue was extracted with ethyl acetate (3 \times 50 ml)



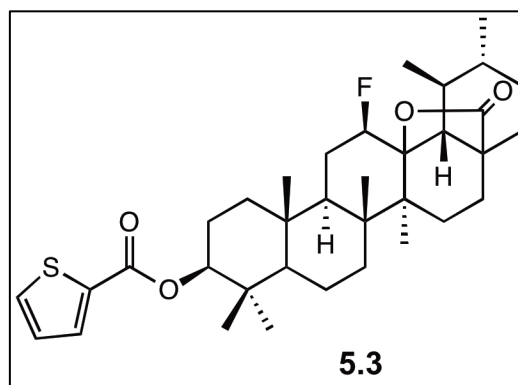
from water (20 ml). The resulting organic phase was washed with 5% HCl aqueous solution (50 ml), water (50 ml), and 10% NaCl aqueous solution (50 ml), dried over Na_2SO_4 , filtered, and concentrated to dryness. The crude residue was purified by preparative TLC (petroleum ether:ethyl acetate 50:25) to give **5.2** as a light yellow solid (65.8%). Mp 264.7 – 268.4 $^\circ\text{C}$. IR (KBr): $\nu = 3137.62, 3118.33, 2958.27, 2927.41, 2877.27, 1770.33, 1724.05, 1567.84, 1473.35, 1392.35, 1294.0, 1184.08, 1122.37, 1014.37, 937.23, 761.74$ cm^{-1} . ^1H NMR (400 MHz, CDCl_3): $\delta = 7.58$ (dd, $J = 1.8, 0.7$ Hz, 1H, H-furoyl), 7.13 (dd, $J = 3.6; 0.6$ Hz, 1H, H-furoyl), 6.50 (dd, $J = 3.4, 1.7$ Hz, 1H, H-furoyl), 4.87 (dt, $J = 46.5, 8.5$ Hz, 1H, H-12), 4.71 (dd, $J = 10.9, 5.0$ Hz, 1H, H-3), 1.23 (s, 3H), 1.21 (s, 3H), 1.15 (d, $J = 6.3$ Hz, 3H), 0.98 (6H), 0.96 (3H), 0.92 (s, 3H). ^{13}C

Chapter 5 | Synthesis and cytotoxic activity of novel UA derivatives

NMR (100 MHz, CDCl₃): δ = 179.06 (C28), 158.79 (OCO), 146.37 (C-furoyl), 145.18 (C2'-furoyl), 117.62 (C-furoyl), 111.86 (C-furoyl), 92.11 (d, J = 14.3 Hz, C13), 89.79 (d, J = 186.0 Hz, C12), 81.32 (C3), 55.58, 52.73 (d, J = 3.5 Hz), 49.30 (d, J = 9.2 Hz), 45.37, 44.08 (d, J = 2.9 Hz), 42.73, 39.71, 38.88, 38.59, 38.31, 37.24, 34.06, 31.52, 30.90, 28.12, 27.81, 25.61 (d, J = 19.1 Hz), 23.82, 22.57, 19.59, 18.71, 17.74, 17.39, 16.92, 16.70 (2C). MS (DI-ESI) (m/z): 569.0 (100%) [M+H]⁺. Anal. Calcd for C₃₅H₄₉FO₅·0.4H₂O: C, 72.99; H, 8.71. Found: C, 72.72; H, 8.98.

3 β -(2-Thiophenecarbonyloxy)-12 β -fluor-urs-13,28 β -olide (**5.3**):

To a stirred mixture of **3.2** (160 mg, 0.34 mmol) in dry benzene (9 ml), Et₃N (0.1 ml) and DMAP (125 mg, 1.02 mmol), under N₂ at r.t., 2-thiophenecarbonyl chloride (0.07 ml, 0.65 mmol) was added. After stirring for 11.5 h at 80 °C, the reaction solvent was removed under reduced pressure, and the resultant residue was extracted

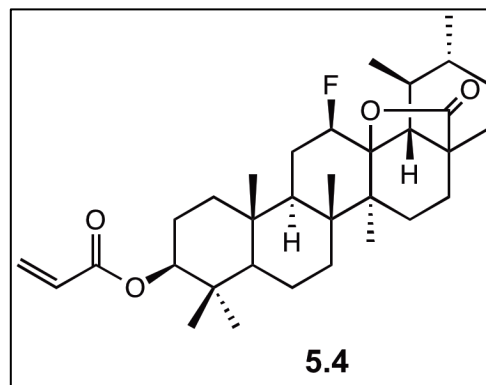


with ethyl acetate (3 × 65 ml) from water (30 ml). The resulting organic phase was washed with 5% HCl aqueous solution (60 ml), water (60 ml), and 10% NaCl aqueous solution (60 ml), dried over Na₂SO₄, filtered, and concentrated to dryness. The crude residue was purified by flash column chromatography (*n*-hexane:ethyl acetate 12:1–10:1) to give **5.3** as a white solid (88.6%). Mp 291.0 – 292.4 °C. IR (KBr): ν = 3112.55, 2973.7, 2929.34, 2875.34, 1766.4, 1710.55, 1529.27, 1457.92, 1419.35, 1357.64, 1263.15, 1099.23, 937.23, 748.24 cm⁻¹. ¹H NMR (400 MHz, CDCl₃): δ = 7.78 (d, J = 3.0 Hz, 1H, H-thiophenyl), 7.54 (d, J = 4.6 Hz, 1H, H-thiophenyl), 7.11–7.09 (m, J = 4.2 Hz, 1H, H4'-thiophenyl), 4.88 (dt, J = 45.7, 8.2 Hz, 1H, H-12), 4.67 (dd, J = 11.3, 4.5 Hz, 1H, H-3), 1.23 (s, 3H), 1.22 (s, 3H), 1.15 (d, J = 6.3 Hz, 3H), 0.98–0.97 (9H), 0.93 (s, 3H). ¹³C NMR (100 MHz, CDCl₃): δ = 179.04 (C28), 162.18 (COO), 134.61 (C2'-thiophenyl), 133.23 (C-thiophenyl), 132.30 (C-thiophenyl), 127.86 (C-thiophenyl), 92.10 (d, J = 14.2 Hz, C13), 89.78 (d, J = 185.8 Hz, C12), 81.62 (C3), 55.59, 52.74 (d, J = 3.5 Hz), 49.28 (d, J = 9.3

Chapter 5 | Synthesis and cytotoxic activity of novel UA derivatives

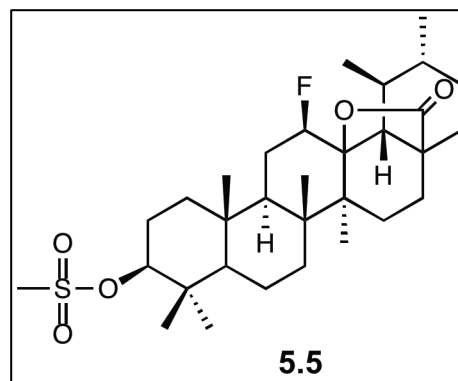
Hz), 45.36, 44.09 (d, $J = 2.9$ Hz), 42.73, 39.71, 38.87, 38.59, 38.33, 37.25, 34.06, 31.52, 30.90, 28.20, 27.81, 25.60 (d, $J = 19.0$ Hz), 23.79, 22.57, 19.59, 18.71, 17.74, 17.40, 16.91, 16.74, 16.69. MS (DI-ESI) (m/z): 584.9 (100%) $[M+H]^+$. Anal. Calcd for $C_{35}H_{49}FO_4S \cdot 0.2EtOAc$: C, 71.25; H, 8.47; S, 5.28. Found: C, 71.57; H, 8.45; S, 4.92.

3 β -Acryloyloxy-12 β -fluor-urs-13,28 β -olide (5.4): To a stirred mixture of **3.2** (145 mg, 0.31 mmol) in dry CH_2Cl_2 (4 ml), Et_3N (0.1 ml) and DMAP (76 mg, 0.62 mmol), under N_2 at 25 °C, acryloyl chloride (0.05 ml, 0.62 mmol) was added. After stirring for 2 h, the reaction was diluted with CH_2Cl_2 (46 ml) and water (20 ml), and the organic phase was separated. The aqueous solution was extracted with CH_2Cl_2 (2 \times 50 ml).



The resulting organic phase was washed with 5% HCl aqueous solution (60 ml), water (60 ml), and 10% NaCl aqueous solution (60 ml), dried over Na_2SO_4 , filtered, and concentrated to dryness to give **5.4** as a white solid (68.1%). Mp 285.1 – 287.2 °C. IR (KBr): $\nu = 2956.34$, 2937.70, 2877.27, 1766.48, 1716.34, 1616.05, 1461.78, 1407.78, 1274.22, 1207.22, 1051.01, 987.37 cm^{-1} . 1H NMR (400 MHz, $CDCl_3$): $\delta = 6.38$ (d, $J = 17.2$ Hz, 1H, = $\underline{C}H$ H), 6.11 (dd, $J = 17.3$, 10.4 Hz, 1H, $OCOC\underline{H}=\underline{C}$), 5.81 (d, $J = 10.6$ Hz, 1H, = $\underline{C}H$ H), 4.87 (dt, $J = 45.7$, 8.4 Hz, 1H, H-12), 4.56 (dd, $J = 10.8$, 5.5 Hz, 1H, H-3), 1.22 (s, 3H), 1.20 (s, 3H), 1.14 (d, $J = 6.3$ Hz, 3H), 0.95–0.96 (6H), 0.89 (s, 3H), 0.87 (s, 3H). ^{13}C NMR (100 MHz, $CDCl_3$): $\delta = 179.04$ (C28), 166.17 (COO), 130.43 ($\underline{C}H_2=\underline{C}H$), 129.14 ($CH_2=\underline{C}H$), 92.11 (d, $J = 14.3$ Hz, C13), 89.70 (d, $J = 186.4$ Hz, C12), 80.78 (C3), 55.58, 52.73 (d, $J = 3.5$ Hz), 49.26 (d, $J = 9.0$ Hz), 45.35, 44.08 (d, $J = 2.9$ Hz), 42.72, 39.70, 38.87, 38.58, 38.13, 37.22, 34.04, 31.51, 30.89, 28.07, 27.80, 25.59 (d, $J = 19.2$ Hz), 23.67, 22.56, 19.58, 18.69, 17.71, 17.38, 16.89, 16.68, 16.64. MS (DI-ESI) (m/z): 528.9 (100%) $[M+H]^+$, 459.1 (10.2%), 458.3 (22.4%), 441.4 (11.8%), 267.0 (54.0%). Anal. Calcd for $C_{33}H_{49}FO_4 \cdot 0.4H_2O$: C, 73.95; H, 9.37. Found: C, 74.16; H, 9.34.

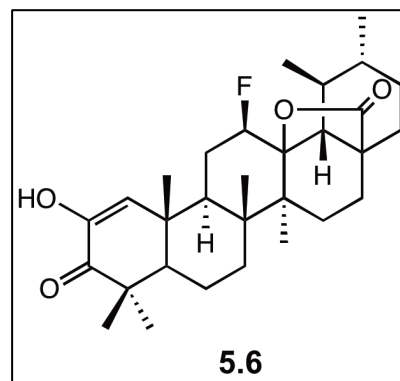
3 β -Methylsulfonyloxy-12 β -fluor-urs-13,28 β -olide (5.5): To a stirred mixture of **3.2** (160 mg, 0.34 mmol) in dry CH₂Cl₂ (4 ml) and Et₃N (0.1 ml), under N₂ at r.t., methanesulfonyl chloride (0.05 ml, 0.65 mmol) was added. After stirring for 2 h, the reaction solvent was removed under reduced pressure, and the resultant residue was extracted with CH₂Cl₂ (3 × 50 ml) from water (20 ml). The resulting organic phase was washed with



water (50 ml), and 10% NaCl aqueous solution (50 ml), dried over Na₂SO₄, filtered, and concentrated to dryness. The crude residue was purified by flash column chromatography (toluene:diethyl ether 11:1–10:1) to give **5.5** as a white solid (69.2%). Mp 154.6 – 157.1 °C. IR (KBr): ν = 2962.12, 2929.34, 2871.49, 1760.69, 1467.56, 1348.0, 1326.79, 1170.58, 935.31 cm⁻¹. ¹H NMR (400 MHz, CDCl₃): δ = 4.86 (dq, J = 45.6, 8.6 Hz, 1H, H-12), 4.34 (dd, J = 10.9, 5.7 Hz, 1H, H-3) 3.02 (s, 3H, CH₃S), 1.21 (s, 3H), 1.19 (s, 3H), 1.14 (d, J = 6.2 Hz, 3H), 1.02 (s, 3H), 0.97–0.95 (6H), 0.86 (s, 3H). ¹³C NMR (100 MHz, CDCl₃): δ = 178.96 (C28), 91.96 (d, J = 14.2 Hz, C13), 89.81 (C3), 89.69 (d, J = 185.9 Hz, C12), 55.69, 52.71 (d, J = 3.5 Hz), 49.19 (d, J = 9.3 Hz), 45.33, 44.06 (d, J = 2.9 Hz), 42.65, 39.69, 39.08, 38.93, 38.72, 38.56, 37.07, 33.99, 31.49, 30.86, 28.23, 27.78, 25.59 (d, J = 19.5 Hz), 25.26, 22.53, 19.56, 18.67, 17.88, 17.34, 16.84, 16.68, 16.27. MS (DI-ESI) (m/z): 552.9 (100%) [M+H]⁺. Anal. Calcd for C₃₁H₄₉FO₅S·0.2EtOAc: C, 66.96; H, 8.94; S, 5.62. Found: C, 67.11; H, 9.08; S, 5.27.

Chapter 5 | Synthesis and cytotoxic activity of novel UA derivatives

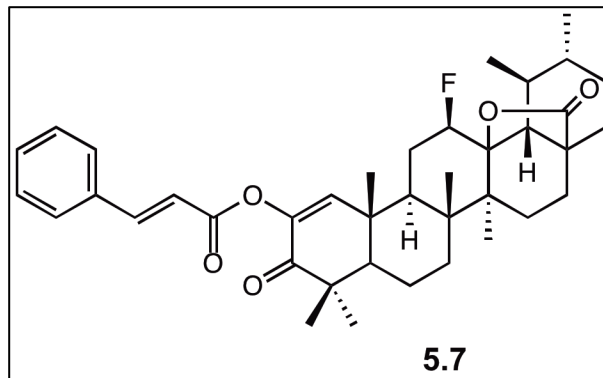
2-Hydroxy-3-oxo-12 β -fluor-urs-1-en-13,28 β -olide (5.6): To a stirred mixture of **3.3** (300 mg, 0.63 mmol) in *t*-BuOH (17 ml) at 25–30 °C, *t*-BuOK (1780 mg, 15.86 mmol) was added, and a constant flux of air was introduced to the system. After 6 h, the reaction mixture was diluted with *t*-BuOMe (100 ml), and neutralized with 1M HCl aqueous solution (80 ml) at 3–5 °C. The aqueous solution was extracted with *t*-BuOMe (2 \times 80 ml), and the resulting organic



phase was washed with water (80 ml), and 10% NaCl aqueous solution (80 ml), dried over Na₂SO₄, filtered, and concentrated to dryness. The crude residue was purified by flash column chromatography (petroleum ether:ethyl acetate 9:1–1:1) to give **5.6** as a yellow solid (72.9%). Mp 306.4 – 309.9 °C. IR (KBr): ν = 3465.45, 2983.34, 2931.27, 2875.34, 1768.4, 1666.2, 1459.85, 1392.35, 1236.15, 1118.51, 939.16 cm⁻¹. ¹H NMR (400 MHz, CDCl₃): δ = 6.43 (s, 1H, H-1), 5.95 (s, 1H, OH), 4.89 (dt, J = 45.7, 6.6 Hz, 1H, H-12), 1.28 (s, 3H), 1.22 (s, 3H), 1.21 (s, 3H), 1.20 (s, 3H), 1.14 (d, J = 6.3 Hz, 3H), 1.12 (s, 3H), 0.96 (d, J = 5.5 Hz, 3H). ¹³C NMR (100 MHz, CDCl₃): δ = 200.89 (C3), 178.84 (C28), 144.31 (C2), 127.56 (C1), 91.94 (d, J = 14.2 Hz, C13), 89.26 (d, J = 186.7 Hz, C12), 54.27, 52.73 (d, J = 3.7 Hz), 45.31, 44.57 (d, J = 9.8 Hz), 44.21 (d, J = 3.0 Hz), 44.17, 43.34, 39.66, 38.48, 38.46, 33.65, 31.43, 30.84, 27.69, 27.16, 25.72 (d, J = 19.9 Hz), 22.48, 21.61, 20.78, 19.57, 19.05, 18.22, 17.27, 16.70. MS (DI-ESI) (m/z): 487.0 (100 %) [M+H]⁺, 114.6 (10.9%), 105.5 (42.4%), 96.6 (55.1%), 95.7 (13.9%). Anal. Calcd for C₃₀H₄₃FO₄·0.5EtOAc: C, 72.42; H, 8.93. Found: C, 72.25; H, 8.85.

2-(*trans*-Cinnamoyloxy)-3-oxo-12 β -fluor-urs-1-en-13,28 β -olide (5.7): To a stirred mixture of

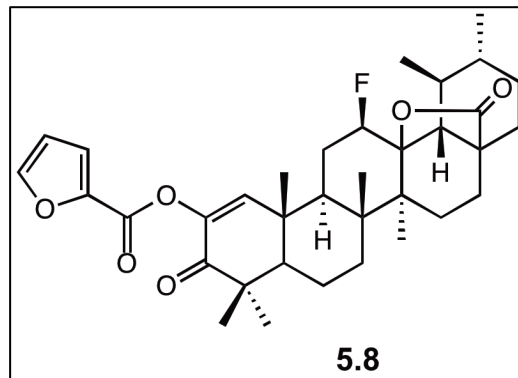
5.6 (165 mg, 0.27 mmol) in dry benzene (6 ml) and THF (1 ml), Et₃N (0.1 ml) and DMAP (93 mg, 0.76 mmol), under N₂ at r.t., cinnamoyl chloride (115 mg, 0.69 mmol) was added. After stirring for 2 h at 80 °C, the reaction solvents were removed under reduced pressure, and



the resultant residue was extracted with ethyl acetate (3 × 60 ml) from water (25 ml). The resulting organic phase was washed with 5% HCl aqueous solution (60 ml), water (60 ml), and 10% NaCl aqueous solution (60 ml), dried over Na₂SO₄, filtered, and concentrated to dryness. The crude residue was purified by preparative TLC (petroleum ether:chloroform 1:10) to give **5.7** as a light yellow solid (62.5%). Mp 176.6 – 180.0 °C. IR (KBr): ν = 3083.62, 3060.48, 2977.55, 2931.27, 2873.42, 1776.12, 1733.69, 1687.41, 1633.41, 1577.49, 1450.21, 1384.64, 1234.22, 1203.36, 1141.65, 1033.66, 981.59, 765.6, 703.89 cm⁻¹. ¹H NMR (400 MHz, CDCl₃): δ = 7.80 (d, *J* = 16.0 Hz, 1H, OCOCH=CH), 7.56–7.53 (m, 2H, H-Ar), 7.41–7.40 (m, 3H, H-Ar), 6.84 (s, 1H, H-1), 6.54 (d, *J* = 16.0 Hz, 1H, OCOCH=CH), 4.91 (dq, *J* = 45.1, 8.4 Hz, 1H, H-12), 1.31 (s, 3H), 1.27 (s, 3H), 1.25 (s, 3H), 1.24 (s, 3H), 1.17 (s, 3H), 1.14 (d, *J* = 6.3 Hz, 3H), 0.97 (d, *J* = 5.6 Hz, 3H). ¹³C NMR (100 MHz, CDCl₃): δ = 197.47 (C3), 178.75 (C28), 165.08 (COO), 147.18 (OCOCH=CH), 143.46 (C2), 143.41 (C1), 134.24 (C-Ar), 130.88 (2C, C-Ar), 129.10 (2C, C-Ar), 128.47 (C-Ar), 116.50 (OCOCH=CH), 91.93 (d, *J* = 14.3 Hz, C13), 89.03 (d, *J* = 186.7 Hz, C12), 53.19, 52.77 (d, *J* = 3.4 Hz), 45.72, 45.33, 44.32 (d, *J* = 2.9 Hz), 43.58 (d, *J* = 9.5 Hz), 43.39, 39.69, 39.50, 38.54, 33.42, 31.44, 30.86, 28.08, 27.73, 25.89 (d, *J* = 20.13 Hz), 22.50, 21.40, 20.48, 19.56, 18.95, 18.56, 17.28, 16.65. MS (DI-ESI) (*m/z*): 616.9 (100%) [M+H]⁺. Anal. Calcd for C₃₉H₄₉FO₅·0.3EtOAc: C, 75.06; H, 8.05. Found: C, 75.04; H, 7.73.

Chapter 5 | Synthesis and cytotoxic activity of novel UA derivatives

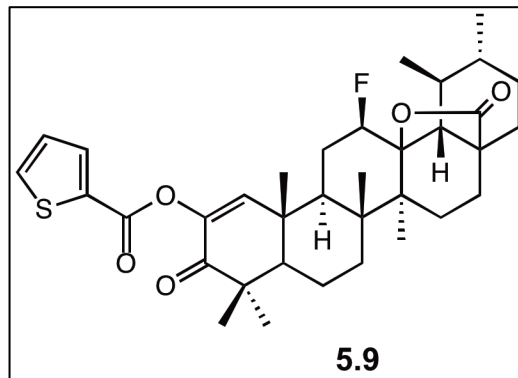
2-(2-Furoyloxy)-3-oxo-12 β -fluor-urs-1-en-13,28 β -olide (5.8): To a stirred mixture of **5.6** (165 mg, 0.34 mmol) in benzene (6 ml), Et₃N (0.1 ml) and DMAP (85 mg, 0.70 mmol) under N₂ at r.t., 2-furoyl chloride (0.07 ml, 0.71 mmol) was added. After stirring for 4 h at 80 °C, the solvent was removed under reduced pressure, and the resultant residue was extracted with ethyl acetate (3 × 60 ml) from



water (25 ml). The resulting organic phase was washed with 5% HCl aqueous solution (60 ml), water (60 ml), and 10% NaCl aqueous solution (60 ml), dried over Na₂SO₄, filtered, and concentrated to dryness. The crude residue was purified by flash column chromatography (petroleum ether:ethyl acetate 11:1–8:1) followed by preparative TLC (petroleum ether:chloroform 1:30) to give **5.8** as a white solid (42.0%). Mp 164.4 – 167.8 °C. IR (KBr): ν = 3139.54, 2977.55, 2933.2, 2873.42, 1774.19, 1745.26, 1687.41, 1577.49, 1471.42, 1392.35, 1294.0, 1172.51, 1095.37, 937.23, 761.74 cm⁻¹. ¹H NMR (400 MHz, CDCl₃): δ = 7.63 (br s, 1H, H-furoyl), 7.32–7.31 (m, 1H, H-furoyl), 6.90 (s, 1H, H-1), 6.56–6.55 (m, 1H, H-furoyl), 4.90 (dq, J = 45.6, 8.4 Hz, 1H, H-12), 1.31 (s, 3H), 1.27 (s, 3H), 1.25 (s, 3H), 1.24 (s, 3H), 1.17 (s, 3H), 1.13 (d, J = 6.4 Hz, 3H), 0.97 (d, J = 5.5 Hz, 3H). ¹³C NMR (100 MHz, CDCl₃): δ = 197.03 (C3), 178.75 (C28), 156.45 (COO), 147.36 (C-furoyl), 143.91 (C1), 143.51 (C2), 142.92 (C-furoyl), 119.93 (C-furoyl), 112.35 (C-furoyl), 91.92 (d, J = 14.4 Hz, C13), 89.11 (d, J = 186.8 Hz, C12), 53.22, 52.77 (d, J = 3.1 Hz), 45.75, 45.33, 44.32 (d, J = 2.8 Hz), 43.54 (d, J = 9.6 Hz), 43.41, 39.69, 39.62, 38.54, 33.42, 31.44, 30.85, 28.00, 27.72, 25.87 (d, J = 19.7 Hz), 22.49, 21.39, 20.38, 19.56, 18.97, 18.52, 17.28, 16.64. MS (DI-ESI) (m/z): 581.1 (100%) [M+H]⁺, Anal. Calcd for C₃₅H₄₅FO₆·0.5EtOAc: C, 71.13; H, 7.9. Found: C, 70.77; H, 7.63.

2-(2-Thiophenecarbonyloxy)-3-oxo-12 β -fluor-urs-1-en-13,28 β -olide (5.9): To a stirred

mixture of **5.6** (165 mg, 0.34 mmol) in dry benzene (6 ml) and THF (1 ml), Et₃N (0.1 ml) and DMAP (92 mg, 0.75 mmol) under N₂ at r.t., 2-thiophenecarbonyl chloride (0.08 ml, 0.75 mmol) was added. After stirring for 2.5 h at 80 °C, the solvents were removed under reduced pressure, and the resultant residue

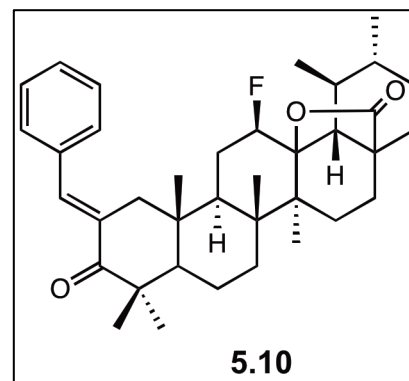


was extracted with ethyl acetate (3 × 60 ml) from water (25 ml). The resulting organic phase was washed with 5% HCl aqueous solution (60 ml), water (60 ml), and 10% NaCl aqueous solution (60 ml), dried over Na₂SO₄, filtered, and concentrated to dryness. The crude residue was purified by preparative TLC (petroleum ether:chloroform 1:25) to give **5.9** as a light yellow solid (57.0%). Mp 317.3 – 320.2 °C. IR (KBr): ν = 3108.69, 2985.27, 2925.48, 2877.27, 1774.19, 1724.05, 1689.34, 1639.2, 1523.49, 1457.92, 1413.57, 1359.57, 1267.0, 1066.44, 935.31, 738.6 cm⁻¹. ¹H NMR (400 MHz, CDCl₃): δ = 7.90 (d, *J* = 3.1 Hz, 1H, H-thiophenyl), 7.64 (d, *J* = 4.6 Hz, 1H, H-thiophenyl), 7.15-7.13 (m, 1H, H_{4'}-thiophenyl), 6.90 (s, 1H, H-1), 4.90 (dq, *J* = 45.6, 8.4 Hz, 1H, H-12), 1.31 (s, 3H), 1.29 (s, 3H), 1.26 (s, 3H), 1.24 (s, 3H), 1.17 (s, 3H), 1.13 (d, *J* = 6.2 Hz, 3H), 0.97 (d, *J* = 5.4 Hz, 3H). ¹³C NMR (100 MHz, CDCl₃): δ = 197.15 (C3), 178.73 (C28), 160.33 (COO), 143.78 (C1), 143.26 (C2), 135.02 (C-thiophenyl), 133.82 (C-thiophenyl), 132.09 (C2'-thiophenyl), 128.14 (C-thiophenyl), 91.91 (d, *J* = 14.4 Hz, C13), 89.12 (d, *J* = 186.9 Hz, C12), 53.28, 52.77 (d, *J* = 3.3 Hz), 45.77, 45.34, 44.32 (d, *J* = 2.8 Hz), 43.59 (d, *J* = 9.7 Hz), 43.41, 39.70, 39.60, 38.55, 33.45, 31.45, 30.86, 28.05, 27.74, 25.88 (d, *J* = 20.0 Hz), 22.50, 21.41, 20.43, 19.57, 18.99, 18.55, 17.28, 16.65. MS (DI-ESI) (*m/z*): 597.0 (100%) [M+H]⁺, MS² (597.0): 597.6 (53.7%), 596.6 (50.0%), 577.3 (84.7%), 555.5 (14.8%), 548.74 (12.4%), 466.8 (40.1%), 449.2 (77.6%), 439.2 (100%), 421.6 (75.1%), 357.6 (13.8%).

Chapter 5 | Synthesis and cytotoxic activity of novel UA derivatives

(E)-2-Benzylidene-3-oxo-12 β -fluor-urs-13,28 β -olide (5.10): To a stirred mixture of **3.3** (165

mg, 0.35 mmol) in methanolic potassium hydroxide (5% w/v) (47 ml) at 40 °C, benzaldehyde (0.21 ml, 2.07 mmol) was added. After stirring for 2.5 h at r.t., the reaction solvent was removed under *vacuum*, and the resultant residue was diluted with water (10 ml), and ethyl acetate (10 ml). The mixture was acidified with 1M HCl aqueous solution (7.5 ml), and extracted



with ethyl acetate (3 × 50 ml). The resulting organic phase was washed with water (50 ml), and 10% NaCl aqueous solution (50 ml), dried over Na₂SO₄, filtered, and concentrated to dryness.

The crude residue was purified by flash column chromatography (petroleum ether:ethyl acetate

13:1–7:1) to give **5.10** as a light yellow solid (58.0%). Mp 184.3 – 188.0 °C. IR (KBr): ν =

3060.48, 2973.7, 2937.05, 2871.49, 1760.69, 1673.91, 1592.91, 1455.99, 1382.71, 1238.08,

1122.37, 939.16, 759.82, 696.18 cm⁻¹. ¹H NMR (400 MHz, CDCl₃): δ = 7.55 (br s, 1H, H-vinyl),

7.44–7.42 (m, 4H, H-Ar), 7.37–7.33 (m, 1H, H-Ar), 4.95 (dt, J = 45.4, 8.4 Hz, 1H, H-12), 3.15 (d,

J = 16.0 Hz, 1H, H-1), 2.28 (d, J = 15.7 Hz, 1H, H-1), 1.27 (s, 3H), 1.25 (s, 3H), 1.18 – 1.17 (m,

6H), 1.15 (s, 3H), 0.97 (d, J = 5.5 Hz, 3H), 0.90 (s, 3H). ¹³C NMR (100 MHz, CDCl₃): δ = 207.46

(C3), 178.85 (C28), 138.25, 135.87, 133.45 (C-Ar), 130.33 (2C, C-Ar), 128.80 (C-Ar), 128.74

(2C, C-Ar), 92.06 (d, J = 14.4 Hz, C13), 89.75 (d, J = 186.1 Hz, C12), 52.97, 52.79 (d, J = 3.6

Hz), 47.28 (d, J = 9.4 Hz), 45.37 (2C), 44.62, 44.25 (d, J = 2.9 Hz), 42.44, 39.73, 38.77, 36.73,

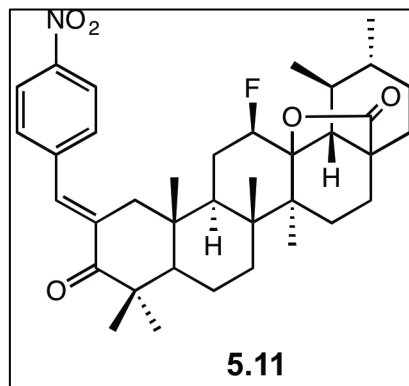
33.15, 31.49, 30.91, 29.55, 27.77, 26.07 (d, J = 19.5 Hz), 22.55, 22.48, 19.86, 19.56, 17.91,

17.16, 16.70, 16.50. MS (DI-ESI) (m/z): 561.6 (100%) [M+H]⁺, 541.4 (23.5%), 513.6 (13.9%).

Anal. Calcd for C₃₇H₄₉FO₃·0.5EtOAc: C, 77.45; H, 8.83. Found: C, 77.17; H, 9.11.

(E)-2-(4-Nitrobenzylidene)-3-oxo-12 β -fluor-urs-13,28 β -olide (5.11): To a stirred mixture of **3.3**

(165 mg, 0.35 mmol) in methanolic potassium hydroxide (5% w/v) (42 ml) at 40 °C, 4-nitrobenzaldehyde (317 mg, 2.10 mmol) was added. After stirring for 2.5 h at r.t., the reaction solvent was removed under *vacuum*, and the resultant residue was diluted with water (10 ml) and ethyl acetate (10 ml). The mixture was acidified with 1M HCl aqueous solution (7.5 ml),



and extracted with ethyl acetate (3 × 50 ml). The resulting organic phase was washed with water (50 ml), and 10% NaCl aqueous solution (50 ml), dried over Na₂SO₄, filtered, and concentrated to dryness. The crude residue was purified by flash column chromatography (petroleum ether:ethyl acetate 12:1–2:1), followed by preparative TLC (petroleum ether:chloroform 1:65) to give **5.11** as a light yellow solid (61.3%). Mp 287.7 – 291.4 °C. IR (KBr): ν = 3112.55, 3081.69, 2981.41, 2931.27, 2871.49, 1762.62, 1735.62, 1679.69, 1604.48, 1521.56, 1455.99, 1344.14, 1238.08, 1112.73, 939.16, 846.6 cm⁻¹. ¹H NMR (400 MHz, CDCl₃): δ = 8.29 (d, *J* = 8.9 Hz, 2H, H-Ar), 7.55–7.53 (m, 3H, H-Ar and H-vinyl), 4.92 (dq, *J* = 45.4, 8.1 Hz, 1H, H-12), 3.06 (d, *J* = 15.9 Hz, 1H, H-1), 2.28 (d, *J* = 15.7 Hz, 1H, H-1), 1.27–1.25 (6H), 1.18–1.16 (9H), 0.98 (d, *J* = 5.9 Hz, 3H), 0.90 (s, 3H). ¹³C NMR (100 MHz, CDCl₃): δ = 206.89 (C3), 178.76 (C28), 147.40 (C-Ar), 142.34 (C-Ar), 136.83 (C2), 135.41 (C-vinyl), 130.67 (2C, C-Ar), 123.96 (2C, C-Ar), 91.94 (d, *J* = 14.0 Hz, C13), 89.51 (d, *J* = 185.2 Hz, C12), 53.07, 52.78 (d, *J* = 3.7 Hz), 47.20 (d, *J* = 9.0 Hz), 45.57, 45.36, 44.53, 44.27 (d, *J* = 3.0 Hz), 42.45, 39.71, 38.78, 36.85, 33.09, 31.47, 30.90, 29.43, 27.78, 26.12 (d, *J* = 19.7 Hz), 22.54 (2C), 19.83, 19.57, 17.92, 17.15, 16.71, 16.51. MS (DI-ESI) (*m/z*): 606.0 (100%) [M+H]⁺, MS2 (606.0): 605.6 (100%), 588.0 (63.6%), 577.4 (20.2%), 576.3 (32.0%), 563.5 (13.8%), 553.6 (19.8%), 544.1 (37.0%), 539.3 (26.1%), 468.3 (30.5%), 458.2 (20.9%), 416.2 (28.1%), 294.2 (8.8%). Anal. Calcd for C₃₇H₄₈FNO₅·0.5EtOAc: C, 72.08 H, 8.07; N, 2.16. Found: C, 71.78; H, 7.76; N 2.24.

Chapter 5 | Synthesis and cytotoxic activity of novel UA derivatives

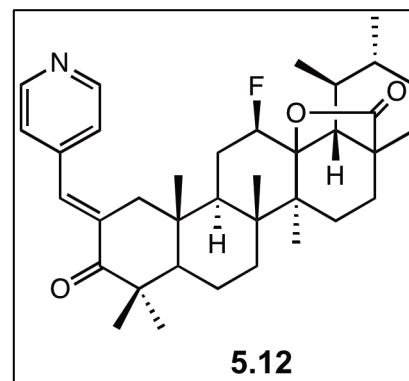
(E)-2-(Pyridine-4-ylmethylidene)-3-oxo-12 β -fluor-urs-13,28 β -olide (5.12): To a stirred

mixture of **3.3** (250 mg, 0.53 mmol) in methanolic potassium hydroxide (5% w/v) (62 ml) at 40 °C, 4-

pyridinecarboxaldehyde (0.25 ml, 2.65 mmol) was added.

After stirring for 4.5 h at r.t., the reaction solvent was removed

under *vacuum*, and the resultant residue was diluted with water (20 ml) and ethyl acetate (20 ml). The mixture was



acidified with 1M HCl aqueous solution (12 ml), and extracted with ethyl acetate (3 × 60 ml). The

resulting organic phase was washed with water (80 ml), and 10% NaCl aqueous solution (80

ml), dried over Na₂SO₄, filtered, and concentrated to dryness. The crude residue was purified by

flash column chromatograph (petroleum ether:ethyl acetate 7:1–1:2) to give **5.12** as a white solid

(55.1%). Mp 300.1 – 301.7 °C. IR (KBr): ν = 3207.04, 2973.7, 2954.41, 2871.49, 1762.62,

1679.69, 1590.98, 1544.7, 1455.99, 1384.64, 1238.08, 1122.37, 1024.02, 939.16 cm⁻¹. ¹H NMR

(400 MHz, CDCl₃): δ = 8.67 (d, J = 5.9 Hz, 2H, H₂',6'-Ar), 7.39 (br s, 1H, H-vinyl), 7.27 (d, J =

5.8 Hz, 2H, H₃',5'-Ar), 4.93 (dq, J = 45.5, 8.6 Hz, 1H, H-12), 3.06 (d, J = 16.0 Hz, 1H, H-1), 2.27

(d, J = 15.9 Hz, 1H, H-1), 1.26 (s, 3H), 1.24 (s, 3H), 1.17 (d, J = 5.7 Hz, 3H), 1.17 (s, 3H), 1.14

(s, 3H), 0.97 (d, J = 5.7 Hz, 3H), 0.89 (s, 3H). ¹³C NMR (100 MHz, CDCl₃): δ = 207.01 (C3),

178.78 (C28), 149.92 (2C, C₂',6'-Ar), 143.67 (C-Ar), 137.71 (C2), 134.66 (C-vinyl), 124.14 (2C,

C₃',5'-Ar), 91.95 (d, J = 14.2 Hz, C13), 89.57 (d, J = 186.4 Hz, C12), 52.99, 52.75 (d, J = 3.7

Hz), 47.14 (d, J = 9.6 Hz), 45.53, 45.33, 44.49, 44.22 (d, J = 2.9 Hz), 42.40, 39.69, 38.74, 36.75,

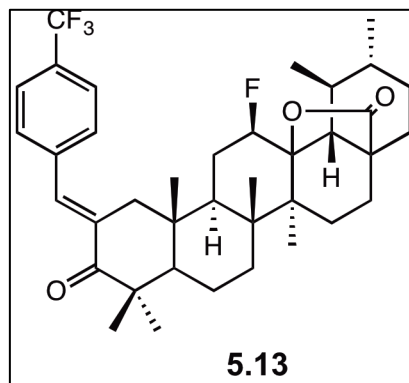
33.04, 31.45, 30.87, 29.36, 27.73, 26.09 (d, J = 19.9 Hz), 22.50, 22.43, 19.78, 19.53, 17.86,

17.11, 16.68, 16.52. MS (DI-ESI) (m/z): 562.5 (100%) [M+H]⁺. Anal. Calcd for

C₃₆H₄₈FNO₃·0.2EtOAc: C, 76.29; H, 8.63; N, 2.42. Found: C, 75.97; H, 8.77; N, 2.58.

(E)-2-(4-(Trifluoromethyl)benzylidene)-3-oxo-12 β -fluor-urs-13,28 β -olide (5.13): To a stirred

solution of **3.3** (165 mg, 0.35 mmol) in methanolic potassium hydroxide (5% w/v) (42 ml) at 40 °C, 4-(trifluoromethyl)benzaldehyde (0.05 ml, 0.37 mmol) was added. After stirring for 10 h at r.t., the reaction solvent was removed under *vacuum*, and the resultant residue was diluted with water (10 ml) and ethyl acetate (10 ml). The mixture was



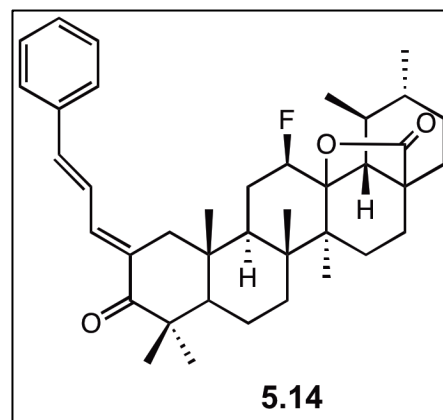
acidified with 1M HCl aqueous solution (7.5 ml), and extracted with ethyl acetate (3 × 50 ml). The resulting organic phase was washed with water (50 ml), and 10% NaCl aqueous solution (50 ml), dried over Na₂SO₄, filtered, and concentrated to dryness. The crude residue was purified by preparative TLC (petroleum ether:chloroform 1:37) give **5.13** as a slight yellow solid (47.4%). Mp 284.4 – 286.8 °C. IR (KBr): ν = 3043.12, 2979.48, 2940.91, 2875.34, 1760.69, 1679.69, 1596.77, 1455.99, 1326.79, 1168.65, 1126.22, 1070.3, 939.16, 840.81 cm⁻¹. ¹H NMR (400 MHz, CDCl₃): δ = 7.69 (d, J = 8.2 Hz, 2H, H-Ar), 7.54 (br s, 1H, H-vinyl), 7.50 (d, J = 8.2 Hz, 2H, H-Ar), 4.93 (dq, J = 45.6, 8.3 Hz, 1H, H-12), 3.09 (d, J = 15.9 Hz, 1H, H-1), 2.25 (d, J = 15.9 Hz, 1H, H-1), 1.27 (s, 3H), 1.25 (s, 3H), 1.18 (d, J = 5.9 Hz, 3H), 1.18 (s, 3H), 1.16 (s, 3H), 0.98 (d, J = 6.1 Hz, 3H), 0.90 (s, 3H). ¹³C NMR (100 MHz, CDCl₃): δ = 207.10 (C3), 178.80 (C28), 139.34 (C-Ar), 136.42 (C-vinyl), 135.44 (C2), 130.24 (2C, C-Ar), 130.39 (q, J = 32.00Hz, C4'-Ar), 124.06 (q, J = 173.00Hz, CF3), 125.68 (d, J = 3.7 Hz, C-Ar), 125.65 (d, J = 5.6 Hz, C-Ar), 91.97 (d, J = 14.4 Hz, C13), 89.62 (d, J = 185.9 Hz, C12), 53.05, 52.78 (d, J = 3.5 Hz), 47.22 (d, J = 9.4 Hz), 45.49, 45.37, 44.45, 44.25 (d, J = 2.9 Hz), 42.45, 39.72, 38.77, 36.80, 33.12, 31.48, 30.90, 29.47, 27.77, 26.10 (d, J = 19.7 Hz), 22.53 (2C), 19.84, 19.57, 17.92, 17.16, 16.70, 16.48. MS (DI-ESI) (m/z): 629.0 (100%) [M+H]⁺, MS2 (629.0): 629.5 (6.0%), 628.3 (20.0%), 627.2 (19.2%), 611.2 (20.1%), 591.1 (9.1%), 583.2 (5.8%), 581.1 (11.3%), 563.4

Chapter 5 | Synthesis and cytotoxic activity of novel UA derivatives

(34.8%), 557.4 (7.7%), 547.9 (14.2%), 517.3 (8.8%), 516.1 (100%). Anal. Calcd for C₃₈H₄₈F₄O₃: C, 72.59; H, 7.69. Found: C, 72.49; H, 7.76.

(E)-2-(2-*trans*-(3-Phenylprop-2-en)-1-ylidene)-3-oxo-12 β -fluor-urs-13,28 β -olide (5.14): To a

stirred solution of **3.3** (165 mg, 0.35 mmol) in methanolic potassium hydroxide (5% w/v) (42 ml) at 40 °C, cinnamaldehyde (0.07 ml, 0.56 mmol) was added. After stirring for 17h at r.t., the reaction solvent was removed under *vacuum*, and the resultant residue was diluted with water (10 ml) and ethyl acetate (10 ml). The mixture was acidified with 1M HCl aqueous solution (7.5 ml), and



extracted with ethyl acetate (3 × 50 ml). The resulting organic phase was washed with water (50 ml), and 10% NaCl aqueous solution (50 ml), dried over Na₂SO₄, filtered, and concentrated to dryness. The crude residue was purified by preparative TLC (petroleum ether:chloroform 1:40) give **5.14** as a yellow solid (31.3%). Mp 212.6 – 215.5 °C. IR (KBr): ν = 3058.55, 3023.84, 2977.55, 2954.41, 2871.49, 1774.19, 1666.2, 1600.63, 1577.49, 1565.91, 1450.21, 1382.71, 1122.37, 985.45, 750.17, 692.32 cm⁻¹. ¹H NMR (400 MHz, CDCl₃): δ = 7.53 (d, *J* = 7.4 Hz, 2H, H-Ar), 7.37 (t, *J* = 7.3 Hz, 2H, H-Ar), 7.33–7.28 (2H, H-Ar, H-vinyl), 6.97 (1H, H-vinyl), 6.95 (1H, H-vinyl), 4.99 (dq, *J* = 45.6, 8.5 Hz, 1H, H-12), 3.07 (d, *J* = 6.1 Hz, 1H, H-1), 1.30 (s, 3H), 1.26 (s, 3H), 1.19 (d, *J* = 6.1 Hz, 3H), 1.14 (s, 3H), 1.11 (s, 3H), 0.99 (d, *J* = 5.7 Hz, 3H), 0.93 (s, 3H). ¹³C NMR (100 MHz, CDCl₃): δ = 206.56 (C3), 178.86 (C28), 141.41 (C-vinyl), 137.99 (C-vinyl), 136.68 (C-Ar), 132.06 (C2), 129.11 (C-Ar), 128.94 (2C, C-Ar), 127.38 (2C, C-Ar), 123.17 (C-vinyl), 92.12 (d, *J* = 14.1 Hz, C13), 89.91 (d, *J* = 185.9 Hz, C12), 53.04, 52.82 (d, *J* = 3.4 Hz), 47.27 (d, *J* = 9.3 Hz), 45.41, 45.20, 44.31 (d, *J* = 2.9 Hz), 43.10, 42.43, 39.74, 38.80, 36.41, 33.26, 31.51, 30.92, 29.49, 27.79, 26.15 (d, *J* = 19.4 HZ), 22.56, 22.47, 19.83, 19.56, 17.95,

Chapter 5 | Synthesis and cytotoxic activity of novel UA derivatives

17.17, 16.66, 16.53. MS (DI-ESI) (m/z): 587.3 (100 %) [M+H]⁺, 567.2 (21.3%). Anal. Calcd for C₃₉H₅₁FO₃·0.2H₂O: C, 79.34; H, 8.77. Found: C, 79.35; H, 8.78.

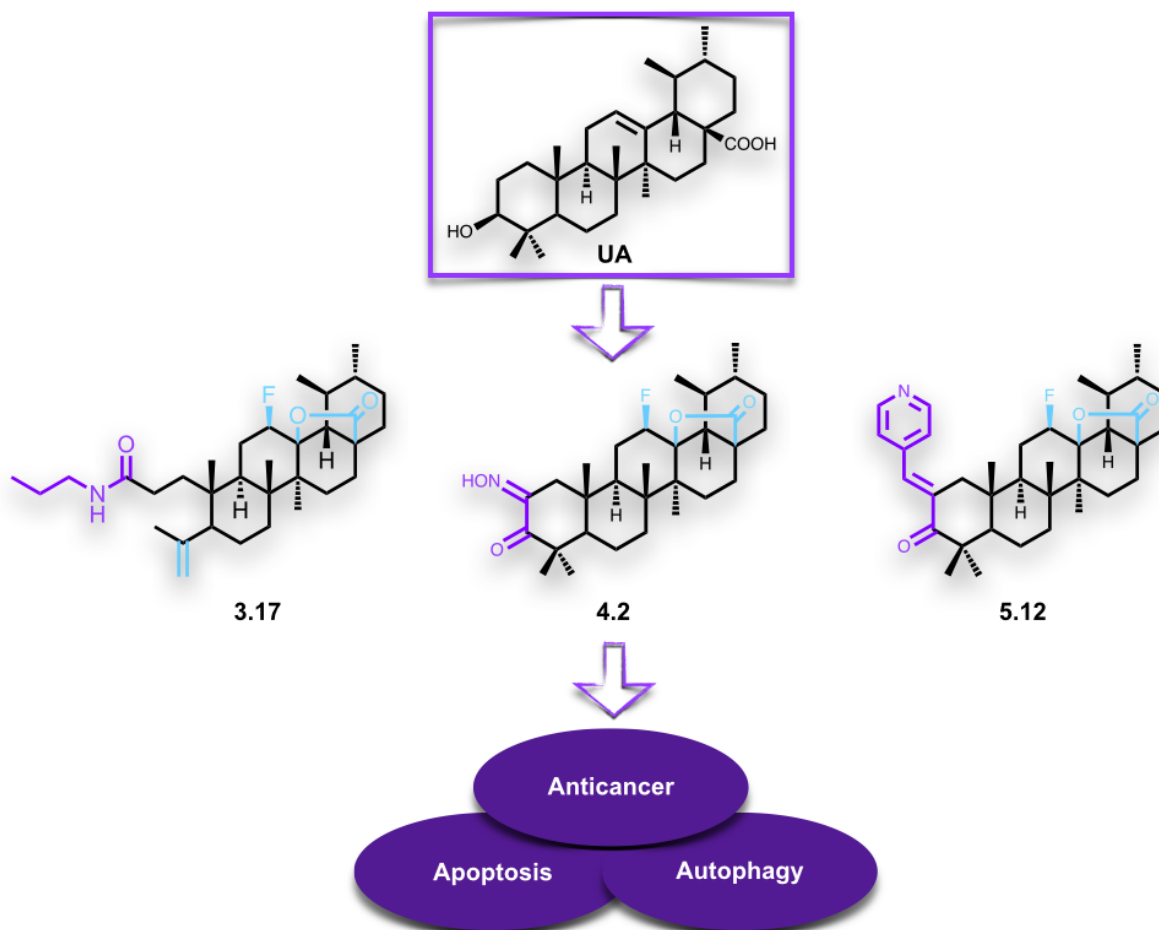
5.4.2. Biology

5.4.2.1. Cell lines and culture, materials and assays

All cell lines, materials and assays were used and performed according to the procedures described in chapter 3.

Chapter 6

Concluding remarks



Chapter 6 | Concluding remarks

Non-small cell lung cancer (NSCLC) is a leading cause of cancer-related deaths worldwide. Despite novel therapeutic strategies, the overall 5-year survival rate in many countries remains less than 15%. These statistics highlight the need for the development of new clinical agents with novel mechanisms of action.

Taking into account the complexity underlying lung cancer, it has been proposed the development of multifunctional drugs that aim at targeting cancer as a complex disease, by modulating the activity of different regulatory networks, and affecting as many hallmarks of cancer as possible.

Natural pentacyclic triterpenoids, particularly ursane-type, have interesting biological properties that could be explored for the design and synthesis of novel multifunctional anticancer derivatives. Ursolic acid (**UA**) can be considered a potential lead because of its promising multitarget anticancer activity, low toxicity and commercial availability.

The main objective of this PhD thesis was to develop new anticancer agents containing an ursane scaffold, as well as to evaluate their anticancer activity against NSCLC cell lines, in 2D and 3D culture models. Moreover, the preliminary mechanism of action responsible for the anticancer activity of the most active derivatives was explored.

This dissertation included three major semisynthetic strategies:

- 1) Synthesis of new ursane derivatives by expansion and cleavage of A-ring, and introduction of nitrogen-containing groups (chapter 3);
- 2) Synthesis of new ursane derivatives with oxime and nitrile groups (chapter 4);
- 3) Synthesis of new ursane derivatives with esters and α,β -unsaturated carbonyl systems (chapter 5).

The semisynthetic strategies selected allowed the successful preparation of new derivatives, with good yields, using simple, cost-effective, and easy-to-handle methods. The novel ursane derivatives were fully characterized by IR, MS and NMR (1D and 2D) techniques, with identification of the exact mass and characteristic signals.

Chapter 6 | Concluding remarks

The newly synthesized derivatives were tested for their ability to inhibit the proliferation of NSCLC cell lines, in monolayer (2D) and spheroid (3D) culture models.

Based on the anticancer results obtained in the monolayer culture model, the structure-activity relationships (SAR) demonstrated that the most active compounds displayed a cleaved A-ring coupled with a secondary amide bearing a small alkyl side chain (**3.17**), an oxime group conjugated with a carbonyl function at A-ring (**4.2**), a cleaved A-ring bearing nitrile and imidazole groups (**4.16**), and an α,β -unsaturated carbonyl system, with an exocyclic double bond, conjugated with a heteroaromatic ring at A-ring (**5.12**). Some of these derivatives maintained the cytotoxicity even in 3D culture systems, albeit a slight increase in their IC₅₀ values. These results demonstrate that the anticancer activity of the ursane scaffold can be improved in order to obtain novel anticancer agents.

The preliminary studies on the anticancer mechanism demonstrated that the newly synthesized **UA** derivatives are able to induce cell death via apoptosis and autophagy. Furthermore, these compounds appear to inherit the multitarget potential of **UA**, by affecting the levels of different proteins involved in the process of cell death. Interestingly, while **UA** is able to induce both extrinsic and intrinsic pathways, these derivatives appear to only activate the extrinsic pathway of apoptosis.

Even though compound **5.12** was not active in the spheroid culture model, it was interesting to understand its mechanism of action on the monolayer culture model, where it seems modulate several RTKs and the PI3K/Akt/mTOR pathway, which have been found deregulated in several types of cancer. The scaffold of this compound should be further explored in order to improve its activity in the 3D culture model.

To gain deeper insight into the anticancer mechanism, the most active compounds have been selected for further *in vitro* studies, particularly with the spheroid culture model in order to evaluate if the same mechanism of action is responsible for the anticancer activity observed, as well as to further explore the molecular pathways involved in their cytotoxicity. Moreover, these

Chapter 6 | Concluding remarks

derivatives should be tested against a non-tumor cell line in order to evaluate their selectivity. Additionally, an *in vivo* study should be performed to validate the use of these compounds as anticancer agents.

In summary, this thesis highlights several semisynthetic strategies that can successfully improve the anticancer activity of **UA**, and simultaneously maintain the multitarget potential of the parent compound. This work also validates the natural product **UA** as a promising lead for the development of new anti-NSCLC agents.

Chapter 7

References



Chapter 7 | References

- 1 National Cancer Institute. What Is Cancer?. *NCI*. <http://www.cancer.gov/about-cancer/what-is-cancer> (2015). Accessed May 23, 2016.
- 2 Hahn, W. C. & Weinberg, R. A. Rules for making human tumor cells. *The New England Journal of Medicine* **347**, 1593–1603, (2012).
- 3 Ferlay, J., Soerjomataram, I., Dikshit, R., Eser, S., Mathers, C., Rebelo, M., Parkin, D. M., Forman, D. & Bray, F. Cancer incidence and mortality worldwide: Sources, methods and major patterns in GLOBOCAN 2012. *International Journal of Cancer* **136**, E359–E386, (2015).
- 4 International Agency for Research on Cancer, WHO. GLOBOCAN 2012: Estimate Cancer Incidence, Mortality and Prevalence Worldwide in 2012. *WHO*. http://globocan.iarc.fr/Pages/fact_sheets_population.aspx. (2012). Accessed May 26, 2016.
- 5 Hanahan, D. & Weinberg, R. A. The Hallmarks of Cancer. *Cell* **100**, 57–70, (2000).
- 6 Hanahan, D. & Weinberg, R. A. Hallmarks of cancer: the next generation. *Cell* **144**, 646–674, (2011).
- 7 Albini, A. & Sporn, M. B. The tumour microenvironment as a target for chemoprevention. *Nature Reviews Cancer* **7**, 139–147, (2007).
- 8 Hengartner, M. O. The biochemistry of apoptosis. *Nature* **407**, 770–776, (2000).
- 9 Ouyang, L., Shi, Z., Zhao, S., Wang, F. T., Zhou, T. T., Liu, B. & Bao, J. K. Programmed cell death pathways in cancer: a review of apoptosis, autophagy and programmed necrosis. *Cell Proliferation* **45**, 487–498, (2012).
- 10 Elmore, S. Apoptosis: a review of programmed cell death. *Toxicologic Pathology* **35**, 495–516, (2007).
- 11 Taylor, R. C., Cullen, S. P. & Martin, S. J. Apoptosis: controlled demolition at the cellular level. *Nature Reviews Molecular Cell Biology* **9**, 231–241, (2008).
- 12 Reed, J. C. Mechanisms of Apoptosis. *American Journal of Pathology* **157**, 1415–1430, (2000).
- 13 Wong, R. S. Apoptosis in cancer: from pathogenesis to treatment. *Journal of Experimental & Clinical Cancer Research* **30**, 87 (2011).
- 14 Lowe, S. W. & Lin, A. W. Apoptosis in cancer. *Carcinogenesis* **21**, 485–495, (2000).
- 15 Vermeulen, K., Van Bockstaele, D. R. & Berneman, Z. N. Apoptosis: mechanisms and relevance in cancer. *Annals of Hematology* **84**, 627–639, (2005).
- 16 Ghobrial, I. M., Witzig, T. E. & Adjei, A. A. Targeting Apoptosis Pathways in Cancer Therapy. *CA: A Cancer Journal for Clinicians* **55**, 178–194, (2005).

Chapter 7 | References

- 17 Plati, J., Bucur, O. & Khosravi-Far, R. Dysregulation of apoptotic signaling in cancer: molecular mechanisms and therapeutic opportunities. *Journal of Cellular Biochemistry* **104**, 1124–1149, (2008).
- 18 Rastogi, R. P. & Sinha, R. P. Apoptosis: Molecular mechanisms and pathogenicity. *EXCLI Journal* **8**, 155–181, (2009).
- 19 Riedl, S. J. & Shi, Y. Molecular mechanisms of caspase regulation during apoptosis. *Nature Reviews Molecular Cell Biology* **5**, 897–907, (2004).
- 20 Hassan, M., Watari, H., AbuAlmaaty, A., Ohba, Y. & Sakuragi, N. Apoptosis and molecular targeting therapy in cancer. *BioMed Research International* **2014**, 150845, (2014).
- 21 Reed, J. C. Apoptosis-targeted therapies for cancer. *Cancer Cell* **3**, 17–22, (2003).
- 22 Brown, J. M. & Attardi, L. D. The role of apoptosis in cancer development and treatment response. *Nature Reviews Cancer* **5**, 213–237, (2005).
- 23 Kasibhatla, S. & Tseng, B. Why Target Apoptosis in Cancer Treatment *Molecular Cancer Therapeutics* **2**, 573–580, (2003).
- 24 Ferreira, C. G., Epping, M., Kruyt, F. A. E. & Giaccone, G. Apoptosis: Target of Cancer Therapy. *Clinical Cancer Research* **8**, 2024–2034, (2002).
- 25 Denton, D., Xu, T. & Kumar, S. Autophagy as a pro-death pathway. *Immunology & Cell Biology* **93**, 35–42, (2015).
- 26 Wirawan, E., Vanden Berghe, T., Lippens, S., Agostinis, P. & Vandenabeele, P. Autophagy: for better or for worse. *Cell Research* **22**, 43–61, (2012).
- 27 Tsujimoto, Y. & Shimizu, S. Another way to die: autophagic programmed cell death. *Cell Death & Differentiation* **12 Suppl 2**, 1528–1534, (2005).
- 28 Fulda, S. & Kogel, D. Cell death by autophagy: emerging molecular mechanisms and implications for cancer therapy. *Oncogene* **34**, 5105–5113, (2015).
- 29 Shintani, T. & Klionsky, D. J. Autophagy in health and disease: a double-edged sword. *Science* **306**, 990–995, (2004).
- 30 Li, X., Xu, H. L., Liu, Y. X., An, N., Zhao, S. & Bao, J. K. Autophagy modulation as a target for anticancer drug discovery. *Acta Pharmacologica Sinica* **34**, 612–624, (2013).
- 31 Jain, M. V., Paczulla, A. M., Klonisch, T., Dimgba, F. N., Rao, S. B., Roberg, K., Schweizer, F., Lengerke, C., Davoodpour, P., Palicharla, V. R., Maddika, S. & Los, M. Interconnections between apoptotic, autophagic and necrotic pathways: implications for cancer therapy development. *Journal of Cellular and Molecular Medicine* **17**, 12–29, (2013).

Chapter 7 | References

- 32 Wood, S. L., Pernemalm, M., Crosbie, P. A. & Whetton, A. D. Molecular histology of lung cancer: from targets to treatments. *Cancer Treatment Reviews* **41**, 361–375, (2015).
- 33 Reck, M., Heigener, D. F., Mok, T., Soria, J.-C. & Rabe, K. F. Management of non-small-cell lung cancer: recent developments. *The Lancet* **382**, 709–719, (2013).
- 34 Rami-Porta, R., Crowley, J. J. & Goldstraw, P. The Revised TNM Staging System for Lung Cancer. *Annals of Thoracic and Cardiovascular Surgery* **15**, 4–9, (2009).
- 35 Nana-Sinkam, S. P. & Powell, C. A. Molecular biology of lung cancer: Diagnosis and management of lung cancer, 3rd ed: American College of Chest Physicians evidence-based clinical practice guidelines. *Chest* **143**, e30S–39S, (2013).
- 36 Kan, Z., Jaiswal, B. S., Stinson, J., Janakiraman, V., Bhatt, D., Stern, H. M., Yue, P., Haverty, P. M., Bourgon, R., Zheng, J., Moorhead, M., Chaudhuri, S., Tomsho, L. P., Peters, B. A., Pujara, K., Cordes, S., Davis, D. P., Carlton, V. E., Yuan, W., Li, L., Wang, W., Eigenbrot, C., Kaminker, J. S., Eberhard, D. A., Waring, P., Schuster, S. C., Modrusan, Z., Zhang, Z., Stokoe, D., de Sauvage, F. J., Faham, M. & Seshagiri, S. Diverse somatic mutation patterns and pathway alterations in human cancers. *Nature* **466**, 869–873, (2010).
- 37 Cufer, T. & Knez, L. Update on systemic therapy of advanced non-small-cell lung cancer. *Expert Review of Anticancer Therapy* **14**, 1189–1203, (2014).
- 38 Salgia, R. Diagnostic challenges in non-small-cell lung cancer: an integrated medicine approach. *Future Oncology* **11**, 489–500, (2015).
- 39 Rosell, R., Bivona, T. G. & Karachaliou, N. Genetics and biomarkers in personalisation of lung cancer treatment. *The Lancet* **382**, 720–731, (2013).
- 40 Sanchez-Cespedes, M., Parrella, P., Esteller, M., Nomoto, S., Trink, B., Engles, J. M., Westra, W. H., Herman, J. G. & Sidransky, D. Inactivation of LKB1/STK11 Is a Common Event in Adenocarcinomas of the Lung. *Cancer Research* **62**, 3659–3662, (2002).
- 41 Ding, L., Getz, G., Wheeler, D. A., Mardis, E. R., McLellan, M. D., Cibulskis, K., Sougnez, C., Greulich, H., Muzny, D. M., Morgan, M. B., Fulton, L., Fulton, R. S., Zhang, Q., Wendl, M. C., Lawrence, M. S., Larson, D. E., Chen, K., Dooling, D. J., Sabo, A., Hawes, A. C., Shen, H., Jhangiani, S. N., Lewis, L. R., Hall, O., Zhu, Y., Mathew, T., Ren, Y., Yao, J., Scherer, S. E., Clerc, K., Metcalf, G. A., Ng, B., Milosavljevic, A., Gonzalez-Garay, M. L., Osborne, J. R., Meyer, R., Shi, X., Tang, Y., Koboldt, D. C., Lin, L., Abbott, R., Miner, T. L., Pohl, C., Fewell, G., Haipek, C., Schmidt, H., Dunford-Shore, B. H., Kraja, A., Crosby, S. D., Sawyer, C. S., Vickery, T., Sander, S., Robinson, J., Winckler, W., Baldwin, J., Chirieac, L. R., Dutt, A., Fennell, T., Hanna, M., Johnson, B. E., Onofrio, R. C., Thomas, R. K., Tonon, G., Weir, B. A., Zhao, X., Ziaugra, L., Zody, M. C., Giordano, T., Orringer, M. B., Roth, J. A., Spitz, M. R., Wistuba, II, Ozenberger, B., Good, P. J., Chang, A. C., Beer, D. G., Watson, M. A., Ladanyi, M., Broderick, S., Yoshizawa, A., Travis, W. D., Pao, W., Province, M. A., Weinstock, G. M., Varmus, H. E., Gabriel, S. B., Lander, E. S., Gibbs, R. A., Meyerson, M. & Wilson, R. K. Somatic mutations affect key pathways in lung adenocarcinoma. *Nature* **455**, 1069–1075, (2008).

Chapter 7 | References

- 42 Gill, R. K., Yang, S. H., Meerzaman, D., Mechanic, L. E., Bowman, E. D., Jeon, H. S., Roy Chowdhuri, S., Shakoori, A., Dracheva, T., Hong, K. M., Fukuoka, J., Zhang, J. H., Harris, C. C. & Jen, J. Frequent homozygous deletion of the LKB1/STK11 gene in non-small cell lung cancer. *Oncogene* **30**, 3784–3791, (2011).
- 43 Korsse, S. E., Peppelenbosch, M. P. & van Veelen, W. Targeting LKB1 signaling in cancer. *Biochimica et Biophysica Acta* **1835**, 194–210, (2013).
- 44 Matsumoto, S., Iwakawa, R., Takahashi, K., Kohno, T., Nakanishi, Y., Matsuno, Y., Suzuki, K., Nakamoto, M., Shimizu, E., Minna, J. D. & Yokota, J. Prevalence and specificity of LKB1 genetic alterations in lung cancers. *Oncogene* **26**, 5911–5918, (2007).
- 45 NICE, National Institute for Health and Care Excellence. NICE guideline for Lung Cancer: diagnosis and management. *NICE*. <http://www.nice.org.uk/guidance/cg121/resources/lung-cancer-diagnosis-and-management-35109444863941>. (2011). Accessed May 31, 2016.
- 46 Felip, E., Gridelli, C., Baas, P., Rosell, R., Stahel, R. & Panel, M. Metastatic non-small-cell lung cancer: consensus on pathology and molecular tests, first-line, second-line, and third-line therapy: 1st ESMO Consensus Conference in Lung Cancer; Lugano 2010. *Annals of Oncology* **22**, 1507–1519, (2011).
- 47 Pinn, S. New drug therapies, dedicated specialists and desperately-ill patients-but who will fly the flag for service developments in lung cancer as NHS budgets come under pressure? *Ecancermedicalscience* **5**, 209, (2011).
- 48 National Cancer Institute. Small Cell Lung Cancer Treatment (PDQ[®]) - Health Profession version. *NIH*. <http://www.cancer.gov/types/lung/hp/small-cell-lung-treatment-pdq>. (2016). Accessed June 7, 2016.
- 49 Jadus, M. R., Natividad, J., Mai, A., Ouyang, Y., Lambrecht, N., Szabo, S., Ge, L., Hoa, N. & Dacosta-Iyer, M. G. Lung cancer: a classic example of tumor escape and progression while providing opportunities for immunological intervention. *Clinical & Developmental Immunology* **2012**, 160724, (2012).
- 50 Gurib-Fakim, A. Medicinal plants: traditions of yesterday and drugs of tomorrow. *Molecular Aspects of Medicine* **27**, 1–93, (2006).
- 51 Newman, D. J. & Cragg, G. M. Natural Products as Sources of New Drugs from 1981 to 2014. *Journal of Natural Products*, **79**, 629–661(2016).
- 52 Cragg, G. M. & Newman, D. J. Biodiversity: A continuing source of novel drug leads. *Pure and Applied Chemistry* **77**, (2005).
- 53 Rouhi, A. M. Rediscovering Natural Products. *Chemical & Engineering News Archive* **81**, 77–91, (2003).
- 54 Demain, A. L. & Vaishnav, P. Natural products for cancer chemotherapy. *Microbial Biotechnology* **4**, 687–699, (2011).

Chapter 7 | References

- 55 Cragg, G. M., Grothaus, P. G. & Newman, D. J. Impact of Natural Products on Developing New Anti-Cancer Agents. *Chemical Reviews* **109**, 3012–3043, (2009).
- 56 Balunas, M. J. & Kinghorn, A. D. Drug discovery from medicinal plants. *Life sciences* **78**, 431–441, (2005).
- 57 Mann, J. Natural products in cancer chemotherapy: past, present and future. *Nature Reviews Cancer* **2**, 143–148, (2002).
- 58 Liby, K. T., Yore, M. M. & Sporn, M. B. Triterpenoids and rexinoids as multifunctional agents for the prevention and treatment of cancer. *Nature Reviews Cancer* **7**, 357–369, (2007).
- 59 Pfisterer, P. H., Wolber, G., Efferth, T., Rollinger, J. M. & Stuppner, H. Natural Products in Structure-Assisted Design of Molecular Cancer Therapeutics. *Current Pharmaceutical Design* **16**, 1718–1741, (2010).
- 60 Cheng, A.-X., Lou, Y.-G., Mao, Y.-B., Lu, S., Wang, L.-J. & Chen, X.-Y. Plant Terpenoids: Biosynthesis and Ecological Functions. *Journal of Integrative Plant Biology* **49**, 179–186, (2007).
- 61 Oldfield, E. & Lin, F. Y. Terpene biosynthesis: modularity rules. *Angewandte Chemie International Edition in English* **51**, 1124–1137, (2012).
- 62 Kirby, J. & Keasling, J. D. Biosynthesis of plant isoprenoids: perspectives for microbial engineering. *Annual Review of Plant Biology* **60**, 335–355, (2009).
- 63 Kuttan, G., Pratheeshkumar, P., Manu, K. A. & Kuttan, R. Inhibition of tumor progression by naturally occurring terpenoids. *Pharmaceutical Biology* **49**, 995–1007, (2011).
- 64 Sawai, S. & Saito, K. Triterpenoid biosynthesis and engineering in plants. *Frontiers in Plant Science* **2**, 25, (2011).
- 65 Salminen, A., Lehtonen, M., Suuronen, T., Kaarniranta, K. & Huuskonen, J. Terpenoids: natural inhibitors of NF-kappaB signaling with anti-inflammatory and anticancer potential. *Cellular and Molecular Life Sciences* **65**, 2979–2999, (2008).
- 66 Xu, R., Fazio, G. C. & Matsuda, S. P. T. On the origins of triterpenoid skeletal diversity. *Phytochemistry* **65**, 261–291, (2004).
- 67 Salvador, J. A. R., Moreira, V. M., Goncalves, B. M., Leal, A. S. & Jing, Y. Ursane-type pentacyclic triterpenoids as useful platforms to discover anticancer drugs. *Natural Product Reports* **29**, 1463–1479, (2012).
- 68 Thimmappa, R., Geisler, K., Louveau, T., O'Maille, P. & Osbourn, A. Triterpene biosynthesis in plants. *Annual Review of Plant Biology* **65**, 225–257, (2014).
- 69 Sheng, H. & Sun, H. Synthesis, biology and clinical significance of pentacyclic triterpenes: a multi-target approach to prevention and treatment of metabolic and vascular diseases. *Natural Product Reports* **28**, 543–593, (2011).

Chapter 7 | References

- 70 Salvador, J. A. R., Leal, A. S., Alho, D. P. S., Gonçalves, B. M. F., Valdeira, A. S., Mendes, V. I. S. & Jing, Y. Highlights of Pentacyclic Triterpenoids in the Cancer Settings, in *Studies in Natural Product Chemistry*. In: Atta-ur-Rahman Ed. Elsevier. Ch. 2, 41, 33–73, (2014).
- 71 Safe, S. H., Prather, P. L., Brents, L. K., Chadalapaka, G. & Jutooru, I. Unifying Mechanisms of Action of the Anticancer Activities of Triterpenoids and Synthetic Analogs. *Anticancer Agents in Medicinal Chemistry* **12**, 1211–1220, (2012).
- 72 Kim, J., Jang, D. S., Kim, H. & Kim, J. S. Anti-lipase and lipolytic activities of ursolic acid isolated from the roots of *Actinidia arguta*. *Archives of Pharmacal Research* **32**, 983–987, (2009).
- 73 Caligiani, A., Malavasi, G., Palla, G., Marseglia, A., Tognolini, M. & Bruni, R. A simple GC-MS method for the screening of betulinic, corosolic, maslinic, oleanolic and ursolic acid contents in commercial botanicals used as food supplement ingredients. *Food Chemistry* **136**, 735–741, (2013).
- 74 Simon, A., Najid, A., Chulia, A. J., Delage, C. & Rigaud, M. Inhibition of lipoxygenase activity and HL60 leukemic cell proliferation by ursolic acid isolated from heather flowers (*Calluna vulgaris*). *Biochimica et Biophysica Acta* **1125**, 68–72, (1992).
- 75 Chowdhury, S. S., Islam, M. N., Jung, H. A. & Choi, J. S. In vitro antidiabetic potential of the fruits of *Crataegus pinnatifida*. *Research in Pharmaceutical Sciences* **9**, 11–22, (2014).
- 76 Siddiqui, B. S., Sultana, I. & Begum, S. Triterpenoidal constituents from *Eucalyptus camaldulensis* var. *obtusa* leaves. *Phytochemistry* **54**, 861–865, (2000).
- 77 Janicsák, G., Veres, K., Zoltán Kakasy, A. & Máthé, I. Study of the oleanolic and ursolic acid contents of some species of the Lamiaceae. *Biochemical Systematics and Ecology* **34**, 392–396, (2006).
- 78 He, Q. Q., Yang, L., Zhang, J. Y., Ma, J. N. & Ma, C. M. Chemical constituents of gold-red apple and their alpha-glucosidase inhibitory activities. *Journal of Food Science* **79**, C1970–1983, (2014).
- 79 Awad, R., Muhammad, A., Durst, T., Trudeau, V. L. & Arnason, J. T. Bioassay-guided fractionation of lemon balm (*Melissa officinalis* L.) using an in vitro measure of GABA transaminase activity. *Phytotherapy Research* **23**, 1075–1081, (2009).
- 80 Banno, N., Akihisa, T., Tokuda, H., Yasukawa, K., Higashihara, H., Ukiya, M., Watanabe, K., Kimura, Y., Hasegawa, J. & Nishino, H. Triterpene acids from the leaves of *Perilla frutescens* and their anti-inflammatory and antitumor-promoting effects. *Bioscience, Biotechnology, and Biochemistry* **68**, 85–90, (2004).
- 81 Ringbom, T., Segura, L., Noreen, Y., Perera, P. & Bohlin, L. Ursolic Acid from *Plantago major*, a Selective Inhibitor of Cyclooxygenase-2 Catalyzed Prostaglandin Biosynthesis. *Journal of Natural Products* **61**, 1212–1215, (1998).

Chapter 7 | References

- 82 Yamai, H., Sawada, N., Yoshida, T., Seike, J., Takizawa, H., Kenzaki, K., Miyoshi, T., Kondo, K., Bando, Y., Ohnishi, Y. & Tangoku, A. Triterpenes augment the inhibitory effects of anticancer drugs on growth of human esophageal carcinoma cells in vitro and suppress experimental metastasis in vivo. *International Journal of Cancer* **125**, 952–960, (2009).
- 83 Machado, D. G., Neis, V. B., Balen, G. O., Colla, A., Cunha, M. P., Dalmarco, J. B., Pizzolatti, M. G., Prediger, R. D. & Rodrigues, A. L. Antidepressant-like effect of ursolic acid isolated from *Rosmarinus officinalis* L. in mice: evidence for the involvement of the dopaminergic system. *Pharmacology Biochemistry and Behavior* **103**, 204–211, (2012).
- 84 Rodrigues, M. R., Kanazawa, L. K., das Neves, T. L., da Silva, C. F., Horst, H., Pizzolatti, M. G., Santos, A. R., Baggio, C. H. & Werner, M. F. Antinociceptive and anti-inflammatory potential of extract and isolated compounds from the leaves of *Salvia officinalis* in mice. *Journal of Ethnopharmacology* **139**, 519–526, (2012).
- 85 Schwaiger, S., Zeller, I., Polzelbauer, P., Frotschnig, S., Laufer, G., Messner, B., Pieri, V., Stuppner, H. & Bernhard, D. Identification and pharmacological characterization of the anti-inflammatory principal of the leaves of dwarf elder (*Sambucus ebulus* L.). *Journal of Ethnopharmacology* **133**, 704–709, (2011).
- 86 Huang, Y., Nikolic, D., Pendland, S., Doyle, B. J., Locklear, T. D. & Mahady, G. B. Effects of cranberry extracts and ursolic acid derivatives on P-fimbriated *Escherichia coli*, COX-2 activity, pro-inflammatory cytokine release and the NF-kappa beta transcriptional response in vitro. *Pharmaceutical Biology* **47**, 18–25, (2009).
- 87 Wozniak, L., Skapska, S. & Marszalek, K. Ursolic Acid-A Pentacyclic Triterpenoid with a Wide Spectrum of Pharmacological Activities. *Molecules* **20**, 20614–20641, (2015).
- 88 Liu, J. Pharmacology of oleanolic acid and ursolic acid. *Journal of Ethnopharmacology* **49**, 57–68, (1995).
- 89 Kashyap, D., Tuli, H. S. & Sharma, A. K. Ursolic acid (UA): A metabolite with promising therapeutic potential. *Life Sciences*, (2016).
- 90 Salvador, J. A. R. & Moreira, V. M. Semisynthetic Pentacyclic Triterpenoids in the cancer setting: Ursolic acid and its Derivatives, in *Pentacyclic Triterpenes as Promising Agents in Cancer*. In: Salvador, J. A. R. Ed. Nova Science Publishers. Ch. 8, 249–276 (2010).
- 91 Novotný, L., Vachálková, A. & Biggs, D. Ursolic acid: an anti-tumorigenic and chemopreventive activity. Minireview. *Neoplasma* **48**, 241–246, (2001).
- 92 Wang, X., Zhang, F., Yang, L., Mei, Y., Long, H., Zhang, X., Zhang, J., Qimuge, S. & Su, X. Ursolic acid inhibits proliferation and induces apoptosis of cancer cells in vitro and in vivo. *Journal of Biomedicine and Biotechnology* **2011**, 419343, (2011).
- 93 Xiang, F., Pan, C., Kong, Q., Wu, R., Jiang, J., Zhan, Y., Xu, J., Gu, X. & Kang, X. Ursolic Acid Inhibits the Proliferation of Gastric Cancer Cells by Targeting miR-133a. *Oncology Research* **22**, 267–273, (2014).

Chapter 7 | References

- 94 Huang, C. Y., Lin, C. Y., Tsai, C. W. & Yin, M. C. Inhibition of cell proliferation, invasion and migration by ursolic acid in human lung cancer cell lines. *Toxicology in Vitro* **25**, 1274–1280, (2011).
- 95 Huang, H.-C., Huang, C.-Y., Lin-Shiau, S.-Y. & Lin, J.-K. Ursolic acid inhibits IL-1 β or TNF- α -induced C6 glioma invasion through suppressing the association ZIP/p62 with PKC- ζ and downregulating the MMP-9 expression. *Molecular Carcinogenesis* **48**, 517–531, (2009).
- 96 Lin, J., Chen, Y., Wei, L., Hong, Z., Sferra, T. J. & Peng, J. Ursolic acid inhibits colorectal cancer angiogenesis through suppression of multiple signaling pathways. *International Journal of Oncology* **43**, 1666–1674, (2013).
- 97 Cardenas, C., Quesada, A. R. & Medina, M. A. Effects of ursolic acid on different steps of the angiogenic process. *Biochemical and Biophysical Research Communications* **320**, 402–408, (2004).
- 98 Gao, N., Cheng, S., Budhraj, A., Gao, Z., Chen, J., Liu, E. H., Huang, C., Chen, D., Yang, Z., Liu, Q., Li, P., Shi, X. & Zhang, Z. Ursolic acid induces apoptosis in human leukaemia cells and exhibits anti-leukaemic activity in nude mice through the PKB pathway. *British Journal of Pharmacology* **165**, 1813–1826, (2012).
- 99 Kim, K. H., Seo, H. S., Choi, H. S., Choi, I., Shin, Y. C. & Ko, S. G. Induction of apoptotic cell death by ursolic acid through mitochondrial death pathway and extrinsic death receptor pathway in MDA-MB-231 cells. *Archives of Pharmacal Research* **34**, 1363–1372, (2011).
- 100 Zhang, Y., Kong, C., Zeng, Y., Wang, L., Li, Z., Wang, H., Xu, C. & Sun, Y. Ursolic acid induces PC-3 cell apoptosis via activation of JNK and inhibition of Akt pathways in vitro. *Molecular Carcinogenesis* **49**, 374–385, (2010).
- 101 Lee, H.-Y., Chung, H.-Y., Kim, K.-H., Lee, J.-J. & Kim, K.-W. Induction of differentiation in the cultured F9 teratocarcinoma stem cells by triterpene acids. *Journal of Cancer Research and Clinical Oncology* **120**, 513–518, (1994).
- 102 Deng, L., Zhang, R., Tang, F., Li, C., Xing, Y.-Y. & Xi, T. Ursolic acid induces U937 cells differentiation by PI3K/Akt pathway activation. *Chinese Journal of Natural Medicines* **12**, 15–19, (2014).
- 103 Pathak, A. K., Bhutani, M., Nair, A. S., Ahn, K. S., Chakraborty, A., Kadara, H., Guha, S., Sethi, G. & Aggarwal, B. B. Ursolic acid inhibits STAT3 activation pathway leading to suppression of proliferation and chemosensitization of human multiple myeloma cells. *Molecular Cancer Research* **5**, 943–955, (2007).
- 104 Hsu, Y. L., Kuo, P. L. & Lin, C. C. Proliferative inhibition, cell-cycle dysregulation, and induction of apoptosis by ursolic acid in human non-small cell lung cancer A549 cells. *Life Sciences* **75**, 2303–2316, (2004).
- 105 Weng, H., Tan, Z. J., Hu, Y. P., Shu, Y. J., Bao, R. F., Jiang, L., Wu, X. S., Li, M. L., Ding, Q., Wang, X. A., Xiang, S. S., Li, H. F., Cao, Y., Tao, F. & Liu, Y. B. Ursolic acid

Chapter 7 | References

- induces cell cycle arrest and apoptosis of gallbladder carcinoma cells. *Cancer Cell International* **14**, 96–106, (2014).
- 106 Wang, J., Liu, L., Qiu, H., Zhang, X., Guo, W., Chen, W., Tian, Y., Fu, L., Shi, D., Cheng, J., Huang, W. & Deng, W. Ursolic acid simultaneously targets multiple signaling pathways to suppress proliferation and induce apoptosis in colon cancer cells. *PLoS One* **8**, e63872, (2013).
- 107 Shen, S., Zhang, Y., Zhang, R., Tu, X. & Gong, X. Ursolic acid induces autophagy in U87MG cells via ROS-dependent endoplasmic reticulum stress. *Chemico-Biological Interactions* **218**, 28–41, (2014).
- 108 Bonaccorsi, I., Altieri, F., Sciamanna, I., Oricchio, E., Grillo, C., Contartese, G. & Galati, E. M. Endogenous reverse transcriptase as a mediator of ursolic acid's anti-proliferative and differentiating effects in human cancer cell lines. *Cancer letters* **263**, 130–139, (2008).
- 109 Zheng, Q. Y., Li, P. P., Jin, F. S., Yao, C., Zhang, G. H., Zang, T. & Ai, X. Ursolic acid induces ER stress response to activate ASK1-JNK signaling and induce apoptosis in human bladder cancer T24 cells. *Cellular Signalling* **25**, 206–213, (2013).
- 110 Wang, J. S., Ren, T. N. & Xi, T. Ursolic acid induces apoptosis by suppressing the expression of FoxM1 in MCF-7 human breast cancer cells. *Medical Oncology* **29**, 10–15, (2012).
- 111 Yeh, C. T., Wu, C. H. & Yen, G. C. Ursolic acid, a naturally occurring triterpenoid, suppresses migration and invasion of human breast cancer cells by modulating c-Jun N-terminal kinase, Akt and mammalian target of rapamycin signaling. *Molecular Nutrition & Food Research* **54**, 1285–1295, (2010).
- 112 Li, Y., Lu, X., Qi, H., Li, X., Xiao, X. & Gao, J. Ursolic Acid Induces Apoptosis Through Mitochondrial Intrinsic Pathway and Suppression of ERK1/2 MAPK in HeLa Cells. *Journal of Pharmacological Sciences* **125**, 202–210, (2014).
- 113 Achiwa, Y., Hasegawa, K. & Udagawa, Y. Regulation of the phosphatidylinositol 3-kinase-Akt and the mitogen-activated protein kinase pathways by ursolic acid in human endometrial cancer cells. *Bioscience, Biotechnology, and Biochemistry* **71**, 31–37, (2007).
- 114 Prasad, S., Yadav, V. R., Sung, B., Reuter, S., Kannappan, R., Deorukhkar, A., Diagaradjane, P., Wei, C., Baladandayuthapani, V., Krishnan, S., Guha, S. & Aggarwal, B. B. Ursolic acid inhibits growth and metastasis of human colorectal cancer in an orthotopic nude mouse model by targeting multiple cell signaling pathways: chemosensitization with capecitabine. *Clinical Cancer Research* **18**, 4942–4953, (2012).
- 115 Cha, H. J., Bae, S. K., Lee, H. Y., Lee, O. H., Sato, H., Seiki, M., Park, B. C. & Kim, K. W. Anti-Invasive Activity of Ursolic Acid Correlates with the Reduced Expression of Matrix Metalloproteinase-9 (MMP-9) in HT1080 Human Fibrosarcoma Cells. *Cancer Research* **56**, 2281–2284, (1996).

Chapter 7 | References

- 116 Mizushima, Y., Iida, A., Ohta, K., Sugawara, F. & Sakaguchi, K. Novel triterpenoids inhibit both DNA polymerase and DNA topoisomerase. *Biochemical Journal* **350**, 757–763, (2000).
- 117 Son, H. S., Kwon, H. Y., Sohn, E. J., Lee, J. H., Woo, H. J., Yun, M., Kim, S. H. & Kim, Y. C. Activation of AMP-activated protein kinase and phosphorylation of glycogen synthase kinase3 beta mediate ursolic acid induced apoptosis in HepG2 liver cancer cells. *Phytotherapy Research* **27**, 1714–1722, (2013).
- 118 Lin, C. C., Huang, C. Y., Mong, M. C., Chan, C. Y. & Yin, M. C. Antiangiogenic potential of three triterpenic acids in human liver cancer cells. *Journal of Agricultural and Food Chemistry* **59**, 755–762, (2011).
- 119 Lauthier, F., Taillet, L., Trouillas, P., Delage, C. & Simon, A. Ursolic acid triggers calcium-dependent apoptosis in human Daudi cells. *Anti-Cancer Drugs* **11**, 737–745, (2000).
- 120 Wu, J., Zhao, S., Tang, Q., Zheng, F., Chen, Y., Yang, L., Yang, X., Li, L., Wu, W. & Hann, S. S. Activation of SAPK/JNK mediated the inhibition and reciprocal interaction of DNA methyltransferase 1 and EZH2 by ursolic acid in human lung cancer cells. *Journal of Experimental & Clinical Cancer Research* **34**, 99, (2015).
- 121 Liu, K., Guo, L., Miao, L., Bao, W., Yang, J., Li, X., Xi, T. & Zhao, W. Ursolic acid inhibits epithelial-mesenchymal transition by suppressing the expression of astrocyte-elevated gene-1 in human nonsmall cell lung cancer A549 cells. *Anticancer Drugs* **24**, 494–503, (2013).
- 122 Wang, W., Sui, H., Qi, C., Li, Q., Zhang, J., Wu, S., Mei, M., Lu, Y., Wan, Y., Chang, H. & Guo, P. Ursolic acid inhibits proliferation and reverses drug resistance of ovarian cancer stem cells by downregulating ABCG2 through suppressing the expression of hypoxia-inducible factor-1 α in vitro. *Oncology Reports* **36**, 428–440, (2016).
- 123 Song, Y. H., Jeong, S. J., Kwon, H. Y., Kim, B., Kim, S. H. K. & Yoo, D. Y. Ursolic Acid from *Oldenlandia diffusa* Induces Apoptosis via Activation of Caspases and Phosphorylation of Glycogen Synthase Kinase 3 Beta in SK-OV-3 Ovarian Cancer Cells. *Biological and Pharmaceutical Bulletin* **35**, 1022–1028, (2012).
- 124 Prasad, S., Yadav, V. R., Sung, B., Gupta, S. C., Tyagi, A. K. & Aggarwal, B. B. Ursolic acid inhibits the growth of human pancreatic cancer and enhances the antitumor potential of gemcitabine in an orthotopic mouse model through suppression of the inflammatory microenvironment. *Oncotarget* **7**, 13182–13196, (2016).
- 125 Li, J., Liang, X. & Yang, X. Ursolic acid inhibits growth and induces apoptosis in gemcitabine-resistant human pancreatic cancer via the JNK and PI3K/Akt/NF-kappaB pathways. *Oncology Reports* **28**, 501–510, (2012).
- 126 Meng, Y., Lin, Z. M., Ge, N., Zhang, D. L., Huang, J. & Kong, F. Ursolic Acid Induces Apoptosis of Prostate Cancer Cells via the PI3K/Akt/mTOR Pathway. *The American Journal of Chinese Medicine* **43**, 1471–1486, (2015).
- 127 Shanmugam, M. K., Manu, K. A., Ong, T. H., Ramachandran, L., Surana, R., Bist, P., Lim, L. H., Kumar, A. P., Hui, K. M. & Sethi, G. Inhibition of CXCR4/CXCL12 signaling

Chapter 7 | References

- axis by ursolic acid leads to suppression of metastasis in transgenic adenocarcinoma of mouse prostate model. *International Journal of Cancer* **129**, 1552–1563, (2011).
- 128 Aguiriano-Moser, V., Svejda, B., Li, Z. X., Sturm, S., Stuppner, H., Ingolic, E., Hoger, H., Siegl, V., Meier-Allard, N., Sadjak, A. & Pfragner, R. Ursolic acid from *Trailliaedoxa gracilis* induces apoptosis in medullary thyroid carcinoma cells. *Molecular Medicine Reports* **12**, 5003–5011, (2015).
- 129 Manu, K. A. & Kuttan, G. Ursolic acid induces apoptosis by activating p53 and caspase-3 gene expressions and suppressing NF-kappaB mediated activation of bcl-2 in B16F-10 melanoma cells. *International Immunopharmacology* **8**, 974–981, (2008).
- 130 Leng, S., Hao, Y., Du, D., Xie, S., Hong, L., Gu, H., Zhu, X., Zhang, J., Fan, D. & Kung, H. F. Ursolic acid promotes cancer cell death by inducing Atg5-dependent autophagy. *International Journal of Cancer* **133**, 2781–2790, (2013).
- 131 Chen, H., Gao, Y., Wang, A., Zhou, X., Zheng, Y. & Zhou, J. Evolution in medicinal chemistry of ursolic acid derivatives as anticancer agents. *European Journal of Medicinal Chemistry* **92**, 648–655, (2015).
- 132 Suh, N., Honda, T., Finlay, H. J., Barchowsky, A., Williams, C., Benoit, N. E., Xie, Q. W., Nathan, C., Gribble, G. W. & Sporn, M. B. Novel Triterpenoids Suppress Inducible Nitric Oxide Synthase (iNOS) and Inducible Cyclooxygenase (COX-2) in Mouse Macrophages. *Cancer Research* **58**, 717–723, (1998).
- 133 Najid, A., Simon, A., Cook, J., Chablerabinovitch, H., Delage, C., Chulia, A. J. & Rigaud, M. Characterization of Ursolic Acid as a Lipoxygenase and Cyclooxygenase Inhibitor Using Macrophages, Platelets and Differentiated HI-60 Leukemic-Cells. *FEBS Letters* **299**, 213–217, (1992).
- 134 Honda, T., Finlay, H. J., Gribble, G. W., Suh, N. & Sporn, M. B. New enone derivatives of oleanolic acid and ursolic acid as inhibitors of nitric oxide production in mouse macrophages. *Bioorganic & Medicinal Chemistry Letters* **7**, 1623–1628, (1997).
- 135 Honda, T. R., BV; Bore, L; Finlay, HJ; Favaloro, FG; Suh, N; Wang, YP; Sporn, MB; Gribble, GW. Synthetic Oleanane and Ursane Triterpenoids with Modified Rings A and C: A series of highly active inhibitors of nitric oxide production in mouse macrophages. *Journal of Medicinal Chemistry* **43**, 4233–4246, (2000).
- 136 Honda, T., Gribble, G. W., Suh, N., Finlay, H. J., Rounds, B. V., Bore, L., Favaloro Jr., F. G., Wang, Y. & Sporn, M. B. Novel Synthetic Oleanane and Ursane Triterpenoids with Various Enone Functionalities in Ring A as Inhibitors of Nitric Oxide Production in Mouse Macrophages. *Journal of Medicinal Chemistry* **43**, 1866–1877, (2000).
- 137 Chadalapaka, G., Jutooru, I., McAlees, A., Stefanac, T. & Safe, S. Structure-dependent inhibition of bladder and pancreatic cancer cell growth by 2-substituted glycyrrhetic and ursolic acid derivatives. *Bioorganic & Medicinal Chemistry Letters* **18**, 2633–2639, (2008).
- 138 Leal, A. S., Wang, R., Salvador, J. A. R. & Jing, Y. Synthesis of novel ursolic acid heterocyclic derivatives with improved abilities of antiproliferation and induction of p53,

Chapter 7 | References

- p21^{waf1} and NOXA in pancreatic cancer cells. *Bioorganic & medicinal chemistry* **20**, 5774–5786, (2012).
- 139 Leal, A. S., Wang, R., Salvador, J. A. R. & Jing, Y. Semisynthetic ursolic acid fluorolactone derivatives inhibit growth with induction of p21^(waf1) and induce apoptosis with upregulation of NOXA and downregulation of c-FLIP in cancer cells. *ChemMedChem* **7**, 1635–1646, (2012).
- 140 Ma, C. M., Cai, S. Q., Cui, J. R., Wang, R. Q., Tu, P. F., Hattori, M. & Daneshtalab, M. The cytotoxic activity of ursolic acid derivatives. *European Journal of Medicinal Chemistry* **40**, 582–589, (2005).
- 141 Tu, H. Y., Huang, A. M., Wei, B. L., Gan, K. H., Hour, T. C., Yang, S. C., Pu, Y. S. & Lin, C. N. Ursolic acid derivatives induce cell cycle arrest and apoptosis in NTUB1 cells associated with reactive oxygen species. *Bioorganic & Medicinal Chemistry* **17**, 7265–7274, (2009).
- 142 Bai, K. K., Chen, F. L., Yu, Z., Zheng, Y. Q., Li, Y. N. & Guo, Y. H. Synthesis of [3beta-acetoxy-urs-12-en-28-oyl]-1-monoglyceride and investigation on its anti-tumor effects against BGC-823. *Bioorganic & Medicinal Chemistry* **19**, 4043–4050, (2011).
- 143 Shao, J. W., Dai, Y. C., Xue, J. P., Wang, J. C., Lin, F. P. & Guo, Y. H. In vitro and in vivo anticancer activity evaluation of ursolic acid derivatives. *European Journal of Medicinal Chemistry* **46**, 2652–2661, (2011).
- 144 Meng, Y. Q., Liu, D., Cai, L. L., Chen, H., Cao, B. & Wang, Y. Z. The synthesis of ursolic acid derivatives with cytotoxic activity and the investigation of their preliminary mechanism of action. *Bioorganic & Medicinal Chemistry* **17**, 848–854, (2009).
- 145 Meng, Y., Song, Y., Yan, Z. & Xia, Y. Synthesis and in vitro cytotoxicity of novel ursolic acid derivatives. *Molecules* **15**, 4033–4040, (2010).
- 146 Liu, D., Meng, Y. Q., Zhao, J. & Chen, L. G. Synthesis and Anti-tumor Activity of Novel Amide Derivatives of Ursolic Acid. *Chemical Research in Chinese Universities* **24**, 42–46, (2008).
- 147 Meng, Y. Q., Zhang, L. F., Liu, D. Y., Liu, L. W., Zhang, Y. & Zhao, M. J. Synthesis and antitumor activity evaluation of novel ursolic acid derivatives. *Journal of Asian Natural Products Research* **18**, 280–288, (2016).
- 148 Hua, S. X., Huang, R. Z., Ye, M. Y., Pan, Y. M., Yao, G. Y., Zhang, Y. & Wang, H. S. Design, synthesis and in vitro evaluation of novel ursolic acid derivatives as potential anticancer agents. *European Journal of Medicinal Chemistry* **95**, 435–452, (2015).
- 149 Liu, M. C., Yang, S. J., Jin, L. H., Hu, D. Y., Xue, W., Song, B. A. & Yang, S. Synthesis and cytotoxicity of novel ursolic acid derivatives containing an acyl piperazine moiety. *European Journal of Medicinal Chemistry* **58**, 128–135, (2012).
- 150 Rashid, S., Dar, B. A., Majeed, R., Hamid, A. & Bhat, B. A. Synthesis and biological evaluation of ursolic acid-triazolyl derivatives as potential anti-cancer agents. *European Journal of Medicinal Chemistry* **66**, 238–245, (2013).

Chapter 7 | References

- 151 Chen, L., Qiu, W., Tang, J., Wang, Z. F. & He, S. Y. Synthesis and bioactivity of novel nitric oxide-releasing ursolic acid derivatives. *Chinese Chemical Letters* **22**, 413–416, (2011).
- 152 Dar, B. A., Lone, A. M., Shah, W. A. & Qurishi, M. A. Synthesis and screening of ursolic acid-benzylidene derivatives as potential anti-cancer agents. *European Journal of Medicinal Chemistry* **111**, 26–32, (2016).
- 153 Lin, R. X., Gong, L. L., Fan, L. M., Zhao, Z. K. & Yang, S. L. Role of ursolic acid chalcone, a synthetic analogue of ursolic acid, in inhibiting the properties of CD133⁺ sphere-forming cells in liver stem cells. *International Journal of Clinical and Experimental Pathology* **8**, 1427–1434, (2015).
- 154 Finlay, H. J., Honda, T., Gribble, G. W., Danielpour, D., Benoit, N. E., Suh, N., Williams, C. & Sporn, M. B. Novel A-ring cleaved analogs of oleanolic and ursolic acids which affect growth regulation in NRP.152 prostate cells. *Bioorganic & Medicinal Chemistry Letters* **7**, 1769–1772, (1997).
- 155 Pattabiraman, V. R. & Bode, J. W. Rethinking amide bond synthesis. *Nature* **480**, 471–479, (2011).
- 156 Roughley, S. D. & Jordan, A. M. The medicinal chemist's toolbox: an analysis of reactions used in the pursuit of drug candidates. *Journal of Medicinal Chemistry* **54**, 3451–3479, (2011).
- 157 Valeur, E. & Bradley, M. Amide bond formation: beyond the myth of coupling reagents. *Chemical Society Reviews* **38**, 606–631, (2009).
- 158 Ghose, A. K., Viswanadhan, V. N. & Wendoloski, J. J. A Knowledge-Based Approach in Designing Combinatorial or Medicinal Chemistry Libraries for Drug Discovery. 1. A Qualitative and Quantitative Characterization of Known Drug Databases. *Journal of Combinatorial Chemistry* **1**, 55–68, (1999).
- 159 Carey, J. S., Laffan, D., Thomson, C. & Williams, M. T. Analysis of the reactions used for the preparation of drug candidate molecules. *Organic & Biomolecular Chemistry* **4**, 2337–2347, (2006).
- 160 Dunetz, J. R., Magano, J. & Weisenburger, G. A. Large-Scale Applications of Amide Coupling Reagents for the Synthesis of Pharmaceuticals. *Organic Process Research & Development* **20**, 140–177, (2016).
- 161 Klose, J., Bienert, M., Mollenkopf, C., Wehle, D., Zhang, C.-w., Carpinoc, L. A. & Henklein, P. 2-Propanephosphonic acid anhydride (T3P)-mediated segment coupling and head-to-tail cyclization of sterically hindered peptides. *Chemical Communications*, 1847–1848, (1999).
- 162 Patterson, D. E., Powers, J. D., LeBlanc, M., Sharkey, T., Boehler, E., Irdam, E. & Osterhout, M. H. Development of a Practical Large-Scale Synthesis of Denaglipatin Tosylate. *Organic Process Research & Development* **13**, 900–906, (2009).

Chapter 7 | References

- 163 Sharnabai, K. M., Nagendra, G., Vishwanatha, T. M. & Sureshbabu, V. V. Efficient synthesis of N-protected amino/peptide Weinreb amides from T3P and DBU. *Tetrahedron Letters* **54**, 478–482, (2013).
- 164 Wissmann, H. & Kleiner, H.-J. New Peptide Synthesis. *Angewandte Chemie International Edition in English* **19**, 133–134, (1980).
- 165 Waghmare, A. A., Hindupur, R. M. & Pati, H. N. Propylphosphonic anhydride (T3P[®]): An expedient reagent for organic synthesis. *Review Journal of Chemistry* **4**, 53–131, (2014).
- 166 Meudt, A., Scherer, S. & Nerdinger, S. Process for preparing nitriles and isonitriles by dehydration reactions with propanephosphonic anhydride. US Patent 2007/0161813 A1, filled January 15, 2005 and issued July 12, 2007.
- 167 Meudt, A., Nerdinger, S. & Boehm, C. Process for preparing nitriles by elimination reactions. US Patent 7,939,688 B2, filled July 5, 2006 and issued May 10, 2011.
- 168 Bohm, H. J., Banner, D., Bendels, S., Kansy, M., Kuhn, B., Muller, K., Obst-Sander, U. & Stahl, M. Fluorine in medicinal chemistry. *Chembiochem* **5**, 637–643, (2004).
- 169 Gillis, E. P., Eastman, K. J., Hill, M. D., Donnelly, D. J. & Meanwell, N. A. Applications of Fluorine in Medicinal Chemistry. *Journal of Medicinal Chemistry* **58**, 8315–8359, (2015).
- 170 Shah, P. & Westwell, A. D. The role of fluorine in medicinal chemistry. *Journal of Enzyme Inhibition and Medicinal Chemistry* **22**, 527–540, (2007).
- 171 Hagmann, W. K. The Many Roles for Fluorine in Medicinal Chemistry. *Journal of Medicinal Chemistry* **51**, 4359–4369, (2008).
- 172 Swallow, S. Fluorine in medicinal chemistry. *Progress in Medicinal Chemistry* **54**, 65–133, (2015).
- 173 Wang, J., Sanchez-Rosello, M., Acena, J. L., del Pozo, C., Sorochinsky, A. E., Fustero, S., Soloshonok, V. A. & Liu, H. Fluorine in pharmaceutical industry: fluorine-containing drugs introduced to the market in the last decade (2001–2011). *Chemical Reviews* **114**, 2432–2506, (2014).
- 174 Isanbor, C. & O'Hagan, D. Fluorine in medicinal chemistry: A review of anti-cancer agents. *Journal of Fluorine Chemistry* **127**, 303–319, (2006).
- 175 Liang, T., Neumann, C. N. & Ritter, T. Introduction of fluorine and fluorine-containing functional groups. *Angewandte Chemie International Edition* **52**, 8214–8264, (2013).
- 176 Murphy, C. D. & Sandford, G. Recent advances in fluorination techniques and their anticipated impact on drug metabolism and toxicity. *Expert Opinion on Drug Metabolism & Toxicology* **11**, 589–599, (2015).
- 177 Kirk, K. L. Fluorination in Medicinal Chemistry: Methods, Strategies, and Recent Developments. *Organic Process Research & Development* **12**, 305–321, (2008).

Chapter 7 | References

- 178 Zhang, F. & Song, J. Z. A novel general method for preparation of α -fluoro- α -arylcarboxylic acid. Direct fluorination of silyl ketene acetals with Selectfluor®. *Tetrahedron Letters* **47**, 7641–7644, (2006).
- 179 Promega. *CellTiter-Blue® Cell Viability Assay Technical Bulletin*. Promega Corporation 1–15.
- 180 Riss, T. L., Moravec, R. A., Niles, A. L., Benink, H. A., Worzella, T. J. & Minor, L. Cell Viability Assays, in *Assay Guidance Manual*. In: Sittampalam, G. S., Coussens, N. P. & Nelson, H. Ed. Bethesda (MD): Eli Lilly & Company and the National Center for Advancing Translational Sciences (2016).
- 181 Yamada, K. M. & Cukierman, E. Modeling tissue morphogenesis and cancer in 3D. *Cell* **130**, 601–610, (2007).
- 182 Zanoni, M., Piccinini, F., Arienti, C., Zamagni, A., Santi, S., Polico, R., Bevilacqua, A. & Tesei, A. 3D tumor spheroid models for in vitro therapeutic screening: a systematic approach to enhance the biological relevance of data obtained. *Scientific Reports* **6**, 19103, (2016).
- 183 Weiswald, L. B., Bellet, D. & Dangles-Marie, V. Spherical cancer models in tumor biology. *Neoplasia* **17**, 1–15, (2015).
- 184 Kunz-Schughart, L. A., Freyer, J. P., Hofstaedter, F. & Ebner, R. The use of 3-D cultures for high-throughput screening: the multicellular spheroid model. *Journal of Biomolecular Screening* **9**, 273–285, (2004).
- 185 Hirschhaeuser, F., Menne, H., Dittfeld, C., West, J., Mueller-Klieser, W. & Kunz-Schughart, L. A. Multicellular tumor spheroids: an underestimated tool is catching up again. *Journal of Biotechnology* **148**, 3–15, (2010).
- 186 Thoma, C. R., Zimmermann, M., Agarkova, I., Kelm, J. M. & Krek, W. 3D cell culture systems modeling tumor growth determinants in cancer target discovery. *Advanced Drug Delivery Reviews* **69–70**, 29–41, (2014).
- 187 Hoffmann, O. I., Ilmberger, C., Magosch, S., Joka, M., Jauch, K. W. & Mayer, B. Impact of the spheroid model complexity on drug response. *Journal of Biotechnology* **205**, 14–23, (2015).
- 188 Stadler, M., Walter, S., Walzl, A., Kramer, N., Unger, C., Scherzer, M., Unterleuthner, D., Hengstschlager, M., Krupitza, G. & Dolznig, H. Increased complexity in carcinomas: Analyzing and modeling the interaction of human cancer cells with their microenvironment. *Seminars in Cancer Biology* **35**, 107–124, (2015).
- 189 Correa, R. J. M., DiMattia, G. E. & Shepherd, T. G. Primary Epithelial Ovarian Cancer Cells form Spheroids when Cultured on Corning® Ultra-Low Attachment Surfaces. *Corning*.
http://csmedia2.corning.com/LifeSciences/media/pdf/CLS_AN_127_Customer_appl_Primary_Epithelial_Ovarian_Cancer_Cells_Spheroids_Ultra_Low_Attach_Surface.pdf. Accessed June 22, 2016.

Chapter 7 | References

- 190 Promega. *CellTiter-Glo® Luminescent Cell Viability Assay Technical Bulletin*. Promega Corporation 1–14.
- 191 Vermes, I., Haanena, C., Steffens-Nakkena, H. & Reutellingspergerb, C. A novel assay for apoptosis Flow cytometric detection of phosphatidylserine expression on early apoptotic cells using fluorescein labelled Annexin V. *Journal of Immunological Methods* **184**, 39–51, (1995).
- 192 Gouill, S. L., Podar, K., Harousseau, J.-L. & Anderson, K. C. Mcl-1 Regulation and Its Role in Multiple Myeloma. *Cell Cycle* **3**, 1259–1262, (2014).
- 193 Paglin, S., Hollister, T., Delohery, T., Hackett, N., McMahon, M., Sphicas, E., Domingo, D. & Yahalom, J. A. Novel Response of Cancer Cells to Radiation Involves Autophagy and Formation of Acidic Vesicles. *Cancer Research* **61**, 439–444, (2001).
- 194 Yoshimori, T., Yamamoto, A., Moriyama, Y., Futai, M. & Tashiro, Y. Bafilomycin A1, a Specific Inhibitor of Vacuolar-type H⁺-ATPase, Inhibits Acidification and Protein Degradation in Lysosomes of Cultured Cells *The Journal of Biological Chemistry* **266**, 17707–17712, (1991).
- 195 Klionsky, D. J., Elazar, Z., Seglen, P. O. & Rubinsztein, D. C. Does bafilomycin A1 block the fusion of autophagosomes with lysosomes? *Autophagy* **4**, 849–850, (2014).
- 196 Glick, D., Barth, S. & Macleod, K. F. Autophagy: cellular and molecular mechanisms. *The Journal of Pathology* **221**, 3–12, (2010).
- 197 Barth, S., Glick, D. & Macleod, K. F. Autophagy: assays and artifacts. *The Journal of Pathology* **221**, 117–124, (2010).
- 198 Vellai, T. Autophagy genes and ageing. *Cell Death & Differentiation* **16**, 94–102, (2009).
- 199 Ruvinsky, I. & Meyuhas, O. Ribosomal protein S6 phosphorylation: from protein synthesis to cell size. *Trends in Biochemical Sciences* **31**, 342–348, (2006).
- 200 Fleming, F. F., Yao, L., Ravikumar, P. C., Funk, L. & Shook, B. C. Nitrile-containing pharmaceuticals: efficacious roles of the nitrile pharmacophore. *Journal of Medicinal Chemistry* **53**, 7902–7917, (2010).
- 201 Kalgutkar, A. S. & Dalvie, D. K. Drug discovery for a new generation of covalent drugs. *Expert Opinion on Drug Discovery* **7**, 561–581, (2012).
- 202 Hunt, J. T., Ding, C. Z., Batorsky, R., Bednarz, M., Bhide, R., Cho, Y., Chong, S., Chao, S., Gullo-Brown, J., Guo, P., Kim, S. H., Lee, F. Y. F., Leftheris, K., Miller, A., Mitt, T., Patel, M., Penhallow, B. A., Ricca, C., Rose, W. C., Schmidt, R., Slusarchyk, W. A., Vite, G. & Manne, V. Discovery of (R)-7-Cyano-2,3,4,5-tetrahydro-1-(1H-imidazol-4-ylmethyl)-3-(phenylmethyl)-4-(2-thienylsulfonyl)-1H-1,4-benzodiazepine (BMS-214662), a Farnesyltransferase Inhibitor with Potent Preclinical Antitumor Activity. *Journal of Medicinal Chemistry* **43**, 3587–3595, (2000).

Chapter 7 | References

- 203 Reid, T. S. & Beese, L. S. Crystal Structures of the Anticancer Clinical Candidates R115777 (Tipifarnib) and BMS-214662 Complexed with Protein Farnesyltransferase Suggest a Mechanism of FTI Selectivity. *Biochemistry* **43**, 6877–6884, (2004).
- 204 Fradet, Y. Bicalutamide (Casodex®) in the treatment of prostate cancer. *Expert Review of Anticancer Therapy* **4**, 37–48, (2014).
- 205 Berenyi, A., Minorics, R., Ivanyi, Z., Ocsovszki, I., Ducza, E., Thole, H., Messinger, J., Wolfling, J., Motyan, G., Mernyak, E., Frank, E., Schneider, G. & Zupko, I. Synthesis and investigation of the anticancer effects of estrone-16-oxime ethers in vitro. *Steroids* **78**, 69–78, (2013).
- 206 Choi, S. J., Lee, J. E., Jeong, S. Y., Im, I., Lee, S. D., Lee, E. J., Lee, S. K., Kwon, S. M., Ahn, S. G., Yoon, J. H., Han, S. Y., Kim, J. I. & Kim, Y. C. 5,5'-substituted indirubin-3'-oxime derivatives as potent cyclin-dependent kinase inhibitors with anticancer activity. *Journal of Medicinal Chemistry* **53**, 3696–3706, (2010).
- 207 Qu, H. E., Huang, R. Z., Yao, G. Y., Li, J. L., Ye, M. Y., Wang, H. S. & Liu, L. Synthesis and pharmacological evaluation of novel bisindole derivatives bearing oximes moiety: identification of novel proapoptotic agents. *European Journal of Medicinal Chemistry* **95**, 400–415, (2015).
- 208 Santos, R. C., Salvador, J. A.R., Cortes, R., Pachon, G., Marin, S. & Cascante, M. New betulinic acid derivatives induce potent and selective antiproliferative activity through cell cycle arrest at the S phase and caspase dependent apoptosis in human cancer cells. *Biochimie* **93**, 1065–1075, (2011).
- 209 Santos, R. C., Salvador, J. A. R., Marin, S., Cascante, M., Moreira, J. N. & Dinis, T. C. Synthesis and structure-activity relationship study of novel cytotoxic carbamate and N-acylheterocyclic bearing derivatives of betulin and betulinic acid. *Bioorganic & Medicinal Chemistry* **18**, 4385–4396, (2010).
- 210 Santos, R. C., Salvador, J. A. R., Marin, S. & Cascante, M. Novel semisynthetic derivatives of betulin and betulinic acid with cytotoxic activity. *Bioorganic & Medicinal Chemistry* **17**, 6241–6250, (2009).
- 211 Leal, A. S., Wang, R., Salvador, J. A. R. & Jing, Y. Synthesis of novel heterocyclic oleanolic acid derivatives with improved antiproliferative activity in solid tumor cells. *Organic & Biomolecular Chemistry* **11**, 1726–1738, (2013).
- 212 Bednarczyk-Cwynar, B., Zaprutko, L. & Froelich, A. Beckmann rearrangement of oxime obtained from oleanolic acid. Structure elucidation of the initial oxime. *Journal of Molecular Structure* **1053**, 115–121, (2013).
- 213 Galaiko, N. V., Nazarov, A. V., Tolmacheva, I. A., Slepukhin, P. A., Vikharev, Y. B., Maiorova, O. A. & Grishko, V. V. Synthesis of triterpene A-condensed azoles. *Chemistry of Heterocyclic Compounds* **50**, 65–75, (2014).
- 214 Huneck, S. Photochemische Umsetzungen, III; Triterpene, XI: Die Darstellung von 3-Oxo-2-diazo-lupen-(20(29)) sowie 3-Oxo-2-diazo-oleanen-(12)-säure-(28)-methylester

Chapter 7 | References

- und deren photochemische Umwandlung in A-Nor-Verbindungen. *Chemische Berichte* **98**, 2284–2290, (1965).
- 215 Tolmacheva, I. A., Nazarov, A. V., Maiorova, O. A. & Grishko, V. V. Synthesis of Lupane and 19 β ,28-epoxy-18 α -oleanane 2,3-seco-derivatives based on betulin. *Chemistry of Natural Compounds* **44**, 606–611, (2008).
- 216 Sommerwerk, S., Heller, L., Kuhfs, J. & Csuk, R. Urea derivatives of ursolic, oleanolic and maslinic acid induce apoptosis and are selective cytotoxic for several human tumor cell lines. *European Journal of Medicinal Chemistry* **119**, 1–16, (2016).
- 217 Ferris, A. F. α -Oximino Ketones. IV. The “Normal” and “Abnormal” Beckmann Rearrangements. *Journal of Organic Chemistry* **25**, 12–18, (1960).
- 218 Liby, K. T. & Sporn, M. B. Synthetic oleanane triterpenoids: multifunctional drugs with a broad range of applications for prevention and treatment of chronic disease. *Pharmacological Reviews* **64**, 972–1003, (2012).
- 219 Sporn, M. B., Liby, K. T., Yore, M. M., Fu, L., Lopchuk, J. M. & Gribble, G. W. New synthetic triterpenoids: potent agents for prevention and treatment of tissue injury caused by inflammatory and oxidative stress. *Journal of Natural Products* **74**, 537–545, (2011).
- 220 Yang, C. *LKB1 Deficient Non-small Cell Lung Cancer Cells are Vulnerable to Energy Stress Induced by ATP Depletion (Master of Science Thesis)*. The University of Texas Health Science Center at Houston, TX, USA. Retrieved from Library Digitalcommons@The Texas Medical Center 49 (2014).
- 221 Bazzaro, M., Anchoori, R. K., Mudiam, M. K., Issaenko, O., Kumar, S., Karanam, B., Lin, Z., Isaksson Vogel, R., Gavioli, R., Destro, F., Ferretti, V., Roden, R. B. & Khan, S. R. α,β -Unsaturated carbonyl system of chalcone-based derivatives is responsible for broad inhibition of proteasomal activity and preferential killing of human papilloma virus (HPV) positive cervical cancer cells. *Journal of Medicinal Chemistry* **54**, 449–456, (2011).
- 222 Priyadarsini, K. I. The chemistry of curcumin: from extraction to therapeutic agent. *Molecules* **19**, 20091–20112, (2014).
- 223 Rucker, H., Al-Rifai, N., Rasclé, A., Gottfried, E., Brodziak-Jarosz, L., Gerhauser, C., Dick, T. P. & Amslinger, S. Enhancing the anti-inflammatory activity of chalcones by tuning the Michael acceptor site. *Organic & Biomolecular Chemistry* **13**, 3040–3047, (2015).
- 224 Sun, J. F., Hou, G. G., Zhao, F., Cong, W., Li, H. J., Liu, W. S. & Wang, C. Synthesis, antiproliferative and multidrug resistance reversal activities of heterocyclic α,β -unsaturated carbonyl compounds. *Chemical Biology & Drug Design*, (2016).
- 225 Gonçalves, B. M. F., Salvador, J. A. R., Marín, S. & Cascante, M. Synthesis and biological evaluation of novel asiatic acid derivatives with anticancer activity. *RSC Advances* **6**, 3967–3985, (2016).
- 226 Perrin, C. L. & Chang, K. L. The Complete Mechanism of an Aldol Condensation. *The Journal of Organic Chemistry*, (2016).

Chapter 7 | References

- 227 Smith, M. B & March, J. *March's Organic Chemistry: Reactions, Mechanisms, and Structure*. Sixth edition. John Wiley & Sons (2006).
- 228 Wang, Z. Claisen-Schmidt Condensation, in *Comprehensive Organic Name Reactions and Reagents*. John Wiley & Sons, Ch. 145, 660–664 (2010).
- 229 Urban, M., Sarek, J., Klinot, J., Korinkova, G. & Hajduch, M. Synthesis of A-Seco Derivatives of Betulinic Acid with Cytotoxic Activity. *Journal of Natural Products* **67**, 1100–1105, (2004).
- 230 LoPiccolo, J., Blumenthal, G. M., Bernstein, W. B. & Dennis, P. A. Targeting the PI3K/Akt/mTOR pathway: effective combinations and clinical considerations. *Drug Resistance Updates* **11**, 32–50, (2008).
- 231 Porta, C., Paglino, C. & Mosca, A. Targeting PI3K/Akt/mTOR Signaling in Cancer. *Frontiers in Oncology* **4**, 64, (2014).
- 232 Xu, K., Liu, P. & Wei, W. mTOR signaling in tumorigenesis. *Biochimica et Biophysica Acta* **1846**, 638–654, (2014).
- 233 Noguchi, M., Hirata, N. & Suizu, F. The links between AKT and two intracellular proteolytic cascades: Ubiquitination and autophagy. *Biochimica et Biophysica Acta (BBA) - Reviews on Cancer* **1846**, 342–352, (2014).
- 234 Okumura, E., Fukuhara, T., Yoshida, H., Hanada Si, S., Kozutsumi, R., Mori, M., Tachibana, K. & Kishimoto, T. Akt inhibits Myt1 in the signalling pathway that leads to meiotic G2/M-phase transition. *Nature Cell Biology* **4**, 111–116, (2002).
- 235 Mueller, S. & Haas-Kogan, D. A. WEE1 Kinase As a Target for Cancer Therapy. *Journal of Clinical Oncology* **33**, 3485–3487, (2015).
- 236 Chow, J. P. & Poon, R. Y. The CDK1 inhibitory kinase MYT1 in DNA damage checkpoint recovery. *Oncogene* **32**, 4778–4788, (2013).
- 237 Chow, J. P., Poon, R. Y. & Ma, H. T. Inhibitory phosphorylation of cyclin-dependent kinase 1 as a compensatory mechanism for mitosis exit. *Molecular and Cellular Biology* **31**, 1478–1491, (2011).
- 238 Matheny, R. W., Jr. & Adamo, M. L. PI3K p110 alpha and p110 beta have differential effects on Akt activation and protection against oxidative stress-induced apoptosis in myoblasts. *Cell Death & Differentiation* **17**, 677–688, (2010).
- 239 Takeuchi, K. & Ito, F. Receptor Tyrosine Kinases and Targeted Cancer Therapeutics. *Biological and Pharmaceutical Bulletin* **34**, 1774–1780, (2011).
- 240 Hojjat-Farsangi, M. Small-molecule inhibitors of the receptor tyrosine kinases: promising tools for targeted cancer therapies. *International Journal of Molecular Sciences* **15**, 13768–13801, (2014).

Chapter 7 | References

- 241 Regad, T. Targeting RTK Signaling Pathways in Cancer. *Cancers (Basel)* **7**, 1758–1784, (2015).
- 242 Lombardi, D. & Lasagni, L. Cell-cycle Alterations in Post-mitotic Cells and Cell Death by Mitotic Catastrophe, in *Cell Biology-New Insights*. In: Najman, S. Ed. INTECH, Ch 3 (2016).
- 243 Vermeulen, K., Van Bockstaele, D. R. & Berneman, Z. N. The cell cycle: a review of regulation, deregulation and therapeutic targets in cancer. *Cell Proliferation* **36**, 131–149, (2003).
- 244 Zitouni, S., Nabais, C., Jana, S. C., Guerrero, A. & Bettencourt-Dias, M. Polo-like kinases: structural variations lead to multiple functions. *Nature Reviews Molecular Cell Biology* **15**, 433–452, (2014).
- 245 Zhang, Z., Zhang, G. & Kong, C. FOXM1 participates in PLK1-regulated cell cycle progression in renal cell cancer cells. *Oncology Letters* **11**, 2685–2691, (2016).